The role of the zinc transporter ZIP7 in adaptive immunity

A thesis submitted for the degree of

Doctor of Philosophy

Jie Yan

Corpus Christi College

DPhil in Clinical Medicine

Supervisors Prof. Richard J Cornall

Dr. Mukta Deobagkar-Lele

Nuffield Department of Medicine

University of Oxford

Hilary 2025

Acknowledgements

This project and thesis would not have been possible without enormous support and guidance from the institutions and individuals mentioned below.

Firstly, I would like to thank from the bottom of my heart my supervisors, Professor Richard Cornall and Dr Mukta Deobagkar-Lele. Not only did Richard offer me constructive suggestions, but he also provided a shoulder for me to lean on. When I first came to Oxford in the middle of the pandemic, his help made my life much easier. He also provided insightful revisions and feedback to my progress reports, transfer essay, DPhil confirmation report and thesis, which prompted me to think harder in a critical way. He has been such a blessing to me in everything he does. I'm particularly grateful to Mukta as she has been super patient and generous in helping me to fully grasp mouse work and bioinformatic analysis. All the regular catch-up discussions with her empowered me to take my studies the extra mile. Whenever I made some progress or won a prize, however small, she was always the one with the brightest smile. If one day I have students of my own to guide, she will be the example I would try to emulate.

I am indebted to the China Scholarship Council-Chinese Academy of Medical Sciences Oxford Institute (CSC-COI) and the MRC Human Immunology Unit (HIU) for their financial support and research funding. Especially, I would like to express my heartfelt gratitude to Professor Tao Dong, the co-founder of COI, for taking me into the MD/PhD High-level Medical Innovative Talent Program and for inspiring me regarding

how to develop a solid career in the long run. I won't take this experience for granted and I hope to contribute to the COI someday.

This ZIP7 project has involved a series of mouse models and cutting-edge single-cell RNA sequencing technology. Without all the unrelenting efforts from Tanya Cheetham, Peter Hinton and all the FGF staff, Ruddy Montandon and the core FACS facility staff, Moustafa Attar and Novogene, the achievements attained so far in this project would not have been possible.

The Cornall/Bull group is like a supportive family. I appreciate Katherine's brilliant suggestions throughout my project. To me, she is also a perfect example of a female physician-scientist who can balance research, clinical practice and family. Tanya has provided over the years invaluable support in every way. More impressively, she makes the lab a lot less like a workplace and more like a caring community. It has been a great pleasure to work with the brilliant postdoctoral researchers, DPhil students and research assistants in the Cornall/Bull lab and within the Wellcome Trust Centre for Human Genetics (WTCHG). Special thanks go to Aneesha Bhandari, Jianwei Cui, Jenny Back, Belinda Ameyaw, Rose Hodgson, Megan Matthews, Jessica Kepple, Tianen He, Rui Qi, Thomas Nicol and Thomas Hiron.

I want to give my deepest appreciation to Professor O'Callaghan, Dr Davies and Dr Fernandes for being my transfer and/or DPhil confirmation examiners.

I'm particularly grateful to the WTCHG, COI, MRC Weatherall Institute of Molecular Medicine (WIMM) and Corpus Christi College for organising various activities for communication, such as talks, seminars, together days and formal dinners.

To my previous supervisor in America, Professor Min Li, I owe a great debt. Without his guidance, I would not have gone down the rabbit hole of ZIPs. Thank you also for sending me birthday wishes every year no matter where I am. Thanks also go to

my previous supervisors in China, Professor Jie Chen and Dr Shuangni Yu, for their constant support.

A special thank you to Jia (Daisy) Liu and George Taylor, not only for spending hours helping me improve my English but also for standing by me amidst my ups and downs.

I couldn't be more grateful for the kindness of my parents, relatives and friends, who encouraged me to take a great adventure around the world. Your unconditional support goes a long way.

Abstract

The zinc transporter SLC39A7, or ZIP7, is critical for early B cell development, but its role in peripheral adaptive immunity remains incompletely defined. Since ZIP7 hypomorphic mutations preferentially affect B cells over T cells in humans and in murine models, we hypothesize that lymphocyte lineage-specific requirements and differential adaptive responses determine the varying phenotypic consequences of ZIP7 deficiency. This thesis investigates the impact of ZIP7 deficiency on B and T cell maintenance, function, and stress adaptation using a series of inducible and tissue-specific mouse models, complemented by single-cell transcriptomics.

Varying degrees of *Ert2*-cre-based ZIP7 deficiency revealed that ZIP7 is essential for maintaining immune cell populations during early development, including pro-B to immature B cells, and thymic late DN to DP T cells. *Cr2-cre* and *Cd4-cre* conditional knockout models also confirmed that marginal zone B and mature T cells exhibit intrinsic survival disadvantages under ZIP7 deficiency, especially in competitive settings. Functionally, ZIP7-deficient B cells failed to mount robust humoral responses to both T-independent and T-dependent antigens. Adoptive transfer models revealed inefficient recruitment and survival of B cells in germinal centres, highlighting a critical role for ZIP7 in sustaining B cell persistence during immune activation.

Single-cell RNA sequencing further uncovered a conserved stress signature marked by high *Atf4* and *Pck2,* and low *Eif2b* expression, consistent with a split

integrated stress response. While stress-marked T cells activated broader compensatory pathways, B cells mounted a more limited adaptive response, potentially contributing to their heightened vulnerability. Divergent mTORC1 activity further suggested lineage-specific compensatory strategies under ZIP7-induced stress.

Together, this work identifies ZIP7 as a non-redundant regulator of lymphocyte fitness under metabolic stress. It defines gene dosage-dependent thresholds of ZIP7 sufficiency across immune cell subsets and highlights transcriptional stress adaptation as a critical vulnerability in ZIP7-deficient cells—offering insights with potential translational relevance for primary immunodeficiencies.

List of Abbreviations

Abbreviation	Full name
4PL	4-parameter logistic
ADT	Antibody-derived tag
AE	Acrodermatitis enteropathica
AID	Activation-induced cytidine deaminase
AP	Alkaline phosphatase
APCs	Antigen-presenting cells
BCR	B-cell receptor
BM	Bone marrow
BMMCs	Bone marrow-derived mast cells
c-ISR	Canonical ISR
CB2	Cannabinoid receptor 2
CIs	Confidence intervals
CLR	Centred log-ratio
CM	Central memory
CSR	Class switch recombination
cTECs	Cortical thymic epithelial cells
DCs	Dendritic cells
DEGs	Differentially expressed genes
DL1	Delta-like 1
DN	Double-negative
DP	Double-positive
DZ	Dark zone
EDCI	1-ethyl-3-(3-dimethylaminopropyl) carbodiimide
Egr2	Early growth response 2
EM	Effector memory
ER	Endoplasmic reticulum
ERAD	ER-associated degradation
ETPs	Early thymic progenitors
FACS	Fluorescence-activated cell sorting
FAO	Fatty acid oxidation
FCS	Fetal calf serum

FcμR	Fcμ receptor
FDCs	Follicular dendritic cells
Fo I	Follicular I
Fo II	Follicular II
GC	Germinal centre
gDNA	Genomic DNA
GF	Germ-free
GO	Gene Ontology
HDR	Homology-directed repair
HEL	Hen egg lysozyme
HELtg	Expressing HEL antigen
HEVs	High endothelial venules
HSCs	Hematopoietic stem cells
HTO	Hashtag oligonucleotide
hZIP7	Human ZIP7
ICTs	Ion channels and transporters
Ig	Immunoglobulin
Ig-tg	Ig transgenic
IRF4	Interferon regulatory factor 4.
IS	Immunological synapse
ISR	Integrated stress response
LMPPs	Lymphoid-primed multipotent progenitors
lssDNA	long single-stranded DNA
LZ	Light zone
MACS	Magnetic-activated cell sorting
MARCO	Macrophage receptor with collagenous structure
MD4	α-HEL BCR transgenic mice lacking HEL antigen expression
MHC	Major histocompatibility complex
MLNs	Mesenteric lymph nodes
MLPs	Multi-lymphoid progenitors
MS	Mass spectrometry
mTECs	Medullary thymic epithelial cells
MTs	Metallothioneins
MZ	Marginal zone
MZBs	Marginal zone B cells
MZP	MZ precursors
non-tg	Non-transgenic
NP	4-hydroxy-3-nitrophenylacetyl
NP-CGG	NP-conjugated chicken gamma globulin
nTreg	Natural regulatory T
OXPHOS	Oxidative phosphorylation
PALS	Periarteriolar lymphoid sheath
PFOS	Perfluorooctane sulfonate

PI3K	Phosphoinositide 3-kinase
PIDs	Primary immunodeficiency diseases
pre-BCR	Pre-B cell receptor
Pre–B cells	Precursor B cells
pro-B cells	Progenitor B cells
ROS	Reactive oxygen species
RT	Room temperature
s-ISR	Split integrated stress response
S1P	Sphingosine-1-phosphate
S1PR1	S1P receptors
scRNA-seq	Single-cell RNA sequencing
SCS	Subcapsular sinus
SHM	Somatic hypermutation
SLC	Surrogate light chain
SP	Single-positive
SPF	Specific pathogen-free
SRC	Spare respiratory capacity
T1	Transitional 1
T2	Transitional 2
T3	Transitional 3
TCRs	T cell receptors
TD	Thymus-dependent
TECs	Thymic epithelial cells
Tfh	T follicular helper
TI	Thymus-independent
TMDs	Transmembrane domains
TRAs	Tissue-restricted antigens
Treg	Regulatory T
TRPM7	Transient receptor potential subfamily M member 7
TSSP	Thymus-specific serine protease
UPR	Unfolded protein response
WBC	White blood cell
WT	Wild-type
XLA	X-linked agammaglobulinemia
ZIPs	Solute carrier family 39 transporters (ZRT/IRT-like proteins)
ZnTs	Solute carrier family 30 transporters

List of Figures

List of Appendices

Table of Contents

Chapter

1 Introduction

1.1 Overview: Insights from primary immunodeficiency research

Primary immunodeficiency diseases (PIDs) are genetic disorders that impair immune system function[1]. Their prevalence varies from 1/2,000 to 1/100,000 based on databases from multicentre registers in America[2], Europe[3], Australia and New Zealand[4], China[5], or Japan[1]. The reported prevalence in some countries suggests that PIDs are more common than generally thought. PIDs are estimated to occur in 6-8 million people worldwide[6]. The aggregated number and accompanying risks of infection[7] and autoimmune diseases[8] take a toll on the public health system.

As the prototype of PID, X-linked agammaglobulinemia (XLA) exemplifies the synergy between clinical observations and technological advancements. From its first clinical description in 1952[9] to the identification of pre-B cell developmental blocks in the 1970s[10,11] and *BTK* mutations as its genetic basis in 1993[12,13], XLA has paved the way for understanding immune system biology. These insights culminated in the development of BTK-targeted therapies[14], illustrating how PIDs bridge patient care and immunological discovery.

Advances in genome sequencing[15-17] have accelerated the identification of novel genes associated with PIDs[18,19]. Among these, researchers in the US and Newcastle,

identified six patients with agammaglobulinemia carrying multiple loss-of-function variants in *SLC39A7* (*ZIP7*)[20], which encodes a zinc transporter. In collaboration with this groups, and using germline *Zip7*$^{P198A/P198A}$ mice, our group revealed a B cell-intrinsic developmental block beyond the pre-B cell stage. These findings raised intriguing questions: What role does ZIP7 play in peripheral B and T cells? Why do ZIP7 hypomorphic mutations predominantly affect B cell function, sparing T cells? Given that complete ZIP7 knockout causes embryonic lethality, how can we investigate the effects of more severe ZIP7 deficiencies in the immune system?

This thesis explores the impact of ZIP7 deficiency on B cell and T cell function, focusing on how varying gene dosages influence adaptive immunity. Through conditional knockout mouse models[21-24] and single-cell RNA sequencing (scRNA-seq)[25-27] , I aim to elucidate the role of ZIP7 in lymphocyte homeostasis, immune responses, and integrated stress pathways. By combining *in vivo* and *in silico* approaches, this work seeks to bridge gaps in our understanding of ZIP7 in immunity.

1.2 B cells in development and immunity

This year marks the 60th anniversary of the recognition of B cells as a distinct lymphocyte lineage in 1965, separate from their functionally intertwined counterparts, T cells[28]. B cells mediate humoral immunity, while T cells contribute to both humoral and cellular immunity, establishing these lymphocytes as central pillars of adaptive immunity, which complements natural barriers and innate immunity to protect against pathogens. This section reviews the development and functions of these two lineages, with a particular focus on B cells and recent advancements.

1.2.1 Early B cell development

Hematopoietic precursor cells undergo an ordered maturation and selection process to become functional B or T cells. Since the majority B cells develop in the bone marrow (BM), especially well-characterised in mouse models, the following section will focus on their BM-dependent stages.

1.2.1.1 Hematopoietic stem cells and their reconstitution

Hematopoietic stem cells (HSCs), although rare–comprising only one in 10,000 nucleated BM cells[29]–serve as the foundation for haematopoiesis. Early lymphoid progenitors[30,31], such as lymphoid-primed multipotent progenitors (LMPPs) in mice[32] or multilymphoid progenitors (MLPs) in human[33], differentiate into B cell progenitors[34] within the BM microenvironment. Stromal cells in the BM niche support this process by secreting essential factors and providing contact-dependent signals[35]. Recent studies have revealed additional sites of B cell development, such as the meninges, where pro-B cells from calvarial HSCs mature independently of circulation[36,37], suggesting unique microenvironments beyond the BM.

The most widely used *in vivo* assay to track and quantify hematopoietic reconstitution is the competitive repopulation of lethally irradiated mice using CD45 disparate congenic donor cells. This approach allows differentiation to occur in a physiologic environment. Among transplanted BM cells, the Lin^- $Sca\text{-}1^+$ fraction, which constitutes only 0.05% of BM cells, possesses hematopoietic reconstitution potential. Even as few as 100 cells can efficiently achieve long-term multilineage hematopoiesis[38]. Sequential analysis of hematopoietic reconstitution shows that myeloid and B-lymphoid lineages emerge earlier (2–3 weeks post-transplantation) than T-lymphoid lineages (4 weeks post-transplantation)[39]. Notably, T cells exhibit higher radiation resistance than B cells,

leading to a greater persistence of host-derived T cells after irradiation[40]. BM-transplanted chimeras are a valuable experimental strategy, particularly when a gene knockout is embryonically lethal, donor cell yield is low, or when validating whether a phenotype is cell-intrinsic[20].

1.2.1.2 BM-dependent stages of B cell development

B cell development in the BM follows a stepwise progression, commonly classified using Hardy Fractions in mice[41,42]. These stages reflect key immunoglobulin (Ig) gene rearrangement events.

Progenitor B cells (Pro-B cells)

Lineage commitment begins at the pre-pro-B stage (Fraction A)[43], marked by the expression of B220, a CD45 isoform. These $CD19^{-}$ $B220^{+}$ cells express low CD24 and are biased toward B cell fate[43,44]. At this stage, Ig gene rearrangement has not yet initiated[44]. Instead, transcription factors such as PU.1, Ikaros, E2A, EBF1, and Pax5 establish B cell identity[45,46]. Pax5 plays a pivotal role by repressing alternative lineage programs and activating CD19 expression[47,48], marking full B cell commitment.

In early pro–B cells (Fraction B), IgH recombination begins with D–J joining[41], followed by V–DJ rearrangement in late pro-B cells (Fraction C)[49]. This process is tightly regulated by the spatial organization of the *Igh* locus (~2.8 Mb) and chromatin architecture. Studies[50-53] show that D and J segments, being closest to the recombination centre, are joined first. RAG-mediated scanning and cohesin-driven loop extrusion then bring distal VH segments into proximity for V–DJ joining.

Structurally, the RAG endonuclease functions as a Y-shaped heterotetramer: the RAG1 dimer forms the core, while RAG2 sits at the tips[54,55]. RAG1 contains two zinc-binding sites essential for structural integrity and DNA cleavage activity[54,56,57].

A productive V_HDJ_H rearrangement allows transcription and splicing of a mature μ heavy chain mRNA[58]. The resulting μ heavy chain protein assembles into the pre-B cell receptor, marking the transition from the pro-B cell to the pre-B cell stage.

Precursor B cells (Pre–B cells)

The formation of the pre–B cell receptor (pre-BCR), comprising the μ heavy chain, surrogate light chain (SLC), and Igα/Igβ, marks the transition to the large pre-B cell stage (Fraction C′), the most proliferative phase of B cell development. The SLC is composed of two invariant polypeptides, Vpre-B and λ5[59,60], and functions as a checkpoint to assess whether the μ chain can form a functional complex with future light chains. Approximately 50% of μ chains successfully pair with the SLC to form a functional pre-BCR[61].

Pre-BCR signaling triggers multiple rounds of cell division, leading to clonal expansion of cells expressing productive IgH rearrangements[62]. As cytoplasmic SLC becomes diluted with each division, proliferation gradually ceases[62], and cells transition into a resting state as small pre–B cells.

At the small pre-B cell stage (Fraction D)[63], RAG1 and RAG2 are re-expressed, initiating V–J recombination at the κ or λ light chain loci[64]. A successful light chain rearrangement allows pairing with the preformed μ chain to form a complete IgM B cell receptor (BCR) on the cell surface.

To ensure clonal specificity, allelic exclusion at the heavy chain[65] and light chain[66] loci restricts expression to a single IgH and a single IgL allele. Inevitably, the resulting naïve BCR repertoire includes not only non-self–reactive antibodies but also a fraction of autoreactive or polyreactive ones[67]. These potentially harmful B cells must

be eliminated or inactivated through central tolerance mechanisms within the BM before further maturation.

Immature B cells

Immature B cells (Fraction E) represent the first developmental stage at which a complete BCR, surface IgM paired with Igα and Igβ, is expressed. This intact BCR delivers essential tonic survival signals[68,69], primarily via the phosphoinositide 3-kinase (PI3K) pathway[70], independently of antigen engagement[71].

Notably, up to 55%–75% of newly generated immature B cells initially express self-reactive BCRs[67]. Cells with low or no self-reactivity are permitted to exit the BM and enter peripheral lymphoid tissues, where additional tolerance mechanisms are applied. In contrast, approximately 30%–35% of immature B cells exhibit medium to high avidity for self-antigens[67] and are retained in the BM to undergo central tolerance processes.

Central B cell tolerance is primarily driven by the avidity of BCR–self-antigen interactions, a combination of antigen affinity and availability[72-74]. Studies using both genetically modified[75,76] and wild-type (WT) polyclonal[77,78] mouse models demonstrate that central tolerance is mainly achieved through receptor editing[79,80], while clonal deletion[72,81] serves as a secondary safeguard[75]. Upon sensing self-antigen, BCR signaling is attenuated, leading to suppression of the PI3K pathway. This permits the nuclear translocation of the transcription factor FOXO1, which upregulates RAG1/2 expression and initiates further light chain rearrangement to revise autoreactive receptors[82,83].

Through these mechanisms, central tolerance enables the removal or revision of self-reactive clones, ensuring the development of a diverse yet self-tolerant B cell repertoire essential for immune homeostasis.

1.2.2 Peripheral B cell subtypes

Upon exiting the BM, immature B cells undergo additional selection and differentiation processes while gradually integrating into the mature, long-lived B cell pool. Peripheral B cells have been traditionally classified into distinct subsets based on their phenotypic markers, anatomical localization, and functional properties, each with specific requirements for development and maintenance. However, these classical classifications do not fully capture the heterogeneity of each B cell subset, making them insufficient to fully resolve B cell diversity at a single-cell resolution. Advances in genomics, proteomics, and genetically modified models have provided deeper insights into the complexity of peripheral B cell populations. Here, I will focus on the main peripheral B cell subtypes in mice and discuss how recent technological advances have refined our understanding of their identity and function.

1.2.2.1 Transitional B cells

Following marrow egress, immature B cells undergo peripheral selection, and only a subset ultimately integrates into the long-lived mature B cell pool[84,85]. These newly emigrated cells, termed transitional B cells, progress through defined stages, namely transitional 1 (T1) and transitional 2 (T2), before attaining full maturity[86,87].

T1 B cells retain key phenotypic characteristics of their BM counterparts, including high CD24 (heat-stable-antigen, HSA)[84] and CD93/AA4.1 expression, while lacking follicular markers such as CD23 and IgD and displaying low levels of CD21. In contrast, T2 B cells upregulate CD23 and IgD while maintaining CD93 expression, serving as a branching point for differentiation into either follicular or marginal zone (MZ) B cells.

T1 to T2 transition: survival and selection mechanisms

The transition from T1 to T2 is a highly regulated process, ensuring the survival and proper selection of non-autoreactive B cells. A recent study using Rosa26^{INDIA} reporter mice demonstrated that immature B cells undergo extensive apoptosis immediately upon entering circulation, peaking at the T1 stage and gradually declining from T2 to follicular B cells. This apoptosis is primarily driven by insufficient BCR- and BAFF-mediated survival signals, rather than clonal deletion[88].

The integrity of BCR signaling plays a crucial role in this transition. Disruptions in this pathway, such as loss of the Ig-α cytoplasmic tail[86] or impaired PI3K/Akt activation in SPPL2a$^{-/-}$ mice[89], can arrest T1 progression. Tonic BCR signaling is particularly essential, with BAFF-R providing additional survival support[90]. In BAFF-R$^{-/-}$ and BLyS$^{-/-}$ mice, B cell development is arrested at the T1 stage, resulting in a near-total loss of T2, MZ and follicular B subsets, whereas B-1 cells remain largely unaffected[91,92].

Beyond survival, the strength of BCR signaling dictates whether a transitional B cell undergoes positive or negative selection[93]. Cells receiving insufficient tonic BCR signaling fail to acquire survival cues[69], leading to apoptosis and exclusion from the mature B cell pool. In contrast, intermediate-strength BCR signaling supports positive selection, promoting transitional cell survival and differentiation. However, when BCR signaling is excessively strong, antigen-driven activation induces negative selection, leading to clonal deletion or anergy to prevent autoreactive B cells from populating the mature B cell compartment.

In addition to intrinsic signaling thresholds, the splenic microenvironment refines the transitional B cell compartment. T1 cells initially localize to the outer periarteriolar lymphoid sheath (PALS), whereas T2 cells migrate into the follicular zone, where they further mature[86,94,95].

T3 B cells: anergic B cells rather than a distinct transitional subset?

Transitional 3 (T3) B cells express CD93 and exhibit a mature follicular B cell-like profile (IgM^{low} $CD23^{+}$), leading to their initial classification as an intermediate stage in linear development[87]. However, accumulating evidence suggests that T3 B cells are more accurately classified as a subset of anergic B cells rather than a distinct transitional stage.

First, anergic Ig-transgenic B cells, such as ArsA1[96] and α-HELtgHELtg[74] (which carry both α-HEL BCR and HEL antigen transgenes), exhibit a T3-like marker profile indistinguishable from that of WT C57BL/6 mice, indicating a shared functional state.

Second, if T3 B cells represented a mandatory developmental stage, they should be present in all B cell populations regardless of antigen reactivity. However, in MD4 mice[74] (α-HELtg, carrying only the α-HEL BCR transgene but lacking HEL antigen expression), T1 and T2 B cell subsets are intact, yet T3 B cells are nearly absent[97], suggesting that T3 B cells arise in response to BCR self-reactivity rather than as a default step in B cell maturation.

Third, if T3 B cells reflect an anergic state rather than a necessary developmental transition, non-autoreactive B cells should acquire a T3 phenotype upon exposure to self-antigen. Indeed, when MD4-derived B cells were transferred into HELtg recipients (expressing HEL antigen), they rapidly downregulated IgM, upregulated CD93, and acquired a T3-like phenotype, further supporting the notion that T3 B cells emerge as a consequence of antigen-driven tolerance rather than as an intrinsic developmental phase.

Finally, studies estimate that ~50% of newly generated B cells enter an anergic state within a normal immune repertoire. These physiologically occurring anergic B cells share functional characteristics with T3 B cells and anergic B cells from immunoglobulin-transgenic models, including attenuated BCR-mediated signaling and failure to mount an immune response upon antigen-receptor stimulation[97].

Given this evidence, this thesis adopts the term "anergic B cells" to describe this population, particularly in the Results section regarding the annotation of splenic B cell subtypes from scRNA-seq clustering.

High-throughput analyses reveal molecular features of transitional B cell subsets

While classical studies have delineated the phenotypic and functional transitions between T1, T2, and anergic B cells, recent high-throughput analyses have provided a deeper molecular resolution into these subsets.

Proteomic profiling of sorted splenic T1 ($CD19^+$ $CD93^+$ IgM^+ $CD23^–$), T2 ($CD19^+$ $CD93^+$ IgM^+ $CD23^+$), MZ ($CD19^+$ $CD93^–$ $CD21^+$ $CD23^–$) and follicular ($CD19^+$ $CD93^–$ $CD21^–$ $CD23^+$) B cells from C57BL/6 mice by quantitative label-free high-resolution mass spectrometry (MS) suggests that T1 B cells exhibit distinct molecular signatures compared to later transitional and mature follicular B cells[98]. Specifically, a subset of proteins, including ZEB2, DUSP10, and SERINC5, were uniquely enriched in T1 cells. Additionally, T1 cells displayed elevated expression of lactate/pyruvate/amino acid/fatty acid transporters (SLC16A1, SLC1A5, SLC7A5, SLC27A1), potentially supporting their rapid turnover and susceptibility to selection pressures. In contrast, T2 and follicular B cells shared largely overlapping transcriptomic and proteomic landscapes, with few distinguishing molecular features, reinforcing the notion that T2 serves as an intermediate stage before full maturation into follicular or MZ B cells rather than a distinct functional subset.

Microarray analysis identified *Egr2, Nab2* and *Nrgn* as genes highly expressed in anergic α-HELtgHELtg B cells compared to antigen-naive α-HELtg B cells[99], which was further validated by qPCR in both physiologic and transgenic anergic B cells[97]. Notably, *Egr2* (early growth response 2) exhibited the highest specificity to anergic B cells, whereas Nab2 and Nrgn were also upregulated in WT T1 and T2 B cells[97]. As a zinc-

finger nuclear transcription factor, Egr2 serves as a critical regulator of the T cell anergy program[100]. In B cells, conditional deletion of *Egr2* in *Egr3*$^{-/-}$ *Egr2*$^{f/f}$ *Cd19-cre* mice leads to a striking accumulation of CD21^{low} CD23^{low} mature B cells, which transcriptionally resemble CD21^{low}/age-associated/atypical memory B cells and are associated with a disruption of B cell tolerance[101]. This underscores the essential role of Egr2 in maintaining peripheral B cell tolerance.

In summary, the transitional B cell stage represents a critical checkpoint in immune homeostasis, ensuring that only functionally competent and self-tolerant B cells integrate into the mature B cell repertoire.

1.2.2.2 Follicular B cells

After successfully passing the transitional B cell stage, a subset of B cells differentiates into follicular B cells, the dominant naïve B cell population, while a smaller proportion adopts a MZ B cell fate. Follicular B cell differentiation is primarily dictated by BCR signaling strength, with additional contributions from BAFF and integrin-mediated interactions. Strong BCR signalling, below the threshold for inducing anergy, promotes follicular B cell differentiation via activation of kinases such as Btk and PLCγ2. Consistently, mice deficient in Btk or PLCγ2 exhibit a marked reduction in follicular B cells, while MZ B cell development remains largely unaffected[102,103]. Additionally, CXCR5-mediated chemotaxis plays a crucial role in guiding follicular B cell precursors into follicles[95,104], where they receive survival signals from BAFF and the follicular microenvironment[105]. By contrast, MZ B cell differentiation is favoured by relatively weaker BCR signalling, combined with Notch2 activation and BAFF-mediated NFκB signalling, which will be discussed in the next section.

In the spleen, naïve follicular B cells and T cells reside in the inner white pulp, surrounded by MZ macrophages and MZ B cells. However, this structured compartmentalization, along with the spatial expression of chemokines such as Ccr7 and Cxcl13, is disrupted in the absence of microbiota-derived antigen exposure, as demonstrated by a scRNA-seq and Stereo-seq study that directly compared spleens from WT specific pathogen-free (SPF) and WT germ-free (GF) mice[106]. Follicular B cells primarily remain in a recirculating quiescent state until encountering cognate antigens. Upon activation, follicular B cells exhibit diverse differentiation fates. While a fraction enters the germinal centre (GC) reaction, undergoing clonal expansion, somatic hypermutation (SHM), and class switch recombination (CSR), others differentiate directly into short-lived plasmablasts, contributing to the extrafollicular response. Thus, follicular B cells represent a dynamic and functionally diverse population.

Heterogeneity within follicular B cells

Early studies proposed that follicular B cells could be subdivided into Follicular I (Fo I) (IgD^{hi} IgM^{low} $CD21^{mid}$) and Follicular II (Fo II) (IgD^{hi} IgM^{hi} $CD21^{mid}$) subsets[107]. FO II B cells exhibit higher basal tyrosine phosphorylation and greater proliferation upon BCR stimulation, suggesting a more activated state compared to FO I B cells. Transcriptomic analyses further indicate that FO II B cells are enriched for genes involved in lymphocyte and complement activation, as well as RNA binding, implying a higher transcriptional activity[108]. Conversely, a study analysing the metabolic state of follicular B cells reported a downregulation of genes associated with peptide biosynthesis, ribosome biogenesis, and oxidative phosphorylation, which was interpreted as a metabolic quiescence phenotype characteristic of follicular B cells. However, this study selectively examined only FO I B cells, potentially overlooking FO II B cells, which exhibit a slightly more activated state[109]. Although the classification of FO I and FO II B cells is not widely

accepted, these findings highlight the need for a refined perspective when investigating follicular B cell heterogeneity, particularly in FACS-sorted, CITE-seq-integrated splenic $CD45^+$ single-cell transcriptomic data, which will be further explored in this study.

Follicular B cell activation and migration

Follicular B cell heterogeneity is also reflected in their dynamic nature. While most follicular B cells remain in a quiescent recirculating state, a subset undergoes different stages of activation, priming for further differentiation. This activation not only alters their transcriptional state but also drives changes in chemokine receptor expression, orchestrating their migration within the spleen.

Upon antigen engagement, CXCL13–CXCR5 signaling enhances BCR-mediated B cell activation by promoting membrane ruffling and LFA-1-supported adhesion, facilitating antigen gathering at the immune synapse and integrating BCR signaling in motile B cells[110]. Meanwhile, CCR7 expression is rapidly upregulated in activated B cells, increasing their responsiveness to CCL19 and CCL21, which guide their migration toward the T–B border for interaction with primed T cells. In this process, CXCR5, which retains B cells within follicles via CXCL13, counterbalances CCR7-driven movement, maintaining a dynamic equilibrium between follicular retention and T-zone entry[111].

Beyond the T–B border, additional cues further refine activated B cell positioning. Upregulation of EBI2 promotes their migration toward the outer follicle and interfollicular regions, facilitating early extrafollicular responses. As the GC reaction initiates, EBI2 expression is downregulated, allowing B cells to access the follicle centre and participate in affinity maturation[112,113].

The subsequent regulation of follicular B cells in the germinal centre will be further discussed in Section 1.3.2.4 GC B cells.

1.2.2.3 MZ B cells

MZ B cells are one of immune populations on the front line, because of their strategic location and versatile functions, blurring the boundaries between innate and adaptive immunity.

MZ B cells in mice reside in the marginal zone, a region situated between the marginal sinus of the white pulp and the red pulp, where they efficiently capture blood-borne antigens. Unlike follicular B cells, MZ B cells exhibit a state of active readiness. When antigen is recognised, they differentiate with unmatched speed into plasmablasts that secrete IgM antibodies[114-116], providing protection akin to innate immune responses[117].

In addition to their rapid response to thymus-independent (TI) antigens, MZ B cells also participate in thymus-dependent (TD) immune responses, leveraging their antigen presentation capacity to enhance T cell-mediated immunity. By expressing high levels of complement receptor CD21, MZ B cells efficiently capture complement-opsonized antigens and transport them to follicular dendritic cells (FDCs)[118]. Beyond antigen transport, MZ B cells also function as antigen-presenting cells (APCs). Through CR2/CD21-mediated trogocytosis, they acquire MHC-II peptide complexes from dendritic cells (DCs) and present them to T helper cells, bypassing the need for intracellular antigen processing[119].

This dual function enables MZ B cells to participate in TD responses through two distinct pathways. In the follicular pathway, upon antigen uptake, MZ B cells cells down-regulate S1P receptors and upregulate CXCR5, allowing them to migrate into the follicle and deposit antigens on FDCs[118,120], thereby facilitating TD antibody responses. In an extrafollicular setting, $CD1d^{+}$ MZ B cells activate iNKT cells, leading to rapid lipid-specific IgM and IgG production[121,122], while $DCIR2^{+}$ dendritic cells provide antigens that allow MZ B cells to engage directly with T helper cells and secrete IgG1[123].

Given their critical roles in both TI and TD immunity, the loss of MZ B cells severely compromises humoral protection. Identifying the underlying causes of MZ B cell depletion is therefore essential. Mouse models have provided insights into both direct and indirect factors contributing to MZ B cell loss.

BCR and downstream signaling cascade defects

While BCR signaling supports MZ B cell development, it is not the sole determinant of its maintenance. CD79a (Igα), a core BCR component, and CD19, a key co-receptor that amplifies PI3K activation, are both essential for MZ B cell development, as their deficiency leads to a marked reduction of MZ B cells while leaving the follicular B cell compartment intact[124-127]. However, BCR signaling defects can selectively impair MZ B cell maintenance or affect both MZ and follicular B cell compartments to varying degrees[128-130]. For example, Aiolos deficiency results in MZ B cell loss but leads to an expansion of the follicular B cell compartment[129,130], whereas Aiolos$^{-/-}$ Xid double knockout mice restore MZ B cells, suggesting that Btk-mediated excessive BCR signaling prevents MZ B cell differentiation in Aiolos$^{-/-}$ mice[129]. Furthermore, not all BCR-associated molecules are required for MZ B cell maintenance, as the deletion of Cd21[129] does not lead to MZ B cell loss.

Nevertheless, since BCR-mediated clonal selection is coordinated with survival (TNF receptor family) and migration (G-protein-coupled receptors) cues, evaluating BCR signaling remains essential to exclude its potential involvement in MZ B cell loss.

Developmental defects

MZ B cell fate is primarily determined by weak to moderate BCR signalling, combined with Notch2 activation and BAFF-mediated NF-κB signalling. Upon encountering

Delta-like 1 (DL1) in the splenic red pulp, Notch2-expressing B cells commit to the MZ B cell lineage[131]. Notch2 signaling is essential for MZ B cell generation, as demonstrated by the complete absence of MZ B cells in mice lacking Notch2, its downstream transcription factor RBP-J, or its ligand Dll1[132-134]. Similarly, NF-κB signaling through the BAFF pathway is indispensable for MZ B cell differentiation, as evidenced by the significant reduction of MZ B cells in mice lacking NF-κB components, including p50, p65, or c-Rel[135].

One possible cause of MZ B cell loss is an upstream defect in precursor populations. However, the developmental trajectory of MZ B cell precursors remains unclear. Initially, MZ B cell precursors were proposed to arise from T2 B cells (sIgM^{hi} sIgD^{hi} CD21/35^{hi} CD23^{+})[86] in the B cell follicle, leading to the designation T2-MZ precursor (MZP) cells[129,133,136,137]. Some studies suggested that MZ B cell precursors resemble follicular-like IgM^{hi} IgD^{hi} CD21^{hi} B cells, which have not yet received adequate BCR signal to commit to a long-lived follicular fate[129]. Another candidate population consists of CD1d^{hi} CD23$^{int/hi}$ CD21/35^{hi} IgM^{hi} B cells, as their numbers decline in parallel with MZ B cells in Notch2-deficient mice[133,136]. However, the lack of lineage-tracing evidence leaves open the possibility that these reductions result from secondary effects rather than a direct precursor-product relationship.

Alternatively, some studies suggest that T1 B cells may directly contribute to MZ B cell generation. This hypothesis is supported by CDR3 repertoire analysis, which shows that MZ B cells are enriched in “fetal-type” B cell receptors lacking N regions (N^{-}), a feature shared with T1 B cells[138]. Further evidence comes from ADAM10-expressing T1 cells, which exclusively differentiate into MZ B cells upon transfer into Rag2$^{-/-}$ mice. In contrast, ADAM10-negative T1 and T2 cells give rise to both follicular and MZ B cells[139].

The unresolved nature of MZ B cell precursor development makes their identification particularly challenging due to the lack of definitive markers. A study using alternative gating strategies in $CD19^{-/-}$ mice produced seemingly contradictory findings. While transitional MZ B cell precursors ($CD23^{high}$ $CD93^{high}$ within the $CD1d^{high}$ IgM^{high} subset) and follicular precursors of MZ B cells ($CD93^{low}$ $CD23^{high}$ within the $CD1d^{high}$ IgM^{high} subset) appeared largely intact (0.44% vs. 0.42% in WT; 0.3% vs. 0.67% in WT, respectively), the overall frequency of combined transitional and follicular MZ precursors was reduced by 30%. This discrepancy underscores the challenge of defining MZ precursors and the influence of gating strategies on their identification[126].

In this study, I define MZ precursors using the gating strategy $B220^{+}$ $CD19^{+}$ $CD93^{-}$ IgM^{hi} $CD21^{hi}$ IgD^{hi} $CD23^{hi}$ (Supplementary Figure 14). Notably, this gating strategy may preferentially enrich for T2-MZP-derived MZ precursors. Given the unresolved nature of MZ precursor classification, this selection could introduce a potential bias in defining the MZ precursor population.

Lifespan and survival defects

MZ B cells exhibit an extended lifespan compared to follicular B cells, with turnover kinetics indicating a half-life of approximately 5 months[140,141]. Their population is dynamically regulated by a balance between survival signals, apoptosis, and activation-induced cell death.

The near-total loss of MZ and follicular B cells in BAFF-deficient mice[105] closely resembles the phenotype observed in BAFF-R-deficient mice[91], supporting BAFF-R as the primary receptor mediating BAFF's survival signals. One outcome of non-canonical NF-κB signaling is the upregulation of anti-apoptotic molecules, including Bcl-2, which plays a crucial role in promoting B cell survival[142,143]. However, Bcl-2 overexpression in BAFF-R-deficient mice restores follicular B cells but fails to rescue MZ B

cells[91,144,145], suggesting that BAFF provides survival cues beyond apoptosis inhibition, which are essential for MZ B cell maturation.

Besides BAFF, Fcμ receptor (FcμR) supports MZ B cell homeostasis by sustaining tonic BCR signalling. Its deficiency results in a selective reduction of MZ B cells due to increased apoptosis and accelerated turnover[146]. Additionally, post-transcriptional regulation by RNA-binding protein ZFP36L1 has emerged as a key mechanism governing MZ B cell survival. Conditional deletion of ZFP36L1 leads to a marked depletion of MZ B cells and their precursors while largely sparing follicular B cells, underscoring its critical role in maintaining MZ B cell survival, turnover, and identity[147].

Upon immune activation, TACI and TLR4 signaling promote Fas-mediated apoptosis of MZ B cells. LPS stimulation induces Fas and FasL expression in a TACI-dependent manner, and TACI-deficient mice exhibit impaired MZ B cell apoptosis following TLR4 activation[148]. This suggests that TACI signaling counterbalances survival pathways by driving activation-induced turnover of MZ B cells.

Together, these distinct yet interconnected pathways coordinate the survival, renewal, and adaptive regulation of the MZ B cell pool.

Retention and migration defects

MZ B cells rely on a delicate balance of chemotactic signalling, adhesion, and cell-cell interactions to remain within the MZ while dynamically shuttling between compartments in response to antigenic stimuli. Disruptions in these mechanisms lead to MZ B cell loss or mislocalization, impairing immune responses to blood-borne antigens.

In mice, the blood passing through the MZ contains sphingosine-1-phosphate (S1P), MZ B cell positioning in the MZ requires S1P receptors (S1PR1) to overcome attraction to follicular CXCL13[118,120,149]. In *S1pr1*$^{-/-}$ fetal liver chimeric mice, MZ B cells fail to localize to the MZ and instead mislocalize into follicles[120]. Similarly,

cannabinoid receptor 2 (CB2), another Gαi-coupled receptor, contributes to MZ B cell retention. In CB2-deficient ($Cnr2^{-/-}$) mice, exhibit a reduction in MZ B cell numbers, with a subset of cells displaced into the blood[150], suggesting that losing chemotactic receptors affecting the balance between MZ B cell and compartment populations.

Beyond chemotactic signals, integrin-mediated adhesion and actin reorganization provides an additional layer of control over MZ B cell retention. Integrins such as LFA-1 (αLβ2) and VLA-4 (α4β1) bind to ICAM-1 and VCAM-1, respectively, on stromal cells, stabilizing MZ B cell positioning[151]. The key role of cytoskeletal remodelling in the positioning of MZ B cells is evidenced by the phenotype of mice lacking the related molecules Pyk2[152], Lsc[153], Wasp[154], or Rac2[155,156]. These mice have normal numbers of follicular B cells but low numbers of MZ B cells, along with impaired antibody responses.

Cell-cell interactions within the MZ further contribute to MZ B cell retention. The interaction between CD97, an adhesion GPCR, and its ligand CD55 on red blood cells is one such mechanism. In *Cd97*$^{-/-}$ mice, MZ B cells are significantly reduced in number, and a portion is found in circulation. The same phenotype is observed in *Cd55*$^{-/-}$ mice, further confirming the role of CD55-CD97 interactions in anchoring MZ B cells within the MZ[157]. Mouse MZ B cells receive further retention signals from MZ macrophages via the scavenger receptor MARCO (macrophage receptor with collagenous structure)[158], it has been shown that trafficking and retention of MZ B cell require specific macrophage-B cell interactions.

Thus, loss of MZ B cells could be attributed to insufficient precursor differentiation, impaired retention or survival within the MZ, or accelerated differentiation into plasma cells. Additionally, nutritional deficiencies may further exacerbate the vulnerability of

these metabolically active and multifunctional MZ B cells. How such metabolic stress affects MZ B cell homeostasis remains to be explored.

1.2.2.4 GC B cells

The humoral immune response relies on the GC reaction to generate plasma cells that secrete high-affinity antibodies and memory B cells, ensuring long-term protection against invading pathogens. As a highly dynamic microenvironment, the GC undergoes strict spatial and temporal regulation within secondary lymphoid organs following antigenic stimulation.

To investigate when and how external factors influence GC B cells, it is essential to consider three key aspects: how antigen-specific B cells are recruited into the GC, how they interact with other immune cells and persist within the GC, and how they ultimately differentiate into plasma cells and memory B cells exiting the GC.

Recruitment

The initiation of the GC response is marked by the recruitment of antigen-specific B cells and T follicular helper (Tfh) cells. Upon antigen stimulation, naïve B cells activate within the follicle and migrate to the B/T boundary or interfollicular zone, where they interact with $CD4^+$ T cells to receive essential activation signals[159-161]. During this phase, T cells upregulate Bcl6, committing to the Tfh lineage, while Bcl6 expression in B cells remains low and only becomes detectable by day 2[160,162].

By day 2, T cells acquire a Tfh-like phenotype ($CXCR5^+$ $PD\text{-}1^+$ $GL7^+$) and migrate into the follicle, preceding B cells to establish a GC-supportive environment[160]. $Bcl6^+$ B cells then enter the follicle, cluster near FDCs, and initiate the GC microenvironment. Meanwhile, some antigen-specific B cells transiently accumulate near the

subcapsular sinus (SCS), where they receive additional signals before either returning to the follicle or differentiating into plasmablasts[113,160,163]. By day 3–4, $Bcl6^+$ B cells establish the nascent GC, while Tfh cells further mature, supporting affinity maturation and selection.

Although this migration pattern may seem circuitous, it ensures B cells receive sufficient T cell help before entering the GC. The GC is a highly competitive environment, where only B cells that acquire optimal T cell signals survive and progress. For instance, EBI2, a G-protein-coupled receptor, directs B cells to the outer follicle before GC entry. EBI2 deficiency ($EBI2^{-/-}$) leads to premature B cell accumulation in the follicle centre, limiting T cell interactions and reducing the early TD antibody response[113]. This highlights the importance of precise B cell positioning in coordinating effective GC initiation.

Retention and interaction

By Day 5–6, GC B cells undergo rapid clonal expansion within the FDC network, significantly increasing GC size. During this phase, activation-induced cytidine deaminase (AID) initiates SHM, introducing point mutations into Ig variable regions and altering BCR affinity[164].

As the immune response progresses (Days 7–8), the GC becomes compartmentalized into a dark zone (DZ) and a light zone (LZ). The DZ is the site of SHM-driven BCR diversification, while the LZ supports affinity-based selection. GC B cells migrate between these zones in response to distinct chemokine gradients, ensuring iterative cycles of mutation and selection[165,166]. In the LZ, B cells acquire antigen from FDCs[167] and compete for Tfh cell signals. Only high-affinity B cells receive sufficient Tfh-derived survival and proliferative signals, enabling them to re-enter the DZ for further rounds of expansion[166,168], while low-affinity B cells undergo apoptosis and are cleared by

macrophages[169,170]. This affinity-coupled, contact-dependent maturation underscores that both BCR affinity and the ability to acquire Tfh signals dictate the fate of GC B cells[166,171,172].

Exit and differentiation

B cells with the highest antigen affinity exit the GC and differentiate into plasma cells or memory B cells[173]. This transition begins with the downregulation of Pax5 and Bcl6, releasing repression on plasma cell-associated genes[174]. As a result, IRF4 shifts from its GC-associated role in promoting Ig class switching (low expression) to driving plasma cell differentiation (high expression)[175,176]. Meanwhile, STAT3 mediates IL-21-driven plasma cell differentiation and cooperates with IRF4 to activate Blimp-1, committing the cell to the plasma cell fate[177-179]. Once expressed, Blimp-1 induces unfolded protein response (UPR) genes, allowing the cell to adapt to high-rate antibody secretion[180,181]. Long-lived plasma cells then migrate to the BM, where they sustain high-affinity antibody production.

1.3 T cells in development and immunity

Unlike B cells, which recognize antigens directly, T cells rely on T cell receptors (TCRs) to recognize peptides presented by major histocompatibility complex (MHC) molecules. This fundamental difference necessitates a repertoire that is both functional and self-tolerant, while also allowing for developmental specialization and adaptive responsiveness.

1.3.1 T cell development and differentiation

1.3.1.1 T cell development and selection in the thymus

T cells develop in the thymus through a highly regulated process that ensures their functionality and self-tolerance. Their differentiation follows a series of developmental checkpoints that integrate signals from the thymic microenvironment to guide lineage commitment and selection.

From progenitors to the DN2 stage: T cell commitment

T cells originate from early thymic progenitors (ETPs), which derive from BM-derived progenitors colonizing the thymus[182,183]. These progenitors reside within the heterogeneous double-negative 1 (DN1) population ($CD4^-$ $CD8^-$ $CD25^-$ $CD44^+$)[184,185], but only a subset are true T cell precursors[186].

In uncommitted precursors, Notch signalling, triggered by Delta-like ligands in the thymic microenvironment, initiates T cell lineage commitment. This signaling cascade leads to the downregulation of Flt3 and upregulation of CD25, marking early differentiation[187,188]. Transcription factors such as TCF-1[189-191], GATA-3[192], and Bcl11b[193,194] cooperate with Notch signaling to reinforce T cell lineage specification. GATA-3, a zinc-finger transcription factor, acts early to promote ETP differentiation, as evidenced by the exclusive reduction of ETPs observed in $Gata3^{-/-}$ mice[192]. As differentiation progresses, Bcl11b, another zinc-finger transcription factor, becomes indispensable for restricting alternative fates such as NK-cell differentiation. In $Bcl11b^{-/-}$ mice, T cell development is arrested at the DN2 stage, leading to an accumulation of aberrant DN1-like cells[193].

At the DN2 stage ($CD44^+$ $CD25^+$), thymocytes reach their first developmental checkpoint. Here, committed T cell progenitors emerge as c-Kit^+ $CD44^+$ $CD25^+$ DN2 cells, which then progress toward the DN3 stage.

Late DN stages: β-selection and lineage fate decision

At the DN3 stage (c-Kit^- $CD44^-$ $CD25^+$), thymocytes complete V(D)J recombination of the TCRβ gene, undergoing β-selection, a critical checkpoint that determines further differentiation and proliferation. Thymocytes that successfully express a functional TCRβ chain assemble a pre-TCR complex, comprising TCRβ, pre-TCRα (pTα), and CD3 molecules. Pre-TCR signaling ensures that only cells with productive TCRβ rearrangement survive and continue development[195]. If instead TCRγ and TCRδ gene rearrangement is successful, and the γδTCR transmits sufficiently strong signals, DN3 cells adopt the γδ T cell fate[196]. However, cells failing to productively rearrange TCRβ are eliminated. Coordinated Notch and pre-TCR signaling play a pivotal role in ensuring successful β-selection at this stage[197-199].

Following β-selection, DN3 cells downregulate CD25 and transition into the DN4 stage (c-Kit^- $CD44^-$ $CD25^-$), where they undergo extensive proliferation before differentiating into double-positive (DP) thymocytes ($CD4^+$ $CD8^+$).

Positive and negative selection in the DP stage

In mice, TCRα gene rearrangement is initiated at the DP stage. Upon successful rearrangement, DP thymocytes express a complete αβTCR complex. Their fate is then determined by the strength and duration of TCR interactions with self-peptide–MHC ligands presented by thymic epithelial cells (TECs). The transition between positive and negative selection occurs within a narrow affinity window, ensuring central tolerance while allowing functional T cells to mature[200].

DP thymocytes undergo positive selection primarily in the thymic cortex, ensuring their ability to recognize self-MHC molecules. This process is driven by cortical thymic epithelial cells (cTECs), which present a specialized repertoire of peptides via distinct proteolytic pathways. For MHC class I antigen presentation, cTECs express the unique β5t proteasome subunit (PSMB11), forming the thymoproteasome essential for $CD8^+$ T cell selection. β5t-deficient mice exhibit severe defects in $CD8^+$ T cell positive selection[201]. For MHC class II antigen presentation, cTECs uniquely express cathepsin L and thymus-specific serine protease (TSSP), both of which shape the $CD4^+$ T cell repertoire. Cathepsin L deficiency reduces $CD4^+$ T cell diversity[202]. Thymocytes with intermediate TCR affinity for self-MHC survive selection and continue maturation, while those with too weak or too strong interactions undergo apoptosis. This fine-tuned selection process ensures the development of functional yet self-tolerant T cells.

Negative selection, which eliminates self-reactive thymocytes to prevent autoimmune responses, occurs primarily in the thymic medulla. This process is mediated by medullary thymic epithelial cells (mTECs) and DCs. mTECs express the autoimmune regulator AIRE, which facilitates ectopic expression of tissue-restricted antigens (TRAs), crucial for eliminating autoreactive T cells[203]. DCs contribute to negative selection by presenting blood-borne antigens, acquiring mTEC-derived antigens, or cross-presenting peripheral antigens transported into the thymus[204-206]. Thymocytes that bind self-antigens with high affinity undergo apoptosis, ensuring self-tolerance. Additionally, some $CD4^+$ T cells differentiate into $FOXP3^+$ $CD4^+$ $CD25^+$ natural regulatory T (nTreg) cells in the medulla, further suppressing autoimmunity[207].

Due to the stringent selection process, only 1%-5% of initial thymocytes successfully develop into mature $CD4^+$ or $CD8^+$ single-positive (SP) T cells[208]. These SP thymocytes

undergo final maturation and exit the thymus, migrating into peripheral lymphoid organs, where they can be activated upon encountering foreign antigens.

1.3.1.2 Differences between naïve and memory T cells

After exiting the thymus, T cells home to secondary lymphoid organs, migrating between blood and peripheral tissues to perform immune surveillance. Naïve T cells, which have not yet encountered antigen, remain in a quiescent state. Upon antigen recognition via MHC molecules, naïve T cells activate, proliferate, and differentiate into effector T cells that mediate immune responses. While most effector T cells undergo apoptosis after pathogen clearance, a subset persists as memory T cells, ensuring faster and stronger responses upon re-exposure to the same antigen[209-211].

In mice, T cells are classified into three major subsets based on their function and phenotype: naïve T cells, central memory (CM) T cells, and effector memory (EM) T cells. In the absence of antigen exposure, these subsets exhibit intrinsic differences, particularly in phenotype, metabolism, and survival.

Phenotype

Naïve T cells express CD62L and CCR7, enabling homing to lymphoid tissues via high endothelial venules (HEVs)[212,213], but have low CD44 expression, distinguishing them from memory T cells. CM T cells retain CD62L and CCR7 while upregulating CD44, allowing continued circulation through lymphoid organs. In contrast, EM T cells downregulate CD62L and CCR7[214], express CXCR3[215], facilitating migration to peripheral tissues, and rapidly produce cytokines such as IFN-γ and IL-4[216,217].

Metabolism

Although both naïve and memory T cells exist in a quiescent state, their metabolic profiles differ to support their distinct functions. Naïve T cells primarily depend on oxidative phosphorylation (OXPHOS) for ATP production, sustaining basal homeostasis with minimal nutrient uptake. Memory T cells, in contrast, exhibit higher mitochondrial mass and spare respiratory capacity (SRC), enabling them to utilize fatty acid oxidation (FAO) more efficiently[218]. This metabolic flexibility supports long-term survival and rapid energy mobilization upon reactivation. While CM T cells predominantly rely on FAO and OXPHOS, EM T cells have been suggested to favour glycolysis, though many studies do not explicitly distinguish between them[219-221].

Survival

Naïve T cells require continuous self-MHC interactions and IL-7 signals to maintain homeostasis and longevity[222-224]. In their absence, they undergo apoptosis. Memory T cells, in contrast, exhibit enhanced longevity due to increased expression of anti-apoptotic proteins such as Bcl-2[225]. Their persistence depends on cytokine-mediated survival signals, primarily IL-7 and IL-15, and they can undergo homeostatic proliferation when necessary to maintain their numbers[210,223,226]. Among memory subsets, CM T cells possess greater proliferative capacity and self-renewal, whereas EM T cells, despite their shorter lifespan, are more differentiated and primed for rapid immune responses in peripheral tissues[211,214]. This balance between longevity and immediate responsiveness ensures immune readiness upon pathogen re-exposure.

Thus, naïve and memory T cells, though distinct, function complementarily. These intrinsic differences may explain why naïve and memory T cells respond differently to environmental changes.

1.3.2 Nutrients as Signal 4: Licensing and regulating T cell function

Upon encountering an antigen, naïve T cells recognise peptide–MHC complexes via the TCR, with $CD4^+$ T cells interacting with MHC class II and $CD8^+$ T cells with MHC class I[227,228]. However, antigenic stimulation alone is insufficient for full activation. Additional costimulatory signals, primarily mediated by CD28 binding to CD80/CD86 on APCs, are required to prevent anergy and promote expansion[229,230]. Finally, cytokines in the microenvironment direct T cell differentiation into specific effector subsets, such as IL-12 promoting Th1 cells[231]. Together, T cells activation, proliferation, and differentiation in adaptive immunity are orchestrated by three classical signals: antigen recognition (Signal 1), costimulation (Signal 2), and cytokine signaling (Signal 3).

However, emerging evidence suggests that nutrients such as glucose, amino acids, and lipids are not merely metabolic substrates but function as an instructive signal ("Signal 4") that is essential for complete T cell activation and function. For example, TCR (Signal 1) and costimulation (Signal 2) only partially activate mTORC1, whereas full activation requires nutrient-derived signals, particularly amino acids and glucose. Once activated, mTORC1 drives metabolic reprogramming, supporting T cell expansion and effector differentiation[232,233]. Beyond mTORC1, several nutrient-sensing pathways integrate environmental nutrient availability to regulate T cell metabolism and immune responses. AMPK functions as an energy sensor, maintaining T cell effector function under nutrient-restricted conditions[234]. Similarly, SREBP regulates $CD8^+$ T cell activation and differentiation by sensing lipid levels[235].

Nutrient deprivation and the Integrated Stress Response (ISR)

Nutrient depletion is a potent trigger of the ISR, a central adaptive mechanism that responds to environmental stressors such as amino acid starvation, glucose limitation, and ER stress[236,237]. In immune cells, ISR activation suppresses global protein synthesis

while selectively inducing ATF4 and stress-adaptive genes, thereby modulating metabolic adaptation, differentiation, and immune function. While ISR plays a protective role in stress adaptation, severe or prolonged metabolic stress can overwhelm its capacity, leading to impaired T cell function, anergy, or even apoptosis.

Nutrient depletion can occur in the tissue microenvironment, particularly under conditions of rapid cell proliferation, inflammation, or metabolic stress, where various cell types, including immune cells and tumour cells, compete for glucose, amino acids, and lipids. For example, tumour cells upregulate SLC6A6, leading to increased taurine uptake and subsequent depletion of taurine in immune cells. Taurine deficiency elevates ER stress and upregulates ATF4, which subsequently induces immune checkpoint expression and promotes T cell exhaustion[238]. Similarly, amino acid deprivation (e.g., tryptophan depletion) activates the GCN2 kinase, initiating the ISR program that suppresses T cell proliferation and induces anergy[237].

Collectively, these findings suggest that Signal 4 is indispensable for optimal T cell activation and immune function. By integrating environmental nutrient availability with immune signalling, nutrients actively shape T cell metabolism, survival, and immune responses.

1.4 Zinc transporters in immune regulation and beyond

Various ion channels and transporters (ICTs) are expressed in both innate and adaptive immune cells, facilitating ion influx and efflux across cellular membranes or release from intracellular organelles. These processes enable immune cells to rapidly adapt to environmental changes during activation, differentiation, and interaction. However, the function of ICTs is not limited to maintaining ion homeostasis. For example, conditional deficiency of transient receptor potential subfamily M member 7 (TRPM7)–a Mg^{2+}-

permeable, nonselective channel with serine/threonine kinase activity–results in developmental arrest at the DN3 stage in the thymus (*Trpm7*$^{f/-}$ *Lck-cre*)[239], at the pro-B stage in the BM (*Trpm7*$^{f/f}$ *CD79a-cre*)[240], impaired gut colonization in TRPM7 kinase-dead mutant mice (*Trpm7*$^{R/R}$)[241], and reduced total cellular Mg^{2+} along with defects in proliferation and viability in DT-40 B cells (inducible *Trpm* deficiency)[242]. These findings underscore the necessity of employing multiple genetic models—including mutation, conditional deletion, compound models, and inducible deletion—to investigate ICTs, particularly those that are embryonically lethal when completely knocked out.

Although ion channels represent the second-largest class of protein targets after G protein-coupled receptors[243], their roles in immune regulation remain largely underexplored. This thesis focuses on the function of a zinc transporter, primarily in B and T cells.

1.4.1 Zinc

Zinc is an essential trace element present in all body tissues, with the majority stored in muscle and bone (85%), followed by the skin and liver (11%)[244]. Since its discovery in 1958[245], zinc deficiency has been recognized as a major global health concern, particularly in children, with an estimated 453,207 zinc-attributable deaths among children under five in 2004[246]. Despite efforts to mitigate this issue, follow-up studies indicate that zinc deficiency remains widespread, affecting nearly half of children in surveyed regions[247].

Clinically, zinc deficiency compromises immune defence, increasing susceptibility to infections such as diarrhoea, pneumonia, and malaria, as demonstrated in multiple randomized trials[246]. During the COVID-19 pandemic, zinc-deficient patients exhibited higher complication rates, prolonged hospital stays, and increased mortality[248].

While zinc supplementation is commonly recommended to mitigate infections, evidence on its effectiveness is inconsistent. A Cochrane review of 34 studies concluded that zinc has minimal impact on cold prevention but may shorten its duration. However, the certainty of this evidence is low[249]. Conversely, a recent randomized controlled trial reported that twice-daily oral zinc reduced 30-day mortality, ICU admissions, and symptom duration in COVID-19 patients (ClinicalTrials.gov, NCT05212480). Yet, the study's mixed patient population (hospitalized and outpatients) may have diluted specific subgroup effects[250].

1.4.1.1 Zinc homeostasis and immune function

Zinc serves as a cofactor for approximately 3,000 metalloproteins, constituting about 9% of the eukaryotic proteome, with the majority being enzymes (47%) or transcription factors (44%)[251]. Beyond its structural role, zinc also functions as an intracellular signaling molecule, dynamically responding to extracellular stimuli. Intracellular Zn^{2+} signaling occurs at different timescales: early zinc signaling happens within seconds to minutes after stimulation, involving a rapid increase in cytoplasmic zinc levels ('zinc wave') that transduces intracellular signals independently of transcription[252,253]. This process primarily relies on the release of zinc from intracellular stores, such as the endoplasmic reticulum (ER) or metallothioneins (MTs)[254]. In contrast, late zinc signaling occurs over hours to days, driven by changes in zinc transporter expression, which alter cellular zinc import and export capacities[255,256].

Within cells, zinc is largely sequestered in organelles such as the ER, Golgi apparatus, and mitochondria[254], whereas cytosolic free zinc levels remain minimal[257]. This spatial organization highlights zinc's role in precise cellular regulation, ensuring that zinc availability is tightly controlled. The maintenance of zinc homeostasis is

orchestrated by three major protein families: solute carrier SLC39 (ZRT/IRT-like proteins, ZIPs), cation diffusion facilitators SLC30 (ZnTs), and MTs[258]. Among them, ZIP transporters (14 members) mediate zinc import into the cytoplasm from extracellular sources or organelle stores, whereas ZnT transporters (10 members) facilitate zinc efflux or its sequestration into organelles. Studies have shown that loss of a single ZIP transporter significantly reduces cellular zinc transport capacity, yet total cellular zinc levels often remain unchanged due to compensatory upregulation of other transporters[256,259].

Zinc plays indispensable roles in both innate and adaptive immunity, regulating immune cell development, activation, and maturation. For example, in innate immunity zinc enhances cGAS-STING signaling by promoting cGAS-DNA phase separation, which facilitates cGAMP production and boosts type I interferon responses, thereby strengthening antiviral and antimicrobial immunity[260]. In adaptive immunity, zinc stabilizes CD4/CD8-Lck interactions via a 'zinc clasp' structure, ensuring proper TCR initiation[261]. Following TCR stimulation, subsynaptic accumulation of cytoplasmic zinc lowers the T cell activation threshold, allowing enhanced responses to suboptimal stimuli and promoting T cell activation by low-affinity antigens or low-dose stimulation[253].

1.4.1.2 Zinc in cellular stress responses

During physiological activation, proliferation, and pathogen clearance, cells–such as macrophages[262], B cells, and intestinal epithelial stem cells[263]–experience increased metabolic and proteostatic demands. This is often accompanied by reactive oxygen species (ROS) production and, in secretory cells, an accumulation of unfolded proteins. However, excessive accumulation can lead to oxidative stress, ER stress, and mitochondrial dysfunction. Although zinc is neither a direct ROS scavenger nor an ER stress sensor, it

is essential for maintaining cellular resilience by supporting antioxidant defences and stress-adaptive pathways.

Zinc deficiency disrupts these homeostatic mechanisms, leading to oxidative stress due to impaired antioxidant enzyme activity[264], ER stress characterized by increased UPR markers[265-268], and mitochondrial dysfunction[266,267]. These stress responses can be interconnected–ROS accumulation exacerbates ER stress[265], which further disturbs Ca^{2+} balance and mitochondrial integrity[267]. Persistent stress may trigger caspase activation and pro-apoptotic signalling[264,266,267,269-271], contributing to cellular dysfunction and eventual cell death.

Given these protective effects, disruptions in zinc homeostasis–such as those caused by zinc transporter deficiencies–may compromise cellular stress resilience.

1.4.2 Zinc transporters

The ZIP family is evolutionarily conserved across eukaryotes and some prokaryotes. Based on sequence similarity, ZIP transporters are classified into four subfamilies: ZIP I, ZIP II, LIV-1, and GufA[272] (Figure 1-1A). Most ZIP proteins have six to eight transmembrane domains (TMDs), with both N- and C-termini exposed to the extracellular space in plasma membrane-localized ZIPs or to the vesicular lumen in organellar ZIPs[273]. Nine out of 14 human ZIPs, including ZIP7, belong to the LIV-1 subfamily, characterized by a conserved HEXPHEXGD motif within TMD V and a histidine-rich loop between TMDs III and IV–both crucial for metal binding and transport. The amphipathic TMDs IV and V form a transmembrane cavity that mediates zinc translocation[273].

In this section, I will focus on the roles of ZIPs (Figure 1-1B) in adaptive immune responses, excluding ZIP7, which will be discussed separately in the next section. The

emphasis will be on ZIPs whose functions in immune cells have been validated by genetic evidence (e.g., knockout mice or mutations in human patients). Additionally, representative ZnTs will be briefly mentioned at the end of this section.

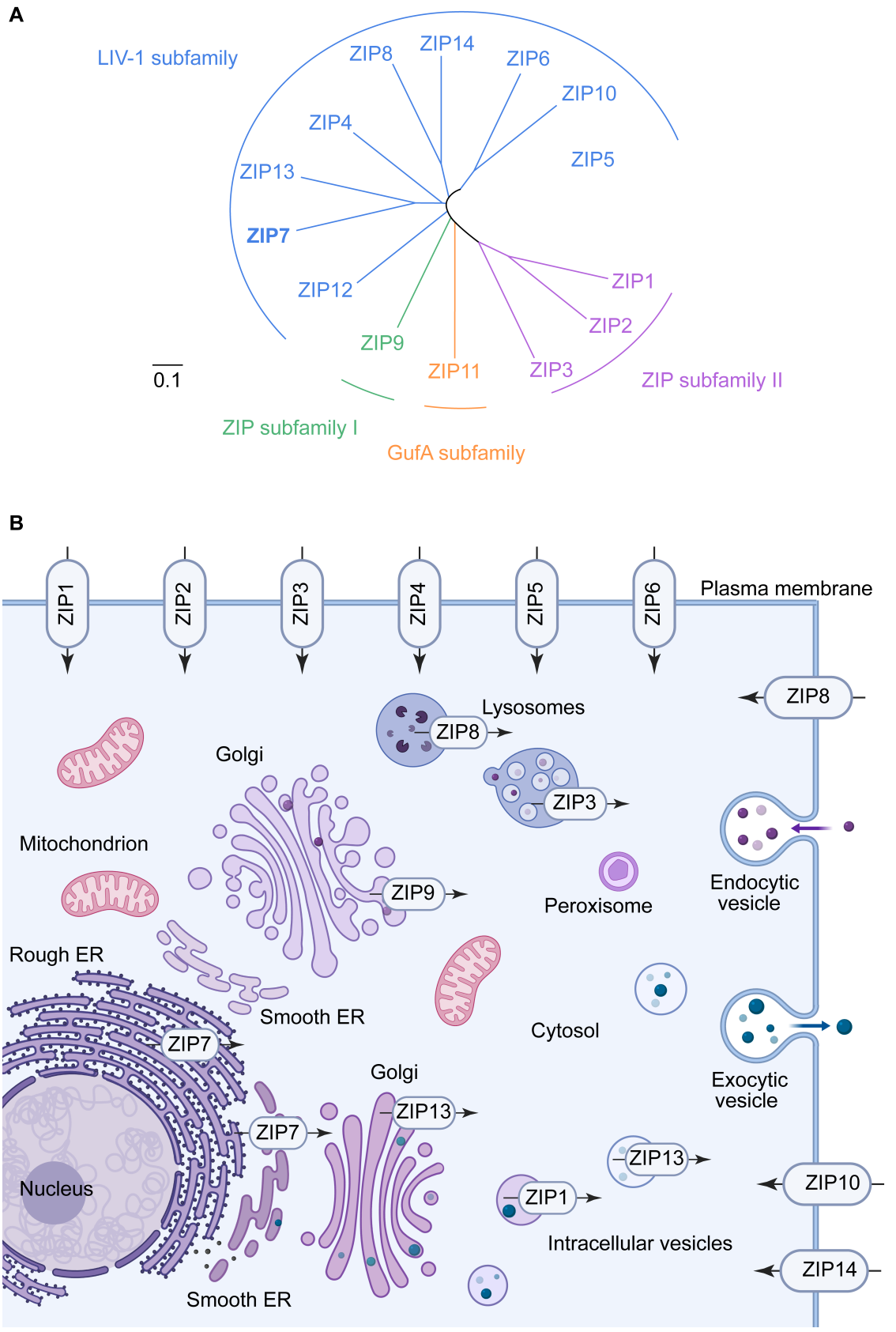

Figure 1-1: Phylogenetic classification and subcellular localization of human ZIP family. A. Phylogenetic relationships of human Zinc transporters. This figure is adapted from[274], where the phylogenetic tree was generated using protein sequences of human Zinc transporters retrieved from NCBI. Sequences were aligned with ClustalW2, and the tree was

constructed using the TreeDyn program. The scale bar represents the evolutionary distance. In this version, the classification of Zinc transporters has been added, categorizing them into four subfamilies: ZIP subfamily I (ZIP9), GufA subfamily (ZIP11), ZIP subfamily II (ZIP1-3), and LIV-1 subfamily (ZIP4-8, ZIP10, ZIP12-14). B. Subcellular localization of human Zinc transporters. This figure illustrates a simplified representation of Zinc transporters' subcellular distribution, with arrows indicating the directions of zinc transport. The localization and expression of Zinc transporters vary depending on tissue type, cell specificity, zinc status, and other regulatory signals. Created with BioRender.

1.4.2.1 ZIPs in B cell development and function

Among the ZIP family, ZIP10[271], ZIP7[20] and ZIP9[275] are the only members reported to be involved in B cell biology (Figure 1-2).

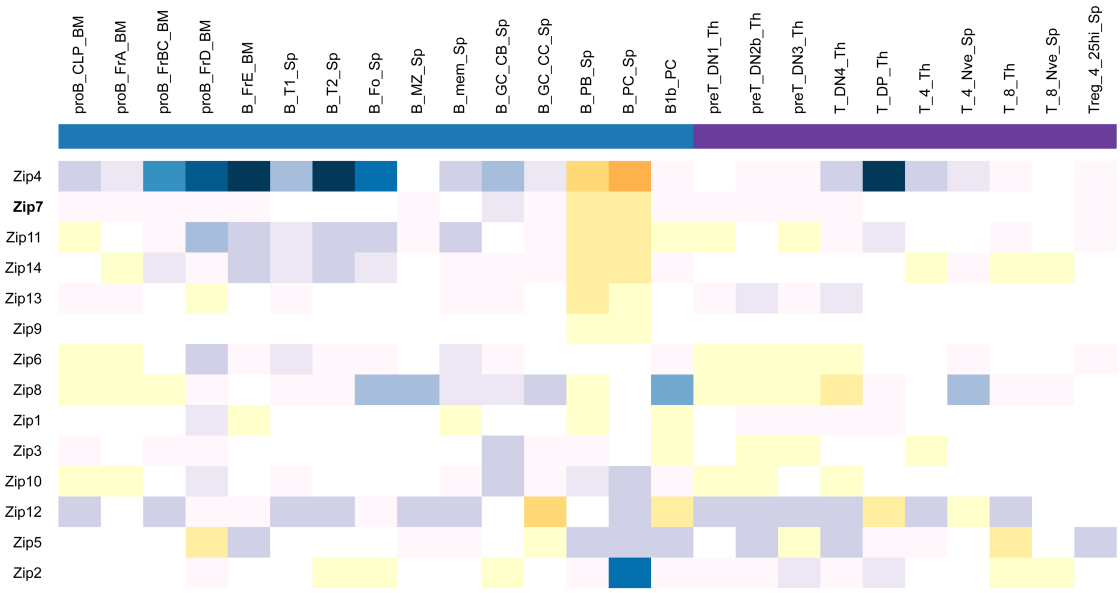

Figure 1-2: Expression of ZIP transporters in mouse B and T cell subsets.
This heatmap shows the expression of 14 ZIP transporters in mouse B and T cell subsets using ImmGen RNA-seq data[276]. Expression values are normalized by DESeq2. Warmer colours (yellow to orange) indicate higher expression, while cooler colours (blue) indicate lower expression. B and T cell subsets are grouped under blue and purple bars, respectively. ZIP7 is highlighted in bold.

B cell development

ZIP10 and ZIP7 regulate B cell development at different stages through distinct mechanisms. ZIP10, highly expressed in pro-B cells, is essential for early B cell survival, as its

deficiency leads to caspase activation and apoptosis. In contrast, ZIP7 is required for BCR-dependent selection at later stages, and its absence results in a pre-B to immature B cell developmental block due to increased phosphatase activity and impaired BCR signalling[20,271].

The ZIP10 study used $B220^+$ IgM^- $CD19^+$ $CD43^+$ gating to define pro-B cells in *Zip10$^{f/f}$ Mb1-cre* mice and observed a marked reduction in this population. However, two key considerations remain unaddressed. First, while ZIP10 deficiency resulted in pro-B cell loss, the study did not directly assess whether this phenotype was B cell intrinsic. Although *in vitro* differentiation data were provided, this system does not fully recapitulate the *in vivo* BM microenvironment, leaving open the possibility of extrinsic factors contributing to the phenotype. Second, although Hardy fraction analysis (Fractions A, B, and C/C') was performed, the control data did not show the expected progressive decline in cell numbers from Fraction A to C/C', as typically observed in B6 mice. While this discrepancy does not invalidate the conclusion that ZIP10 is critical for early B cell survival, it suggests that the fraction-specific effects of ZIP10 deficiency require further clarification.

Peripheral B cell function

ZIP10 plays multiple roles in peripheral B cell homeostasis and function. Mice with ZIP10 deletion in peripheral B cells (*Cd74 (Ii)-cre* cKO) exhibited reduced follicular B cell numbers and shortened lifespan, suggesting that ZIP10 is crucial for long-lived B cell persistence. Functionally, ZIP10 acts as a negative regulator of BCR signalling, as its deficiency leads to hyperactivation of SYK, LYN, ERK, AKT, and NF-κB, impairing B cell proliferation upon BCR cross-linking. Additionally, ZIP10-deficient mice show defective GC formation and significantly reduced TD and TI antibody responses[259].

However, since ZIP10 deletion also reduces mature B cell numbers, it remains unclear whether the impaired TD and TI responses stem from a direct functional requirement or a consequence of reduced peripheral B cell populations. Adoptive transfer of mixed WT and ZIP10-deficient B cells would help clarify this distinction.

Zinc transporters in BCR signalling

In addition to ZIP10, ZIP9 has been implicated in BCR signaling regulation, but with an opposite effect. ZIP9-deficient DT40 B cells exhibit reduced AKT and ERK phosphorylation upon BCR activation due to increased phosphatase activity, leading to excessive dephosphorylation of key signaling molecules[275].

Taken together, ZIP7 and ZIP9 deficiencies dampen BCR signalling, leading to increased phosphatase activity and reduced phosphorylation of AKT and ERK, ultimately impairing B cell differentiation and proliferation. In contrast, ZIP10 deficiency leads to hyperactivated BCR signalling, due to reduced CD45R phosphatase activity, causing excessive phosphorylation of SYK, ERK, AKT, and NF-κB, which also disrupts B cell proliferation.

The distinct effects of ZIP deficiencies suggest that Zinc homeostasis is finely tuned in a B cell subtype- and context-dependent manner, ensuring a balance between activation, proliferation, and survival.

1.4.2.2 ZIPs in T cell development and activation

Among the ZIP family, ZIP3, ZIP6, and ZIP8 are the only members reported to be involved in T cell biology.

T cell development

Causative evidence linking Zinc transporters to T cell development is limited, but existing data suggest that thymocytes are the most vulnerable lymphocyte subset under zinc stress.

The only direct evidence comes from zebrafish, where *zip6* deficiency reduces T lymphocytes due to increased apoptosis rather than impaired proliferation[277]. In mammals, *Zip7*$^{P198A/P198A}$ does not affect T cell development[20], and *Zip3*$^{-/-}$ mice show no T cell phenotype under normal conditions. However, under a zinc-deficient diet for 21 days, *Zip3*$^{-/-}$ mice exhibit exacerbated thymic atrophy and reduced DP ($CD4^+$ $CD8^+$) thymocytes[278], suggesting a supportive but non-essential role in thymic maintenance.

Thymic atrophy and lymphopenia are also features of acrodermatitis enteropathica (AE)[279,280], a disorder caused by *ZIP4* mutations[281,282], but whether ZIP4 directly affects thymocytes remains unclear. A *Zip4 villin-Ert2-cre* knockout model mimics AE but lacks specificity to lymphocytes[283], making it difficult to determine ZIP4's role in T cell development.

Overall, Zinc transporters appear to support thymic development rather than being indispensable for peripheral T cell maintenance. However, their cell-intrinsic roles and potential impact under more severe ZIP deficiency remain to be explored.

T cell activation

Among the 14 Zinc transporters, only ZIP6, ZIP7, ZIP8, and ZIP14 are consistently upregulated during the early stages of T cell activation across different models, including human peripheral T cells, Jurkat cells, and murine splenic T cells stimulated with anti-CD3/anti-CD28[256]. Among these, ZIP6 and ZIP8 are reported playing distinct but complementary roles in this process.

ZIP6 is constitutively localized in lipid rafts of the T cell membrane and accumulates at the immunological synapse (IS) upon TCR stimulation. This translocation is accompanied by Zap70-mediated phosphorylation, which enhances its zinc transport activity[284]. ZIP6-deficient T cells maintain normal zinc homeostasis at rest, but upon activation, they show impaired zinc influx and a severely compromised activation program[256]. Consequently, ZIP6 deficiency disrupts CD69 and CD25 upregulation and reduces IL-2 production[253,256], highlighting its essential role in early T cell priming.

Unlike ZIP6, which imports extracellular zinc, ZIP8 mobilizes intracellular zinc by releasing it from lysosomes into the cytoplasm following TCR activation. This zinc influx inhibits calcineurin, thereby sustaining CREB phosphorylation and enhancing IFN-γ production[255]. Functionally, ZIP8 knockdown significantly reduces IFN-γ and perforin secretion[255], both of which are critical for Th1 and cytotoxic T cell responses.

While ZIP6 facilitates early TCR signaling and IS formation, ZIP8 primarily regulates effector functions by promoting IFN-γ production. Whether other Zinc transporters contribute to T cell activation remains underexplored, especially in *in vivo* models.

T cell differentiation

Currently, there is no direct evidence linking Zinc transporters to T cell differentiation. Instead, most studies focus on the broader relationship between zinc availability and T cell polarization. Zinc deficiency in humans and *in vitro* models is associated with a Th1/Th2 imbalance and impaired Treg induction[285,286]. This imbalance is characterized by selective impairment of Th1 cytokine production, such as IL-2 and IFN-γ[287,288]. Zn^{2+} and Ca^{2+} signals act synergistically to promote IFN-γ production, highlighting the importance of zinc in Th1 differentiation. While ZIP8 has been shown to enhance IFN-γ production[255] and ZIP6 promotes IL-2 secretion[256,284], no ZIP knock-out models have

specifically examined whether T cell differentiation into Th1, Th2, or regulatory T (Treg) cells is affected.

Studies investigating the roles of Zinc transporters in both B and T cells simultaneously remain scarce. For example, ZIP10 is highly expressed in immune tissues, including the thymus, spleen, lymph nodes, and BM B cells. In this study[271], *Zip10$^{f/f}$ Rosa26$^{ERT2\text{-}cre}$* mice were used to analyse ZIP10 function, yet its potential effects on T cells were not reported. This omission limits insights into whether ZIP transporters exert cell-type-specific effects or regulate B and T cells to different extents. Regardless of whether the findings in T cells were positive or negative, reporting these results could have provided valuable data on whether ZIP transporters influence lymphocyte subsets differentially.

1.4.2.3 ZnTs in immune regulation and beyond

ZnTs primarily function as zinc exporters, counterbalancing ZIP-mediated zinc uptake. Among the ten ZnTs, ZnT1 and ZnT5 stand out for their characterized functions in immune cells, offering insights that may complement ZIP research.

ZnT5 is highly expressed in BM-derived mast cells (BMMCs) and predominantly localizes to the Golgi apparatus. While ZnT5 deletion does not affect mast cell development, it selectively impairs delayed-type allergic responses by disrupting PKC-β translocation to the plasma membrane. This impairs NF-κB-dependent cytokine production but leaves mast cell degranulation intact. As a result, *Znt5*$^{-/-}$ mice exhibit defective delayed-type hypersensitivity while retaining normal immediate-type allergic reactions[289].

ZnT1 localization varies across species but is generally found in the plasma membrane, ER, and endosomes[290-293]. Myeloid-specific *Znt1* knockout (*Znt1$^{f/f}$ LysM-cre*) in a chronic inflammation-associated HCC model leads to heightened inflammation and

increased macrophage PD-L1 expression, contributing to immune evasion. Mechanistically, ZnT1 deficiency reduces endosomal Zn^{2+} levels, impairing PD-L1 and TLR4 internalization. This results in increased PD-L1 surface expression and IL-6 production, collectively suppressing $CD8^+$ T cell cytotoxicity and promoting an immunosuppressive tumour microenvironment, facilitating tumour progression[292].

Beyond zinc homeostasis, ZnT1 also functions as a Cu^{2+}- or Ca^{2+}-coupled zinc exporter[293,294]. Notably, ZnT1 is critical for intestinal stem cell survival by regulating cuproptosis, a copper-dependent cell death pathway not observed in ZIPs[294].

1.4.3 ZIP7

1.4.3.1 ZIP7: Localization and functional properties

ZIP7 is a highly conserved zinc transporter found across diverse species, from plants and Drosophila to mammals[20,295,296]. The human ZIP7 gene is located on chromosome 6 near the MHC class II region, and its mouse ortholog lies on chromosome 17, near the MHC class I region. Their protein sequences share 85.15% identity. As a member of the LIV-1 subfamily, ZIP7 shares core structural features with other ZIP transporters, while also exhibiting unique functional properties.

Intracellular metal transport

Unlike other members of the LIV-1 subfamily, ZIP7 is not localised to the plasma membrane but instead resides on intracellular membranes, primarily in the ER, and is also found in the Golgi apparatus and mitochondria, depending on the cell type[297-299]. This subcellular distribution enables ZIP7 to mediate dynamic metal transport between organelles, particularly between the ER and mitochondria, which exhibit extensive physical and functional interactions[300,301]. For example, ER-localised ZIP7 interacts with VDAC3

on the mitochondrial membrane to facilitate Fe^{2+} transfer, thereby preventing iron dyshomeostasis and ferroptosis in hepatocytes under perfluorooctane sulfonate (PFOS) exposure[302]. In nucleus pulposus cells, ZIP7 forms a complex with the mitochondrial protein NLRX1 to regulate Zn^{2+} trafficking, thereby mitigating mitochondrial damage under oxidative stress[299]. These findings underscore ZIP7 as a critical intracellular metal transporter that coordinates inter-organelle communication, helping cells manage stress and maintain homeostasis.

Gene dosage sensitivity

Evidence from three independent studies consistently demonstrates that patients with ZIP7 deficiency carry either homozygous or compound heterozygous mutations (Figure 1-3), while heterozygous family members exhibit no clinical manifestations[20,303,304]. These findings suggest that disease only arises when both alleles are impaired, and that partial ZIP7 activity is sufficient to sustain normal immune function.

This recessive, dose-sensitive pattern is mirrored in mouse models: homozygous or compound heterozygous mutations (*Zip7*$^{P198A/P198A}$, *Zip7*$^{H199QV/H199QV}$, and *Zip7*$^{P198A/H199QV}$) lead to a developmental block in B cells within the BM, whereas heterozygous mice (carrying one WT allele) maintain normal B cell numbers[20]. In contrast, ZIP7 loss-of-function mutations have more severe consequences in *Drosophila*: homozygous mutations in *Catsup*, the *ZIP7* ortholog, result in lethality at the first instar larval stage[296]. Collectively, these cross-species findings strongly support that ZIP7 pathogenic mutations are hypomorphic.

Gene dosage effects are further underscored by the lethality of any genotype carrying a germline ZIP7 null allele (*Zip7*$^{-/-}$, *Zip7*$^{P198A/-}$, *Zip7*$^{H199QV/-}$), while mice retaining at least one WT allele(*Zip7*$^{+/-}$, *Zip7*$^{P198A/+}$, *Zip7*$^{H199QV/+}$) remain phenotypically normal[20]. A similar dose-dependent effect has been observed in conditional knockout models: *Zip7*

f/f *Lgr5*^{EGFP}*-IRES-creERT2* mice, with complete ZIP7 deletion in Lgr5^{+} stem cells, exhibited an increased ER stress response, and loss of proliferative capacity. In contrast, *Zip7*$^{f/+}$ *Lgr5*^{EGFP}*-IRES-creERT2* mice, which are theoretically expected to exhibit a ~50% reduction in ZIP7 expression, show no such defects[305]. These observations raise intriguing questions about the molecular basis of ZIP7 dosage sensitivity and how different cell types tolerate varying degrees of ZIP7 deficiency.

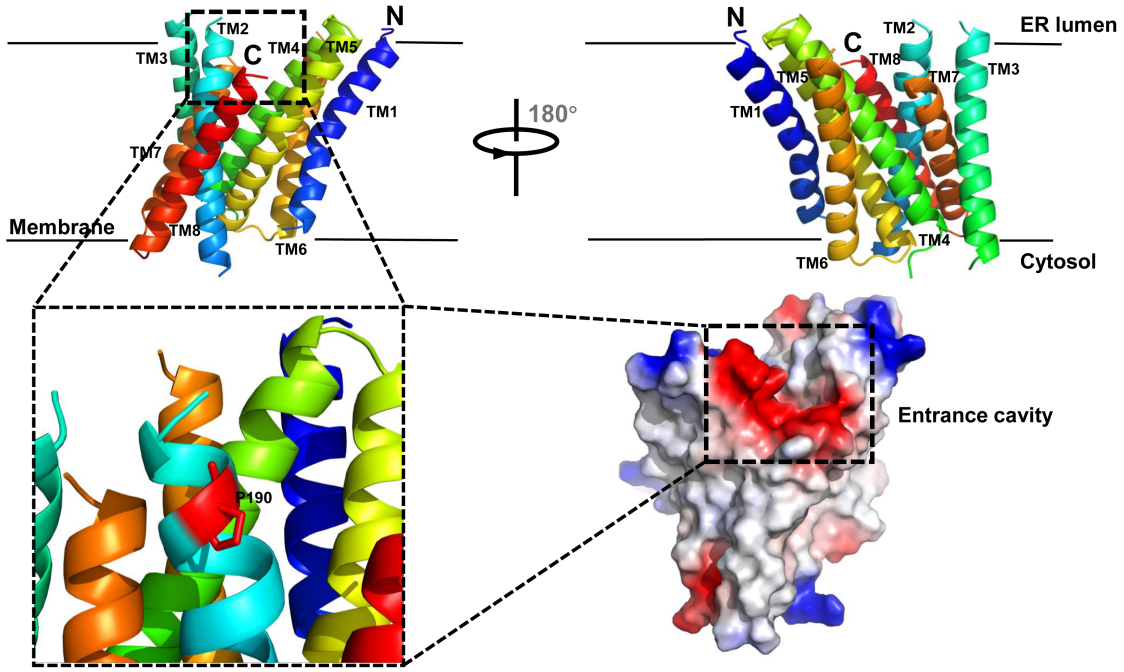

Figure 1-3: Predicted high-confidence transmembrane structure of human ZIP7 (hZIP7) modelled by AlphaFold[306,307] and visualized using PyMOL.
Top panel: Side views of the model. Bottom left: Close-up of the P190 residue (corresponding to P198 in mZIP7). Bottom right: Electrostatic potential surface highlighting the entrance cavity. TM, transmembrane.

1.4.3.2 ZIP7 and ER stress

Dysfunction of ZIP13 and ZIP14 has been shown to exacerbate ER stress, particularly under environmental stressors such as alcohol or high-fat diets[266,308]. Emerging evidence also suggests that ZIP7 plays a key role in modulating ER stress.

Under physiological conditions, ZIP7 is essential for maintaining homeostasis in highly proliferative cells[20,305]. For example, ZIP7 is highly expressed in intestinal crypts, and its conditional deletion in intestinal epithelial cells (*Zip7$^{f/f}$ Villin-creERT2*) induces ER stress in progenitor cells, leading to apoptosis[305]. Notably, zinc supplementation alone fails to rescue this phenotype, suggesting that ZIP7 plays a more specific regulatory role beyond simply increasing intracellular zinc levels[20,305].

In contrast, acute or sustained stress can overwhelm cellular adaptive mechanisms. Proteotoxic stress, marked by the accumulation of misfolded proteins, is a hallmark of many degenerative diseases. Cells respond by activating the UPR, which includes ER-associated degradation (ERAD) to clear damaged proteins. ZIP7 contributes to this process by supplying Zn^{2+} to activate Rpn11, a Zn^{2+}-dependent deubiquitinase essential for proteasomal degradation. In both Drosophila and human cells, ZIP7 and Zn^{2+} act as rate-limiting factors in ERAD. Overexpression of ZIP7 enhances Rh1 clearance and protects photoreceptors in a Drosophila model of retinal degeneration[309].

Given that B cells possess high secretory capacity and robust UPR activity, and that T cells integrate nutrient sensing as activation "Signal 4," these lymphocytes may have distinct dependencies on ZIP7. How do they adapt to ZIP7 deficiency? What role does ZIP7 play during immune activation? While ZIP7 dysfunction has been implicated in neurodegeneration[309], inflammation[305], diabetes[310], and cancer[311,312], its role in peripheral B and T cells remains largely unexplored, apart from our previous work[20].

1.5 Hypothesis and aims of this project

Hypothesis

Given the essential role of ZIP7 in early B cell development and the observed effects of the *Zip7$^{P198A/P198A}$* mutation in T cells[20], I hypothesize that ZIP7 is required for peripheral B cell maintenance, whereas T cells may exhibit greater tolerance to ZIP7 deficiency.

Aims

Aim 1: Does ZIP7 deficiency impair peripheral lymphocyte maintenance?

To investigate whether ZIP7 is required for the maintenance of peripheral B and T cells, this thesis examines models with varying degrees of ZIP7 deficiency while avoiding embryonic lethality and early B cell developmental defects. Chapter 3 characterises inducible *Zip7* knockout models (*Zip7*$^{+/f}$ *Ert2-cre*; *Zip7*$^{P198A/f}$ *Ert2-cre* and *Zip7*$^{f/f}$ *Ert2-cre*), while Chapter 4 focuses on ZIP7 deficiency in mature B cells (*Cr2-cre*) and CD4^{+} T cells (*Cd4-cre*). The phenotypes were assessed in unmanipulated mice and single BM chimeras, followed by mixed BM chimeras to determine whether the observed defects are cell-intrinsic.

Aim 2: How does ZIP7 deficiency impair immune responses?

To determine the impact of ZIP7 deficiency on immune responses, I examined how ZIP7-deficient lymphocytes respond to immunization with TI and TD antigens. These studies revealed defects in antibody production and GC formation. To dissect the underlying mechanisms, adoptive transfer models were used to assess ZIP7's role in key processes such as B cell recruitment into GCs, maintenance within the GC microenvironment, and clonal expansion during immune responses. Chapter 5 characterises these immune deficiencies and evaluates potential contributing factors.

Aim 3: Why do varying degrees of ZIP7 deficiency have different effects on B and T cells?

To investigate why B and T cells exhibit distinct responses to varying degrees of ZIP7 deficiency (*Zip7*$^{+/f}$ *Ert2-cre*; *Zip7*$^{P198A/f}$ *Ert2-cre* and *Zip7*$^{f/f}$ *Ert2-cre*), I employed scRNA-seq as an unbiased, high-throughput approach to identify transcriptional changes

associated with different ZIP7-deficient states. By comparing gene expression profiles across B and T cell subsets in different models, this analysis aimed to uncover molecular signatures and pathways that could explain the differential sensitivity of these lineages to ZIP7 loss. Chapter 6 presents these findings, providing a high-resolution characterisation of the transcriptional landscape of ZIP7-deficient lymphocytes and highlighting potential regulators of the observed phenotypic differences.

In summary, while ZIP7 has been established as a key regulator of early B cell development, its role in peripheral lymphocyte homeostasis and immune responses remains poorly understood. Previous studies have linked zinc transporters to cellular stress responses, but whether ZIP7 deficiency disrupts immune function through similar mechanisms is unclear. By leveraging conditional knockout models, this work investigates how varying degrees of ZIP7 deficiency differentially affect B and T cells, providing new insights into its role in adaptive immunity.

Chapter

2 Materials and Methods

2.1 Animal work

2.1.1 Breeding and maintenance

All animal procedures were conducted in accordance with the United Kingdom Animals (Scientific Procedures) Act 1986 and performed under project license P79A4C5BA. Mice were housed under SPF conditions at the Functional Genetics Facility, with five to six animals per cage. No animals were excluded from analysis. Experimental groups were age- and sex-matched wherever possible. Gating controls were included for flow cytometry as required.

2.1.2 Mouse models

Zip7^{P198A} and *Zip7*^{H199QV} knock-in mouse models

Zip7^{P198A} and *Zip7*^{H199QV} knock-in alleles were previously generated using *CRISPR-Cas9*-mediated mutagenesis targeting exon 2 of *Zip7*[20]. Genotyping was performed by PCR (forward: 5'-GTTCTTAATCGGTGGGAAGCTCC-3'; reverse: 5'-CAGCACAC-CAGTCCCTGGTTTT-3') followed by Sanger sequencing. Homozygous and compound heterozygous animals were intercrossed to generate experimental cohorts.

Zip7^{flox} (*Zip7*^{f}) mouse model

Zip7$^{f/+}$ mice were generated in collaboration with Dr. Ben Davies (Transgenics Core, Wellcome Centre for Human Genetics) using the EASI-CRISPR approach[313]. Two LoxP sites were inserted flanking exon 2 of *Zip7* via *CRISPR/Cas9*-mediated homology-directed repair (HDR), using a long single-stranded DNA (lssDNA) donor template. Microinjections were performed in C57BL/6J zygotes with a mixture of Cas9 protein, two sgRNAs (Zip7A and Zip7B), and the lssDNA template. Embryos were transferred into pseudopregnant CD1 females. Correctly targeted founders were identified by PCR and Sanger sequencing, and two of them were used to establish independent colonies (TGLH and TGML). Founders were backcrossed to C57BL/6J mice for at least six generations. Genotyping was performed by PCR (forward: 5'-CCACCTCATCGCGCATGCCTTGGGTAA-3'; reverse: 5'-CAGTAAAGCATGAAGGGAGACG-3') followed by Sanger sequencing.

Zip7 conditional knockout models

To generate models with varying degrees of ZIP7 deficiency, the previously described alleles were combined with *Ert2-cre* (JAX #008463)[22], *Cr2-cre* (JAX #006368)[23], *Cd4-cre* (JAX #022071)[24], or MD4 transgenic mice (JAX #002595)[74] using a stepwise breeding strategy. For example, to generate ZIP7-deficient models with or without hen egg lysozyme (HEL) antigen specificity, *Cr2-cre* mice were first crossed with *Zip7*$^{P198A/+}$ animals to generate *Zip7*$^{P198A/+}$ *Cr2-cre* offspring, then crossed with *Ig Zip7*$^{f/f}$ mice to produce Ig or non-Ig *Zip7*$^{P198A/f}$ *Cr2-cre* animals.

In summary, inducible models include *Zip7*$^{+/f}$ *Ert2-cre*, *Zip7*$^{P198A/f}$ *Ert2-cre*, and *Zip7*$^{f/f}$ *Ert2-cre*, in which the floxed *Zip7* allele is deleted upon tamoxifen administration. Cell type–specific models include B cell specific (*Zip7*$^{+/f}$ *Cr2-cre*, *Zip7*$^{P198A/f}$ *Cr2-cre*

and *Zip7*$^{H199QV/f}$ *Cr2-cre*) and the T cell specific (*Zip7*$^{+/f}$ *Cd4-cre* and *Zip7*$^{P198A/f}$ *Cd4-cre*) mice.

CD45.1 and CD45.1/2 congenic mice

To distinguish donor and recipient haematopoietic cells in BM chimeras, all recipients were non-transgenic homozygous CD45.1 congenic mice obtained from Biomedical Services (BMS), University of Oxford. In some experiments, WT CD45.1/2 mice maintained in house were used as donors.

2.1.3 Tamoxifen preparation and administration

Tamoxifen (Sigma-Aldrich, T5648) was dissolved at 20 mg/mL in corn oil (Sigma-Aldrich, C8267) by shaking at 37 °C for 2–4 hours until fully dissolved. The solution was stored at 4 °C in the dark and used within one week.

For Cre induction, tamoxifen was administered at 75 mg/kg (body weight) by intraperitoneal (i.p.) injection once daily for five consecutive days, unless specified otherwise. Mice were then rested for 5–7 days before tissue collection or further procedures, with longer intervals used in selected experiments as indicated in the figure legends.

2.1.4 BM transplantation and sample processing

BM chimeras

CD45.1$^+$ recipient mice were lethally irradiated with two doses of 4.5 Gy, separated by a 3-hour interval. Irradiated mice were intravenously injected with BM cells (≥5 × 10^6 total cells), either from a single donor (single chimeras) or a mixture of CD45.1$^+$ control and CD45.2$^+$ experimental BM cells (mixed chimeras). Mice were maintained on

enrofloxacin-supplemented drinking water (10% oral solution) for four weeks post-transplant. Analysis or immunization was performed at least eight weeks after reconstitution.

Sample processing

All mice were euthanised by Schedule 1. Whole blood was collected immediately after euthanasia. Serum was isolated by centrifugation at 17,000 g for 10 minutes, followed by a second spin, and stored at -20 °C. BM (from femurs and tibias), thymus, spleen, and mesenteric lymph nodes (MLNs) were collected. All tissues were kept on ice and processed into single-cell suspensions in pre-chilled RPMI-1640 medium supplemented with 2% fetal calf serum (FCS). Spleen and MLN were mechanically dissociated and filtered through a 70 µm cell strainer. BM was obtained by flushing the bones with medium using a syringe and 25G needle. Where required, splenic red blood cells were lysed for 2 minutes at room temperature (RT) before resuspension in FCS-containing medium. An aliquot of each cell suspension was mixed with white blood cell (WBC) counting fluid (1.5% acetic acid, 0.5% methyl violet) and manually counted using a haemocytometer.

Bulk B-cell enrichment by magnetic-activated cell sorting (MACS)

ACK-lysed splenocytes were purified by negative selection using the MojoSort™ Mouse Pan B Cell Isolation Kit II (BioLegend, #480088), which removes non-B cells ($CD3^+$, $CD4^+$, $CD8a^+$, $CD11c^+$, $CD49B^+$, $Gr\text{-}1^+$, $TER\text{-}119^+$) via biotinylated antibodies and streptavidin-coated magnetic beads. Following magnetic separation, B cells were enriched in the flow-through, while T cells, myeloid cells, and erythroid cells were retained in the magnet. Both fractions were collected for purity assessment and downstream applications.

Fluorescence-activated cell sorting (FACS)-based isolation of B cell subsets

MACS-enriched samples were stained with fluorochrome-conjugated antibodies targeting B-cell surface markers. The following panel was used:

Fusion Laser		Band-pass Filter	Fluorochrome	Antigen	Dilution	Clone	Brand	Catalogue No.
Yellow	561 nm	582/15	PE	CD1d	500	1B1	Invitrogen	12-0011-82
Blue	488 nm	695/40	PerCP/Cyanine5.5	B220	200	RA3-6B2	BioLegend	103236
Yellow	561 nm	780/60	PE/Cyanine7	CD23	300	B3B4	BioLegend	101614
Red	640 nm	670/30	APC	CD93	100	AA4.1	BioLegend	136510
	640 nm	730/45	AF700	CD19	100	6D5	BioLegend	115528
Violet	405 nm	525/50	V500	L/D	200	NA	BioLegend	423102
	405 nm	610/20	BV605	CD21	300	7G6	BD OptiBuild	747763

Cells were gated as follows: lymphocytes → singlets → live cells → $B220^{+}$ $CD19^{+}$ B cells → follicular B cells ($CD21^{Int}$ $CD1d^{-}$ $CD23^{+}$) and MZ B cells ($CD21^{hi}$ $CD1d^{hi}$ $CD23^{-/low}$). Cells were sorted using a BD FACSAria Fusion, and genomic DNA was extracted from the purified subsets for downstream Sanger sequencing (Figure 4-1C–E).

2.1.5 Adoptive transfer experiments

Adoptive transfer of antigen-specific B cells provides a powerful tool for dissecting cell-intrinsic effects on B cell phenotype under defined immunological conditions. In this study, I used HEL-specific MD4 Ig-transgenic B cells from either constitutive or inducible Cre lines as donors, and transferred them into non-Ig-transgenic recipient mice to evaluate the impact of ZIP7 deficiency on GC entry and maintenance. This system offers several advantages, including a fixed BCR specificity, internal competition, and consistent exposure to a WT microenvironment, which minimizes external confounding effects. The adoptive transfer design follows established methods previously described[314], with modifications tailored to each experimental model.

For *Cr2-cre*-based adoptive transfer experiments, donor B cells were MACS-enriched from the spleen or MLNs as previously described. The purity of sorted B cells was verified by flow cytometry and consistently exceeded 90%. CD45.2$^+$ MD4 *Zip7*$^{P198A/f}$ *Cr2-cre* or *Zip7*$^{+/f}$ *Cr2-cre* B cells were mixed at a 1:1 ratio with CD45.1$^+$ MD4 WT B cells. The mixed cell suspension was resuspended in PBS and intravenously injected into CD45.2$^+$ WT recipient mice (2×10^6 total cells per mouse), followed by HEL-SRBC immunisation the next day. All analyses were performed on recipient spleens, with HEL-binding GC and non-GC B cells quantified by flow cytometry on Day 8. The overall setup and immunisation timeline are illustrated in Figure 2-1.

For *Ert2-cre*–based adoptive transfer experiments, CD45.2$^+$ MD4 *Zip7*$^{f/f}$ or MD4 *Zip7*$^{f/f}$ *Ert2-cre* chimeric donor mice were treated with tamoxifen to induce *Zip7*^{f} deletion prior to B cell isolation. The subsequent procedures—including mixing, transfer, and immunisation—were similar to those described above, with slight modifications such as different tissue collection time points. The full schematic is shown in Figure 5-6A.

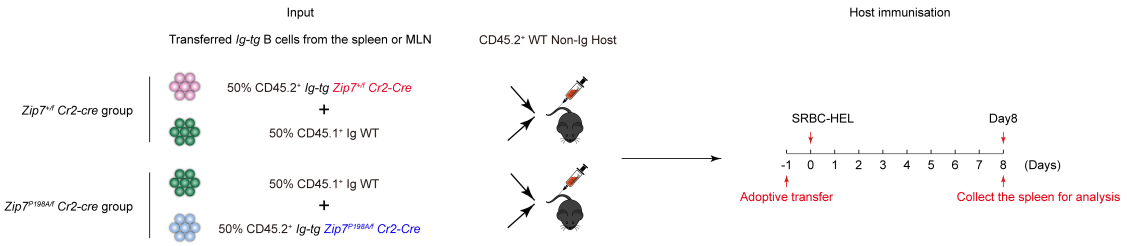

Figure 2-1: Experimental setup for adoptive transfer of Ig-transgenic B cells in the *Cr2-cre* model.
CD45.2$^+$ HEL-specific MD4 B cells were sorted from the spleen or MLNs of *Zip7*$^{+/f}$ *Cr2-cre* or *Zip7*$^{P198A/f}$ *Cr2-cre* mice and mixed at a 1:1 ratio with CD45.1$^+$ MD4 WT B cells. Mixed B cells were transferred into CD45.2$^+$ non-transgenic WT hosts, followed by HEL-SRBC immunisation. Spleens were collected on Day 8 for analysis.

2.1.6 Antigen immunization

NP-Ficoll

Mice were injected intraperitoneally with 50 µg NP-Ficoll (LGC Biosearch Technologies, Middlesex, UK) diluted in PBS. Spleens, MLNs, and BM were harvested 7 days later for flow cytometric analysis, and serum was collected for ELISA.

NP-CGG

Single BM chimeras were immunized intraperitoneally with 50 µg NP-(20–29)-CGG (ChemCruz, Cat. sc-396209A) emulsified 1:1 in alum (Thermo Scientific, Cat. 77161), with a total volume of 300 µL per mouse. A secondary immunization (booster) with 50 µg NP-(20–29)-CGG in PBS was administered on day 42. Sera were collected by tail bleeding (Sarstedt, Cat. 16.444) on days 7, 14, 28, 35 and 46 post-primary immunization (Figure 2-2). All bleeds complied with the UK Home Office guidelines, with <15% of total blood volume collected per 28-day period.

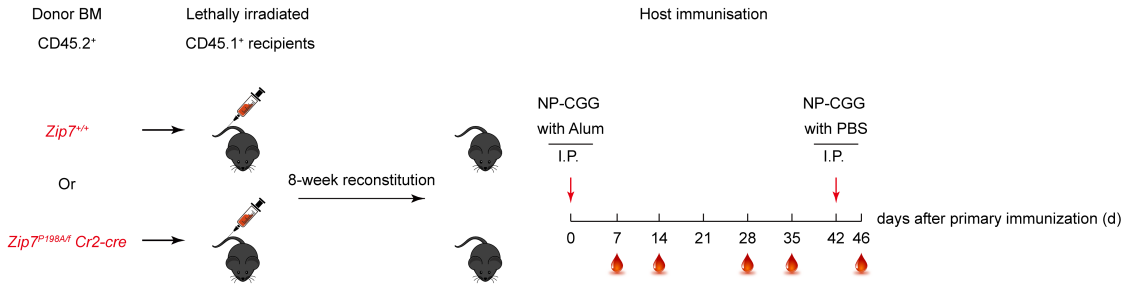

Figure 2-2: Schematic of NP-CGG immunisation in Zip7$^{+/+}$ and *Zip7*$^{P198A/f}$ *Cr2-cre* single BM chimeras.
Recipient mice reconstituted with Zip7$^{+/+}$ and *Zip7*$^{P198A/f}$ *Cr2-cre* BM were immunised intraperitoneally with NP-CGG in alum on Day 0, followed by a booster with NP-CGG in PBS on Day 42. Tail vein bleeds were collected at the indicated time points to assess antibody responses.

SRBCs and HEL-conjugated SRBCs

Sheep red blood cells (SRBCs) (Thermo Scientific Oxoid, Leicestershire, UK) were washed three times in HBSS (Gibco) and resuspended at 2 × 10^9 cells/mL.

To enable the study of antigen-specific responses in B cells derived from MD4 transgenic donors, SRBCs were conjugated to HEL using 1-ethyl-3-(3-dimethylaminopropyl) carbodiimide (EDCI) crosslinking. Briefly, washed SRBCs were resuspended at 10% (v/v) in conjugation buffer (0.35 M mannitol, 0.01 M NaCl in HBSS), incubated with HEL (20 mg/mL) for 10 minutes at 4 °C, followed by the addition of EDCI (100 mg/mL) and incubation for 30–60 minutes at 4 °C with gentle agitation. After four washes with HBSS, cells were counted and adjusted to 2 × 10^9 cells/mL. Conjugation efficiency was verified by flow cytometry using HyHEL9-PerCP-Cy5.5 staining.

For immunization with SRBC or HEL-SRBC, mice were injected intraperitoneally with 150 µL of the cell suspension per flank (total 300 µL per mouse). Spleens were harvested around eight days later for analysis. The schematic for SRBC immunisation in mixed chimeras is shown in Figure 2-3 ; the adoptive transfer–based HEL-SRBC protocol is illustrated separately in Figure 2-1 and Figure 5-6A.

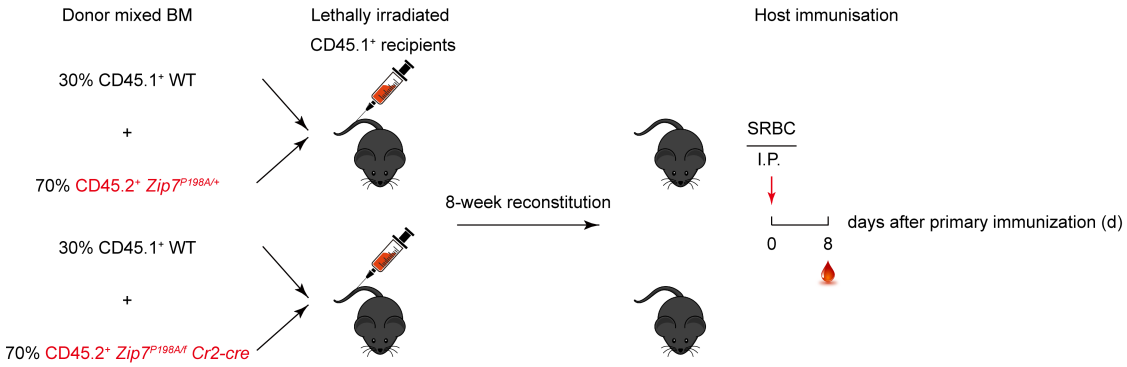

Figure 2-3: Schematic of SRBC immunisation in mixed BM chimeras.
CD45.1$^+$ WT recipients were lethally irradiated and reconstituted with 30% CD45.1$^+$ WT and 70% CD45.2$^+$ donor BM from either CD45.2$^+$ *Zip7*$^{P198A/+}$ or *Zip7*$^{P198A/f}$ *Cr2-cre* mice. Eight weeks post-reconstitution, mice were immunised intraperitoneally with SRBCs, and spleens were harvested on day 8 to evaluate T cell-dependent germinal centre responses.

2.1.7 Flow cytometry analysis

Immunophenotyping by flow cytometry

Cell suspensions were plated at 0.5 × 10^6 cells per well in U-bottom 96-well plates. After a single wash with FACS buffer (DPBS supplemented with 2% FCS, 10 mM HEPES, and 0.05% sodium azide), cells were stained with 25 µL of antibody cocktail containing 10% Fc block for 30 minutes on ice, protected from light.

For detection of HEL-binding B cells, cells were first incubated with 250 ng/mL HEL on ice for 25–30 minutes, washed 2–3 times with FACS buffer, and co-stained with HyHEL9-Pacific Blue in the antibody cocktail for 30 minutes on ice, protected from light.

After two final washes, samples and compensation controls were acquired on a 10-colour BD FACS Canto II (BD Biosciences) with BD FACSDiva and the flow cytometry data were analysed using FlowJo v10.8, v10.9 or v10.10 (FlowJo LLC). Antibodies used for staining surface markers are listed in Table S2-4.

BrdU incorporation assay

For analysis of proliferating cells, mice were injected intraperitoneally with BrdU (1 mg per mouse) and sacrificed 4 hours later. Single-cell suspensions were stained for surface markers as described above, followed by fixation and permeabilisation using the BD Cytofix/Cytoperm kit (BD, Cat. 554714). DNA was denatured with DNase I for 1 hour at 37 °C, and intracellular BrdU was detected using an anti-BrdU antibody (Table S2-4). Flow cytometry data were recorded and analysed as above.

2.2 Molecular biology assays

2.2.1 ELISA

Mouse serum immunoglobulin (IgM, IgG, and IgG3) levels were quantified using sandwich ELISA kits from Bethyl Laboratories (Cat. E90-101 for IgM, E90-131 for IgG, and E90-111 for IgG3). 96-well plates were coated with affinity-purified goat anti-mouse capture antibodies and blocked with 1% BSA in Tris-buffered saline (TBS, pH 8.0). Serial dilutions of reference serum were used to generate a standard curve. Samples were diluted to appropriate concentrations and measured in duplicate. Detection was performed using HRP-conjugated secondary antibodies and TMB substrate (Life Technologies, Cat. 00-4201-56), with absorbance read at 450 nm. Concentrations were calculated by 4-parameter logistic (4PL) curve fitting and reported as relative units multiplied by the dilution factor.

To assess NP-specific antibody responses following immunization, ELISA plates were coated with NP_7-BSA or NP_{25}-BSA (Biosearch Technologies) at 5 μg/mL in bicarbonate buffer. After blocking with 5% fat-free milk, diluted serum samples and standard controls (pooled immune sera) were incubated for 1 hour at 37 °C. Detection was performed using alkaline phosphatase (AP)-conjugated goat anti-mouse IgM or IgG1, followed by development in NPP buffer containing phosphatase substrate (Sigma-Aldrich,

Cat. S0942-200TAB). Absorbance was measured at 405 nm using an ELISA plate reader. NP-specific antibody levels were expressed as arbitrary units, calculated from standard curves using a 4PL model and multiplied by the dilution factor.

2.2.2 DNA extraction and PCR

Genomic DNA was extracted using the DNeasy Blood & Tissue Kit (QIAGEN, Cat. 69504) following the manufacturer's instructions and quantified using a NanoDrop 1000 spectrophotometer (Thermo Fisher Scientific). Touchdown PCR was performed using the BIOTAQ^{TM} PCR Kit (Bioline, Cat. BIO-21071). The primers used to validate Zip7 knockout efficiency were as follows: Forward (F1): 5'–CTGTGGGACTGCTGACCT–3' and Reverse (R1): 5'–ATGTGTGTTTGAAGACAACCGGAA–3'.

2.3 Single-cell RNA sequencing

The Next GEM Single Cell 5' Reagent Kits v2 with Feature Barcode technology (10× Genomics) were used to enable comprehensive single-cell mRNA profiling (Figure 2-4). As inducible ZIP7 gene deletion targets exon 2, its impact on downstream transcript stability or degradation was uncertain. Therefore, the 5' assay was selected over the 3' version, as it captures the 5' end of transcripts and may provide more reliable data under these conditions.

While both 3' and 5' assays are widely used for cell barcoding and gene expression profiling, a recent preprint comparing the two in PBMCs found that the 5' assay captured more exonic molecules and better detected low-abundance, long transcripts[315]. Although not peer-reviewed, this comparative analysis provided objective support for the selection of the 5' assay in this study.

2.3.1 Sample preparation for scRNA-seq

Mouse models and experimental setup

CD45.1$^+$ WT mice were lethally irradiated and reconstituted with CD45.2$^+$ BM cells from *Zip7*$^{+/f}$ *Ert2-cre*, *Zip7*$^{P198A/f}$ *Ert2-cre*, or *Zip7*$^{f/f}$ *Ert2-cre* donors. Following eight weeks of reconstitution, mice received five doses of tamoxifen, and spleens were harvested 7 days after the final dose (n = 3 per group).

Hashtag labelling, CITE-seq and FACS antibody staining

Single-cell suspensions were prepared from spleens following ACK lysis. 2×10^6 cells per sample were transferred into DNA and protein low-binding Eppendorf tubes and labelled with a unique hashtag antibody (TotalSeq-C C0301–C0309) at 0.5 μg per 10^6 cells in 200 μL. After 30 minutes incubation at 4 °C, cells were washed three times with cold FACS buffer and pooled in equal numbers.

The pooled sample was stained with a cocktail of eight CITE-seq antibodies (CD19, CD21, CD93, CD23, CD1d, CD4, CD8a, CD25) and three flow cytometry antibodies (FITC-CD45.1, APC-CD45.2, V550-Live/Dead). Antibody dilutions are listed in Table S2-5. Staining was performed at 4 °C for 30 minutes using 50 μL antibody mix per 10^6 cells, followed by four washes in chilled FACS buffer.

FACS sorting and library preparation

Cells were resuspended in 2% FCS in PBS (sorting buffer) at 10×10^6 cells/mL and sorted on a BD FACSAria Fusion. Live CD45.2$^+$ CD45.1$^-$ lymphocytes with small-to-moderate SSC were gated and collected into FCS-coated low-binding tubes. Sorted cells were pelleted and resuspended in PBS with 0.04% BSA at 1×10^6 cells/mL. Viability and concentration were assessed prior to loading.

Cells were mixed, split into duplicates, and ~30,000 viable cells were captured using the 10X Chromium Controller protocol, followed by library preparation and sequencing.

2.3.2 Library preparation and scRNA-seq

Library preparation

Four separate libraries were generated, corresponding to duplicate samples per condition:

1. 10× transcriptome library for single-cell mRNA profiling

2. A feature barcode library for sample demultiplexing and surface protein identification

Library construction was performed by Dr Moustafa Attar (Computational and Single Cell Genomics Group, Kennedy Institute of Rheumatology, University of Oxford) at the Single Cell and Spatial Genomics Facility.

Sequencing

Libraries were sequenced on a NovaSeq X Plus PE150 platform (Novogene UK). A 1% PhiX control was included to improve base calling accuracy and ensure data quality.

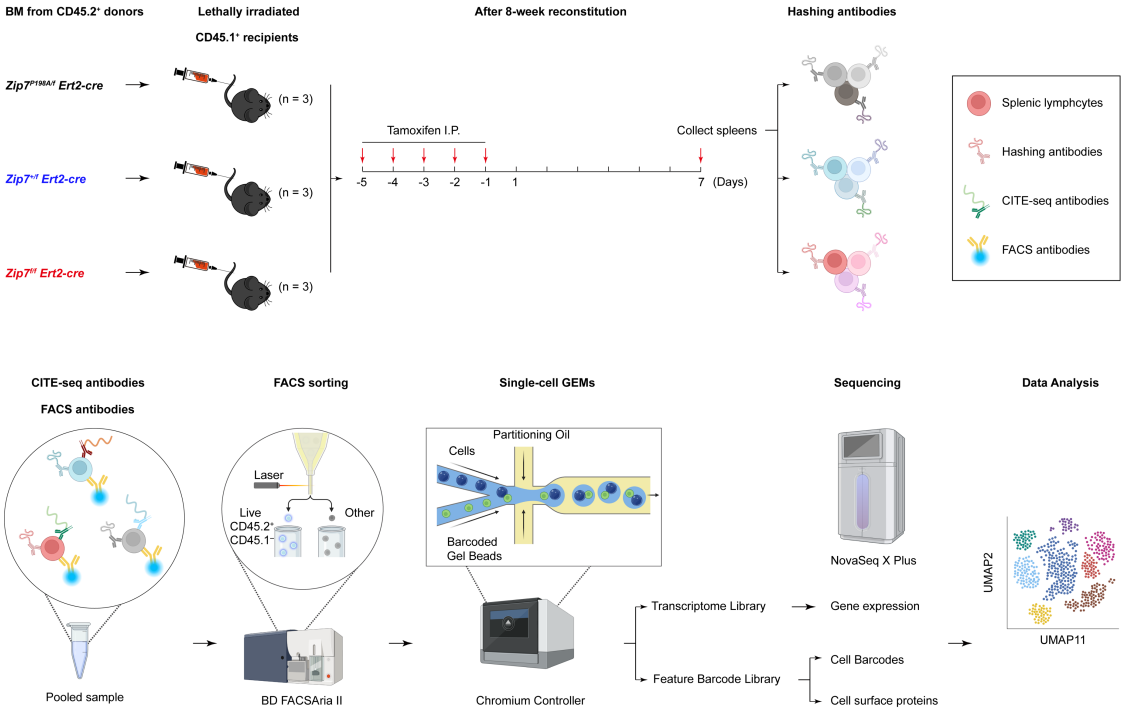

Figure 2-4: Workflow for sample preparation and scRNA-seq with barcode technologies. Spleens were collected after tamoxifen treatment, and splenocytes were labelled with hashtag, CITE-seq, and FACS antibodies. Live CD45.2$^+$ CD45.1$^-$ lymphocytes were sorted and processed for single-cell GEM generation, library preparation, and sequencing. Illustration created with BioRender and Adobe Illustrator.

2.3.3 Bioinformatic analyses

2.3.3.1 Initial data processing and generation of feature-barcode matrices

Raw sequencing data were initially processed by Novogene (UK) Company Limited, including base calling, quality control, and demultiplexing.

Subsequent alignment to the mouse reference genome (mm10; refdata-gex-mm10-2020-A), cell barcode assignment, and gene expression quantification were performed using the Cell Ranger pipeline (v7.2.0, 10× Genomics) by Dr. Mukta Deobagkar. This process produced feature-barcode matrices with filtered gene expression data, which provided the foundation for downstream scRNA-seq analyses.

2.3.3.2 Seurat-based scRNA-seq analysis

Downstream analysis of scRNA-seq data was performed using Seurat (v5.1.0, Satija Lab). A Seurat object was created incorporating RNA, hashtag oligonucleotide (HTO), and antibody-derived tag (ADT) assays to enable integrated analysis and cell type characterisation.

Quality control

Quality control metrics—including the number of detected genes (nFeature_RNA), total UMI counts (nCount_RNA), and the percentage of mitochondrial transcripts (percent.mt)—were visualised using violin and scatter plots to assess sample quality (Figure 2-5A). Cells were excluded if percent.mt exceeded 10% or if nFeature_RNA was below 200 or above 5,500.

Although a 5% mitochondrial cutoff is commonly used to exclude low-quality or dying cells, a higher threshold (10%) was applied here for two reasons:

1. Doublet filtering: Dead or dying cells often show multiple hashtag labels and are removed during doublet exclusion, reducing the need for a strict mitochondrial threshold.
2. ZIP7-deficient cell phenotypes: ZIP7-deficient cells, which are prone to reduced viability, may exhibit naturally elevated mitochondrial gene expression (Figure 2-5B). A stringent filter might exclude these biologically relevant populations.

This adapted cutoff aimed to minimise low-quality cells while retaining potentially important ZIP7-deficient subsets, preserving biological interpretability in downstream analyses.

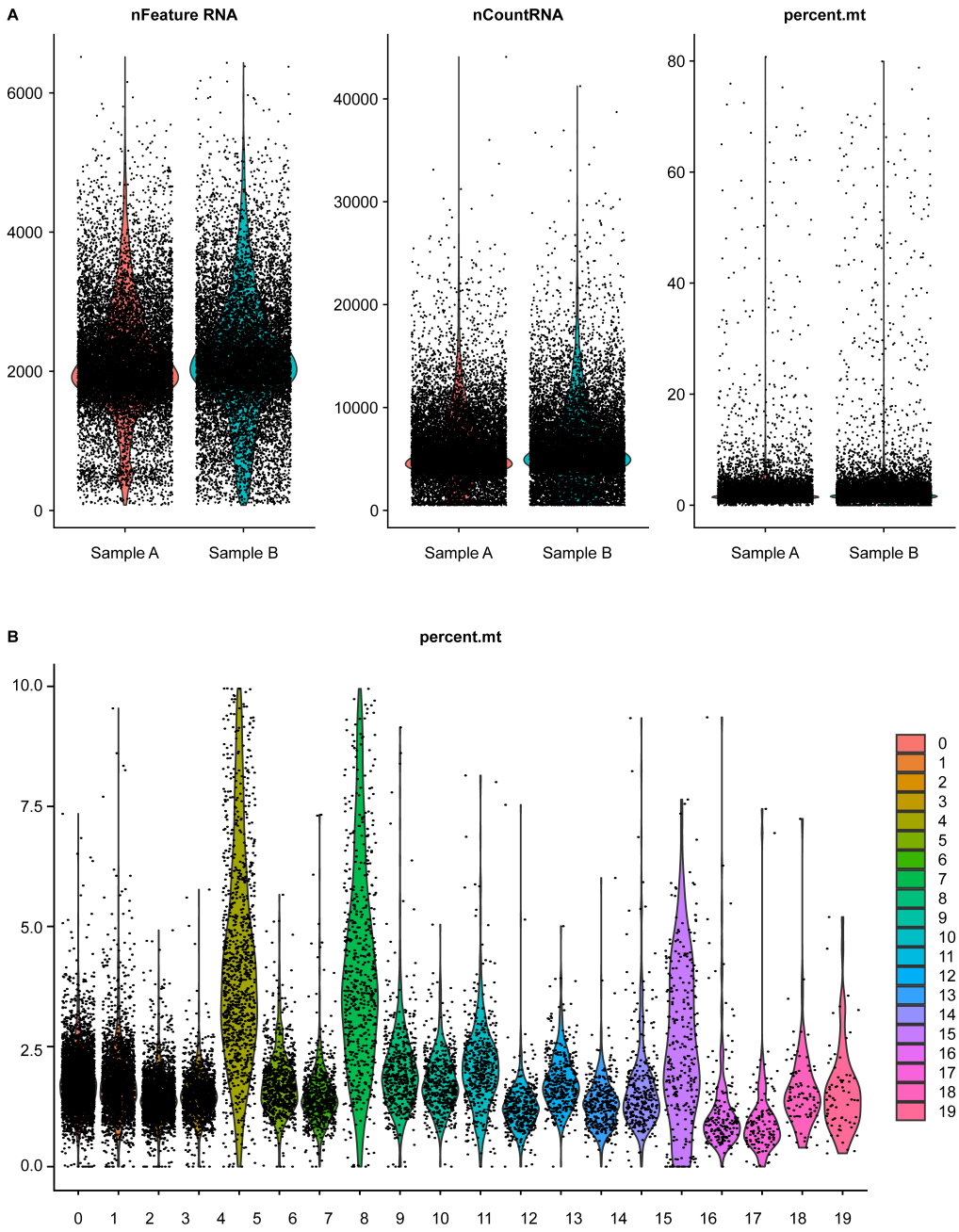

Figure 2-5: Quality control metrics and mitochondrial percentage across clusters. (A) Violin and scatter plots of nFeature_RNA, nCount_RNA, and percent.mt for Sample A and Sample B before filtering. (B) Violin plots of percent.mt across clusters (resolution = 0.8) in pooled data after filtering. Several biologically relevant clusters show percent.mt values exceeding the conventional 5% threshold, supporting the use of a 10% cutoff.

Hashtag demultiplexing and filtering

HTO data were used to assign cells to individual samples, remove doublets and negatives, and map sample identities for downstream analysis.

1. Normalization: HTO counts were normalised using centred log-ratio (CLR) transformation to standardise expression across features.

2. Demultiplexing: Cells were classified as singlets, doublets, or negatives using the HTODemux function in Seurat. A positive quantile threshold of 0.99 was applied to ensure accurate classification (Figure 2-6).

3. Dimensionality reduction: PCA and t-SNE were applied to the HTO assay prior to filtering to visualise sample demultiplexing (Figure 2-6C).

4. Filtering: Only singlet cells were retained for downstream analyses, while doublets and negative cells were excluded.

5. Sample annotation: Singlet cells were further annotated by assigning unique sample IDs (e.g., *Zip7*$^{+/f}$ *Ert2-cre*_1, *Zip7*$^{+/f}$ *Ert2-cre*_2) and group IDs (*Zip7*$^{+/f}$ *Ert2-cre*, *Zip7*$^{P198A/f}$ *Ert2-cre*, or *Zip7*$^{f/f}$ *Ert2-cre*), reflecting biological replicates and experimental conditions.

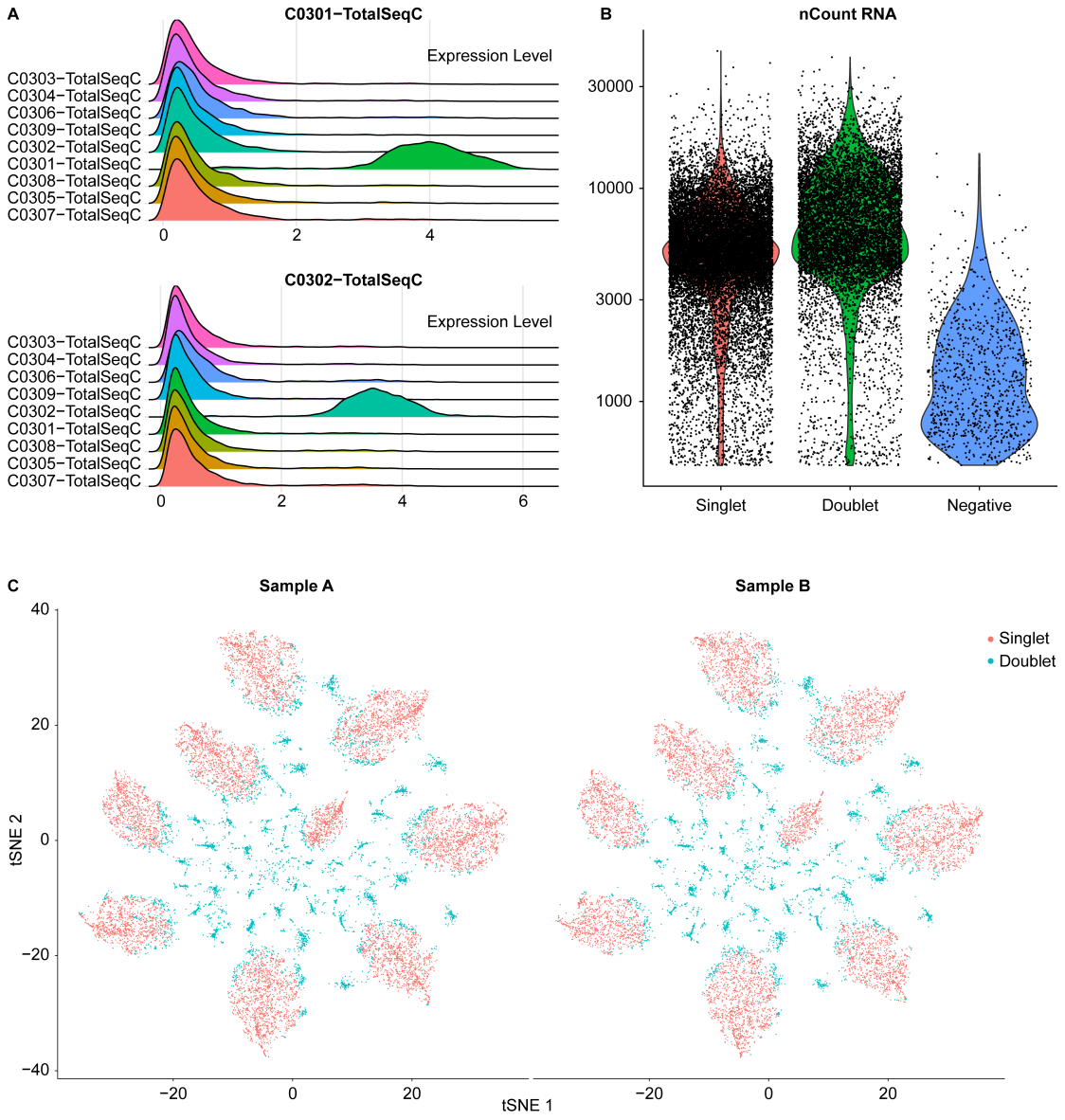

Figure 2-6: Hashtag demultiplexing of pooled scRNA-seq samples.
(A) Ridge plots of normalised HTO expression for two representative hashtags (Total-Seq-C C0301 and C0302), demonstrating distinct signal distribution for cell origin assignment. (B) Violin plots comparing the number of UMIs for singlets, doublets, and negative cells after HTO demultiplexing. Doublets and negatives were excluded from downstream analyses. (C) t-SNE plots of HTO profiles in Sample A and Sample B highlighting singlet (red) and doublet (blue) cell populations. Negatives were excluded from display.

ADT analysis and visualization of protein marker distribution

ADT data were analysed to assess surface protein expression across cell populations:

1. Normalization and dimensionality reduction: ADT counts were normalised using the CLR transformation. PCA was performed on the normalised and scaled data. Feature plots were used to visualise the expression of eight protein markers.

2. Integration of RNA and protein data: RNA and ADT assays were integrated to examine the concordance between mRNA and protein expression, revealing marker-specific relationships (Figure 2-7).

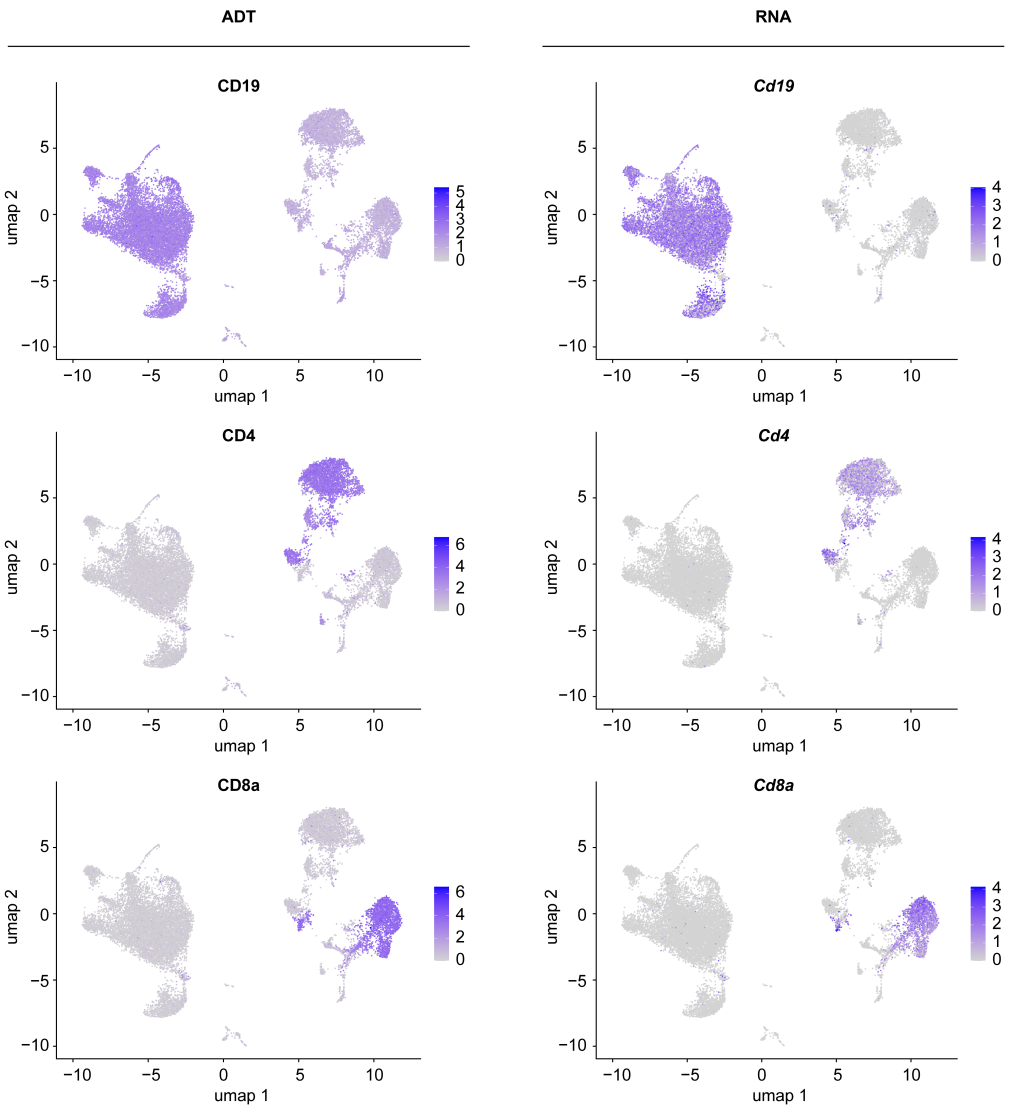

Figure 2-7: Comparison of protein and mRNA expression levels for representative markers CD19, CD4, and CD8a.
UMAP visualisations showing marker expression at the protein level (ADT, left panels) and mRNA level (RNA, right panels). Colour intensity represents normalised expression, with brighter colours indicating higher expression. Data shown are from pooled samples (Sample A and Sample B).

RNA data processing, clustering, and cluster annotation

1. Normalization, feature selection and cell cycle scoring

RNA counts were log-normalised with a scale factor of 10,000 to standardise expression levels across cells. Highly variable features were identified using the "vst" method, with the top 2,000 variable genes selected for downstream analysis. To assess the impact of cell cycle heterogeneity, cell phase scores were calculated based on canonical gene sets for G1, S, and G2/M phases[316] (Figure 2-8). As no major influence on clustering was observed, regression was not applied.

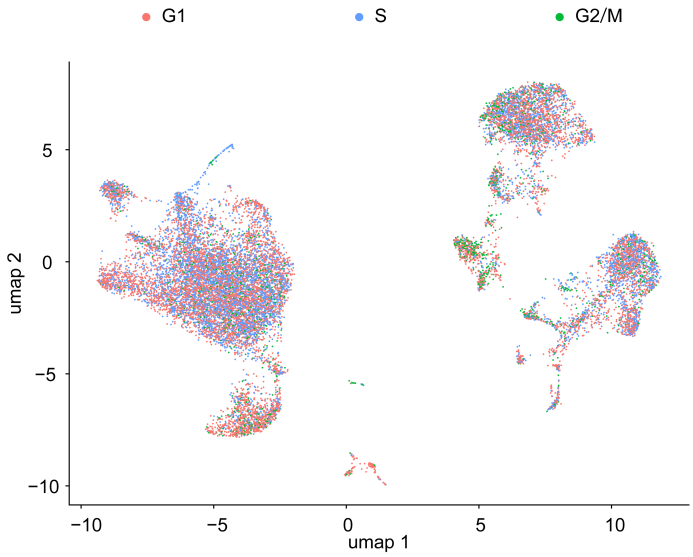

Figure 2-8: UMAP visualization of cell cycle phases.
UMAP plot showing cell cycle classification: G1 (red), S (blue), and G2/M (green). The even distribution of phases across clusters suggests minimal cell cycle–driven transcriptional variation.

2. Dimensionality reduction, clustering, and resolution selection

PCA was used to reduce dimensionality and identify key components for downstream clustering, with the optimal number of PCs determined using an elbow plot. Non-linear dimensionality reduction methods, including UMAP and t-SNE, were applied for visualisation of cellular heterogeneity.

To ensure biologically meaningful resolution of transcriptional subtypes, clustering was performed across a range of resolutions (Res = 0.1–1.5) for each major lymphocyte lineage using clustree plots and UMAP projection. Clustering resolution was selected based on three complementary considerations: (1) cluster stability, assessed using clustree plots (e.g., Supplementary Figure 20); (2) genotype-specific enrichment patterns, particularly ZIP7-deficient groups (*Zip7*$^{P198A/f}$ *Ert2-cre* and *Zip7*$^{f/f}$ *Ert2-cre*), observed in split UMAP projections (e.g., Figure 6-2C, Figure 6-3A, Figure 6-4B); and (3) biological coherence and interpretability of the resulting cluster annotations.

Accordingly, resolution 0.1 was chosen for $CD4^+$ T cells due to early and stable emergence of the ZIP7-deficiency–associated stress cluster. For $CD8^+$ T cells, resolution 0.3 allowed clearer delineation of ZIP7-deficiency–enriched cells. For B cells, resolution 0.6 balanced clustering stability and biological interpretability, enabling the identification of distinct subsets (e.g., MZ, GC/plasma, anergic B cells) and revealing ZIP7-deficiency–associated shifts in cellular composition.

3. Cell cluster annotation

Clusters were annotated by integrating multiple data sources to comprehensively identify immune cell populations. ADT assay data supported initial classification of major cell types, in combination with RNA expression profiles. For each cluster, the top 20 marker genes identified using FindAllMarkers() were analysed using the ImmGen[276] MyGeneSet tool. This allowed comparison of gene expression patterns with sorted immune cell subsets from the ImmGen reference dataset, helping to infer likely cell subtypes. Functional interpretation was further guided by known biological roles of these genes and immunological context. Additionally, HTO distribution patterns revealed that some clusters, primarily composed of ZIP7-deficient cells, exhibited unique

transcriptional signatures consistent with stressed or dying phenotypes, in agreement with previous wet-lab observations.

2.3.3.3 Downstream analysis of scRNA-seq data

To investigate the downstream transcriptional consequences of ZIP7 deficiency, a series of analyses were performed including gene module scoring, statistical comparisons, correlation analysis, and pathway enrichment.

Module scoring (AddModuleScore)

Transcriptional signature scoring was carried out using Seurat's AddModuleScore()[316] function on lineage-specific Seurat objects for B cells, $CD4^+$ T cells, and $CD8^+$ T cells. Stress-associated and functional signatures—including the Shared Stress Signature, the split integrated stress response (s-ISR) signature[317], the Terminal UPR Signature[318], curated Hallmark gene sets from the Mouse MSigDB collection[319,320], and several custom gene modules[321]—were applied. Violin plots displayed raw module scores calculated separately within each cell type, without z-score normalisation, to retain biologically meaningful differences. In contrast, signature scores shown in heatmaps were generated after merging all lineage-specific datasets and applying a unified z-score normalisation within each functional category to enable cross-lineage comparisons.

Statistical testing of module scores

Statistical evaluation of module scores was performed per cluster using the Kruskal–Wallis test to assess overall genotype effects. For clusters with significant differences, pairwise Wilcoxon rank-sum tests were applied between genotype groups, with Bonferroni correction to adjust for multiple comparisons.

Correlation between stress signatures

To further assess the relationship between transcriptional stress programs, Spearman correlation analysis was conducted between the Shared Stress Signature and the s-ISR signature. For each lineage, correlation was assessed both globally (across all cells, coloured by ZIP7 genotype) and at the level of individual transcriptomic clusters. Correlation statistics, including Spearman's R, R^2, and p-values, were reported alongside regression-based visualisations.

Pathway enrichment

Significantly upregulated genes from the most stress-enriched clusters, filtered using an adjusted *p*-value < 0.05 and average $\log_2$ fold-change > 0.3, were selected for Gene Ontology (GO) enrichment analysis. Enrichment was performed using the clusterProfiler package (version 4.12.6), with mouse gene annotations from org.Mm.eg.db. GO terms with adjusted *p*-values below 0.05 were considered significantly enriched. To enable meaningful cross-lineage comparison, enrichment levels were quantified using fold enrichment (observed-to-expected gene frequency ratio), rather than raw gene counts or GeneRatio.

2.4 Reagents and equipment

All reagents, antibodies, consumables, and equipment used in this study were commercially obtained. Full details, including source, catalogue number, dilution, and usage context, are provided in the Appendices: biochemical reagents (Table S2-1), antibodies and reagents used for *ex vivo* stimulation (Table S2-2), buffers and kits (Table S2-3), antibodies for flow cytometry and phospho-flow (Table S2-4), BioLegend antibodies for

CITE-seq and cell hashing (Table S2-5), laboratory consumables and equipment (Table S2-6).

2.5 Statistical analysis

All statistical analyses were performed using GraphPad Prism (version 9.2.0).

The normality of continuous variables was assessed using the Shapiro–Wilk test, and the equality of variances using the *F* test. Based on these assessments: comparisons between two groups were conducted using an unpaired *t*-test or an unpaired *t*-test with Welch's correction if variances were unequal. For multiple pairwise comparisons, Welch's *t*-tests were followed by Holm–Šídák correction to control for false discovery.

For comparisons involving multiple groups, statistical methods were selected according to the experimental design: When two independent variables (e.g. genotype and cluster or cell subset) were analysed simultaneously, two-way ANOVA was used. For genotype comparisons within each cluster, Šídák's multiple comparisons test was applied after two-way ANOVA to focus on within-cluster differences while controlling type I error. For related or hierarchically structured variables (e.g. Hardy fractions A–F), where standard ANOVA assumptions may not hold, mixed-effects analysis was used, followed by Tukey's multiple comparisons test.

Unless otherwise stated, data are presented as mean $\pm$ 95% confidence intervals (CIs). Statistical significance was defined as: $p < 0.05$ (*), $p < 0.01$ (**), $p < 0.001$ (***), and $p < 0.0001$ (****).

Chapter

3 Different degrees of ZIP7 deficiency alter B and T cell subtype cellularity

3.1 Introduction

Proteins play a fundamental role in maintaining physiological homeostasis, with both their quality (absence of mutations) and quantity (expression levels) being crucial. Disruptions in either can lead to pathological conditions such as cancer, immune deficiencies, and genetic disorders.

In the adaptive immune system, somatic mutations are key for generating antigen receptor diversity, a process essential for robust immune responses. However, mutations that go beyond this natural process—such as those affecting genes like *ZIP7*—can disrupt lymphocyte function and lead to immunodeficiencies[20]. For example, monoallelic variants of *TCF3* cause a milder form of PID, while biallelic *null* mutations, which completely abolish TCF3 expression, lead to more severe immunodeficiency[322]. Notably, the same mutation can trigger different effects, complicating the phenotype. A newly described form of combined immunodeficiency is caused by a heterozygous germline mutation in the DNA binding domain of interferon regulatory factor 4 (*IRF4*). Patients with the IRF4^{T95R} mutation exhibit multiple defects in B cell development and function,

driven by reduced transcriptional activity on canonical interferon-stimulated response elements (hypomorph), increased affinity for DNA (hypermorph), and acquired binding to noncanonical sites (neomorph)[323].

Given the intertwined effects of mutations and gene dosage, it is increasingly necessary to design strategies that elucidate their physiological and biochemical consequences in individual cells and biological systems. Mouse models are invaluable for investigating the full spectrum of a gene's functions, especially where human cases are limited due to selective pressures. Based on *Myc* haploinsufficiency and overexpression mouse models, Finkin *et al.* revealed that the more antigen presented to the Tfh cells in the light zone, the more MYC is induced by them. The latter proportionally supports B cell division capacity and residence time in the dark zone, which makes Tfh cells dictate the timing of B cells clonal expansion in the germinal centre[324]. Thus, models with gradient degrees of deficiency or hyperfunction can capture intermediate regulations and stretch the spectrum of the understanding of a gene's functions.

Despite multiple combinations of hypomorphic mutations, the spectrum of the ZIP7 immunodeficiency is narrowly defined and focused on B cells. In both ZIP7$^{P198A/P198A}$ patients and mouse models, an exclusive defect in B cell development is observed, while more severe deficiency cannot be studied due to embryonic lethality[20]. This raises questions about how ZIP7 functions in other cell types and why its effects differ. One approach to address these gaps is to develop a series of inducible models with varying degrees of ZIP7 deficiency—such as *Zip7*$^{+/f}$ *Ert2-cre*, *Zip7*$^{P198A/f}$ *Ert2-cre*, and *Zip7*$^{f/f}$ *Ert2-cre*—to compare their effects on different cell types.

3.2 Generation of tamoxifen-inducible mouse models with varying ZIP7 deficiencies

To control *Zip7* knockout temporally *in vivo*, mice heterozygous for the $Zip7^{P198A}$ or the allele were crossed with the Ig $Zip7^{f/f}$ *Ert2-cre* strain to generate Ig transgenic (Ig-tg) or non-transgenic (non-tg) $Zip7^{+/f}$ *Ert2-cre*, $Zip7^{P198A/f}$ *Ert2-cre* and $Zip7^{f/f}$ *Ert2-cre* mice. Given that germline $Zip7^{-/-}$ causes embryonic death[20] and the relevant animal welfare concerns involved, directly inducing *Zip7* deletion in the whole body was not considered as a viable option. Therefore, subsequent experiments with the *Ert2-cre* models exclusively used irradiated recipients reconstituted with BM from $Zip7^{+/f}$ *Ert2-cre*, $Zip7^{P198A/f}$ *Ert2-cre* and $Zip7^{f/f}$ *Ert2-cre* donors. In this way, following tamoxifen treatment, hematopoietic cells in the recipients (derived from the respective donors) were expected to achieve the following genotypes: $Zip7^{+/-}$, $Zip7^{P198A/-}$ and $Zip7^{-/-}$, respectively (Figure 3-1).

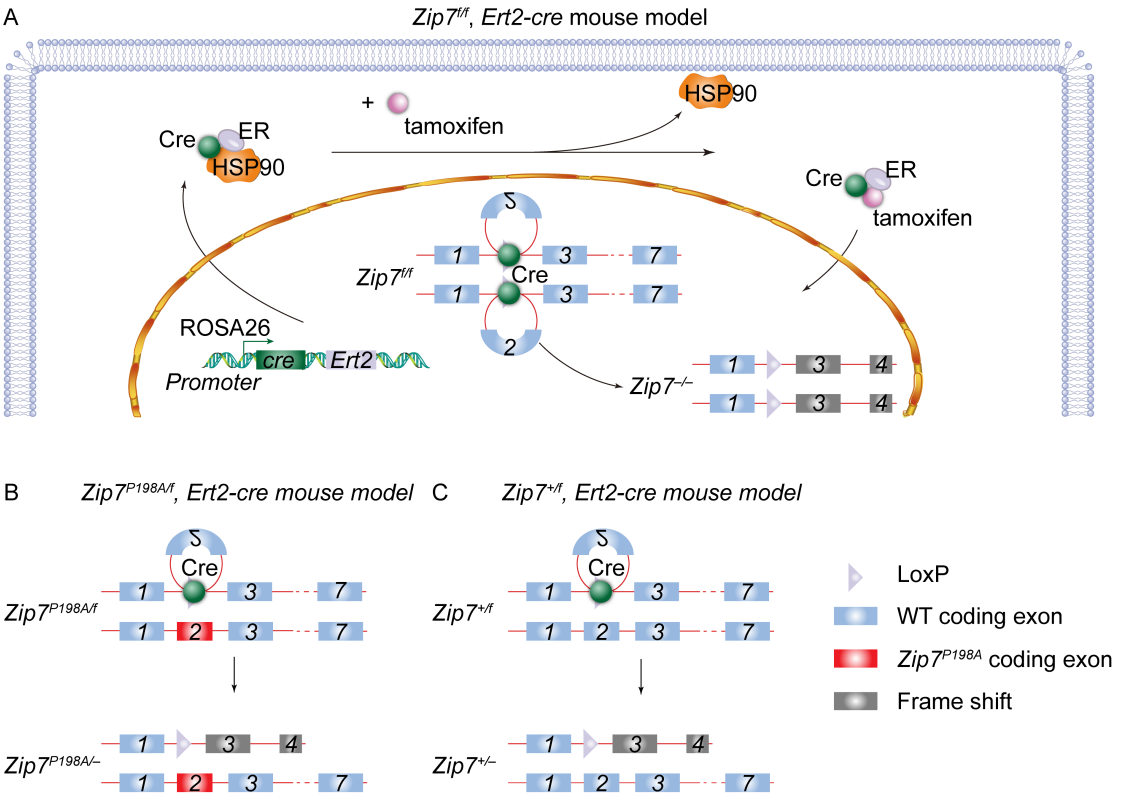

Figure 3-1: Conditional *Zip7* knockout strategies using the tamoxifen-inducible *Ert2-cre* system.
Tamoxifen administration releases Cre–ERT2 from HSP90-mediated cytoplasmic retention[325,326], enabling nuclear translocation and loxP-mediated deletion of *Zip7* exon 2. Shown are expected recombination outcomes in three genotypes: (A) $Zip7^{f/f}$, (B) $Zip7^{P198A/f}$, and (C) $Zip7^{+/f}$ mice carrying the *Ert2-cre* transgene. Cre, Cre recombinase; *Ert2*, mutated ligand-binding domain of the human estrogen receptor; HSP90, heat shock protein 90.

Once tamoxifen has been administered to mice with transplanted BM, three things can happen: 1) at the DNA level, the increasing level of Cre recombinase triggers the deletion of *Zip7* floxed fragments; 2) at the protein level, *de novo* synthesis of intact ZIP7 protein ceases. In the $Zip7^{P198A/f}$ *Ert2-cre* group, the balance may shift towards a relatively greater proportion of mutant ZIP7 protein, whereas in the $Zip7^{f/f}$ *Ert2-cre* group, total ZIP7 protein levels are expected to decline further, as no functional allele remains; 3) at the cellular level, as previously produced intact ZIP7 is depleted or diluted during cell division, cells begin to present a ZIP7-deficient phenotype.

In germline mutagenesis models, mice with at least one intact allele of Zip7 exhibit normal immunological phenotypes[20]. In the *Zip7*^{f}-based inducible models, *Zip7*$^{+/+}$ *Ert2-cre*, *Zip7*$^{+/f}$ *Ert2-cre*, *Zip7*$^{f/f}$ (without Cre) mice treated with Tamoxifen presented some differences in lymphocyte subtype percentages, likely due to individual variability and minor adjustments in FACS staining panels. However, the absolute cell numbers remained consistent across these models (Supplementary Figure 1). Importantly, these variations were negligible compared to the phenotypes observed in *Zip7*$^{f/f}$ *Ert2-cre* and *Zip7*$^{P198A/f}$ *Ert2-cre* models. Therefore, in subsequent experiments, *Zip7*$^{+/+}$ *Ert2-cre*, *Zip7*$^{+/f}$ *Ert2-cre*, *Zip7*$^{f/f}$ (without Cre) mice were used as controls, depending on the experimental context. For visual clarity, control groups are shown in grey across all figures, with the specific control used indicated in each figure legend.

Given that the long-term B cell developmental block in *Zip*$^{P198A/P198A}$ mice results in a profound loss of B cells from the pre-B stage onwards[20], it is reasonable to assume that fewer B cells will be recovered from mice with more severe genotypes (*Zip7*$^{P198A/–}$ and *Zip7*$^{–/–}$) if interrogated too long after Tamoxifen treatment. Therefore, the first question was: at what time point should samples be collected during this dynamic process? Ideally, it should be within a time window wherein *Zip7* has been deleted in the majority of cells, and only minimal amounts of residual intact ZIP7 protein are present in cells, such that peripheral lymphocyte subtypes presenting a ZIP7-deficient phenotype can be recovered at comparable cell numbers across the experiment groups (*Zip7*$^{+/f}$ *Ert2-cre*, *Zip7*$^{P198A/f}$ *Ert2-cre* and *Zip7*$^{f/f}$ *Ert2-cre*).

To address this concern, knockout efficiency was evaluated following tamoxifen treatment. The protocol suggested by the Jackson Laboratory for induction of Cre in adult C57BL/6 mice was adopted as a starting point[327,328]. Accordingly, 75 mg/kg (body weight) Tamoxifen was administered daily by intraperitoneal injection for a defined number of days, followed by a 5- to 7-day waiting period after the last injection.

3.3 Validation of *Zip7* gene deletion

I examined first whether the Tamoxifen-inducible Cre-ERT2 could recognise the Zip7 *loxP* sites and delete the expected fragment. While the *Zip7* floxed allele was efficiently deleted with three to five doses of tamoxifen, followed by a period of 5- to 7-days post the last dose, the intact *Zip7*$^{f/f}$ allele was still detectable at very low levels at the end of the tamoxifen protocol (Figure 3-2). This likely reflects the presence of residual radio-resistant WT cells in the chimeras, such as irradiation-resistant T cells.

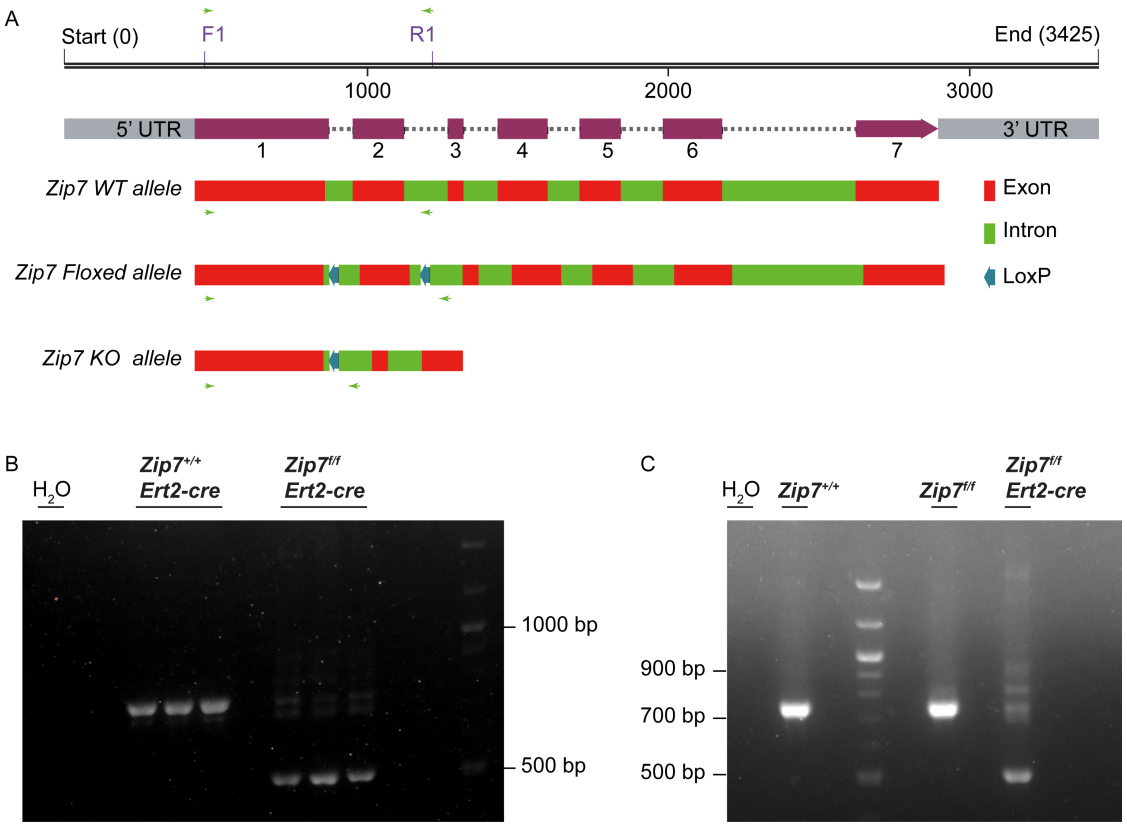

Figure 3-2: PCR-based assessment of *Zip7* floxed allele deletion in *Ert2-cre* mouse models.
(A) Schematic representation of the *Zip7* genomic locus and the primer positions used for genotyping. The upper panel shows the mouse *Zip7* reference sequence, with exons (maroon), introns (dashed lines), and untranslated regions (UTRs, grey). The genotyping primers (green arrows) span exon 1 (forward) and intron 2 (reverse), downstream of the 3' LoxP site. The lower panel illustrates three alleles: the WT allele, the floxed allele (containing two LoxP sites flanking exon 2, +68 bp), and the KO allele (with exon 2 deleted), resulting in a frameshift and premature stop codon. Expected PCR products are:

WT (753 bp), floxed (821 bp), and KO (513 bp). (B) Deletion efficiency in non-transgenic *Zip7*$^{+/+}$ *Ert2-cre* and *Zip7*$^{f/f}$ *Ert2-cre* single BM chimeras. Mice were treated with tamoxifen for 4 consecutive days, and splenic genomic DNA (gDNA) was isolated on Day 10 post-treatment. The 'H_2O' lane is a no-template control containing primers only. (C) Deletion efficiency in Ig-tg *Zip7*$^{f/f}$ and Ig-tg *Zip7*$^{f/f}$ *Ert2-cre* single BM chimeras. Mice received 3 daily doses of tamoxifen, and spleens were harvested on Day 5 after the final injection. A sample from an Ig-tg *Zip7*$^{+/+}$ mouse was used as a WT reference control. UTR, untranslated region; gDNA, genomic DNA.

3.4 Impact of ZIP7 deficiency on B and T cell subtype cellularity

To examine how different degrees of ZIP7 deficiency affect lymphocyte subsets, I generated *Zip7*$^{f/f}$ *Ert2-cre* and *Zip7*$^{P198A/f}$ *Ert2-cre* BM chimeras. Unless otherwise stated, all results in this section derive from the following setup: BM from CD45.2$^+$ donor mice was transplanted into lethally irradiated CD45.1$^+$ WT recipients. After eight weeks of reconstitution, the recipients received five doses of tamoxifen, and tissues were collected one week later. Phenotypes were analysed in BM B cells, splenic B cells, thymocytes, and splenic T cells.

The data presented below are from *Zip7*$^{+/f}$ *Ert2-cre*, *Zip7*$^{P198A/f}$ *Ert2-cre*, and *Zip7*$^{f/f}$ *Ert2-cre* chimeras, some of which were also used for single-cell RNA sequencing (see Chapter 6).

3.4.1 ZIP7 deficiency impairs B-cell development from early to immature stages in the BM

B cells with one intact *Zip7* allele, whether paired with a point mutation (*Zip7*$^{P198A/+}$) or a deletion (*Zip7*$^{+/–}$), undergo normal B cell development in the BM[20]. I sought to investigate the consequences of ablating the remaining intact allele in these settings (*Zip7*$^{P198A/–}$ or *Zip7*$^{–/–}$). The hypothesis was that the loss of the WT allele, combined with a mutation or deletion, would exacerbate the phenotype of the previously reported

Zip7$^{P198A/P198A}$ allele[20], either by disrupting a prior developmental stage or by causing a more pronounced reduction at specific stages.

BM B cells were gated into Hardy Fractions[41,42] to assess the development at each stage (Figure 3-3A). Due to the relatively small number of cells in Fractions B and C, contamination from the larger CD43$^-$ population could potentially mask their true phenotypes. To address this, I applied an IgM$^-$ IgD$^-$ gate before gating the CD43$^+$ population to exclude cells beyond the late-pre-B stage (Supplementary Figure 2).

Zip7$^{P198A/f}$ and *Zip7*$^{f/f}$ *Ert2-cre* BM recipients exhibited a decreased ability to sustain early-stage B cell development. Notably, these mice demonstrated a significantly diminished capacity to maintain late pre-B cells and immature B cells. The proportion of late pre-B cells dropped to 0.43% (95% CI: 0.03–0.83%) in *Zip7*$^{P198A/f}$ *Ert2-cre* and 0.22% (95% CI: 0.08–0.35%) in *Zip7*$^{f/f}$ *Ert2-cre*, compared to 3.22% (95% CI: 2.42–4.01%) in *Zip7*$^{+/f}$ *Ert2-cre* controls. Similarly, immature B cells were reduced to 0.07% in both deficient groups versus 1.55% (95% CI: 1.21–1.90%) in controls. A slight decline was also observed in recirculating B cells, likely reflecting impaired replenishment from upstream proliferating stages (Figure 3-3B, C).

Taken together, while B cells with one intact *Zip7* allele can sustain normal BM development, *Zip7*$^{P198A/f}$ and *Zip7*$^{f/f}$ *Ert2-cre* mice exhibit a marked developmental disadvantage from early stages, which becomes more pronounced in the late pre-B to immature B cells stages.

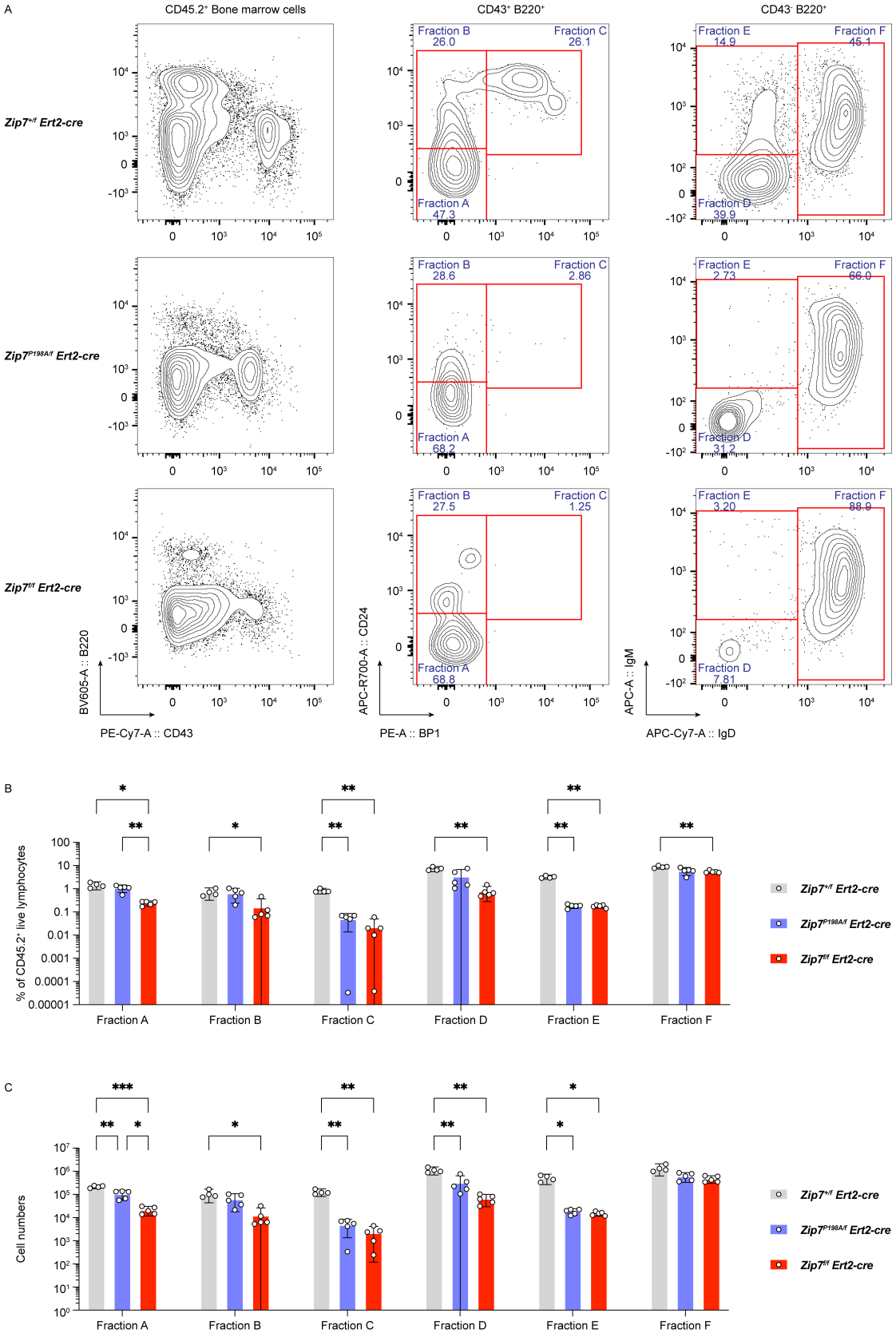

Figure 3-3: ZIP7 deficiency impairs B cell development in the BM.
(A) Representative flow cytometry plots showing Fractions A-F from CD45.2$^+$ BM cells in the *Zip7*$^{+/-}$, *Zip7*$^{P198A/-}$, and *Zip7*$^{-/-}$ chimeric models, based on the gating strategy depicted in Supplementary Figure 2. (B) Percentage and (C) absolute number of CD45.2$^+$

B-lineage cells in Fractions A–F. Each dot represents an individual mouse (n = 4–5 per group). Bars indicate mean ± 95% CI. Statistical analysis using mixed-effects analysis followed by Tukey's multiple comparisons test.

3.4.2 ZIP7 deficiency causes progressive loss of splenic transitional and MZ B cells

To evaluate whether ZIP7-deficient B cells are maintained in the periphery, I analysed splenic B cell subsets in chimeric mice using flow cytometry (Supplementary Figure 3).

In mice reconstituted with *Zip7*$^{P198A/f}$ *Ert2-cre* or *Zip7*$^{f/f}$ *Ert2-cre* BM, significantly fewer transitional B cells were recovered from the spleen, consistent with the reduced numbers of immature B cells observed in the BM (Figure 3-4). While the percentage of follicular B cells appeared relatively increased, their absolute number was reduced along with the overall peripheral B cell count (Figure 3-4B, C).

After 12 days of tamoxifen induction, the *Zip7*$^{P198A/f}$ *Ert2-cre* group exhibited a noticeable loss of MZ B cells, whereas the *Zip7*$^{f/f}$ *Ert2-cre* group maintained their MZ B cell levels (Figure 3-4). However, following a 14-day induction period, the *Zip7*$^{f/f}$ *Ert2-cre* group also displayed a significant reduction in MZ B cells, alongside a decrease in follicular B cells (Figure 3-5).

In summary, both ZIP7-deficient models had fewer transitional B cells in spleen. Interestingly, the loss of *Zip7*$^{P198A/–}$ MZ B cells was observed at an earlier time point than that of *Zip7*$^{–/–}$ MZ B cells. Further investigation is needed to determine whether the decline of MZ B cells in the *Zip7*$^{f/f}$ *Ert2-cre* group is due to the overall greater loss of spleen cells under prolonged induction or due to a MZ-specific requirement for ZIP7.

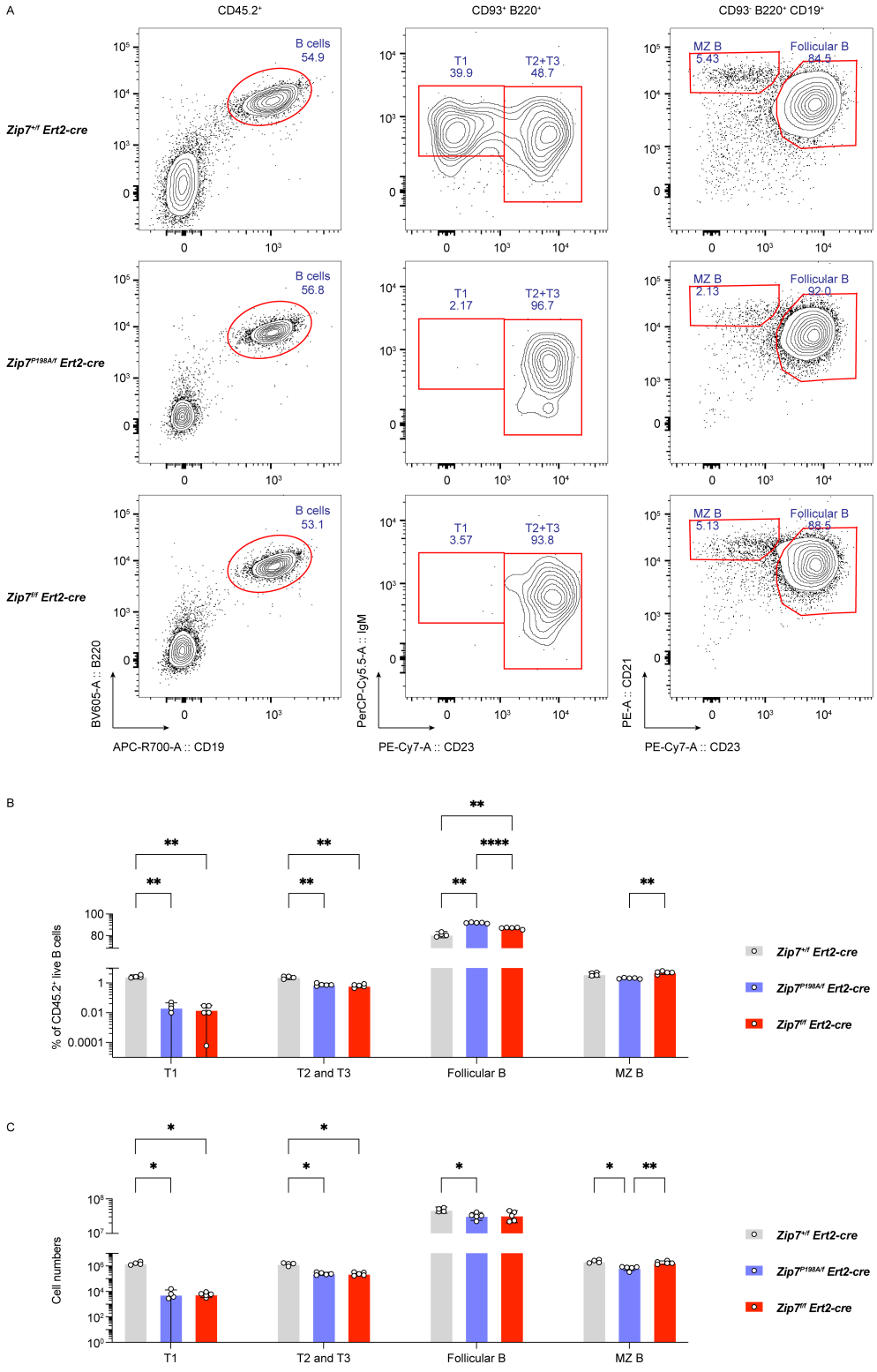

Figure 3-4: ZIP7 deficiency alters splenic B cell subpopulations.
(A) Representative flow cytometry plots showing splenic B cell subsets in *Zip7*$^{+/f}$ *Ert2-cre*, *Zip7*$^{P198A/f}$ *Ert2-cre* and *Zip7*$^{f/f}$ *Ert2-cre* chimeric mice, analysed seven days after tamoxifen treatment. CD45.2^{+} donor B cells were classified into transitional (T1, T2+T3), follicular, and MZ B cell subsets. (B) Proportions of each B cell subtype among CD45.2^{+} live splenic B cells. (C) Corresponding absolute cell numbers. Bars represent group means with 95% CIs (n = 4–5 mice per group). Statistical comparisons were made using mixed-effects analysis with Tukey's post-test.

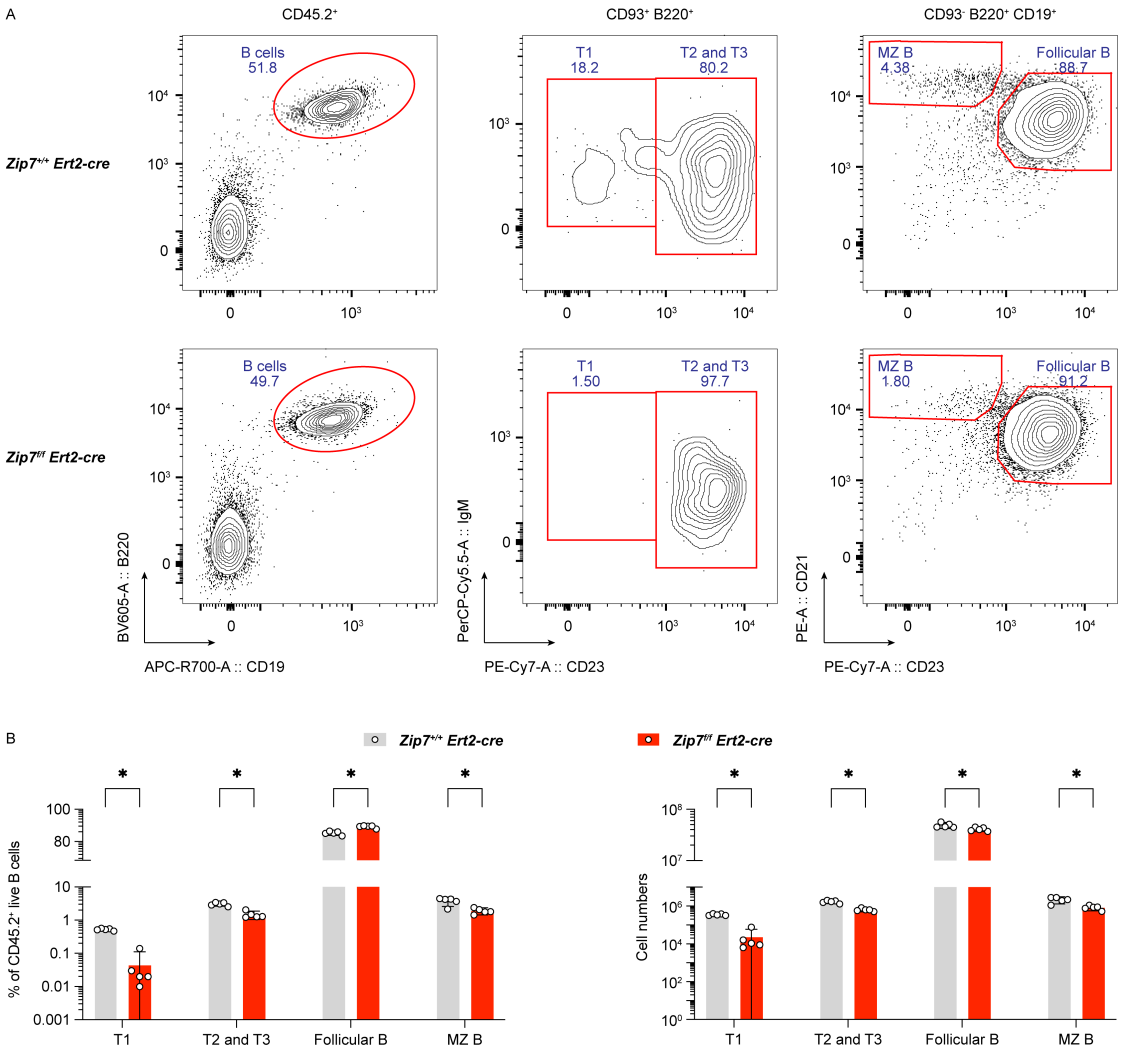

Figure 3-5: Prolonged ZIP7 deficiency leads to a reduction in splenic MZ B cells.
(A) Representative flow cytometry plots showing B cell subtypes (T1, T2+T3, Follicular B and MZ B cells) in the spleen of *Zip7*$^{+/+}$ *Ert2-cre* and *Zip7*$^{f/f}$ *Ert2-cre* single-BM recipient mice. These mice received four doses of tamoxifen, followed by a 10-day waiting period before sample collection. (B) Quantification of the percentage (left panel) and absolute cell numbers (right panel) of splenic B cell subsets. Each dot represents data from an individual mouse and results are presented as mean ± 95% CI. Statistical analysis was performed using unpaired *t* test with Welch's correction, followed by Holm-Šídák's multiple comparisons test.

3.4.3 ZIP7 deficiency impairs early-stage proliferating thymocytes while sparing more mature single-positive thymocytes

To assess the impact of varying degrees of ZIP7 deficiency on thymocyte subsets, I analysed thymus subsets in tamoxifen-treated *Zip7*$^{P198A/f}$ *Ert2-cre* and *Zip7*$^{f/f}$ *Ert2-cre* BM

chimeras (Supplementary Figure 4). Compared with *Zip7*$^{+/f}$ *Ert2-cre* group (Figure 3-6) and other controls such as *Zip7*$^{+/+}$ *Ert2-cre* or *Zip7*$^{f/f}$ (Supplementary Figure 1), which retained an intact thymus after tamoxifen treatment, the thymus from *Zip7*$^{P198A/f}$ *Ert2-cre* and *Zip7*$^{f/f}$ *Ert2-cre* chimeras appeared markedly shrunken and were barely visible upon gross examination, especially in the *Zip7*$^{f/f}$ *Ert2-cre* group. This gross reduction in thymic mass corresponded to a significant drop in total thymocyte numbers across all subsets (Figure 3-6C).

The most substantial loss was observed in the DP cells. While these cells accounted for 92-94% (95% CI) of thymocytes in the *Zip7*$^{f/+}$ *Ert2-cre* control group, they were reduced to 55-60% in *Zip7*$^{P198A/f}$ *Ert2-cre* and to 13-18% in *Zip7*$^{f/f}$ *Ert2-cre* groups. Specifically, the proportion of DP1 and DP2 cells was significantly lower in both ZIP7-deficient groups, with a more pronounced reduction in the *Zip7*$^{f/f}$ *Ert2-cre* group. In contrast, thymocytes beyond the DP3 stage, including SP thymocytes, showed a relative increase in these models, suggesting that while ZIP7 deficiency has a more profound effect on the early DP stages, it does not completely block the maturation and maintenance of SP thymocytes.

The early thymocyte developmental profile in ZIP7-deficient BM chimeras suggests that the transition from DN to DP stages is hindered. While the *Zip7*$^{P198A/f}$ *Ert2-cre* chimeras had increased proportions of DN1-DN4 cells compared to the control (Figure 3-6), the total cell count across these subsets was reduced. In the *Zip7*$^{f/f}$ *Ert2-cre* group, the effect was even more pronounced, with a marked increase in the proportion of DN1 cells but a significant reduction from DN2 onwards, with a corresponding loss of cells across all the DN subsets.

Taken together, ZIP7 is essential for early thymocyte development and for maintaining DP thymocytes. In contrast, its deficiency has a more moderate impact on mature

quiescent SP thymocytes, suggesting that the demand for ZIP7 is greater in the proliferative thymocytes.

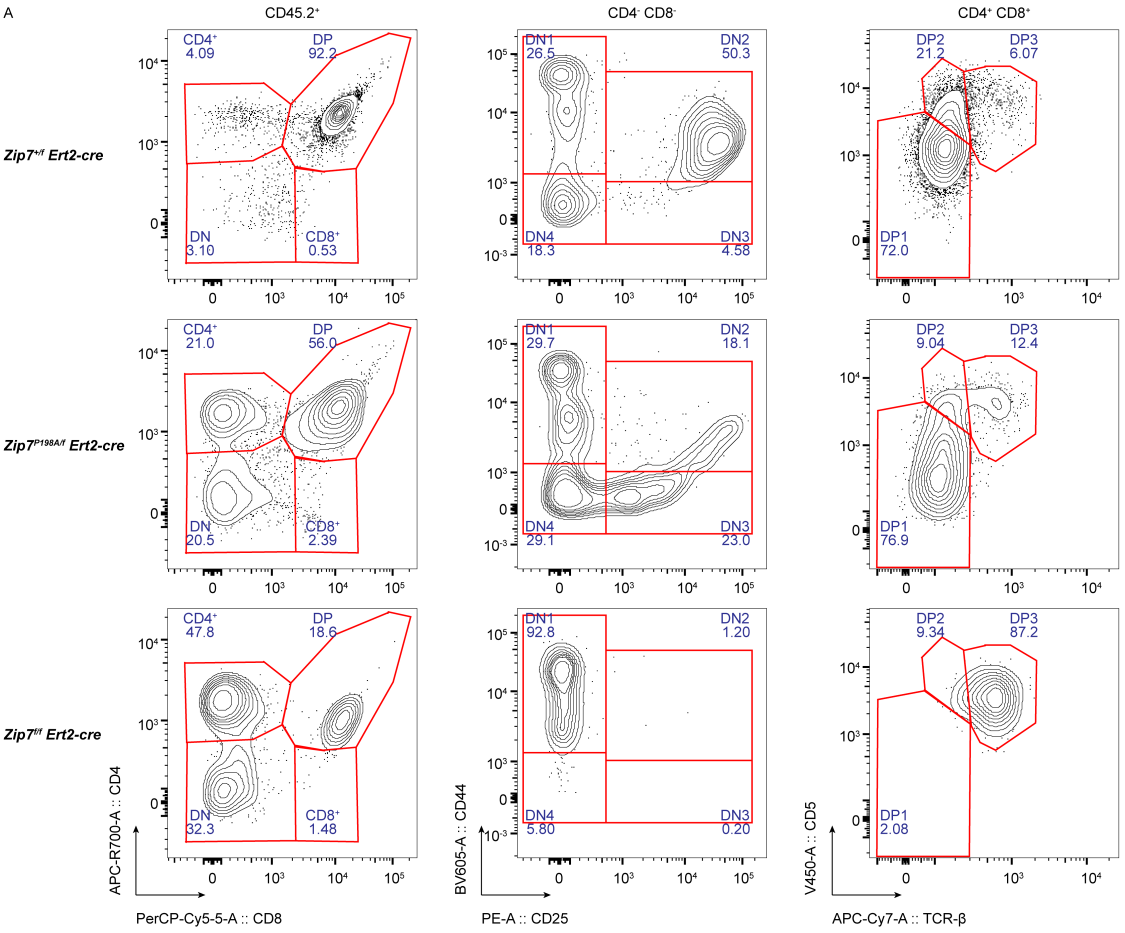
A
CD45.2+
CD4- CD8-
CD4+ CD8+
Zip7+/f Ert2-cre
Zip7P198A/f Ert2-cre
Zip7f/f Ert2-cre
CD4+ 4.09
DP 92.2
DN 3.10
CD8+ 0.53
DN1 26.5
DN2 50.3
DN4 18.3
DN3 4.58
DP2 21.2
DP3 6.07
DP1 72.0
CD4+ 21.0
DP 56.0
DN 20.5
CD8+ 2.39
DN1 29.7
DN2 18.1
DN4 29.1
DN3 23.0
DP2 9.04
DP3 12.4
DP1 76.9
CD4+ 47.8
DP 18.6
DN 32.3
CD8+ 1.48
DN1 92.8
DN2 1.20
DN4 5.80
DN3 0.20
DP2 9.34
DP3 87.2
DP1 2.08
APC-R700-A :: CD4
PerCP-Cy5-5-A :: CD8
BV605-A :: CD44
PE-A :: CD25
V450-A :: CD5
APC-Cy7-A :: TCR-β

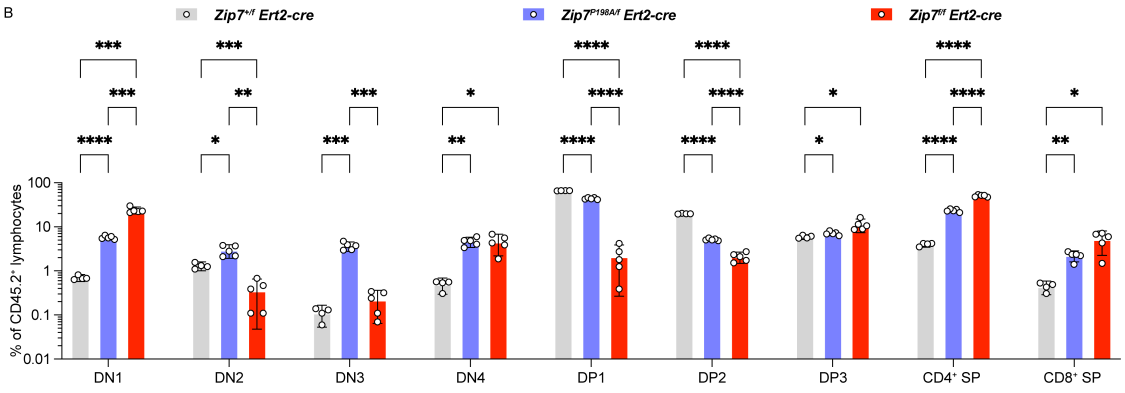
B
Zip7+/f Ert2-cre
Zip7P198A/f Ert2-cre
Zip7f/f Ert2-cre
% of CD45.2+ lymphocytes
DN1
DN2
DN3
DN4
DP1
DP2
DP3
CD4+ SP
CD8+ SP

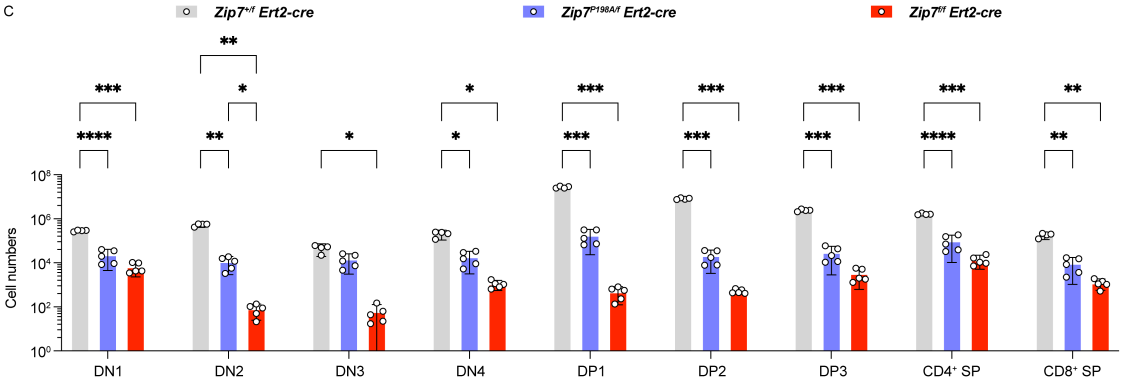
C
Zip7+/f Ert2-cre
Zip7P198A/f Ert2-cre
Zip7f/f Ert2-cre
Cell numbers
DN1
DN2
DN3
DN4
DP1
DP2
DP3
CD4+ SP
CD8+ SP

Figure 3-6: ZIP7 deficiency impairs early thymocyte development but spares mature single-positive cells.
(A) Representative flow cytometry plots showing CD45.2$^+$ donor-derived thymocytes at distinct developmental stages in *Zip7*$^{+/f}$, *Zip7*$^{P198A/f}$ and *Zip7*$^{f/f}$ *Ert2-cre* chimeras. Mice were analysed one week after tamoxifen induction. (B, C) Quantification of the percentage (B) and absolute numbers (C) of CD45.2$^+$ thymocytes at each stage. Each dot represents an individual mouse. Data are shown as mean with 95% CI, with each dot representing an individual mouse. Statistical significance was determined using mixed-effects analysis with Tukey's multiple comparisons test.

3.4.4 ZIP7 deficiency impairs splenic T cell memory subsets while sparing naïve T cells

Given that SP thymocytes were more resilient to ZIP7 loss, I next examined splenic T cell populations by flow cytometry (Supplementary Figure 5).

CD4$^+$ effector memory (EM) T cells and CD4$^+$ central memory (CM) T cells were reduced in both ZIP7-deficient groups compared to the *Zip7*$^{+/f}$ *Ert2-cre* controls (Figure 3-7B, C). Numbers of CD8$^+$ EM T cells were higher in *Zip7*$^{P198A/f}$ *Ert2-cre* than *Zip7*$^{f/f}$ *Ert2-cre* mice, though neither was significantly different from WT controls. This suggests that the mutated ZIP7 protein in the *Zip7*$^{P198A/f}$ *Ert2-cre* model retains partial function that may support CD8$^+$ memory T cell maintenance. In contrast, naïve T cells in both CD4$^+$ and CD8$^+$ subsets were unaffected, indicating that these quiescent T cells are less dependent on ZIP7 for their maintenance (Figure 3-7).

In summary, ZIP7 is essential for maintaining splenic T cell memory subsets, particularly CD4$^+$ memory T cell subsets.

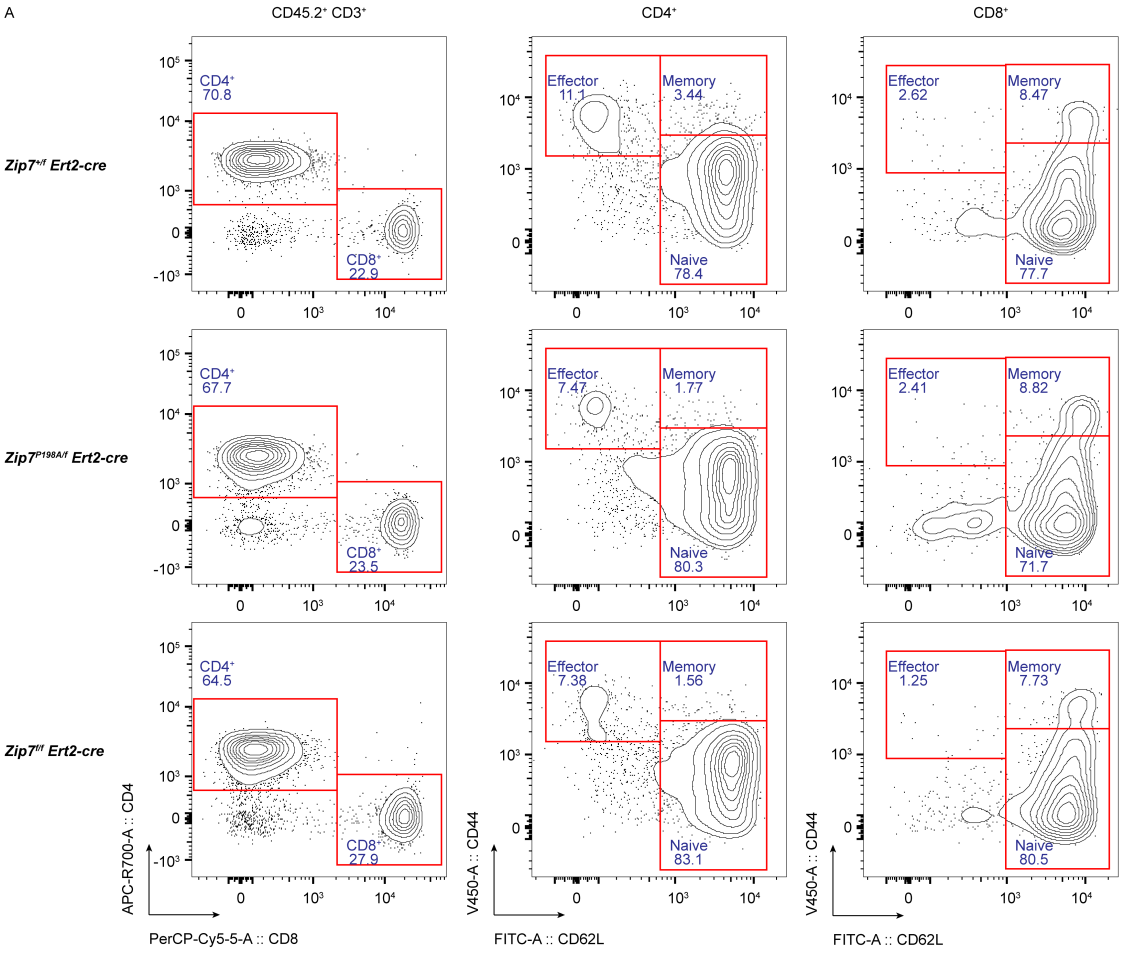
A
CD45.2+ CD3+
CD4+
CD8+
Zip7+/f Ert2-cre
Zip7P198A/f Ert2-cre
Zip7f/f Ert2-cre
CD4+ 70.8
CD8+ 22.9
Effector 11.1
Memory 3.44
Naive 78.4
Effector 2.62
Memory 8.47
Naive 77.7
CD4+ 67.7
CD8+ 23.5
Effector 7.47
Memory 1.77
Naive 80.3
Effector 2.41
Memory 8.82
Naive 71.7
CD4+ 64.5
CD8+ 27.9
Effector 7.38
Memory 1.56
Naive 83.1
Effector 1.25
Memory 7.73
Naive 80.5
APC-R700-A :: CD4
PerCP-Cy5-5-A :: CD8
V450-A :: CD44
FITC-A :: CD62L
V450-A :: CD44
FITC-A :: CD62L

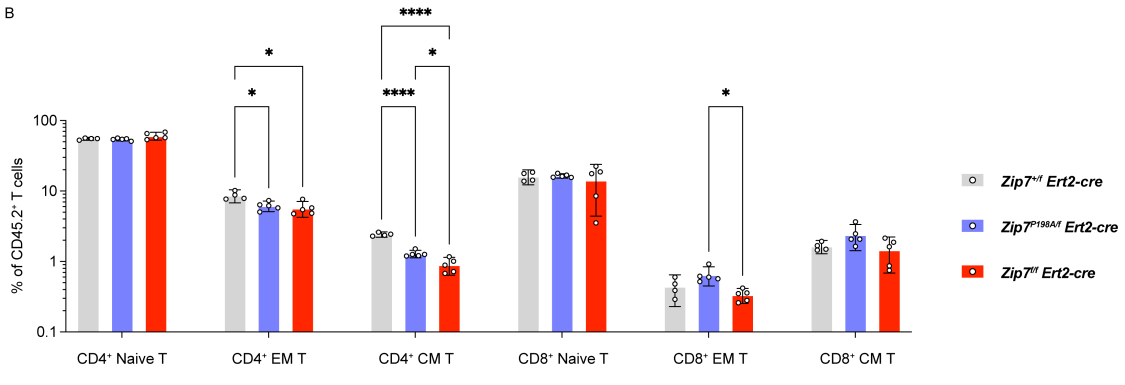
B
% of CD45.2+ T cells
CD4+ Naive T
CD4+ EM T
CD4+ CM T
CD8+ Naive T
CD8+ EM T
CD8+ CM T
Zip7+/f Ert2-cre
Zip7P198A/f Ert2-cre
Zip7f/f Ert2-cre

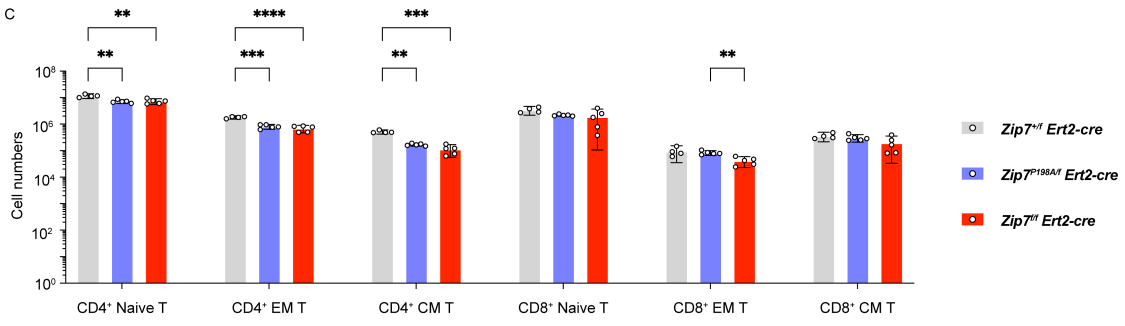
C
Cell numbers
CD4+ Naive T
CD4+ EM T
CD4+ CM T
CD8+ Naive T
CD8+ EM T
CD8+ CM T
Zip7+/f Ert2-cre
Zip7P198A/f Ert2-cre
Zip7f/f Ert2-cre

Figure 3-7: ZIP7 deficiency alters splenic T cell populations, impacting memory and effector subsets.
(A) Representative flow cytometry plots of CD45.2$^+$ donor-derived CD4$^+$ and CD8$^+$ T cells, showing naïve (CD62L$^+$ CD44$^–$), central memory (CD62L$^+$ CD44$^+$) and effector memory (CD62L$^–$ CD44$^+$) subsets in *Zip7*$^{+/f}$, *Zip7*$^{P198A/f}$ and *Zip7*$^{f/f}$ *Ert2-cre* chimeras. Samples were analysed one week after tamoxifen treatment. (B, C) Quantification of subset frequencies (B) and absolute cell numbers (C) within the CD45.2$^+$ T cells. Each dot represents one mouse (n = 4–5 per group). Data are shown as mean ± 95% CI. Statistical analysis was conducted using mixed-effects analysis followed by Tukey's multiple comparisons test.

3.5 Cell-intrinsic requirement for ZIP7 in B and T cell maintenance

To assess whether the loss of specific B and T cell subsets was cell-intrinsic, I generated mixed BM chimeras by transplanting a 1:1 mixture of CD45.2$^+$ ZIP7 WT or ZIP7-deficient BM cells and CD45.1$^+$ or CD45.1/2$^+$ WT internal control BM cells into lethally irradiated CD45.1$^+$ recipients. After 8 weeks of reconstitution, the mice received three or five doses of tamoxifen to induce ZIP7 deletion within hematopoietic cells. Samples were collected at least one week after the final tamoxifen dose.

3.5.1 Cell-intrinsic requirement for ZIP7 during early B cell development

To examine the impact of ZIP7 deficiency on early B cell development, I generated mixed BM chimeras using CD45.2$^+$ *Zip7*$^{P198A/f}$ *Ert2-cre* cells or its Cre-free control (*Zip7*$^{P198A/f}$), mixed at a 1:1 ratio with CD45.1$^+$ WT BM. Comparable donor proportions were confirmed at baseline by gating on B220$^+$ CD19$^+$, B220$^+$ CD43$^+$ and B220$^+$ CD43$^–$ cells (Supplementary Figure 6).

Following tamoxifen treatment, by gating for different BM fractions, I separated CD45.2$^+$ cells from their WT CD45.1$^+$ counterparts to evaluate their relative proportions within each developmental stage (Supplementary Figure 7). Comparative analysis of the chimeras revealed a progressive loss of ZIP7-deficient cells across B cell developmental stages. While WT CD45.2$^+$ *Zip7*$^{P198A/f}$ cells made up over 75% of each BM fraction,

CD45.2$^+$ *Zip7*$^{P198A/f}$ *Ert2-cre* cells were progressively lost through the BM B cell developmental stages. A slight decrease was observed in the Pro-B stage (Fraction B), but this loss became more noticeable from the large pre-B (Fraction C+C') to newly formed B cells (Fraction E), with most of these cells dropping below 25% (Figure 3-8A). These results confirm the increasing vulnerability of Pro-B to immature B cells to ZIP7 deficiency, consistent with single-BM transplanted chimeras.

Whether ZIP7 deletion via *Ert2-cre* affects even earlier stages such as HSCs remains unclear. I considered assessing mouse HSCs[329,330] by canonical markers like lin$^-$, CD150$^+$, Sca1$^+$, c-Kit$^+$, CD34$^-$, Flk2$^-$, and CD48$^-$. However, the scarcity of HSCs in the BM made it difficult to sort cells in sufficient numbers to evaluate *Zip7* deletion efficiency and its early impact on HSCs. As an alternative, I transferred ZIP7-deficient BM into secondary recipients, hypothesizing that if early progenitors were compromised, their capacity to generate and differentiate would be diminished. Since the two chimeric mice chosen as secondary donors were treated with Tamoxifen, the ratio of CD45.2$^+$ to CD45.1$^+$ cells in Fraction A in WT4 and KO4 (see samples marked with an asterisk in Figure 3-8A) were 70.10% to 28.90% and 70.60% to 29.40%, respectively. The KO4 is one of the samples that presented a significant loss from Fraction C to Fraction E of CD45.2$^+$ cells. In the secondary recipient mice, three out of five mice displayed decreases across all the fractions (Figure 3-8B); however, two mice retained around 75% CD45.2$^+$ cells, similar to their control *Zip7*$^{P198A/f}$ counterpart. A possible explanation is that some HSC function is partially maintained in the absence of ZIP7, or more likely, a fraction of HSCs from the secondary donors did not delete *Zip7* and were able to reconstitute the BM B cell niche.

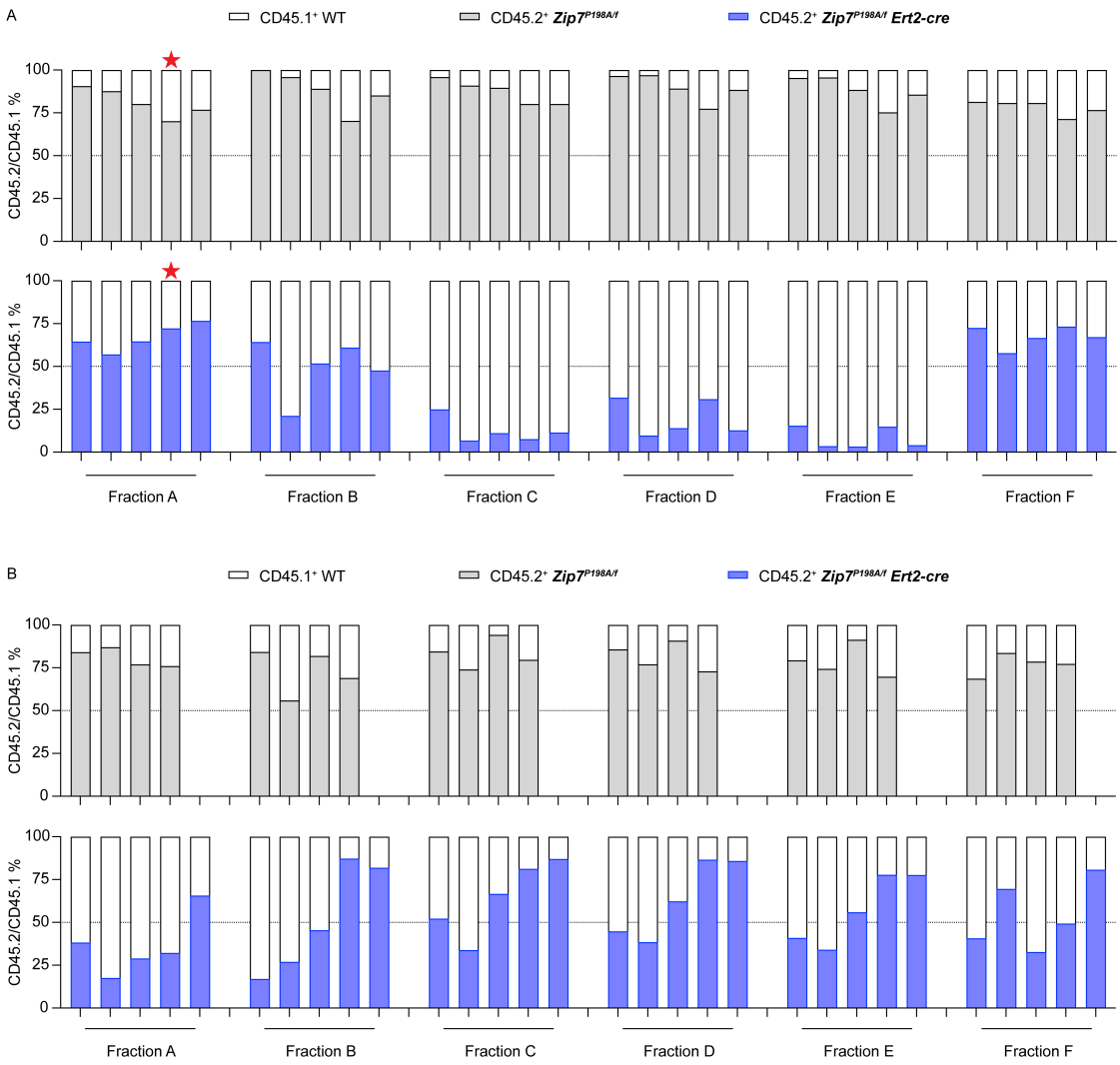

Figure 3-8: Progressive B cell loss in *Zip7*$^{P198A/f}$ *Ert2-cre* chimeras and its maintenance in secondary recipients.
(A) *Zip7*$^{P198A/f}$ *Ert2-cre* BM cells presented noticeable decreases from Fraction C to Fraction E. The stars on the Fraction A mark the individual mice (WT4 and KO4) selected as donors for secondary BM transplantation. (B) BM B cell profiles in secondary recipients reconstituted with BM from WT4 or KO4. Bars indicate relative frequencies of each Hardy Fraction, based on gating in Supplementary Figure 7. CD45.2$^+$ cells represent either WT or ZIP7-deficient donor cells (shaded), and CD45.1$^+$ cells represent internal WT competitors (white). Dashed lines indicate the original CD45.2:CD45.1 donor ratio before transplantation. Each bar represents one mouse (n = 5 per group).

Given that the compound *Zip7*$^{P198A/–}$ model exhibited earlier deficits during BM B cell development compared to the block observed in *Zip7*$^{P198A/P198A}$, I investigated whether varying tamoxifen dosage and timing could reveal differential effects on the phenotypes in *Zip7*$^{f/f}$ *Ert2-cre* mice. On the eighth day after the last treatment, *Zip7*$^{f/f}$ *Ert2-cre* chimeric mice treated with three-doses tamoxifen displayed a significant

reduction in B cell fractions, particularly between Fraction B and Fraction E. This reduction was less evident on day 3, suggesting a progressive effect over time (Figure 3-9A, B). In addition, when *Zip7$^{f/f}$ Ert2-cre* mixed chimeras were treated with a higher tamoxifen dose and given a longer induction period, severe B cell loss occurred, with some mice showing less than 20% CD45.2^{+} donor cells, despite the CD45.2^{+}:CD45.1^{+} mixed chimeras originally being set up at a 60:40 ratio (Figure 3-9C).

In conclusion, the mixed BM chimeras reaffirmed that Fractions B through E are particularly susceptible to sustained ZIP7 deficiency in a cell intrinsic manner, in agreement with findings from the single-BM transplanted models.

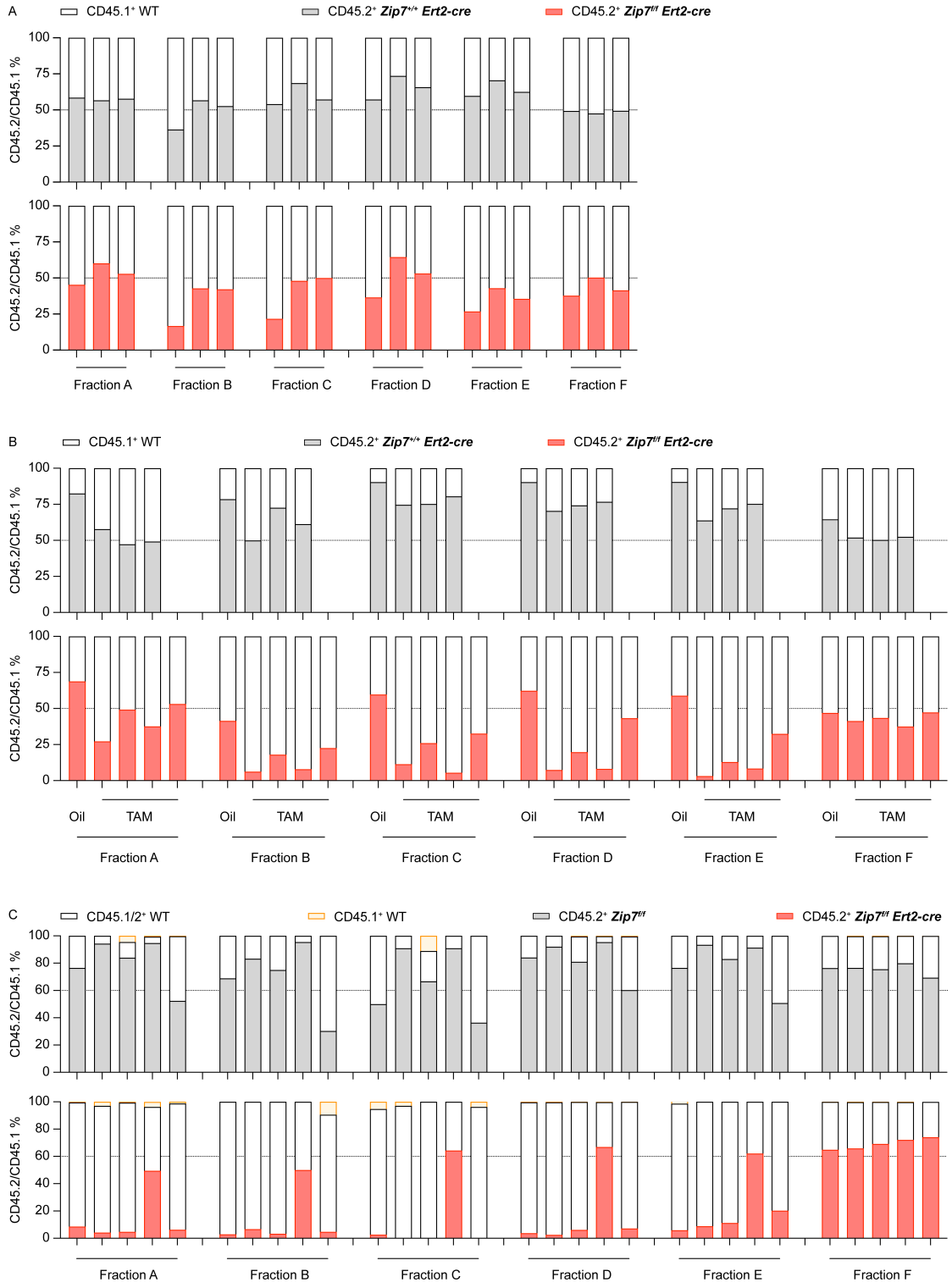

Figure 3-9: Complete knockout *Zip7* presented a noticeable loss of BM B cells from Fraction B to E.

(A-C) *Zip7*$^{f/f}$ *Ert2-cre* chimeric mice and their controls were treated with three doses of tamoxifen and then analysed three days later (A) or eight days later (B), or were treated with five doses of tamoxifen and analysed 13 days post the last dose (C). Each bar represents one mouse, with the filled bars indicating the proportions of CD45.2$^+$ WT or ZIP7-deficient cells and the white bars indicating the CD45.1/2$^+$ internal WT controls. The dashed lines indicate the ratio of CD45.2$^+$ to CD45.1/2$^+$ cells in the donor mixture

prior to transplantation. In Panel B, "TAM" denotes tamoxifen treatment, while "Oil" indicates vehicle-only control; this abbreviation is used consistently throughout the related figures. In Panel C, orange-outlined bars represent residual CD45.1$^+$ recipient-derived thymocytes, which were excluded from comparative analyses.

3.5.2 Intrinsic role of ZIP7 in the progressive loss of MZ B cells under prolonged deficiency

To further explore the impact of ZIP7 deficiency on peripheral B cell subsets in a competitive environment, I extended the analysis to mixed-BM transplanted chimeras, examining B cell subpopulations in the spleen and MLNs by flow cytometry (Supplementary Figure 8). For both *Zip7*$^{P198A/f}$ *Ert2-cre* and *Zip7*$^{f/f}$ *Ert2-cre* chimeras, tamoxifen was administered in five doses, followed by tissue collection at day 7 and day 13 after the final injection, respectively (Figure 3-10A, B).

In agreement with findings from single-BM chimeras, ZIP7 deficiency in both *Zip7*$^{P198A/f}$ *Ert2-cre* and *Zip7*$^{f/f}$ *Ert2-cre* mixed chimeras led to a loss of transitional T1 and MZ B cells, while follicular B cells remained relatively unaffected (Figure 3-10A, B). The reduction in T1 cells is likely to be a downstream effect of the significant loss of immature B cells in the BM. The results highlight that, while follicular B cells are relatively preserved, MZ B cells are susceptible to reduced or absent ZIP7 in a cell-intrinsic manner, especially under prolonged deficiency conditions.

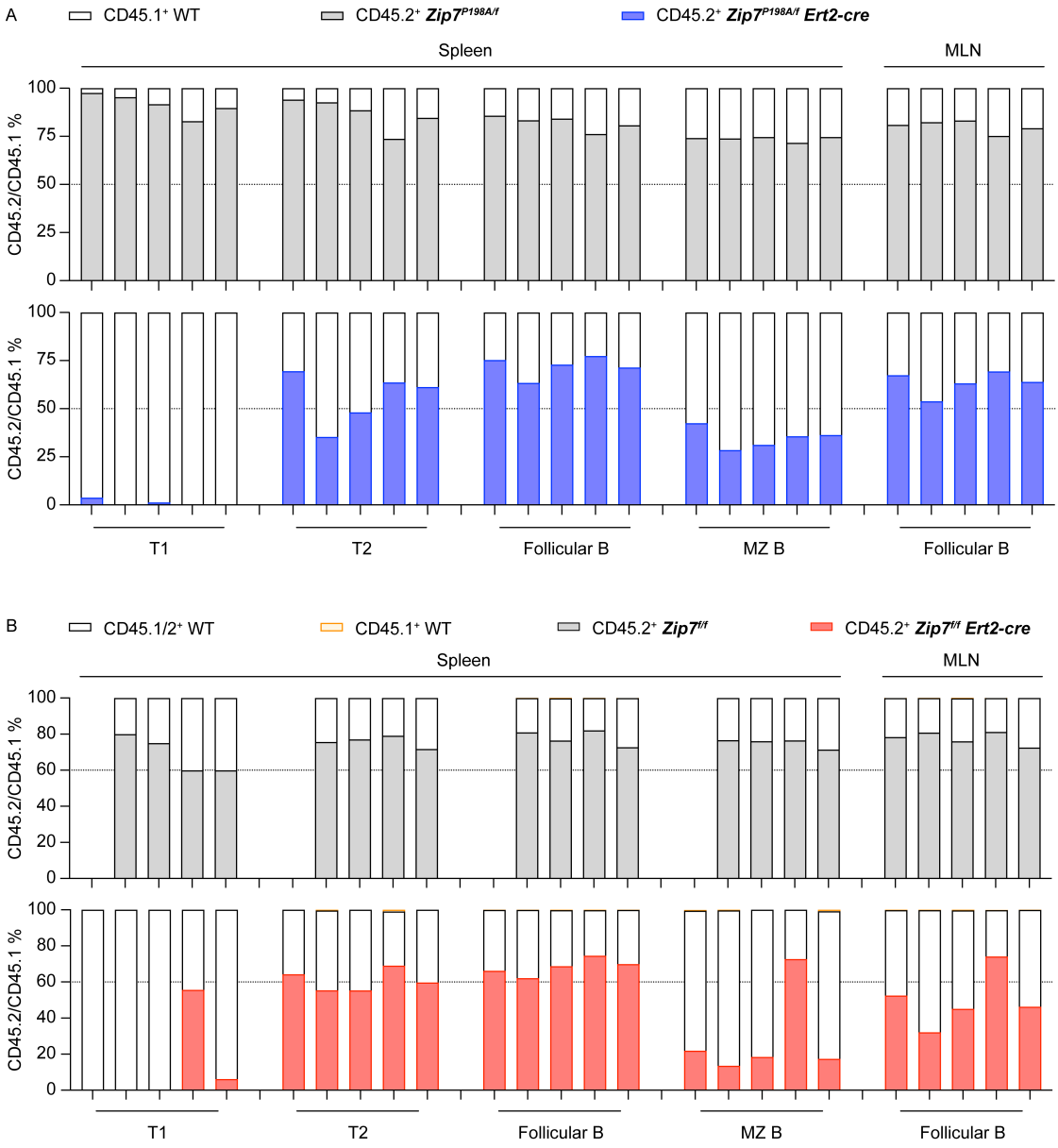

Figure 3-10: ZIP7 deficiencies lead to a reduction in peripheral T1 and MZ B cells. (A) Proportions of T1 and MZ B cells in the *Zip7*$^{P198A/f}$ *Ert2-cre* mice. *Zip7*$^{P198A/f}$ *Ert2-cre* mice were treated with five doses of tamoxifen and waited for seven days after the last dose. (B) *Zip7*$^{f/f}$ *Ert2-cre* mixed chimeras were treated with five doses of tamoxifen and then collected spleen and MLN samples on the 13th day. Each bar in the above charts represents a mouse, with the filled bars indicating the proportions of CD45.2^{+} WT or ZIP7-deficient cells and the white bars indicating the CD45.1/2^{+} internal WT controls. The dashed lines indicate the ratio of CD45.2^{+} to CD45.1/2^{+} cells in the donor mixture prior to transplantation.

3.5.3 Differential impact of ZIP7 loss on thymocyte stages in competitive chimeras

To test whether the cell-intrinsic effects of ZIP7 deficiency observed in single BM chimeras are recapitulated in a competitive environment, I analysed thymocyte development in mixed BM chimeras (Supplementary Figure 9). In these experiments, varying degrees of ZIP7 deficiency affected early T cell development. In *Zip7*$^{P198A/f}$ *Ert2-cre* mixed chimeras, the DN2 and DN3 stages retained a population of CD45.2^{+} donor cells, but a substantial reduction was observed in the DP1 and DP2 thymocytes (Figure 3-11A). This mirrors the findings in single-BM chimeras, where mutated ZIP7 could partially maintain thymocyte populations through the DN stages but faced challenges at the DP stages (Figure 3-6B). In the *Zip7*$^{f/f}$ *Ert2-cre* chimeras, reductions were observed across DN2 through DP stages, with only modest or variable effects on SP cells at this stage (Figure 3-11B). When ZIP7 deficiency was sustained for a longer duration, as in mice analysed at Day 13 post-tamoxifen (Figure 3-11C), further decreases were seen across DN2 to SP stages. However, whether the reduced contribution to CD4^{+} and CD8^{+} SP thymocytes reflects a direct requirement for ZIP7 at the SP stage or a secondary consequence of upstream developmental block remains uncertain. More targeted and sensitive experiments will be needed to determine whether ZIP7 deficiency differentially impacts CD8^{+} versus CD4^{+} thymocyte maturation or survival.

Taken together, the mixed chimeras confirmed that the DP1 and DP2 thymocytes are the most sensitive to ZIP7 deficiency. While the mutated form of ZIP7 in *Zip7*$^{P198A/f}$ *Ert2-cre* can partially support the maintenance of thymocytes in DN2 to DN4, the complete absence of ZIP7 severely impairs progression through these stages. Additionally, under prolonged ZIP7 deficiency, a reduction in SP thymocyte representation may occur, although this could be a downstream effect of defects in earlier precursors.

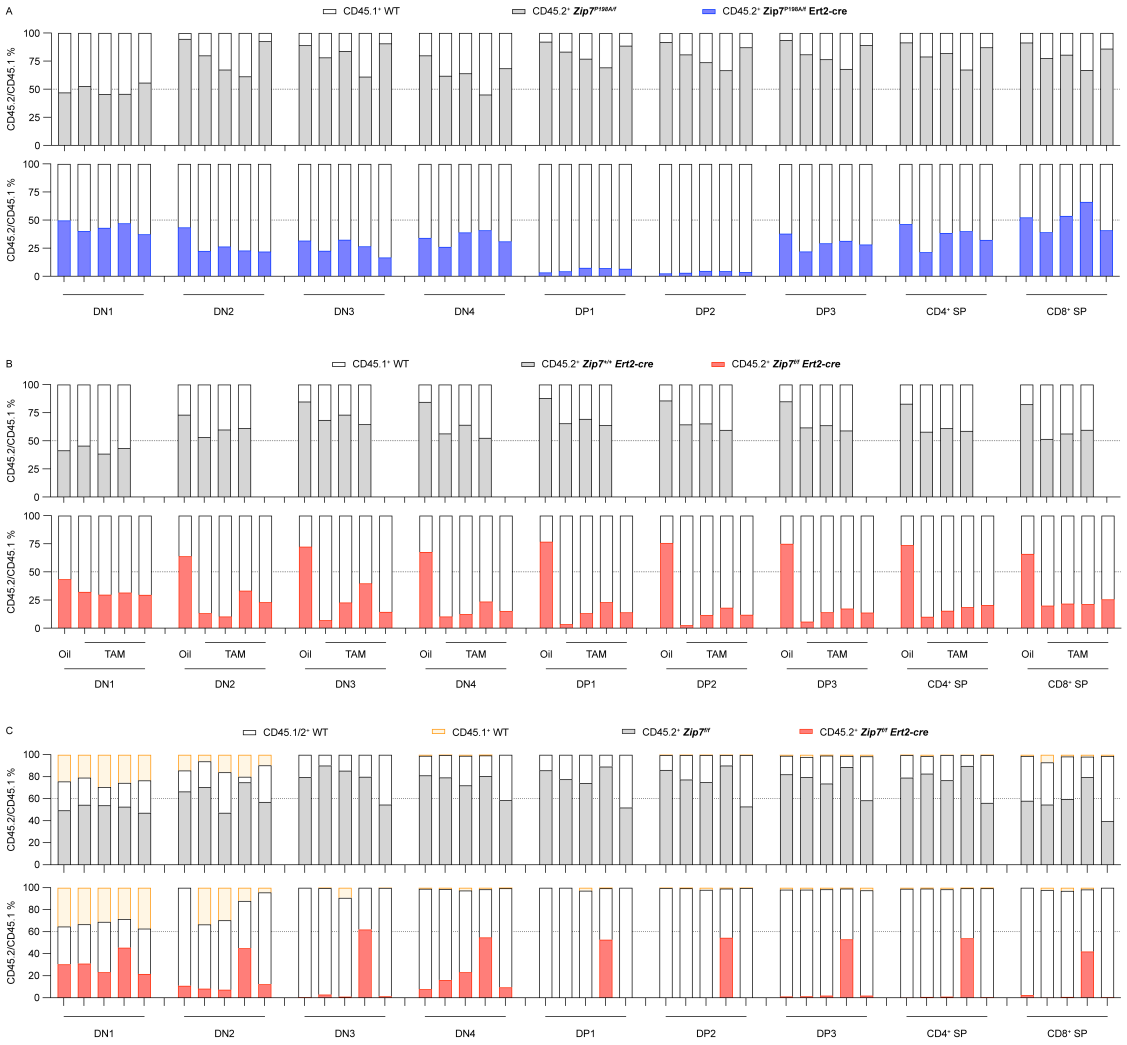

Figure 3-11: Loss of thymocyte subpopulations in the absence of WT ZIP7.
(A) Mixed chimera experiment examining the contribution of WT (CD45.1$^+$): *Zip7*$^{P198A/f}$ (CD45.2$^+$) or WT (CD45.1$^+$): *Zip7*$^{P198A/f}$ *Ert2-cre* (CD45.2$^+$) cells to the pool of thymic subsets. (B-C) Mixed chimeric mice with *Zip7*$^{f/f}$ *Ert2-cre* (CD45.2$^+$) and control counterpart cells were treated with three or five doses of tamoxifen and collected samples on Day 8 (B), and Day 13 (C) post the last dose. Each bar represents one mouse. Orange-outlined bars, where present, indicate CD45.1$^+$ recipient-derived cells.
Note: CD3 was used to distinguish SP thymocytes based on its well-characterised expression pattern, which increases progressively from DN to SP stages[331,332]. CD8$^+$ SP and CD4$^+$ SP cells were thus defined as CD3$^+$ CD8$^+$ CD4$^-$ and CD3$^+$ CD4$^+$ CD8$^-$, respectively, to improve subset resolution.

3.5.4 ZIP7 deficiency impairs memory T cell maintenance

Building on the findings from single-BM chimeras, where ZIP7 deficiency primarily affected $CD4^+$ memory T cells while sparing naïve T cells, I sought to validate these observations in mixed chimeras (Supplementary Figure 10).

In *Zip7*$^{P198A/f}$ *Ert2-cre* mixed-BM chimeras treated with tamoxifen, both $CD4^+$ and $CD8^+$ CM and EM T cells were decreased compared to controls (Figure 3-12A). This decline contrasts with the findings in single-BM chimeras, where the proportions of $CD8^+$ EM T cells and CM T cells within the total T cells were slightly increased. This may because the partial function of the mutated *Zip7*^{P198A} allele, effective in single-BM models, was inadequate against WT competition.

Similarly, the *Zip7*$^{f/f}$ *Ert2-cre* mixed chimeras, particularly with extended tamoxifen induction, presented a marked reduction in $CD4^+$ and $CD8^+$ CM and EM T cells over time (Figure 3-12B, C). This suggests that the maintenance of these subsets also depends on the duration and severity of ZIP7 deficiency.

In both *Zip7*$^{P198A/f}$ *Ert2-cre* and *Zip7*$^{f/f}$ *Ert2-cre* mixed chimeras, naïve $CD4^+$ and $CD8^+$ T cells showed relative resilience to ZIP7 deficiency across different time points and tamoxifen induction protocols (Figure 3-12). This stability suggests naïve T cells are less dependent on ZIP7 function, even under conditions of heightened competition.

Taken together, the mixed chimeras validate the cell-intrinsic role of ZIP7 in maintaining memory T cells, showing that even partial ZIP7 function is insufficient under competitive conditions. Extended ZIP7 deficiency further exacerbates the loss, while Naïve T cells remain unaffected.

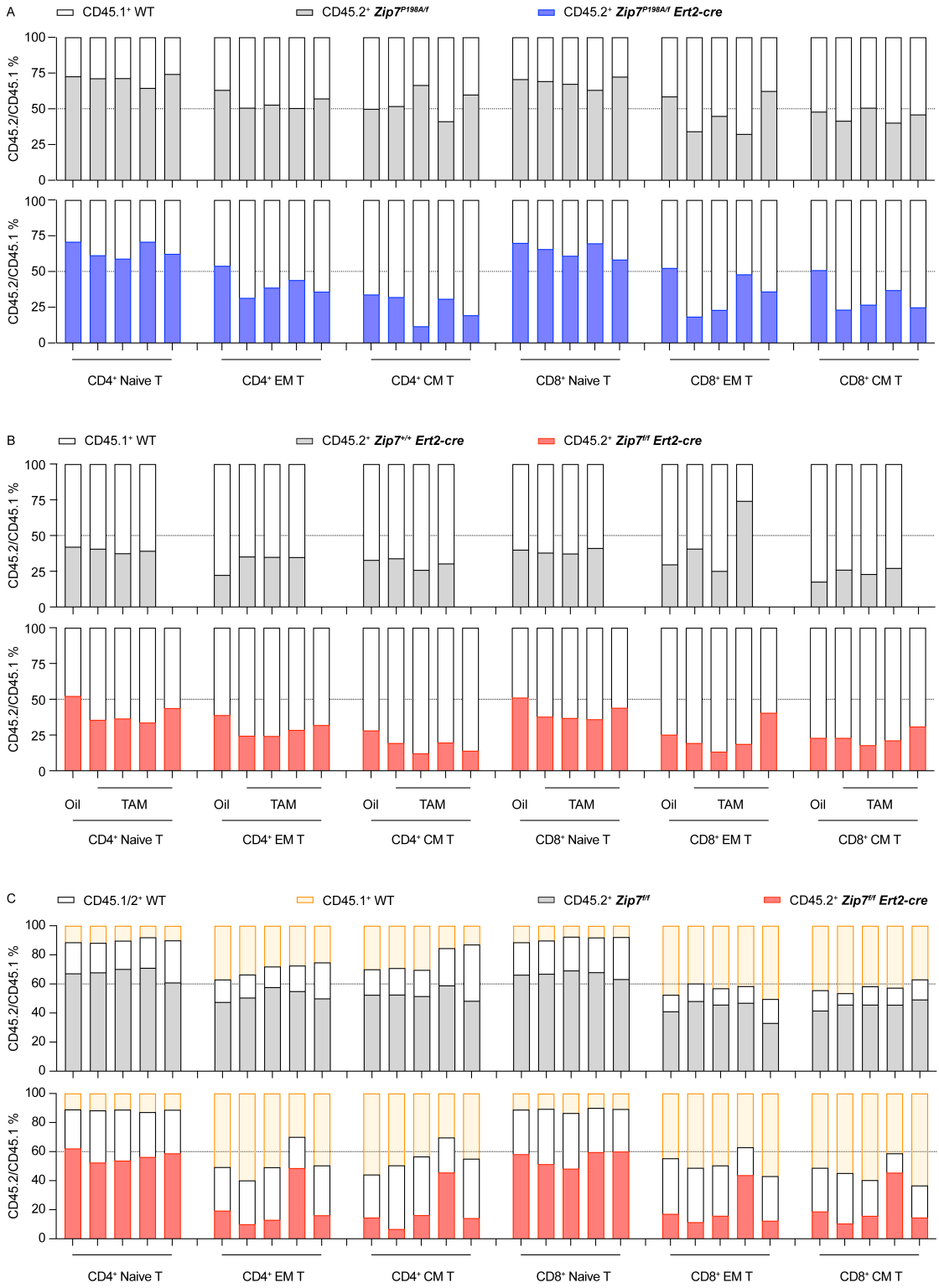

Figure 3-12: Contribution of ZIP7-deficient and WT CD45.2$^+$ cells to splenic T cell subsets in mixed chimera mice.
(A) Spleens were collected from *Zip7*$^{P198A/f}$ *Ert2*-cre mice treated with five doses of tamoxifen and collected on the 7th day after the last dose. (B-C) *Zip7*$^{f/f}$ *Ert2-cre* chimeric mice and their controls were administered three or five doses of tamoxifen, and samples were collected on Day 8 (B) and Day 13 (C). (C) Bar graphs represent the contributions of CD45.2$^+$ (ZIP7-deficient or WT), CD45.1/2$^+$ (internal control), and CD45.1$^+$ (recipient-derived) cells to defined T cell subsets.

3.6 Discussion

In this chapter, I demonstrate that ZIP7 is essential for the development and maintenance of both B and T lymphocyte subtypes, particularly at stages where the cells are undergoing active proliferation or are likely to be experiencing selection pressure. While cells carrying at least one intact ZIP7 allele (*Zip7*$^{+/-}$ or *Zip7*$^{P198A/+}$) remain functional, further loss of the wildtype allele, as in the *Zip7*$^{P198A/-}$ or *Zip7*$^{-/-}$ mice, leads to marked impairments in B cell development from the pro-B to immature stages, and in T cell development from late DN to DP stages. In peripheral organs, MZ B cells and memory T cells were preferentially lost, while quiescent follicular B and naïve T cells remained largely intact. These phenotypes were exacerbated by the degree and duration of ZIP7 deficiency, and were observed in both single- and mixed-BM chimeras. Notably, while the *Zip7*^{P198A} allele provided a partial rescue at early developmental stages, it failed under competitive or prolonged deficiency. Taken together, these findings support a model where ZIP7 is not uniformly required across all lymphocyte populations but is crucial for sustaining immune cell subsets undergoing selection or developmental stress.

Chapter

4 *Cr2-cre* and *Cd4-cre* induced ZIP7 deficiency impair periphery B and T cell maintenance

4.1 Introduction

Tamoxifen-induced models with varying degrees of ZIP7 deficiency have provided valuable insights into ZIP7's role in lymphocyte populations. However, a limitation of these models is that the phenotypes observed in peripheral cells may be influenced by upstream developmental defects. To address this, ZIP7-deficient mouse models driven by *Cr2-cre* and *Cd4-cre* were used to assess effects in mature B and T cells, respectively targeting each lineage while minimizing interference from early developmental stages.

While germline $Zip7^{P198A/-}$ and $Zip7^{H199QV/-}$ models exhibit embryonic lethality[20], use of a *Cr2-cre* conditional knockout model would make it possible to explore the effects specifically in mature B cells. Additionally, the impacts of different degrees of ZIP7 deficiency ($Zip7^{P198A/f}$ *Cr2-cre* and $Zip7^{H199QV/f}$ *Cr2-cre*) on cell maintenance have not been studied.

In this Chapter, I aim to investigate the effects of ZIP7 deficiency on peripheral B- and T cell subsets and determine whether varying levels of ZIP7 deficiency correlate with phenotype severity.

4.2 Efficient deletion of *Zip7^{f}* by *Cr2*-driven Cre recombinase in follicular and MZ B cells

To generate Ig-tg or non-tg *Zip7$^{P198A/f}$ Cr2-cre* mice, I crossed Ig *Zip7$^{f/f}$* mice with *Zip7$^{P198A/+}$ Cr2-cre* mice. The Cre recombinase-driven deletion of the *Zip7^{f}* allele was expected to occur primarily in mature B cells, given the high expression levels of CD21 (*Cr2*) in follicular B cells, MZ B cells and germinal centre B cells, relative to other cell types (Supplementary Figure 11). Notably, follicular dendritic cells also express *Cr2*[333], suggesting that *Zip7* may be conditionally knocked out of in these cells as well.

To evaluate the specificity and efficiency of the *Zip7* conditional knockout, I initially sorted splenic cells into B cell and non-B cell populations using MACS. A negative selection strategy was used to enrich B cells by depleting CD3^{+}, CD4^{+}, CD8a^{+}, CD11c^{+}, CD49b^{+}, Gr-1^{+}, TER-119^{+} cells. Approximately 90% of the sorted B cell fraction consisted of B cells, while 22-31% (95% CI) of cells in the non-B cell fraction were also B cells (Figure 4-1A). After amplifying the targeted genomic region using the same primers as shown in Figure 3-2, PCR results from *Zip7$^{P198A/f}$ Cr2-cre* samples showed deletion of the *Zip7^{f}* allele in both B and non-B fractions, with a higher abundance of truncated PCR products in the B cell fraction (Figure 4-1B). This indicates successful recognition and excision of *LoxP* sites within the *Zip7* gene by Cre recombinase. However, accurately quantifying the knockout efficiency with this method was challenging. Additionally, B cell contamination in the non-B cell fraction due to sorting limitations affected the assessment of knockout specificity.

To address these limitations, MACS-enriched splenocytes were stained with antibodies against CD19, B220, CD93, CD21, CD23, and CD1d, along with a viability dye, to distinguish B-cell subsets by FACS. Follicular B cells were defined as $CD21^{Int}$ $CD1d^{-}$ $CD23^{+}$, and MZ B cells as $CD21^{hi}$ $CD1d^{hi}$ $CD23^{-/low}$, within the live $B220^{+}$ $CD19^{+}$ population. These subsets were sorted from $Zip7^{P198A/f}$, $Zip7^{+/f}$ *Cr2-cre*, and $Zip7^{P198A/f}$ *Cr2-cre* mice for DNA extraction and Sanger sequencing (Figure 4-1C). The full antibody panel is listed in the Methods Section 2.1.4. As expected, the germline $Zip7^{P198A}$ mutation was present only in $Zip7^{P198A/f}$ and $Zip7^{P198A/f}$ *Cr2-cre* mice (Figure 4-1D). In terms of conditional knockout, both follicular and MZ B cells in $Zip7^{+/f}$ *Cr2-cre* mice showed a highly efficiency of $Zip7^{f}$ fragment deletion. Similarly, follicular B cells in $Zip7^{P198A/f}$ *Cr2-cre* mice exhibited efficient knockout, with only minimal residual $Zip7^{f}$ fragments detected in MZ B cells (Figure 4-1E). Overall, Cre recombinase-mediated excision was highly effective in CD21-expressing B cells, specifically in follicular and MZ B cells.

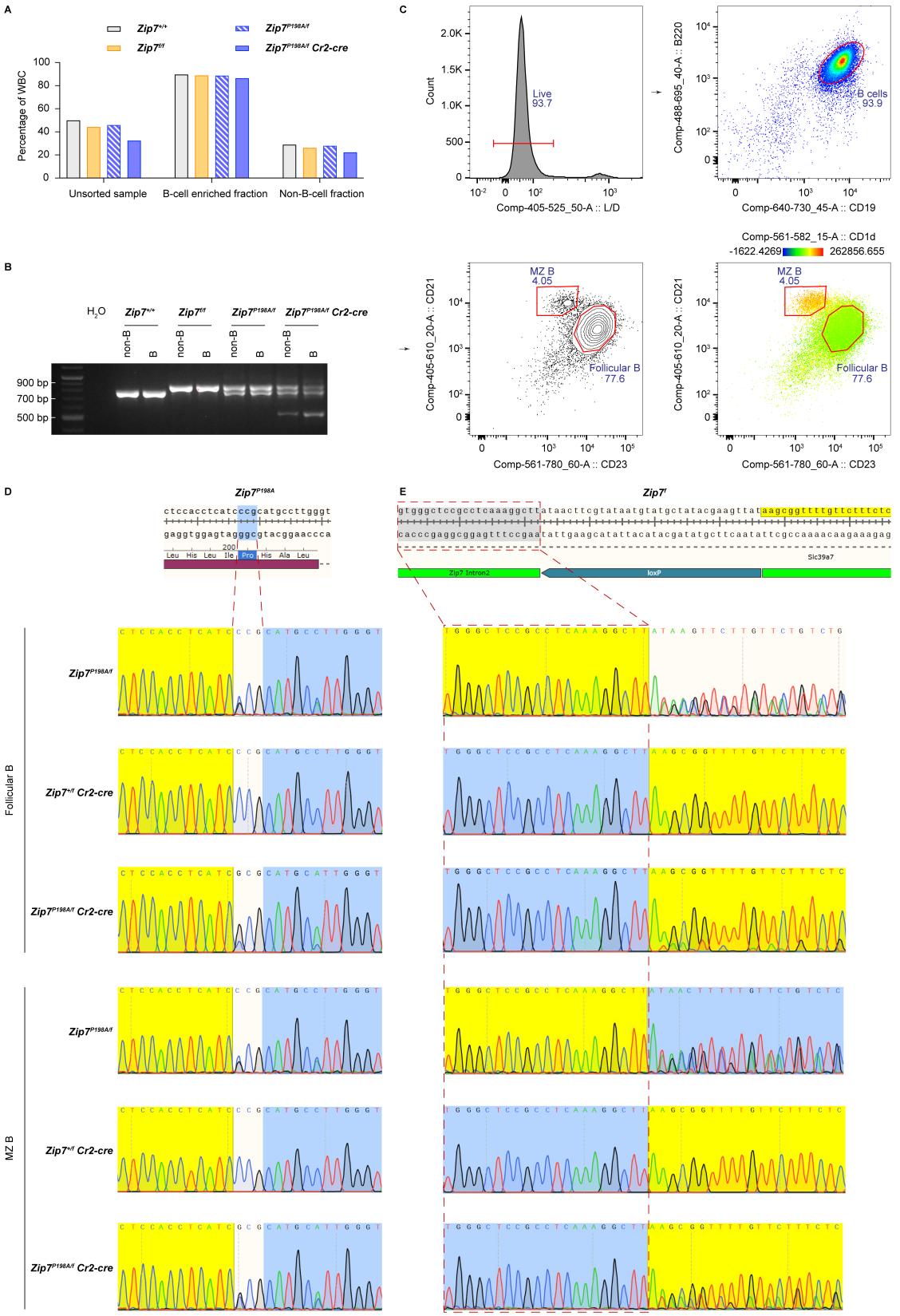

Figure 4-1: Genotype validation of *Cr2-cre*-induced *Zip7* conditional knockout in B cells using PCR and Sanger sequencing.
(A, B) Samples were sorted using a MACS Pan-B isolation kit. (A) The bar graph shows the proportions of B cells in the unsorted sample, the B cell-enriched fraction, and the remaining non-B cell fraction. (B) Genotyping results of these samples. PCR products

for the *Zip7*^{f}, *Zip7*$^{+}$ (*Zip7*^{P198A}), and *Zip7*$^{–}$ alleles were 821 bp, 753 bp and 513 bp, respectively. The 'H_2O' sample serves as a negative control, containing only primers and other reagents without DNA template. (C-E) Samples were enriched by MACS and further sorted by FACS. (C) FACS gating strategy for isolating follicular B cells (CD21^{Int} CD1d$^{–}$ CD23^{+}) and MZ B cells (CD21^{hi} CD1d^{hi} CD23$^{–/low}$) from live B cells. (D-E) Sanger sequencing results. The reference *Zip7*$^{P198A/f}$ DNA sequence is shown in the top row, with subsequent rows displaying sample sequences around the *Zip7*^{P198A} or *Zip7*$^{+}$ site (D) and the downstream *LoxP* site (E).

4.3 Loss of follicular and MZ B cells in *Zip7*$^{P198A/f}$ *Cr2-cre* mice

With effective *Zip7* deletion achieved through *Cr2*-driven Cre recombinase (Figure 4-1), I examined the impact of *Cr2-cre*-induced ZIP7 deficiency on various B cell subsets.

4.3.1 *Zip7*$^{P198A/f}$ *Cr2-cre* reduces mature B cells without disrupting BM B cell development

Unlike mice with *Zip7* germline hypomorphic mutations, which exhibit stunted growth and limited survival[20], *Zip7*$^{P198A/f}$ *Cr2-cre* mice grew normally and survived beyond 50 weeks.

To test the hypothesis that *Cr2-cre*-induced ZIP7 deficiency would not alter B cell development in the BM, I analysed sequential B cell subsets by flow cytometry according to the Hardy fraction scheme (Figure 4-2A). *Zip7*$^{+/f}$, *Zip7*$^{198A/+}$, *Zip7*$^{+/f}$ *Cr2-cre*, and *Zip7*$^{P198A/f}$ *Cr2-cre* mice displayed comparable numbers across multiple developmental stages in BM, from early Pro-B cells to Pre-B cells and up to immature B cells (Figure 4-2B). However, *Zip7*$^{P198A/f}$ *Cr2-cre* mice showed a noticeable reduction in the percentage and number of mature B cells compared to the other three groups (Figure 4-2).

Phenotypic analysis of mice generated from a separate *Zip7*^{f} founder, derived from the same batch of CRISPR reagent-injected embryos and validated by genotyping, also showed a reduction in mature B cells in *Zip7*$^{P198A/f}$ *Cr2-cre* mice, though without

reaching statistical significance. Importantly, early BM B cell developmental stages remained unaffected (Supplementary Figure 12A).

These findings suggest that in this conditional model, intact ZIP7 during early developmental stages and in immature B cells permits normal B cell development and BM egress. However, the observed reduction in recirculating mature B cells returning to the BM indicates that ZIP7 deletion in mature B cells, induced by *Cr2-cre*, negatively affects B cell survival and/or function in the periphery.

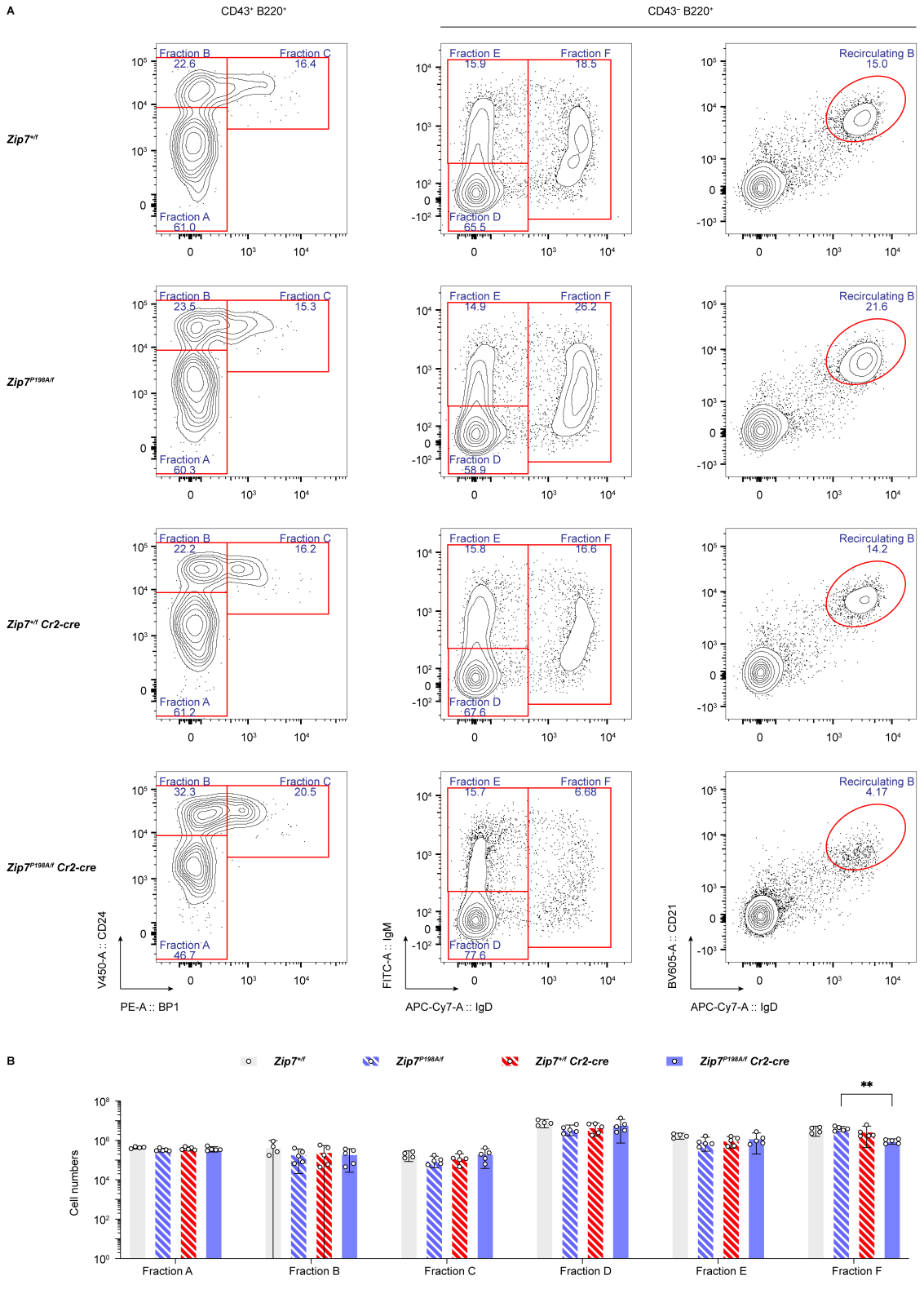

Figure 4-2: B cell development in the BM is unaffected in unmanipulated *Zip7*$^{P198A/f}$ *Cr2-cre* mice.
(A) Representative flow cytometry plots showing B cell development in the BM across different genotypes, with gating on Hardy Fractions A-F and CD21^{+} IgD^{+} CD43^{-} B220^{+} recirculating B cells. (B) Absolute cell numbers of B cell subsets in the BM. Each dot represents an individual mouse (n = 4 or 5 per genotype). Bars represent the mean with

95% CI. Statistical comparisons were performed using mixed-effects analysis with Tukey's multiple comparisons test. **, $p = 0.0055$.

4.3.2 Loss of MZ B cells in *Zip7*$^{P198A/f}$ *Cr2-cre* mice

To investigate further which peripheral B cell subtypes are affected by ZIP7 deficiency, I analysed B cell subsets in the spleen and lymph nodes by flow cytometry (Figure 4-3A).

In the *Cr2-cre* model, the *cre* transgene is introduced through random integration driven by the *Cr2* promoter[71]. This differs from targeted integration models, such as the *Cd79a-cre* model, where native gene expression may be disrupted[334]. In heterozygous *Cd21-cre* transgenic mice, CD21 expression is less likely to be affected. This assumption was validated by confirming that CD21^{+} CD23$^{low/-}$ cells in *Zip7*$^{+/f}$ *Cr2-cre* mice exhibit the characteristic markers of MZ B cells (CD1d^{high} IgM^{high} IgD^{low}), consistent with the MZ B cell phenotype observed in *Zip7*$^{+/f}$ MZ B mice (Supplementary Figure 13).

Zip7$^{P198A/f}$ *Cr2-cre* mice showed a significant reduction in MZ B cells compared to other genotypes (Figure 4-3, Supplementary Figure 12B). The absolute numbers of follicular B cells also decreased, though statistical significance was reached only in some comparisons (Figure 4-3B) and not others (Supplementary Figure 12B). A similar reduction in MZ B cells was observed in Ig-tg *Zip7*$^{P198A/f}$ *Cr2-cre* mice, indicating that this phenotype retained in the monoclonal BCR setting. A modest reduction was also seen in Ig-tg *Zip7*$^{+/f}$ *Cr2-cre* mice, though the underlying cause remains unclear. In contrast, follicular B cell numbers remained comparable to control groups (Figure 4-4).

These findings suggest that ZIP7 deficiency disproportionately impacts peripheral B cells, particularly the MZ B cell population.

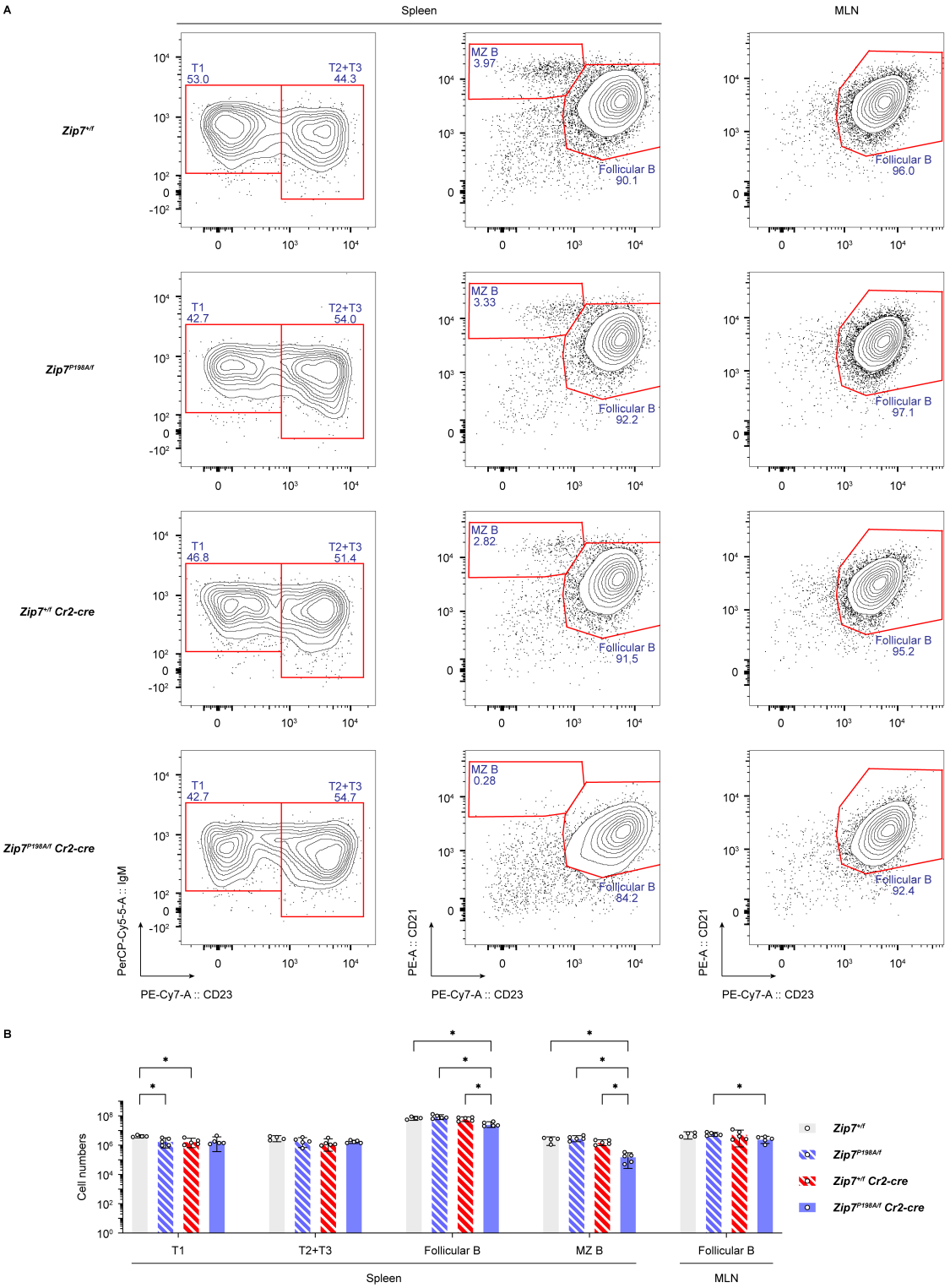

Figure 4-3: Reduction in follicular and MZ B cells in *Zip7*$^{P198A/f}$ *Cr2-cre* mice.
(A) Representative flow cytometric plots of peripheral B cell subsets for each genotype. Percentages of gated cells within the lymphocyte population are shown. Transitional B cells were gated on CD93^{+} B220^{+} live lymphocytes, while follicular B cells and MZ B cells were gated on CD93^{-} B220^{+} CD19^{+} live lymphocytes. (B) Absolute numbers of B cell subsets in the spleen and MLN, presented as mean values with 95% CIs. Each dot

represents an individual mouse. Statistical analyses were conducted using mixed-effects models, followed by Tukey's multiple comparisons test for significance between genotypes. $p < 0.05$ is indicated by *.

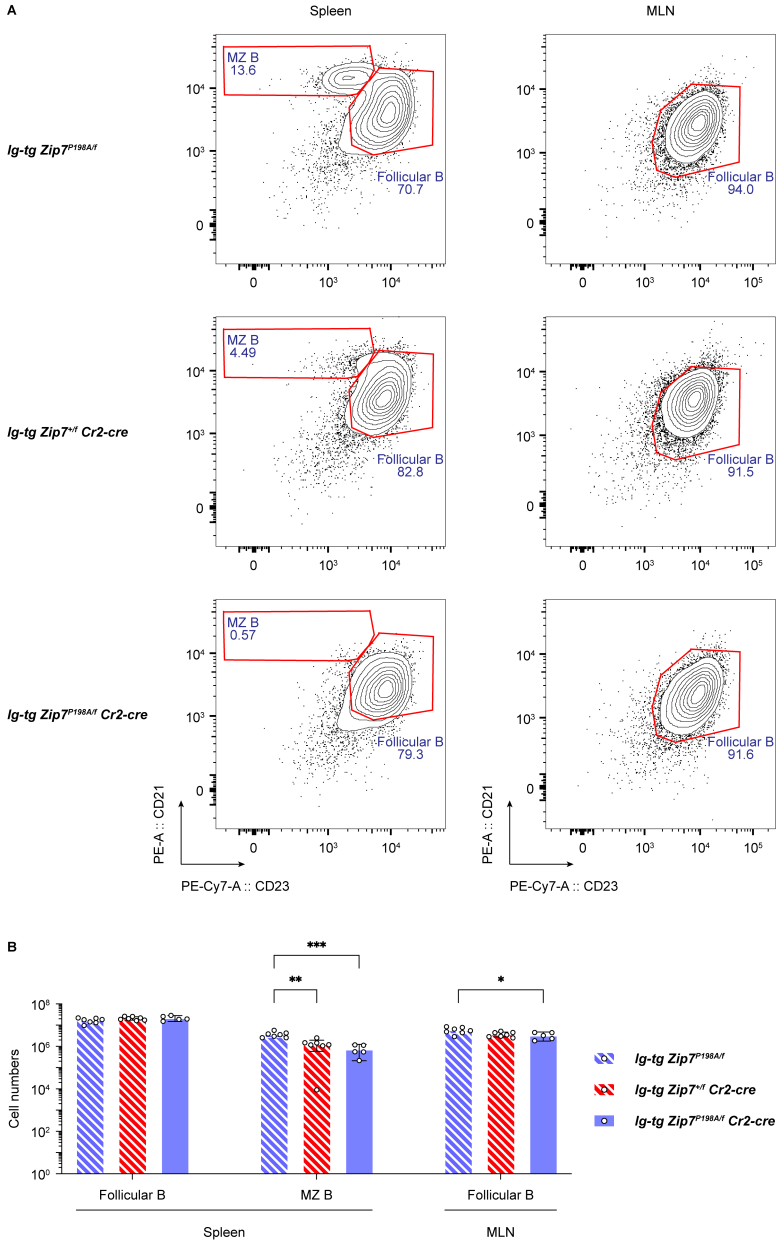

Figure 4-4: Reduction in MZ B Cells in Ig-tg *Zip7*$^{P198A/f}$ *Cr2-cre* mice.
(A) Representative flow cytometry plots of B cell subsets in the spleen and MLN across three genotypes. Percentages of MZ and follicular B cells within the lymphocyte population are shown. (B) Absolute numbers of follicular and MZ B cells in the spleen and MLN. Each dot represents an individual mouse, with values displayed as means and 95% CIs. Statistical analysis was conducted using mixed-effects models, followed by Tukey's multiple comparisons test.

4.3.3 Reduced follicular and MZ B cells in *Zip7$^{P198A/f}$ Cr2-cre* mice

To assess the hematopoietic-specific effects of *Zip7$^{P198A/–}$* independently of other potentially affected systems, I reconstituted lethally irradiated CD45.1$^+$ WT mice with CD45.2$^+$ BM cells from *Zip7$^{198A/f}$*, *Zip7$^{+/f}$ Cr2-cre* or *Zip7$^{P198A/f}$ Cr2-cre* donor mice. In *Zip7$^{P198A/f}$ Cr2-cre* chimeric mice, the absolute number of mature B cells was significantly reduced compared to controls, while B cell development within the BM remained unaffected (Figure 4-5A). This substantial reduction in recirculating B cells was also observed in the spleen, where both follicular and MZ B cells showed marked decreases (Figure 4-5B).

This consistency of these findings across both unmanipulated and chimeric models reinforces that ZIP7 deficiency, driven by *Cr2-cre*, selectively impacts peripheral B cell subsets, particularly follicular and MZ B cells, while sparing B cell development in the BM.

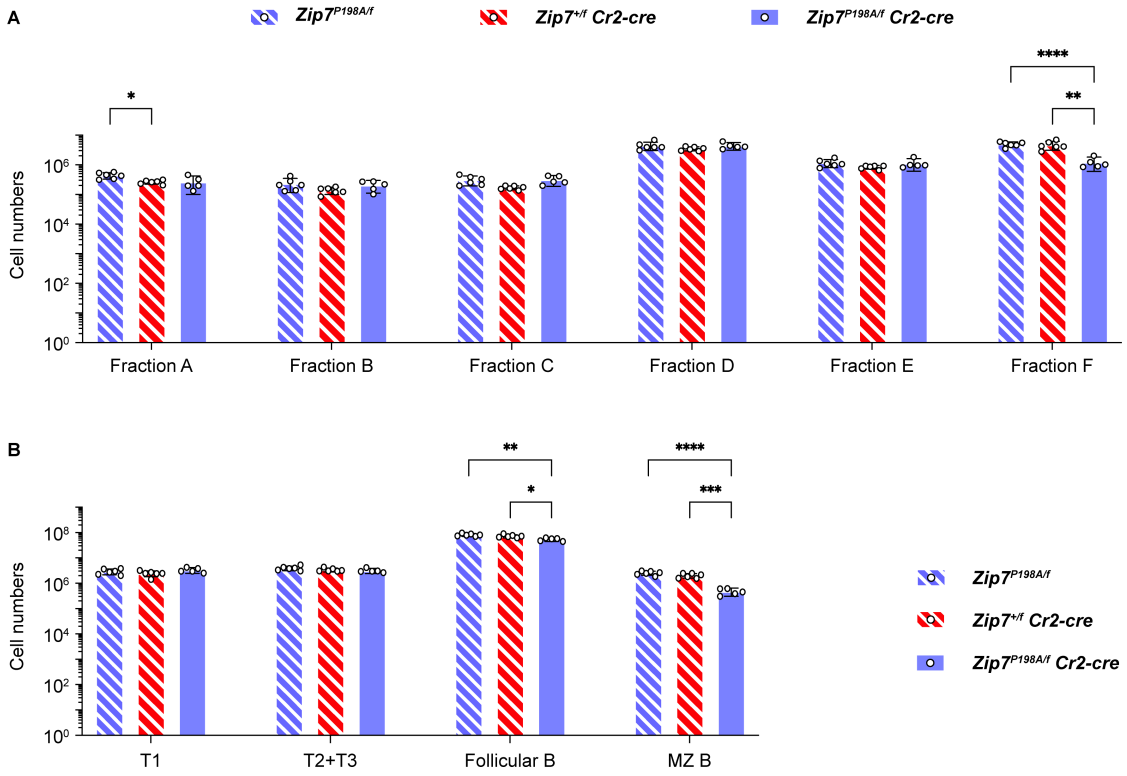

Figure 4-5: Significant reduction in follicular and MZ B cells in *Zip7*$^{P198A/f}$ *Cr2-cre* single-BM transplanted chimeras
(A, B) Absolute numbers of B cell subsets in the BM (A) and spleen (B) are shown. The gating strategy follows that shown in Supplementary Figure 2 and Supplementary Figure 3. Data are presented as mean values with 95% CIs, with n = 5 mice per genotype. Statistical analyses were conducted using mixed-effects models, followed by Tukey's multiple comparisons test.

4.4 Loss of follicular and MZ B cells in *Zip7*$^{H199QV/f}$ *Cr2-cre* and *Zip7*$^{P198A/f}$ *Cr2-cre* mice is cell-intrinsic

To determine whether the observed loss of follicular and MZ cells in ZIP7-deficient mice is cell-intrisic, I utilised a mixed chimera approach. Alongside *Zip7*$^{P198A/f}$ *Cr2-cre* mice, I included *Zip7*$^{H199QV/f}$ *Cr2-cre* mice as an additional ZIP7-deficient model. As mentioned in the Introduction, while the *Zip7*^{H199QV} mutation retains Proline-198, the insertion disrupts the orientation of downstream residues, altering the α-helix structure near the zinc entry site. In mouse models, both germline homozygous *Zip7*$^{P198A/P198A}$ and *Zip7*$^{H199QV/H199QV}$ mutations result in notable B cell immunodeficiency[20].

Although the initial ratio of CD45.1$^+$ WT and CD45.2$^+$ BM cells injected in the mixed chimeras was 50:50, both *Zip7*$^{H199QV/f}$ *Cr2-cre* and *Zip7*$^{P198A/f}$ *Cr2-cre* chimeric mice displayed reduced mature B cells in the BM compared to controls (Figure 4-6). In the peripheral B cell populations, follicular B cells showed a slight reduction, while MZ B cells exhibited a pronounced decrease in both models (Figure 4-7). To assess whether this reduction originated at an earlier developmental stage, I examined MZP, identified by gating CD93$^-$, B220$^+$, CD19$^+$, CD21^{high}, IgM^{high}, IgD$^+$ and CD23$^+$ cells (Supplementary Figure 14). The result indicated that the loss of MZ cells begins at the MZ precursor stage (Figure 4-7).

In summary, these findings support a conclusion that the reduction in MZ and follicular B cells in *Cr2-cre*-driven ZIP7-deficient mice is a cell-intrinsic effect, highlighting that the maintenance of these cells requires intact ZIP7.

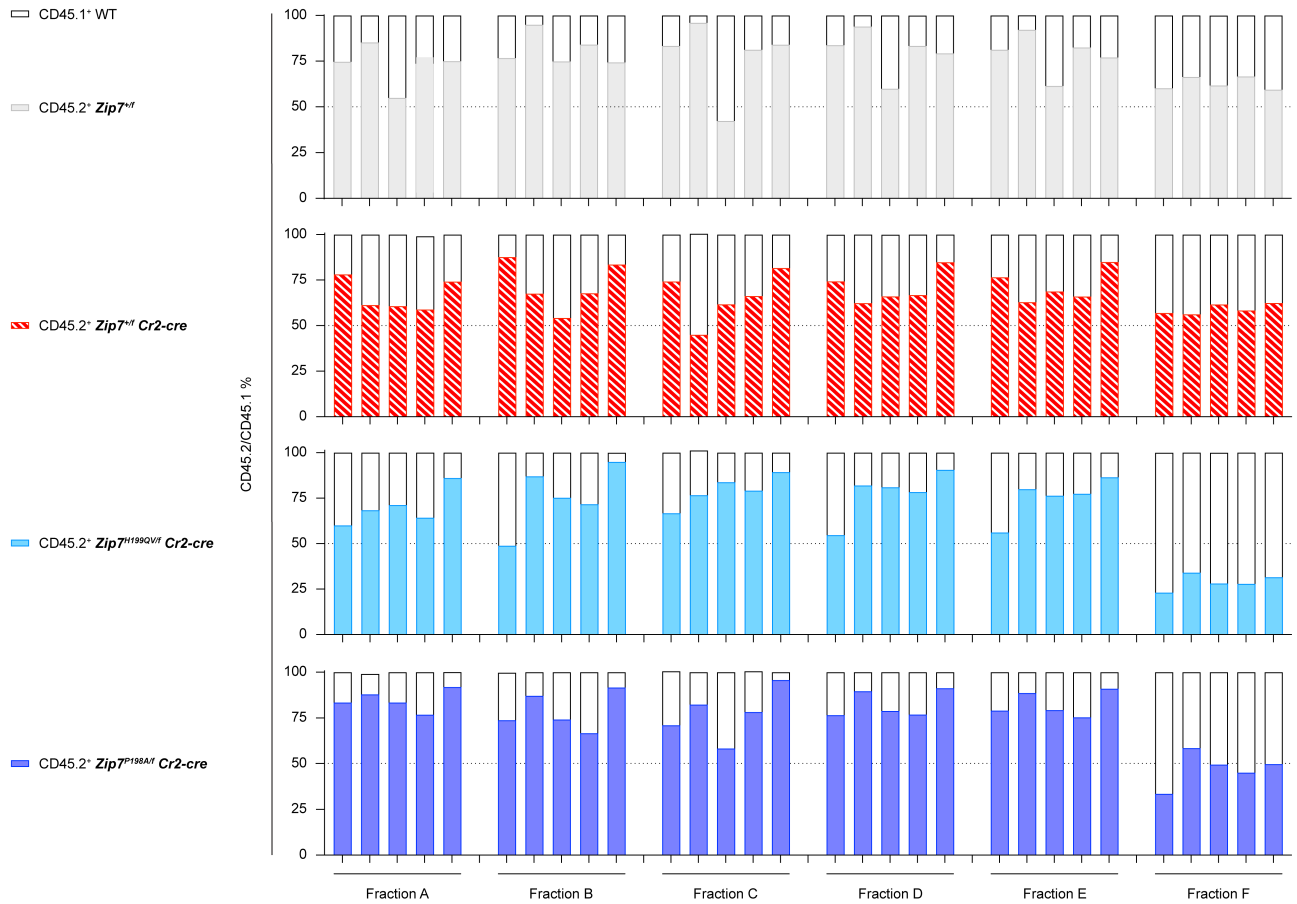

Figure 4-6: Normal BM B cell development in *Cr2-cre*-driven ZIP7-deficient mice, but decreased recirculating mature B cells.
Competitive repopulation analysis of CD45.2$^+$ Zip7$^{+/f}$, Zip7$^{+/f}$ *Cr2-cre*, *Zip7$^{H199QV/f}$ Cr2-cre* and *Zip7$^{P198A/f}$ Cr2-cre* B cell progenitors alongside CD45.2$^+$ WT cells in lethally irradiated recipients. Bars show the percentage contribution of CD45.2$^+$ (coloured) and CD45.1$^+$ (hollow) cells across Hardy Fractions A-F in the BM. Each panel represents chimeric mice with a different CD45.2$^+$ dornor genotype. Each bar corresponds to an individula mouse, with five mice per group.

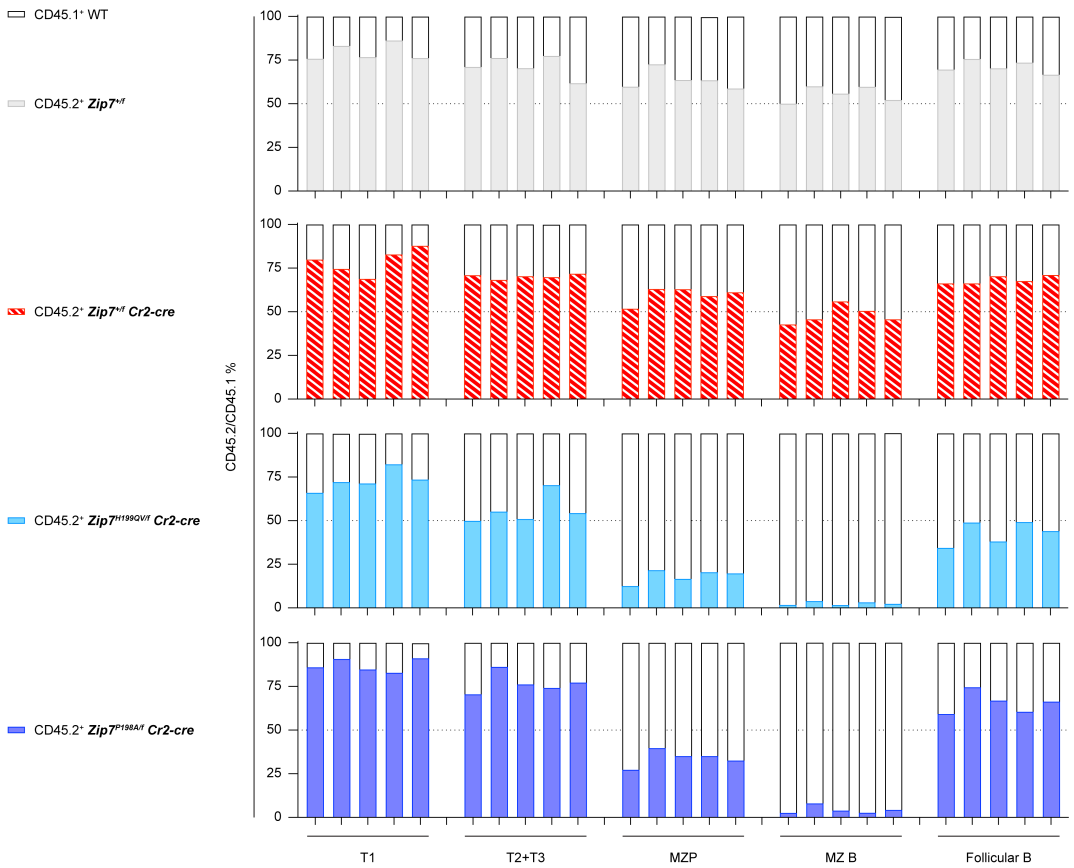

Figure 4-7: Decreased follicular B cells and markedly reduced MZ B precursors and MZ B cells in *Cr2-cre*-driven ZIP7 deficient chimeric mice. This figure shows the relative contribution of CD45.2$^+$ Zip7$^{+/f}$, Zip7$^{+/f}$ *Cr2-cre*, *Zip7$^{H199QV/f}$ Cr2-cre* and *Zip7$^{P198A/f}$ Cr2-cre* donor-derived B cells, compared to CD45.1$^+$ WT cells, within spleen B cell subsets in mixed chimeras. B cell populations analyzed include T1, T2+T3, MZP, MZ B, and follicular B cells, with gating strategy detailed in Supplementary Figure 14. Coloured bars represent CD45.2$^+$ cells from each donor genotype, while hollow bars represent CD45.1$^+$ WT cells. Each panel displays data for one donor genotype, with each bar corresponding to an individual mouse (n = 5 per group).

4.5 *Cd4-cre*-driven ZIP7 deficiency impairs peripheral T cell maintenance without affecting thymic development

To investigate the effect of ZIP7 deficiency specifically in T cells, I crossed *Zip7*$^{f/f}$ mice with *Zip7*$^{P198A/+}$ *Cd4-cre* mice to generate *Zip7*$^{P198A/f}$ *Cd4-cre* mice along with appropriate controls. I examined T cell development and subset distribution in both unmanipulated and chimeric *Zip7*$^{P198A/f}$ *Cd4-cre* mice.

4.5.1 Reduced Naïve T cells in *Zip7*$^{P198A/f}$ *Cd4-cre* mice

Flow cytometric analysis revealed that thymic T cell development was unaffected in unmanipulated *Zip7*$^{P198A/f}$ *Cd4-cre* mice, as absolute cell numbers of thymic subsets (DN1-4, DP1-3, CD4$^+$ SP, and CD8$^+$ SP) were comparable to controls (*Zip7*$^{+/f}$, *Zip7*$^{P198A/f}$, and *Zip7*$^{+/f}$ *Cd4-cre*) (Figure 4-8).

In contrast, splenic T cell analysis revealed a marked reduction in both CD4$^+$ and CD8$^+$ naïve T cells in *Zip7*$^{P198A/f}$ *Cd4-cre* mice. Within the CD8$^+$ compartment, the proportions of CM and EM subsets increased, likely reflecting compensation for naïve T cell loss. In the CD4$^+$ compartment, EM T cell frequencies were similarly elevated, while other subsets, including CM T cells, remained largely unchanged in proportion. A small but statistically significant reduction in CD4$^+$ CM T cell numbers was observed, though its relevance is unclear. Overall, naïve T cell loss emerged as the most robust and consistent phenotype (Figure 4-9).

These results indicate the *Cd4-cre*-driven ZIP7 deficiency impairs the maintenance of naïve T cells in the periphery, though thymic T cell development remains affected.

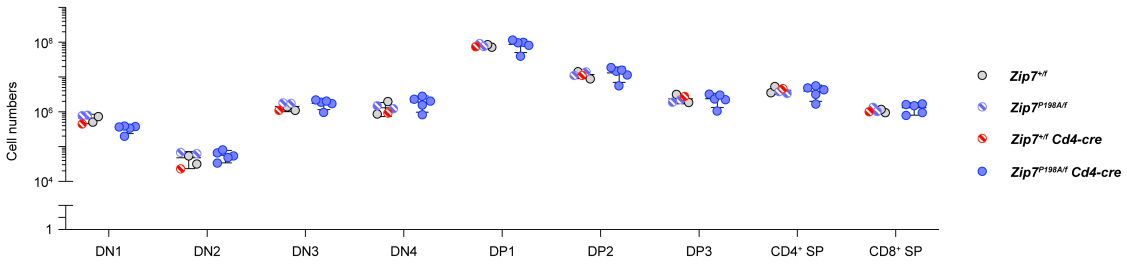

Figure 4-8: No significant differences in thymic T cell subsets in unmanipulated *Zip7*$^{P198A/f}$ *Cd4-cre* mice compared to controls.
This figure shows the absolute cell numbers for each thymic T cell subset in unmanipulated *Zip7*$^{P198A/f}$ *Cd4-cre* mice relative to pooled controls (*Zip7*$^{+/f}$, *Zip7*$^{P198A/f}$, and *Zip7*$^{+/f}$ *Cd4-cre*). Each data point represents an individual mouse. Statistical analysis was conducted using unpaired two-tailed Welch's t-tests with Holm-Šídák correction for multiple comparisons, revealing no significant differences across groups.

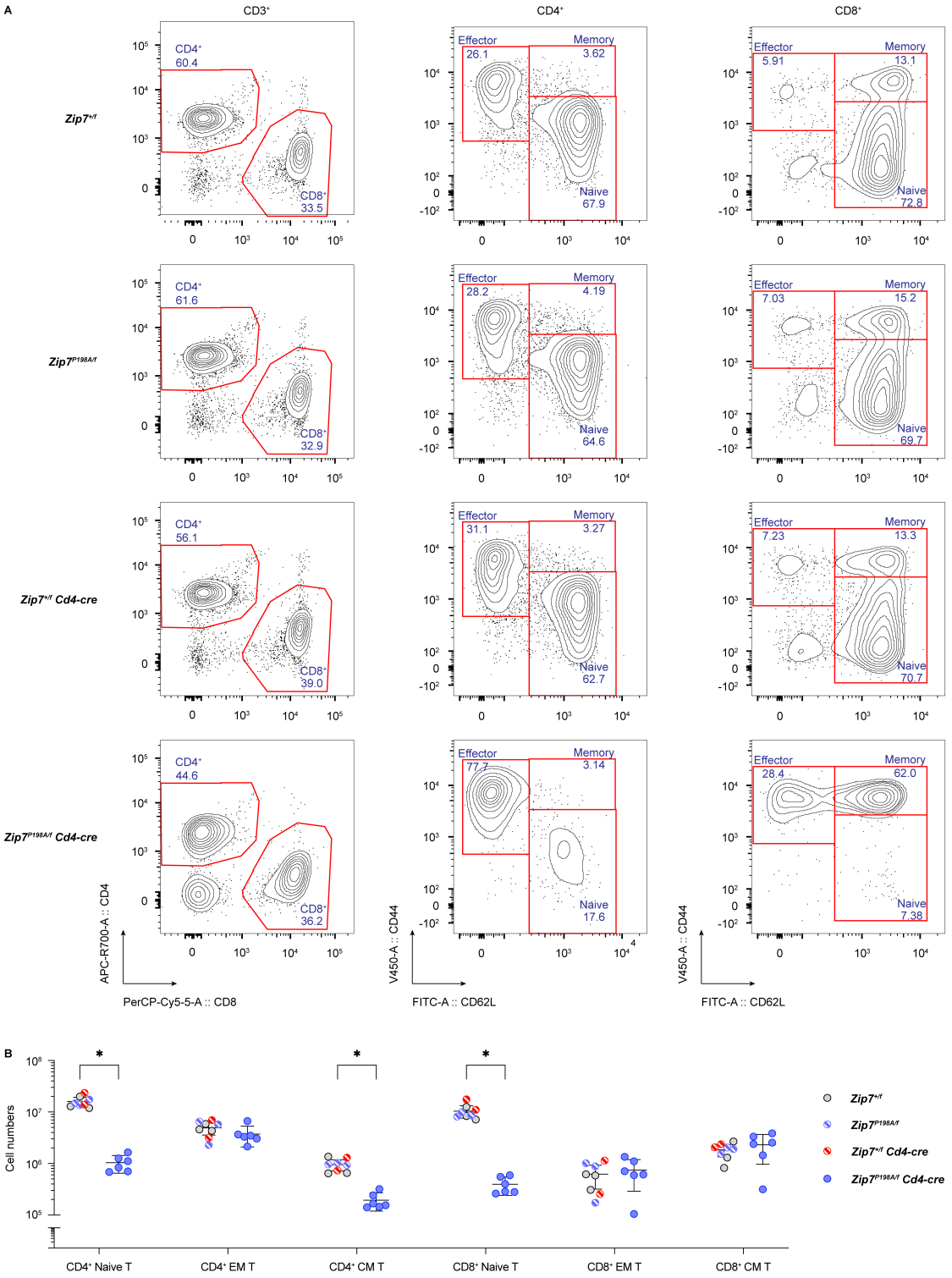

Figure 4-9: Decreased Naïve T cells in unmanipulated *Zip7*$^{P198A/f}$ *Cd4-cre* mice.
(A) Representative flow cytometry plots of splenic CD4$^+$ and CD8$^+$ T cells in unmanipulated mice, displaying CM, EM, and naïve subsets based on CD44 and CD62L expression. (B) Absolute cell numbers of splenic T cell subsets. Data for control mice (*Zip7*$^{+/f}$, *Zip7*$^{P198A/f}$, and *Zip7*$^{+/f}$ *Cd4-cre*) are pooled and compared with *Zip7*$^{P198A/f}$ *Cd4-cre* mice. Each symbol represents an individual mouse. Statistical comparisons were performed using unpaired two-tailed Welch's *t* tests, with Holm-Šídák correction for multiple comparisons (*, $p < 0.05$).

4.5.2 Normal thymic development with reduced peripheral T cell subsets in single-BM transplanted *Zip7$^{P198A/f}$ Cd4-cre* mice

To assess the effects of *Zip7$^{P198A/f}$ Cd4-cre* specifically within the hematopoietic system, I generated single-BM transplanted *Zip7$^{+/f}$ Cd4-cre* or *Zip7$^{P198A/f}$ Cd4-cre* mice.

Thymic T cell development appeared unaffected by ZIP7 deficiency, as the absolute cell numbers of all T cell subsets, including DN1-4, DP1-3, and SP CD4$^+$ and CD8$^+$ thymocytes, were comparable between *Zip7$^{+/f}$ Cd4-cre* and *Zip7$^{P198A/f}$ Cd4-cre* groups (Figure 4-10A). However, the overall T cell number in the periphery of *Zip7$^{P198A/f}$ Cd4-cre* mice was significantly reduced, leading to decreased cell numbers across all subsets in both the spleen and blood (Figure 4-10B).

Collectively, these findings indicate that while thymic T cell development proceeds normally in *Zip7$^{P198A/f}$ Cd4-cre* chimeric mice, ZIP7 is crucial for maintaining adequate numbers of naive and memory T cells in the periphery.

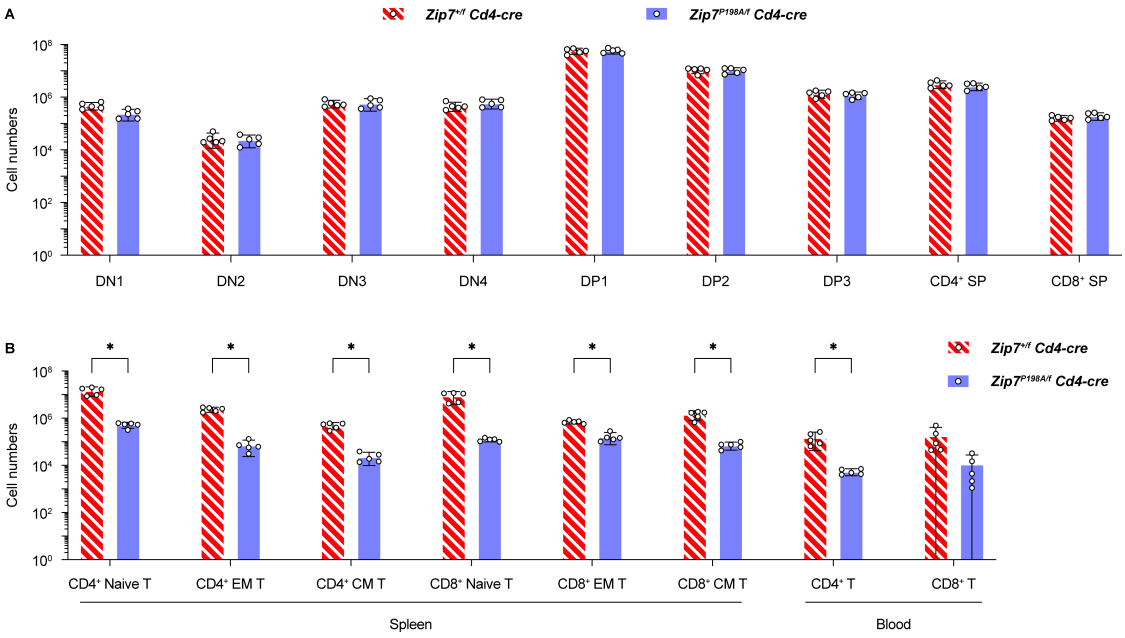

Figure 4-10: Reduced splenic T cell subsets in *Zip7$^{P198A/f}$ Cd4-cre* chimeric mice with normal thymic T cell development
(A-B) Absolute cell numbers of T cell subsets in the thymus (DN1-4, DP1-3, and CD4$^+$ and CD8$^+$ SP), spleen (CD4$^+$ and CD8$^+$ naïve, EM, and CM T cells) and blood (CD4$^+$ T

and CD8$^+$ T cells) in *Zip7*$^{+/f}$ *Cd4-cre* and *Zip7*$^{P198A/f}$ *Cd4-cre* chimeric mice. Each dot represents an individual mouse. Statistical analysis was conducted using unpaired two-tailed Welch's t tests with Holm-Šídák correction for multiple comparisons (*, $p < 0.05$).

4.5.3 Normal thymic development but few donor peripheral T cells in ZIP7-deficient mixed chimeras

To confirm the impact of ZIP7 deficiency on T cell maintenance and survival within a competitive environment, mixed BM chimeras were generated by transplanting a 50:50 mixture of CD45.2$^+$ BM cells from *Zip7*$^{+/f}$, *Zip7*$^{P198A/f}$, *Zip7*$^{+/f}$ *Cd4-cre*, or *Zip7*$^{P198A/f}$ *Cd4-cre* mice, along with CD45.1$^+$ WT BM cells, into lethally irradiated CD45.1$^+$ recipient mice.

Consistent with findings from the single-BM transplanted *Zip7*$^{P198A/f}$ *Cd4-cre* chimeras, thymic T cell development appeared unaffected, as ZIP7-deficient and control cells were represented equally across the thymocyte subsets (Figure 4-11). This indicates that ZIP7 deficiency does not impair thymic T cell maturation.

However, a marked difference was observed in the peripheral T cell compartments. In the spleen, ZIP7-deficient donor-derived T cells from *Zip7*$^{P198A/f}$ *Cd4-cre* were significantly outcompeted by their WT-derived counterparts across all T cell subsets, including naïve, EM, and CM populations of both CD4$^+$ and CD8$^+$ T cells (Figure 4-12). This pattern reflects the substantial reduction of T cells previously observed in single-BM transplanted *Zip7*$^{P198A/f}$ *Cd4-cre* mice and reinforces the conclusion that ZIP7 is essential for the maintenance of T cell subsets in the periphery.

Together, these data highlight that while ZIP7 deficiency does not affect T cell development within the thymus, there is an intrinsic requirement for ZIP7 in sustaining adequate peripheral T cell populations.

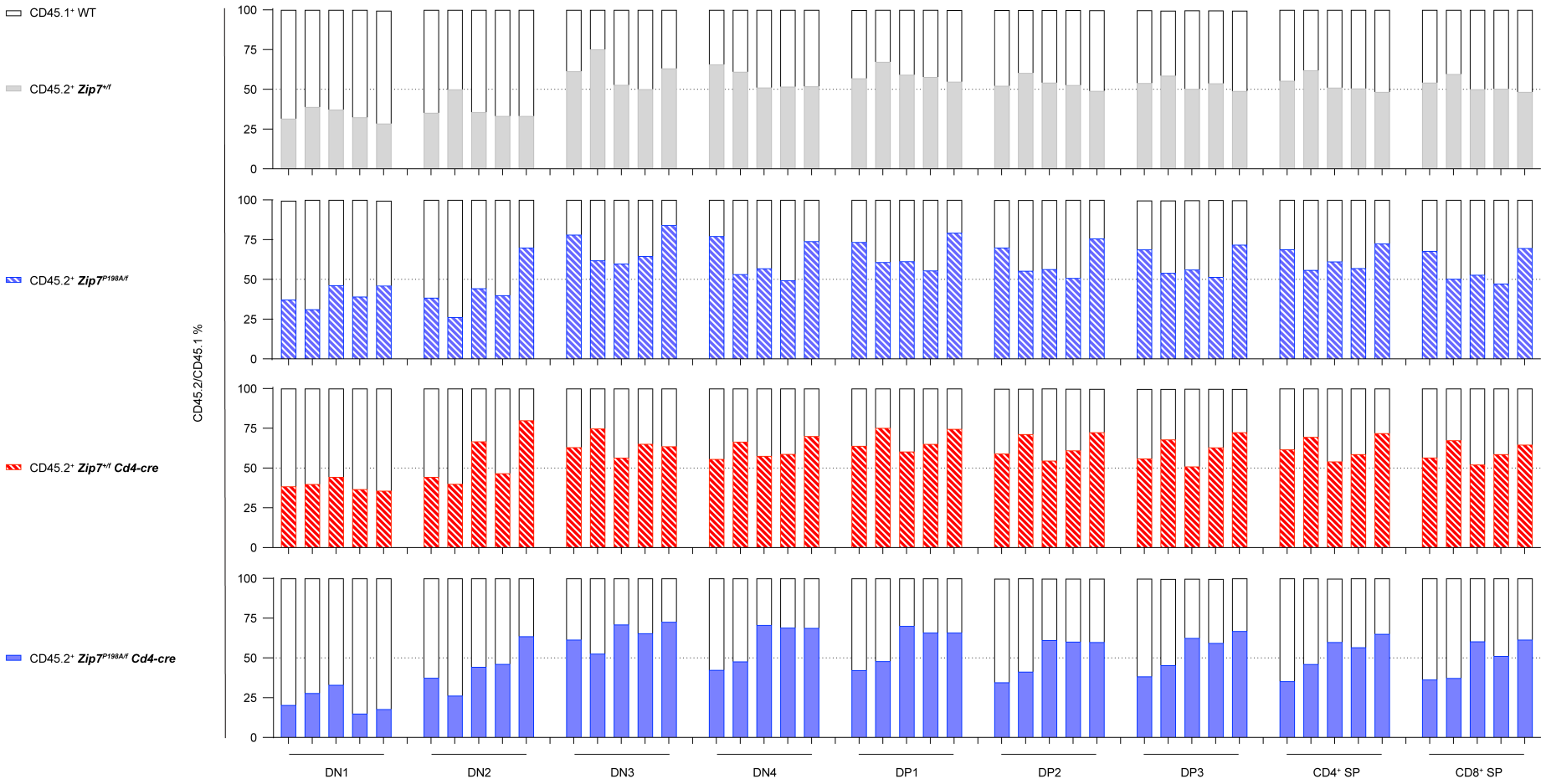

Figure 4-11: ZIP7 deficiency does not affect thymic T cell development in *Cd4-cre* mixed chimeras
Percentage contribution of CD45.2$^+$ *Zip7*$^{+/f}$, *Zip7*$^{P198A/f}$, *Zip7*$^{+/f}$ *Cd4-cre*, and *Zip7*$^{P198A/f}$ *Cd4-cre* donor-derived cells compared to CD45.1$^+$ WT cells across thymic T cell developmental stages in mixed chimeras. Gating for thymic T cell subsets follows the strategy shown in Supplementary Figure 9. The dashed line represents the initial 50:50 ratio of CD45.2$^+$ to CD45.1$^+$ cells in the injected BM mixture.

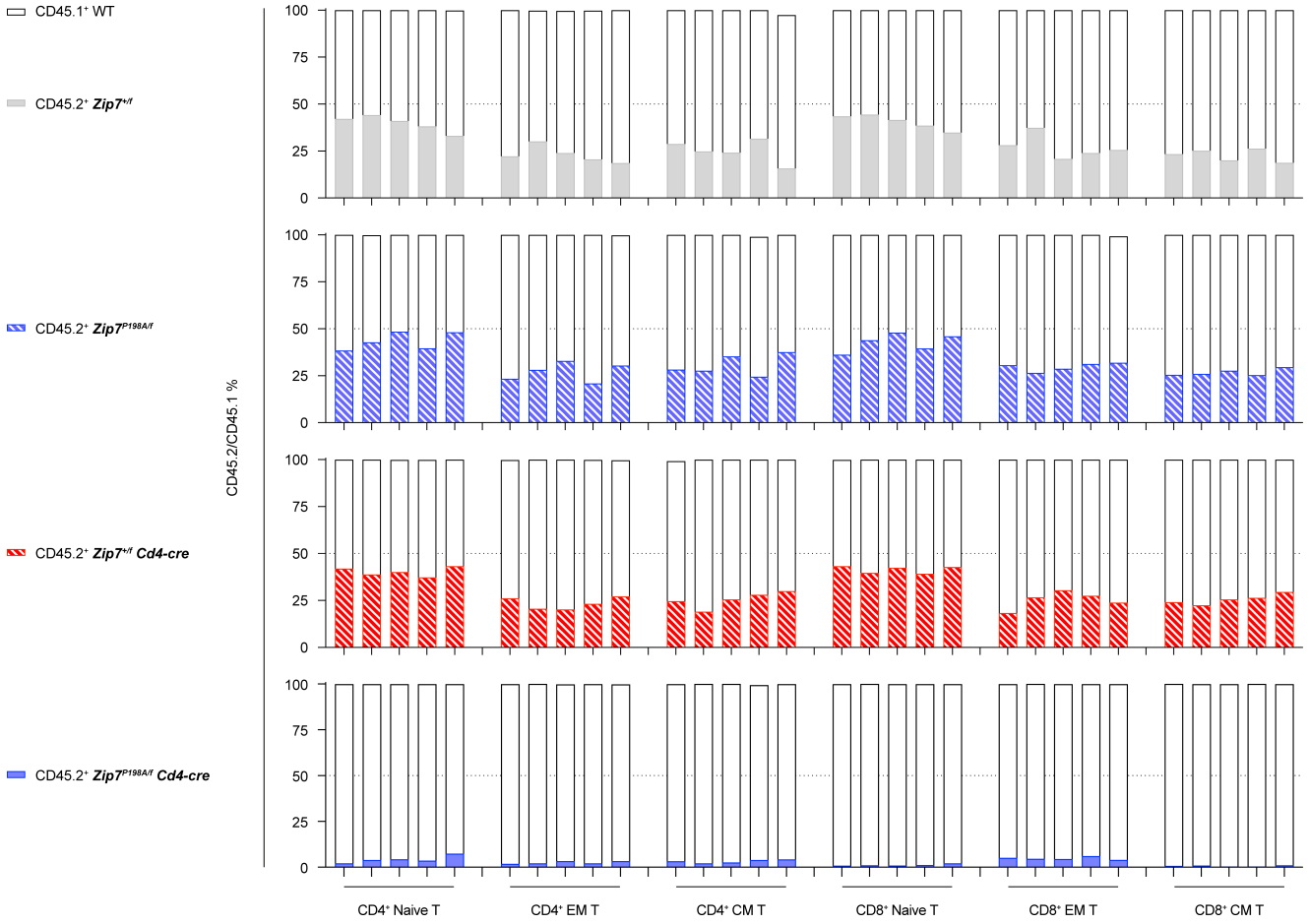

Figure 4-12: Few ZIP7-deficient donor T cells in splenic T cell subsets of mixed chimeras
Each bar represents the proportion of CD45.2$^+$ (coloured) and CD45.1$^+$ (hollow) cells in an individual mouse (n = 5 per group). Gating for splenic T cell subsets follows the strategy shown in Supplementary Figure 10. The dashed line represents the initial 50:50 ratio of CD45.2$^+$ and CD45.1$^+$ cells in the injected BM mixture.

4.6 Discussion

Despite the established role of zinc in T cell signaling and ZIP7 in B cell development, its contribution to peripheral lymphocyte maintenance remained unclear. Using tissue-specific deletion driven by *Cr2-cre* and *Cd4-cre*, the results show that mature lymphocyte subsets differ in their dependence on ZIP7, with MZ B cells and naïve T cells being especially sensitive.

A key limitation of the current analysis is that $Zip7^{f}$ deletion was confirmed only at the genomic level. Due to the lack of a robust antibody suitable for flow cytometry or Western blotting in primary lymphocytes, direct assessment of ZIP7 protein loss—particularly in small subsets—remains challenging. As an orthologous approach, transcript-level confirmation by RT-qPCR could help determine whether Cre-mediated recombination leads to reduced *Zip7* mRNA expression in B and T cells. In parallel, scRNA-seq–based analysis of exon usage may allow estimation of deletion efficiency at single-cell resolution. These strategies are discussed further in the General Discussion (Section 7.7) as part of future validation plans.

MZ B cell loss was consistently observed across multiple contexts—including unmanipulated, Ig-tg, and $Zip7^{P198A/f}$ or $Zip7^{H199QV/f}$ *Cr2-cre* BM chimeras—and competitive repopulation assays confirmed a cell-intrinsic defect. Notably, Ig-tg $Zip7^{+/f}$ *Cr2-cre* mice also displayed a statistically significant reduction in MZ B cells compared to Ig-tg $Zip7^{P198A/f}$ mice lacking *Cr2-cre*. This suggests that the monoclonal BCR background may sensitise the system to reveal subtle gene dosage effects, although the contribution of other factors cannot be excluded. Such an effect was not observed in non-Ig-tg models, and the underlying mechanism remains to be elucidated.

A comparable dose-sensitive phenotype was also observed in T cells. Naïve $CD4^{+}$ and $CD8^{+}$ T cells were markedly reduced in $Zip7^{P198A/f}$ *Cd4-cre* mice, and this deficit was again shown to be cell-intrinsic in mixed chimeras, where ZIP7-deficient donor cells

were severely outcompeted by their WT counterparts. In *Cd4-cre* mice, Cre recombinase expression is initiated at the DP stage and efficiently deletes floxed alleles in both $CD4^+$ and $CD8^+$ lineages[24]. While thymic development was preserved in *Zip7*$^{P198A/f}$ *Cd4-cre* mice, peripheral T cells were markedly reduced, suggesting that ZIP7 is dispensable during late thymocyte maturation but essential for post-thymic T cell survival. Interestingly, germline *Zip7*$^{P198A/P198A}$ mice retain normal T cell numbers in both thymus and periphery[20], indicating that partial ZIP7 activity may suffice under homeostatic conditions. In contrast, the marked reduction of peripheral T cells in *Zip7*$^{P198A/f}$ *Cd4-cre* mice implies that further reduction in ZIP7 dosage—by compound heterozygosity—renders peripheral T cell maintenance untenable. These findings point to a dose-sensitive requirement for ZIP7 in mature T cells and raise the possibility that ZIP7 supports survival or metabolic fitness in the periphery. Further studies assessing proliferation, metabolic capacity, or ZIP7 protein stability may help clarify the underlying mechanisms.

Chapter

5 ZIP7 deficiency alters antibody responses and germinal centre dynamics

5.1 Introduction

In the previous two chapters, phenotyping of various ZIP7 deficiency models demonstrated that an adequate level of intact ZIP7 is crucial for maintaining peripheral lymphocyte subsets. Notably, B cells were more sensitive to ZIP7 loss compared to T cells, with MZ B cells being the most affected.

Building on these findings, I sought to investigate how ZIP7-deficient lymphocytes respond to immunization, focusing on their role in humoral immunity. Using distinct TI and TD antigens, I evaluated the effects of ZIP7 deficiency on antibody production and GC formation. To further understand the precise stages affected, adoptive transfer models with antigen-specific ZIP7-deficient lymphocytes were employed. These models enabled the examination of ZIP7's role in critical processes such as B cell recruitment into GCs, their maintenance within the GC microenvironment, and clonal proliferation during immune responses.

5.2 B cell intrinsic requirement for ZIP7 to mount an effective humoral response

B cells are critical mediators of humoral immunity, orchestrating responses against both TI and TD antigens. To assess the role of ZIP7 in B cell-mediated adaptive immunity, I challenged *Zip7*$^{P198A/f}$ *Cr2-cre* mice with well-characterized TI (NP-Ficoll) and TD (NP-CGG, SRBC) antigens. These models allowed me to systematically evaluate the ability of ZIP7-deficient B cells to mount effective humoral responses across different immunological contexts.

5.2.1 Reduced NP-Ficoll responses in *Zip7*$^{P198A/–}$ B cells

To evaluate the immune response to T cell-independent antigens, I immunized mice with NP-Ficoll, a type II TI antigen consisting of the hapten 4-hydroxy-3-nitrophenylacetyl (NP) conjugated to Ficoll. NP-Ficoll is commonly used to assess BCR-dependent responses, particularly from MZ B cells and B1 cells, and is known to elicit IgM production and class-switching responses[335,336]. Compared to controls with at least one intact *Zip7* allele, *Zip7*$^{P198A/f}$ *Cr2-cre* mice displayed significantly reduced levels of IgM, IgG, and IgG3 antibodies (Figure 5-1). This impaired extrafollicular response may, at least in part, reflect the diminished MZ B cell population in *Zip7*$^{P198A/f}$ *Cr2-cre* mice.

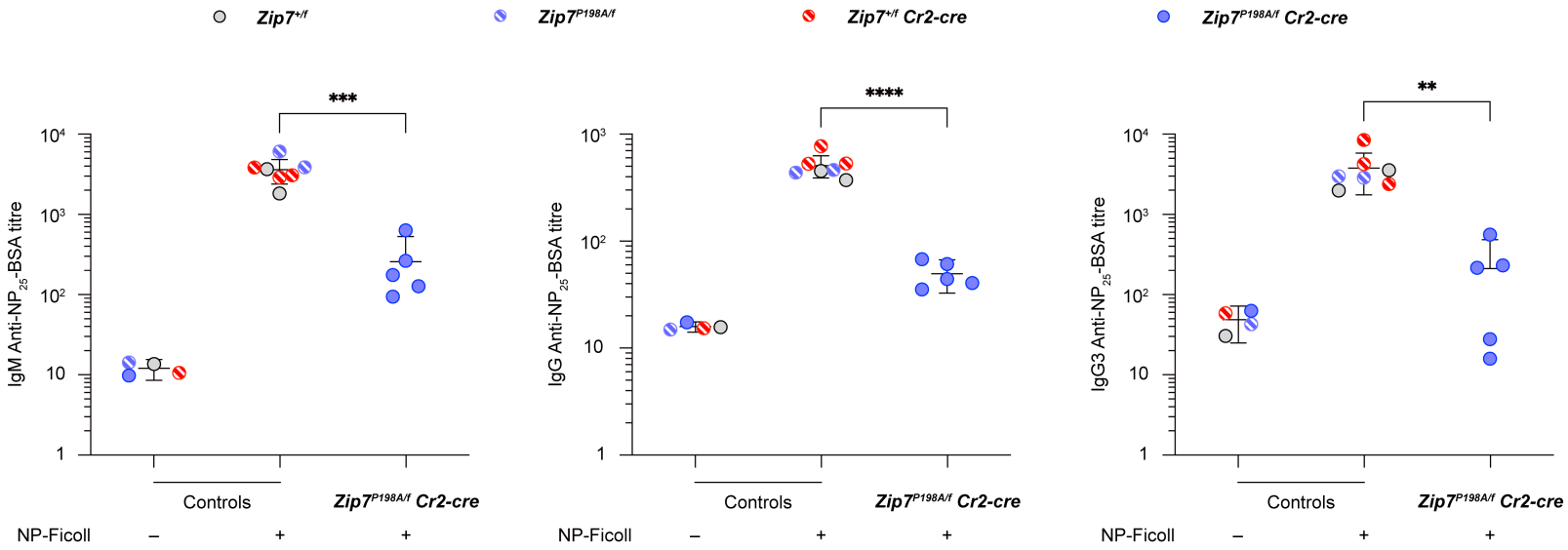

Figure 5-1: Reduced antibody responses to NP-Ficoll in *Zip7*$^{P198A/f}$ *Cr2-cre* mice.
NP-specific IgM (left panel), IgG (middle panel), and IgG3 (right panel) were measured by ELISA on day 8 after NP-Ficoll immunization. Each dot represents an individual mouse. Immunized controls include *Zip7*$^{+/f}$, Zip7$^{P198A/f}$, and *Zip7*$^{+/f}$ *Cr2-cre* mice (as defined in key), pooled for comparison. Unimmunized controls (mice of the same genotypes without immunization) demonstrate baseline non-specific binding. The *p*-value between immunized controls and *Zip7*$^{P198A/f}$ *Cr2-cre* mice was calculated using unpaired *t* test with Welch's correction.

5.2.2 Early IgM suppression and persistent IgG deficiency in NP-specific responses in *Zip7$^{P198A/f}$ Cr2-cre* mice

To evaluate the role of ZIP7 in T cell-dependent antibody production, I immunized Zip7$^{+/+}$ and *Zip7$^{P198A/f}$ Cr2-cre* chimeric mice with NP-conjugated chicken gamma globulin (NP-CGG), followed by a secondary boost on Day 42 (Figure 2-2). Serum samples were collected at multiple timepoints to assess the progression of the immune response, including antibody class switching, production, and affinity maturation.

The serum IgM titres peaked on Day 14 after the primary immunization and showed an increase following the Day 42 boost. Across most timepoints, the levels of NP-specific IgM in *Zip7$^{P198A/f}$ Cr2-cre* mice were comparable to controls, except for a transient reduction on Day 7 post-immunization (Figure 5-2A).

In contrast, whilst total IgG levels increased steadily after primary immunization and peaked around Day 28 in controls, IgG titres in *Zip7$^{P198A/f}$ Cr2-cre* mice were markedly reduced from early stages, indicating a significant defect in IgG production. While the total IgG levels in *Zip7$^{P198A/f}$ Cr2-cre* mice improved over time, they remained consistently lower than in controls (Figure 5-2B). Interestingly, however, the fold-change in IgG titres over time was higher in *Zip7$^{P198A/f}$ Cr2-cre* mice compared to controls (Supplementary Figure 15), suggesting that, despite their initial defect, *Zip7$^{P198A/f}$ Cr2-cre* B cells can respond robustly once engaged in the immune response.

I next examined high-affinity NP-specific IgG titres as a measure of affinity maturation. High-affinity NP-specific IgG levels in the *Zip7$^{P198A/f}$ Cr2-cre* group were consistently lower than those in controls throughout the immune response, even as titres increased over time (Figure 5-2C). Additionally, the proportion of high-affinity IgG relative to total IgG (NP_7/NP_{25} ratio) showed a downward trend in *Zip7$^{P198A/f}$ Cr2-cre* mice, further suggesting impaired affinity maturation (Figure 5-2D).

These results demonstrate that *Zip7*$^{P198A/f}$ *Cr2-cre* B cells can undergo class switching, affinity maturation, and respond to secondary immunization. However, fewer cells contribute to this process from an early stage, leading to reduced antibody production. Despite a greater fold-change in IgG titres over time, the overall IgG levels and antibody affinity maturation were consistently impaired in *Zip7*$^{P198A/f}$ *Cr2-cre* mice compared to controls. This suggests that ZIP7 is essential for optimal B cell responses in T cell-dependent immune challenges.

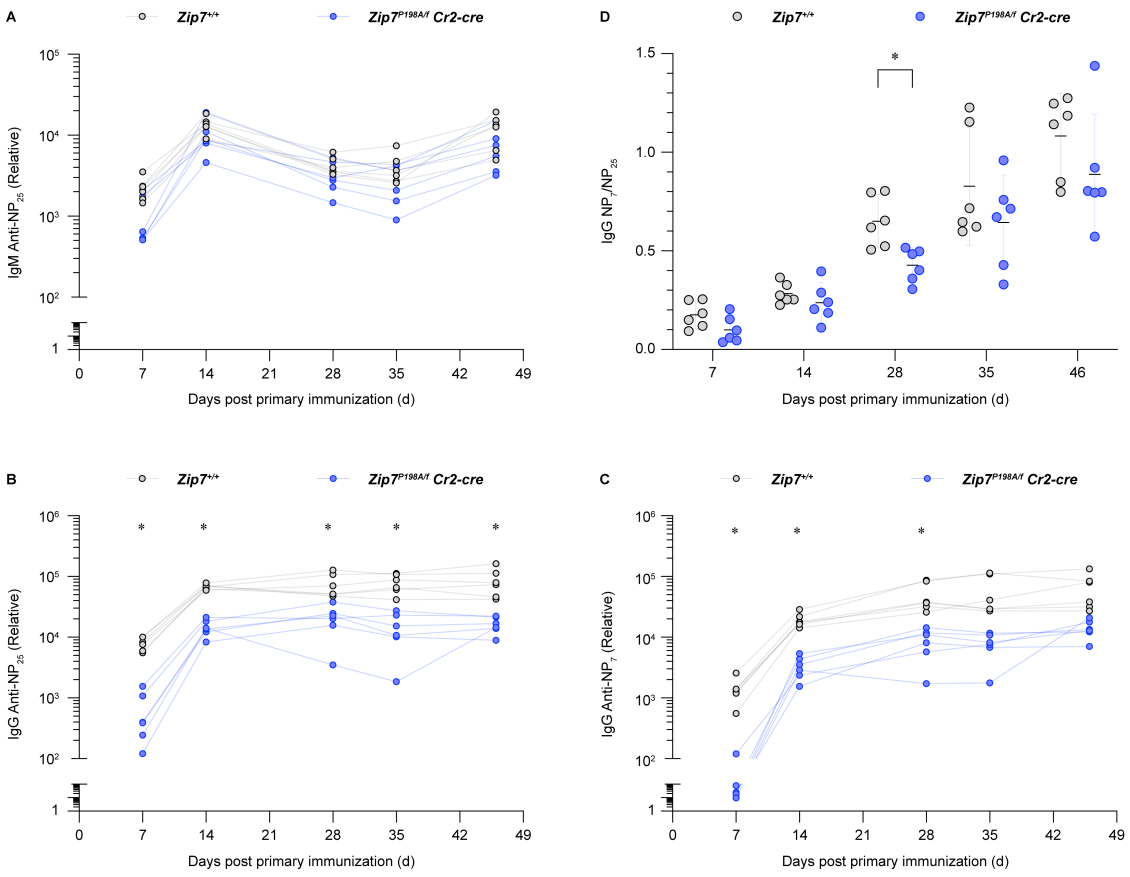

Figure 5-2: Longitudinal monitoring of NP-specific antibody titres after primary and secondary immunization with NP-CGG.
(A-C) Relative titres of NP-specific IgM (A), IgG (B), and high-affinity IgG (C) measured by ELISA at multiple timepoints following primary immunization (Day 0) and secondary immunization (Day 42). Antibody titres were calculated using arbitrary units, determined based on serial dilution and fitted to a 4PL model. (D) Ratio of high-affinity IgG (anti-NP_7) to total IgG (anti-NP_{25}) at each timepoint, reflecting antibody affinity maturation. Data are presented as mean ± 95% CI. Each dot represents an individual mouse. Statistical analysis was conducted using unpaired *t* test with Welch correction, followed by Holm-Šídák's multiple comparisons test.

5.2.3 Cell-intrinsic GC response defects in *Zip7$^{P198A/f}$ Cr2-cre* B cells after SRBC immunization

To address effects that might be compensated by the presence of WT cells or vice versa, a competitive mixed chimera model was employed (Figure 2-3), allowing ZIP7-deficient (CD45.2$^+$) and WT (CD45.1$^+$) B cells to coexist within the same recipient, providing internal controls.

As expected, the development of BM B cells remained unaffected in *Zip7$^{P198A/f}$ Cr2-cre* mixed chimeras, with a reduction observed only in recirculating B cells. In the spleen, the proportion of CD45.2$^+$ *Zip7$^{P198A/f}$ Cr2-cre* follicular B cells mirrored this reduction, while MZ B cells were consistently diminished (Figure 5-3).

Following SRBC immunization, the *Zip7$^{P198A/f}$ Cr2-cre* mixed chimeras exhibited a significant reduction in GC B cells and IgG1$^+$ B cells compared to controls (Figure 5-3). Notably, these defects were observed even in the presence of WT B cells in the same environment, emphasising the intrinsic requirement of ZIP7 for effective GC responses. Additional data from *Zip7$^{P198A/f}$ Cr2-cre* chimeras derived from an independent founder line corroborated these findings (Supplementary Figure 16).

These results demonstrate that ZIP7-deficient B cells exhibit impaired GC responses, even when supported by WT cells, highlighting a B cell intrinsic requirement for ZIP7 in mounting effective immune responses.

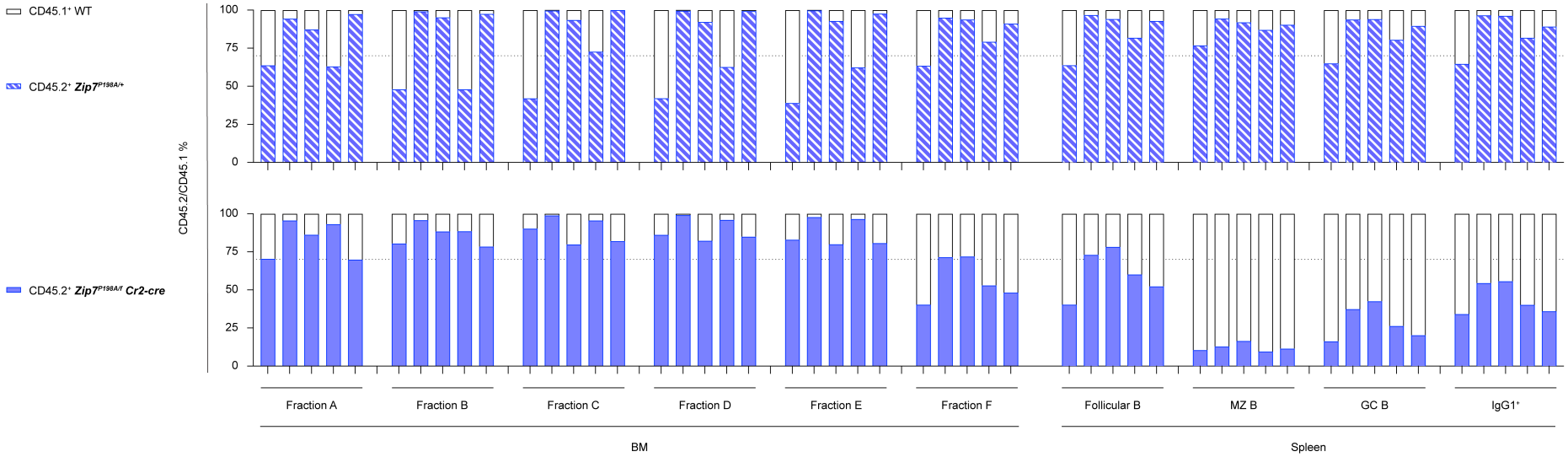

Figure 5-3: Reduced GC B and IgG1$^+$ cells in *Zip7*$^{P198A/f}$ *Cr2-cre* mixed chimeras after SRBC immunization.
Chimeric mice were generated by injecting 70:30 BM mixtures of CD45.2$^+$ *Zip7*$^{P198A/+}$ or *Zip7*$^{P198A/f}$ *Cr2-cre* and CD45.1$^+$ WT BM cells into lethally irradiated recipients. After 8 weeks of reconstitution, mice were immunized with SRBC, and spleens and BM were analysed by flow cytometry on Day 8 post-immunization. The proportion of CD45.1$^+$ (white) and CD45.2$^+$ (coloured) cells within each B cell subset was determined. Columns represent individual mice, with five mice per group. GC B cells were defined as CD95$^+$ GL7$^+$ IgD$^-$ B220$^+$ CD19$^+$ cells.

5.3 ZIP7 deficiency impairs recruitment and survival of GC B cells

The impaired GC functions observed in *Zip7*$^{P198A/–}$ B cells raise questions about whether these defects occur during recruitment, survival, or interactions with other lymphocytes within GCs. To address this, I employed an adoptive transfer model using HEL-specific MD4 B cells, which are characterized by expressing IgM^a and IgD^a with a high affinity anti-HEL specificity (Ig^{HEL})[74].

This model allows precise distinguishing of donor-derived B cells using anti-allotypic monoclonal antibodies and selective activation by HEL or HEL-conjugated antigens, such as HEL-SRBC. Following adoptive transfer, MD4 B cells home to lymphoid organs and, upon HEL-SRBC immunization, engage in T cell-dependent GC responses. This approach provides a robust framework for examining ZIP7-deficient B cell recruitment, survival, and function within GCs under well-controlled conditions.

5.3.1 MZ B cell deficiency alone does not explain impaired GC responses in *Zip7*$^{P198A/f}$ *Cr2-cre* mice

While MZ B cells contribute to GC formation via antigen transport[118,337,338], their selective reduction in *Zip7*$^{P198A/f}$ *Cr2-cre* mice raises the possibility that impaired GC responses arise from MZ deficiency. To test this, I compared the GC outcomes of adoptively transferred B cells derived from spleen or MLNs, which differ in MZ B cell content.

In this experimental setup, I transferred a 50:50 mixture of CD45.2$^+$ MD4 *Zip7*$^{P198A/f}$ *Cr2-cre* or *Zip7*$^{+/f}$ *Cr2-cre* B cells with CD45.1$^+$ MD4 WT B cells into CD45.2$^+$ WT recipient mice. This design ensured that the CD45.1$^+$ MD4 WT B cells served as internal controls, while CD45.2$^+$ B cells from MD4 *Zip7*$^{P198A/f}$ *Cr2-cre* or *Zip7*$^{+/f}$ *Cr2-cre* donors experienced identical environments (Figure 2-1). By minimizing

the influence of external factors, this model provided direct evidence of ZIP7's role in GC B cell formation.

On Day 8 post-immunization, GC B cells ($CD95^+$ $GL7^+$ PNA^+) were analysed (Supplementary Figure 17). $CD45.2^+$ MD4 *Zip7*$^{+/f}$ *Cr2-cre* B cells from spleen or MLN maintained a similar ratio to the input (close to 50%), but $CD45.2^+$ MD4 *Zip7*$^{P198A/f}$ *Cr2-cre* B cells, whether sorted from spleen or MLN, presented significantly lower proportions at 14.26% (7.64 – 20.88%) and 11.75% (-0.74 – 24.25%), respectively (mean with 95% CI; Figure 5-4). Absolute numbers of ZIP7-deficient GC B cells were reduced; however, this reduction was not statistically significant (Figure 5-4).

To further explore whether the reductions in ZIP7-deficient B cells were GC-specific, I performed additional analyses. HEL-binding non-GC B cells were more prevalent than GC B cells in both groups. Among transferred splenic B cells, MD4 *Zip7*$^{P198A/f}$ *Cr2-cre* B cells showed a reduction in non-GC compartments compared to MD4 *Zip7*$^{+/f}$ *Cr2-cre* B cells (Figure 5-5A, B). However, such reductions were not observed in the transferred B cells sorted from the MLN (Figure 5-5C, D).

Together, these findings suggest that the impaired GC responses in *Zip7*$^{P198A/f}$ *Cr2-cre* mice cannot be solely attributed to MZ B cell deficiency. The reductions were more pronounced within the GC than outside it, indicating that the highly competitive and proliferative GC environment poses additional challenges for the survival and maintenance of ZIP7-deficient B cells.

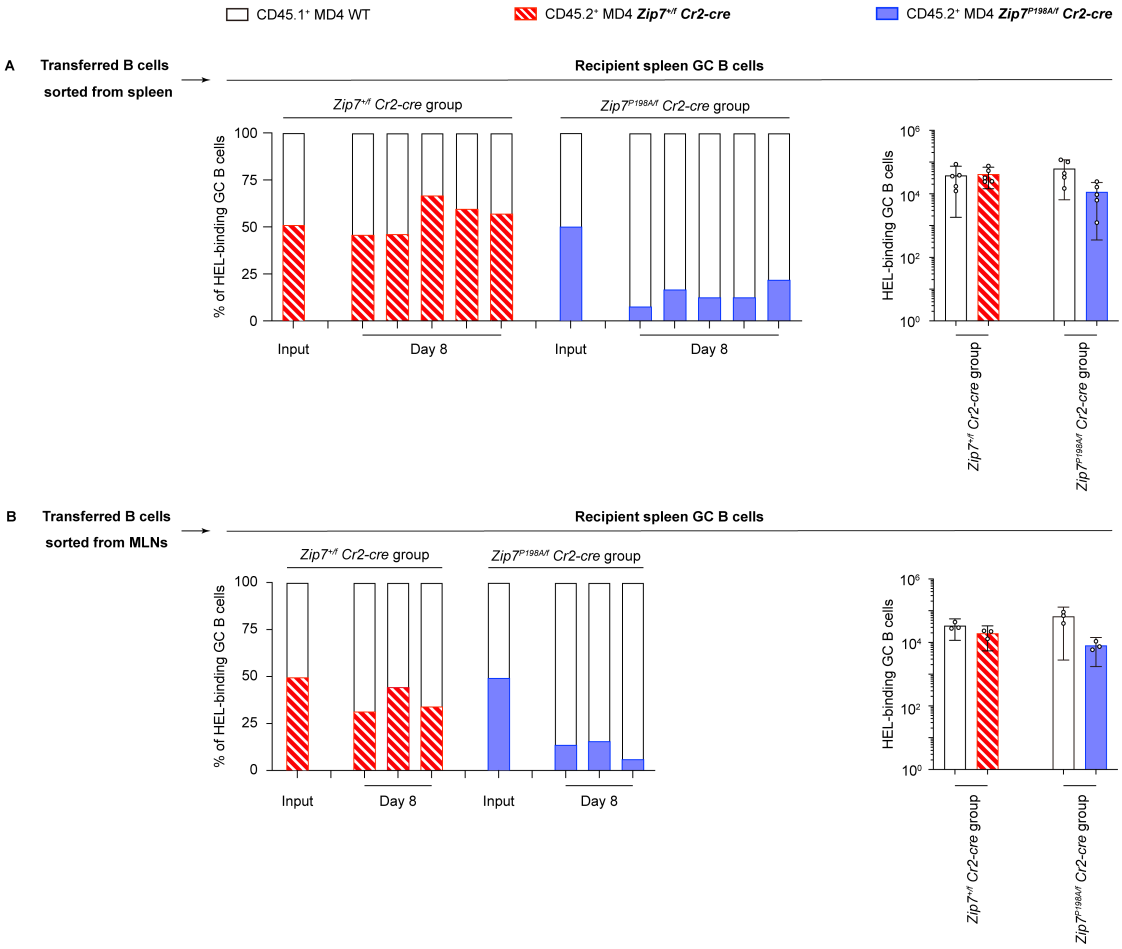

Figure 5-4: ZIP7 deficiency impairs splenic GC B cell formation in the MD4 *Cr2-cre* adoptive transfer model following HEL-SRBC immunization.
GC B cells were analysed in the spleens of recipient mice on Day 8 after immunisation. (A and B) Proportions (left) and absolute numbers (right) of HEL-binding GC B cells ($CD95^+$ $GL7^+$ PNA^+) in recipient spleens. $CD45.1^+$ MD4 WT and $CD45.2^+$ MD4 *Zip7*$^{+/f}$ *Cr2-cre* (red hatched) or *Zip7*$^{P198A/f}$ *Cr2-cre* (blue solid) B cells were sorted from donor spleen (A) or donor MLNs (B) and transferred at a 1:1 ratio into $CD45.2^+$ WT recipients. Each bar on the left represents an individual mouse. On the right, bars indicate means ± 95% CI; each dot represents one mouse. Statistical analysis was performed using unpaired two-tailed Welch's *t*-test with Holm–Šídák correction for multiple comparisons. For details of the adoptive transfer protocol, see Methods Section 2.1.5.

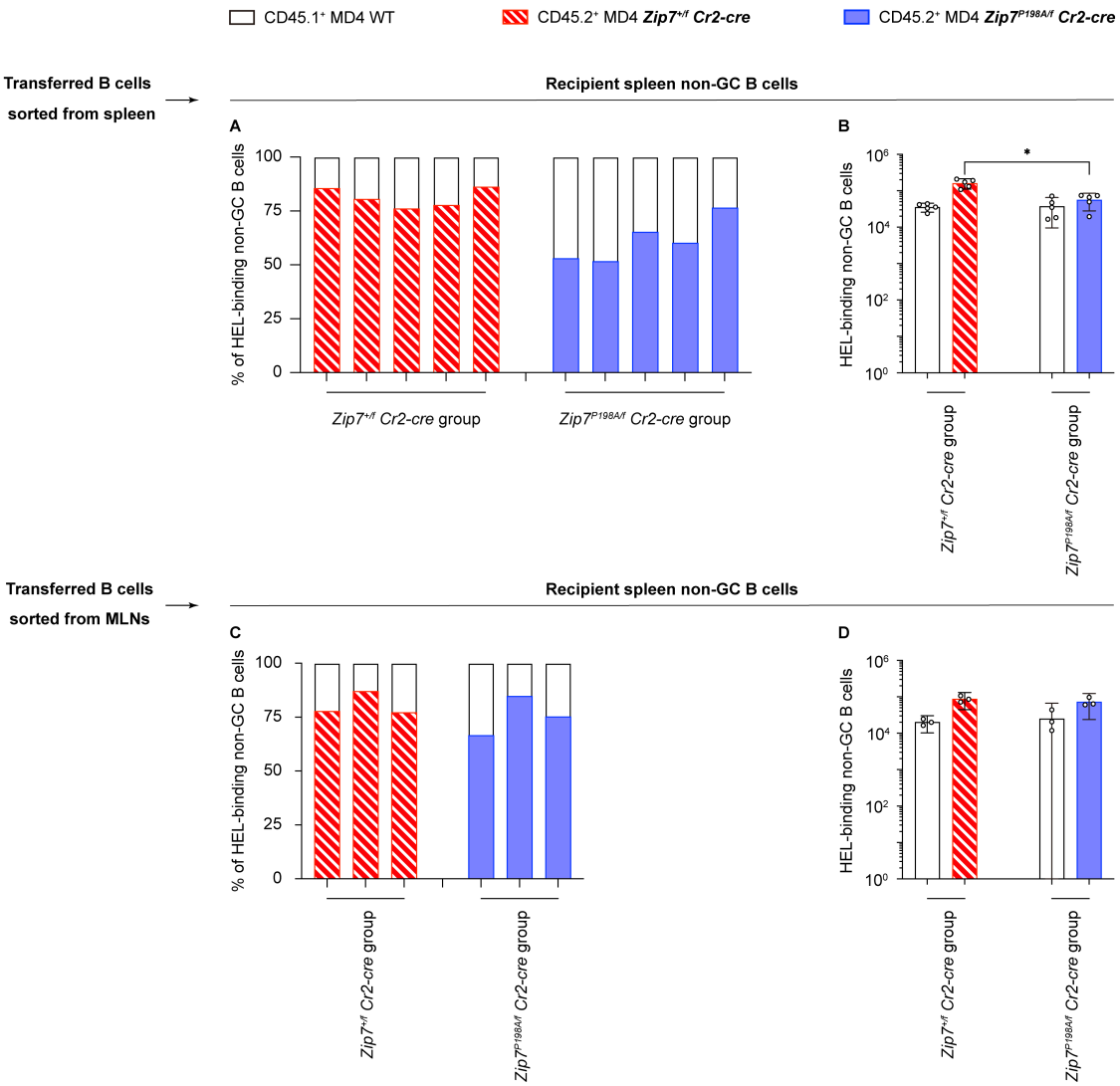

Figure 5-5: HEL-binding non-GC B cells in recipient spleens from the same adoptive transfer experiment shown in Figure 5-4.
(A, C) Proportions of HEL-binding non-GC B cells derived from CD45.2$^+$ (coloured) and CD45.1$^+$ (white) donors, based on transferred B cells sorted from the spleen (A) or MLN (C), eight days post-immunization. Each column represents one mouse.
(B, D) Absolute numbers of HEL-binding non-GC B cells corresponding to transferred B cells sorted from the spleen (B) or MLN (D), eight days post-immunization. The bars represent the mean ± 95% CI, while the dots indicate individual mice. Statistical analyses were performed using unpaired *t* test with Welch correction, followed by Holm-Šídák's multiple comparisons test. For experimental details, see Methods Section 2.1.5.

5.3.2 Impaired GC entry and persistence of ZIP7-deficient B cells

While MZ B cells are unique to the spleen and contribute to GC formation, other micro-environmental differences exist between the spleen and lymph nodes. To address these complexities and validate the GC responses of antigen-specific ZIP7-deficient B cells

under more comparable baseline conditions, I employed the *Ert2-cre* mouse models for additional analyses.

After inducing deletion by tamoxifen in MD4 *Zip7*$^{f/f}$ and MD4 *Zip7*$^{f/f}$ *Ert2-cre* mice, I sorted CD45.2^{+} MD4 *Zip7*$^{f/f}$ or MD4 *Zip7*$^{f/f}$ *Ert2-cre* B cells and mixed each with CD45.1/2^{+} MD4 WT B cells at a 50:50 ratio. The mixed cells were then adoptively transferred into CD45.1^{+} wild-type recipient mice, which were immunised with HEL-SRBC to induce germinal centre formation (Figure 5-6A, B). On Day 9 post-HEL-SRBC immunization, CD45.2^{+} MD4 *Zip7*$^{f/f}$ GC B cells retained their input ratio, while MD4 *Zip7*$^{f/f}$ *Ert2-cre* GC B cells showed a significant reduction in both proportions and absolute numbers (Figure 5-6C, E). To determine whether this reduction was due to uniform depletion or specific accumulation outside the GC, I analysed transferred B cells in non-GC compartments. ZIP7-deficient B cells also showed significant reductions in non-GC compartments (Figure 5-6D, F).

To further investigate whether the observed deficits stemmed from impaired recruitment into GCs or decreased maintenance of ZIP7-deficient B cells, I analysed spleen samples on Day 3 post-HEL-SRBC immunization. At this early stage, MD4 *Zip7*$^{f/f}$ *Ert2-cre* B cells were markedly reduced within GC compartments compared to controls, both in proportion and absolute number (Figure 5-7A, C). In contrast, the reduction was less evident in non-GC compartments (Figure 5-7B, D), suggesting a defect in early GC recruitment or proliferation.

These findings demonstrate that effective recruitment into GCs is deficient and contributes to the reduced presence of ZIP7-deficient B cells observed at later stages. Additionally, the persistence of low numbers in both GC and non-GC compartments by Day 9 highlights maintenance challenges that ZIP7-deficient B cells face as the immune response progresses. This underscores the critical role of ZIP7 in both the initiation and sustained phases of B cell responses to antigenic stimulation.

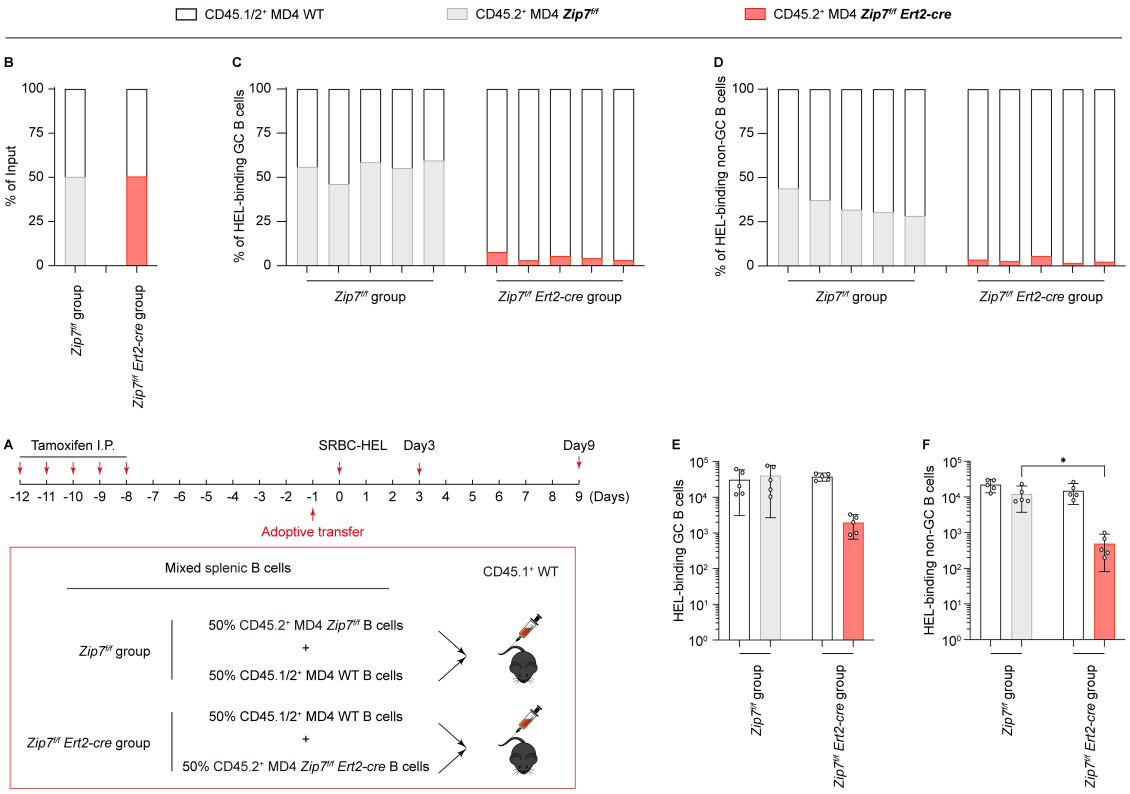

Figure 5-6: Reduced MD4 *Zip7*$^{f/f}$ *Ert2-cre* B cells in both GC and non-GC compartments on Day 9 post-HEL-SRBC immunization.
(A) Experimental setup and timeline. MD4 *Zip7*$^{f/f}$ and MD4 *Zip7*$^{f/f}$ *Ert2-cre* chimeric mice were treated with tamoxifen to induce ZIP7 deletion. One week after the final dose, splenic B cells were sorted and mixed with CD45.1/2^{+} MD4 WT B cells at a 50:50 ratio. These mixtures ('*Zip7*$^{f/f}$ group' and '*Zip7*$^{f/f}$ *Ert2-cre* group' as illustrated) were transferred into CD45.1^{+} WT recipients, followed by HEL-SRBC immunization the next day. (B) Validation of the 50:50 input ratios of CD45.2^{+} and CD45.1/2^{+} donor B cells before adoptive transfer. (C, D) Proportions of transferred MD4 B cells within GC (C) and non-GC (D) compartments in the spleen. (E, F) Absolute numbers of transferred MD4 B cells in GC (E) and non-GC (F) compartments. Bars represent the mean ± 95% CI, and dots indicate individual mice. Statistical analysis was performed using unpaired *t* tests with Welch correction, followed by Holm-Šídák's multiple comparisons test.

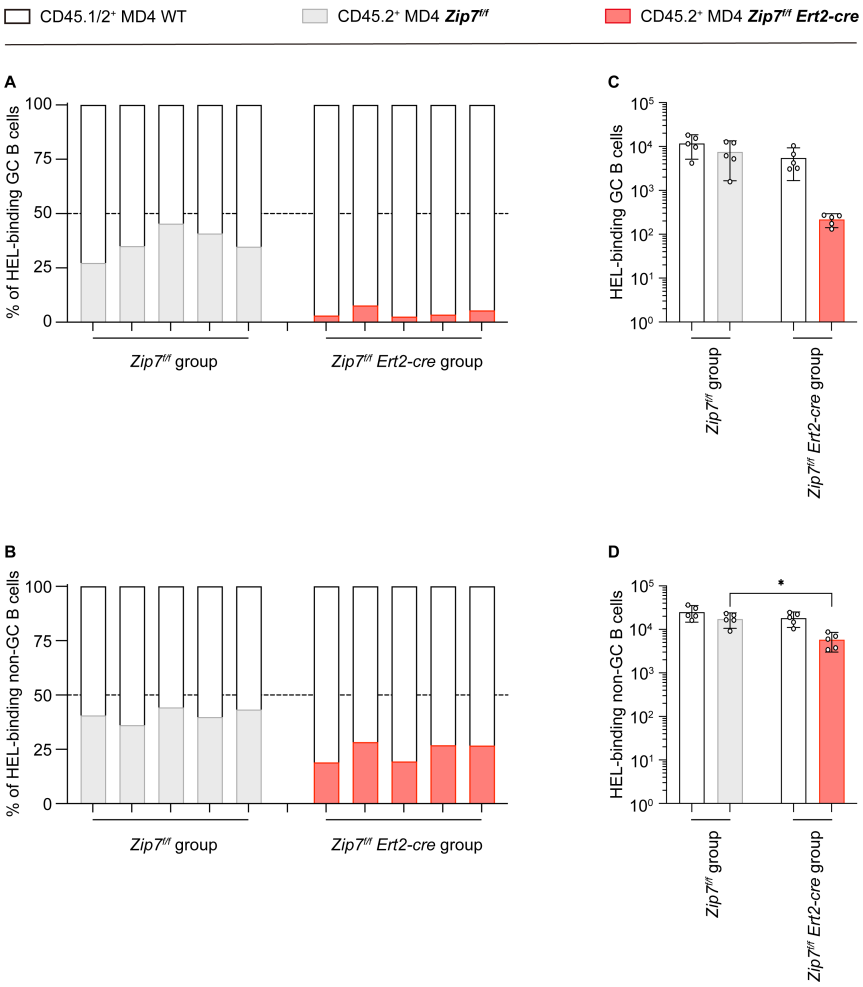

Figure 5-7: Impaired recruitment of MD4 *Zip7*$^{f/f}$ *Ert2-cre* B cells into GC compartments on Day 3 post-HEL-SRBC immunization.
This figure represents an early time point analysis of the same experimental model as in Figure 5-6. (A, B) Proportions of transferred MD4 B cells within GC (A) and non-GC (B) compartments. (C, D) Corresponding absolute numbers of transferred MD4 B cells in GC (C) and non-GC (D) compartments. Bars show the mean value with 95% CI, and dots represent individual mice. Statistical analysis was performed using unpaired *t* tests with Welch correction, followed by Holm-Šídák's multiple comparisons test.

5.3.3 ZIP7-deficient GC B cells exhibit comparable distribution in dark zone and light zone compartments

GCs are specialised microenvironments where B cells proliferate predominantly in the DZ and undergo interactions for selection in the LZ. After observing a significant reduction in transferred MD4 ZIP7-deficient B cells within GCs following HEL-SRBC immunization, I sought to determine whether their distribution within the DZ and LZ was altered.

Given the low number of ZIP7-deficient GC B cells, precise analysis was required to avoid bias. To achieve this, I employed the same tamoxifen-induced deletion and adoptive transfer protocol described in Figure 5-6A but collected spleens on Day 8 post-HEL-SRBC immunization. Tight gating strategies were applied to reliably distinguish $CD45.2^+$ donor-derived and $CD45.1/2^+$ internal control MD4 GC B cells, particularly in the *Zip7*$^{f/f}$ *Ert2-cre* group, where most GC B cells originated from the internal control (Figure 5-8A).

At Day 8, most GC B cells were localized in the LZ. Both $CD45.2^+$ ZIP7 WT and ZIP7-deficient B cells showed comparable distributions between DZ and LZ compartments across groups (Figure 5-8B). The absolute cell numbers of ZIP7-deficient GC B cells were markedly lower in both DZ and LZ compared to their WT counterparts, reflecting the overall reduction in GC B cells (Figure 5-8C). Although numerical differences were observed in dark and light zone cell numbers, none of the comparisons reached statistical significance after Holm–Šídák correction for multiple testing (adjusted $p > 0.05$ for all comparisons).

These findings suggest that while ZIP7 deficiency results in a cell-intrinsic reduction of GC B cells, it does not disrupt their proportional distribution between the DZ and LZ, indicating that the defect is uniformly manifested across these compartments.

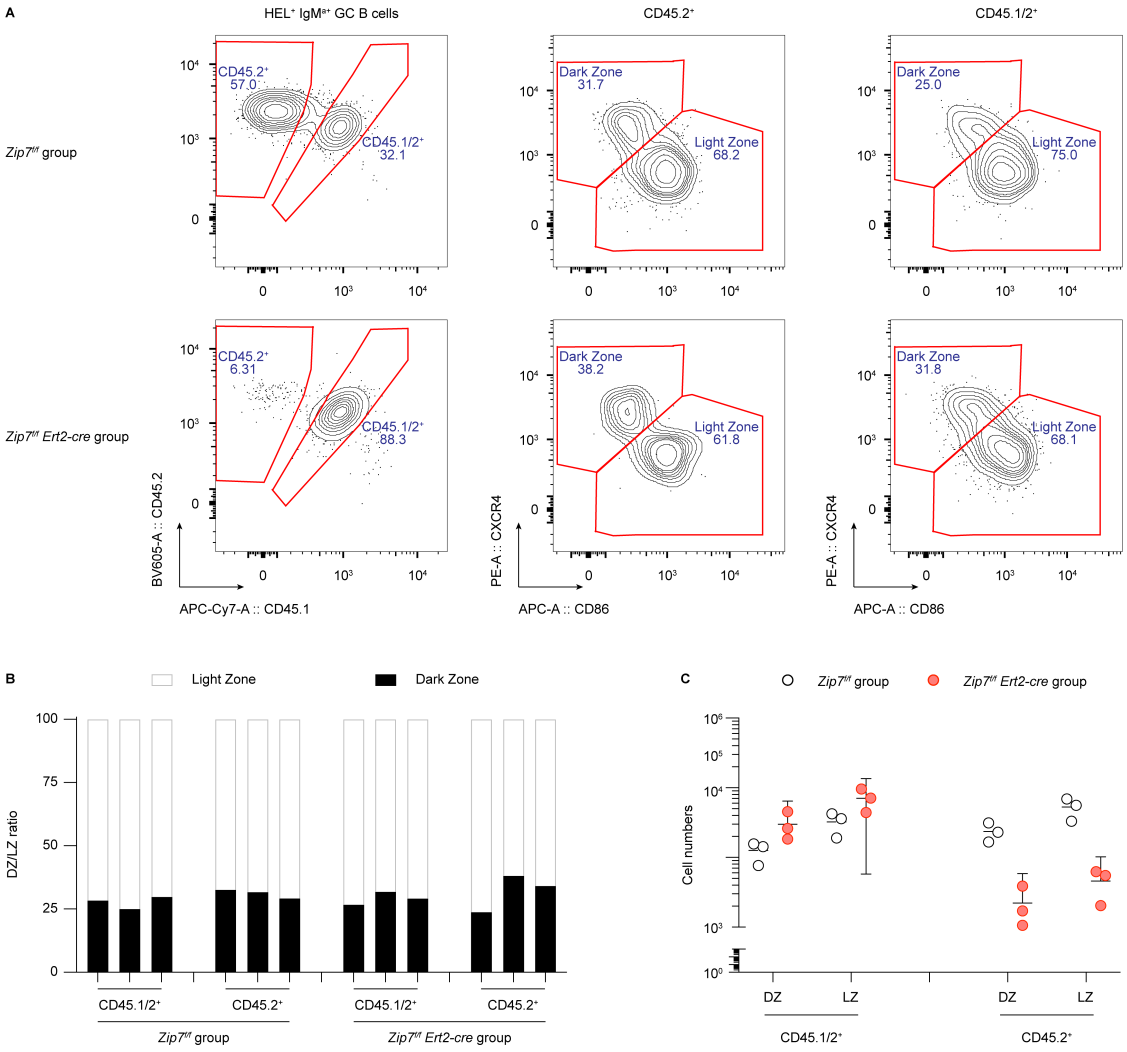

Figure 5-8: Comparable distribution of ZIP7-deficient GC B cells in DZ and LZ compartments within GCs.
(A) Representative FACS plots showing the distribution of CD45.2$^+$ and CD45.1/2$^+$ MD4 GC B cells in the Dark Zone (DZ, CXCR4$^+$ CD86$^-$) and Light Zone (LZ, CXCR4$^-$ CD86$^+$) for the *Zip7$^{f/f}$* and *Zip7$^{f/f}$ Ert2-cre* groups. (B, C) Proportions (B) and absolute cell numbers (C) of CD45.2$^+$ and CD45.1/2$^+$ MD4 GC B cells within DZ and LZ compartments. (B) Each column represents an individual mouse. (C) Bars represent mean values with 95% CIs, and dots indicate individual mice. Statistical analyses were conducted using unpaired *t* tests with Welch correction, followed by Holm-Šídák's multiple comparisons test.

5.3.4 ZIP7-deficient GC B cells maintain proliferation capacity despite their reduced numbers

Having observed a significant reduction in the number of ZIP7-deficient GC B cells but no preferential distribution between the DZ and LZ compartments, I next investigated whether ZIP7 deficiency affects the proliferative capacity of GC B cells.

To evaluate this, I assessed BrdU incorporation, which labels actively proliferating cells during DNA synthesis. BrdU was administered intraperitoneally four hours prior to spleen collection on Day 8 post-HEL-SRBC immunization (Figure 5-9A). The proportion of $BrdU^+$ GC B cells was comparable between $CD45.2^+$ MD4 ZIP7-deficient and ZIP7 WT GC B cells (Figure 5-9B). As expected, the absolute numbers of both $BrdU^+$ and $BrdU^-$ GC B cells were reduced in ZIP7-deficient cells due to the overall decrease in GC B cell numbers (Figure 5-9C). Although numerical differences in GC B cell counts were observed between ZIP7-deficient and WT-like populations, none of the comparisons reached statistical significance after Holm–Šídák correction for multiple testing (adjusted $p > 0.05$ for all cases).

These findings suggest that ZIP7 deficiency does not impair the proliferative capacity of GC B cells within the microenvironment, despite their reduced overall numbers. However, I cannot exclude the possibility that a subset of GC B cells may have escaped Cre-mediated deletion, and thus contributed to the preserved BrdU incorporation.

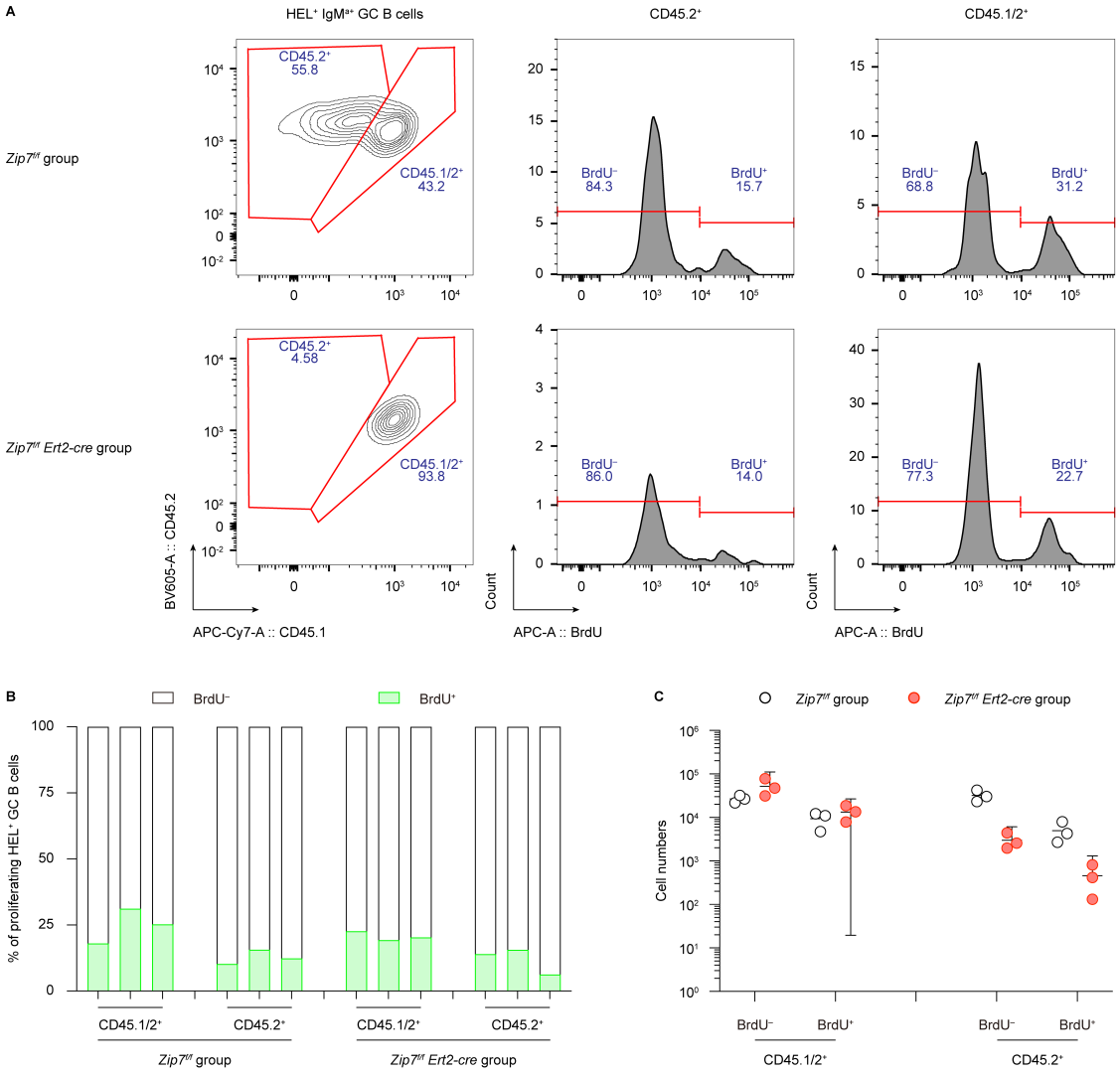

Figure 5-9: ZIP7-deficient GC B cells maintain proliferative capacity despite reduced numbers on Day 8 post-HEL-SRBC immunization.
(A) Representative FACS plots distinguishing CD45.2$^+$ cells and internal control CD45.1/2$^+$ cells within HEL-specific GC B cells (CD95$^+$ GL7$^+$ IgM^{a+} HyHEL9$^+$). Histograms display the percentages of BrdU$^-$ and BrdU$^+$ cells within different MD4 donor-derived GC B cell populations. The BrdU$^+$ threshold was determined using a control mouse that underwent the same adoptive transfer and immunization protocol but did not receive BrdU injection. (B) Proportions of BrdU$^+$ and BrdU$^-$ cells among HEL-specific MD4 GC B cells for each mouse. (C) Absolute numbers of BrdU$^+$ and BrdU$^-$ HEL-specific GC B cells derived from each donor population. Bars represent the mean with 95% CI, and dots indicate individual mice. Statistical analysis was conducted using unpaired *t* tests with Welch correction and Holm-Šídák's multiple comparisons test.

5.3.5 ZIP7-deficient B cells exhibit intrinsic survival defects even without immunization

Since internal factors such as localisation or proliferation did not fully account for the loss of ZIP7-deficient GC B cells, I next assessed whether these cells exhibited an intrinsic survival defect.

To test this possibility, I adoptively transferred cells in unimmunized recipients. As illustrated in Figure 5-6A, spleen samples were collected on Day 3 and Day 9. By Day 3, the proportion of CD45.2$^+$ MD4 ZIP7 WT B cells remained consistent with the input ratio (53%, 48 – 58%), whereas ZIP7-deficient B cells showed a modest reduction to 43% (39 – 47%) (mean, 95% CI; Figure 5-10A). By Day 9, ZIP7-deficient B cells had significantly declined to 8.7% (2 – 15%), even in the absence of antigenic stimulation (mean, 95% CI; Figure 5-10B).

These findings demonstrate that ZIP7-deficient B cells have an intrinsic survival defect that becomes more pronounced over time, independent of external antigenic challenges. Such a survival defect is very likely to result in the significant loss of GC and non-GC B cells observed during immune responses.

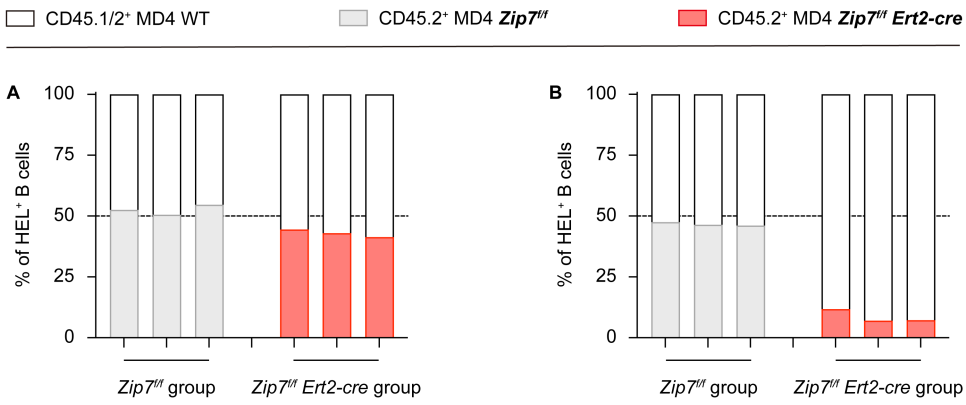

Figure 5-10: Reduction in transferred MD4 ZIP7-deficient B cells in unimmunized recipients over time.
Adoptively transferred spleen samples were collected on Days 3 and 9, corresponding to the immunization timeline of experimental counterparts, as outlined in Figure 5-6A. (A, B) Proportions of transferred MD4 B cells (CD45.2$^+$ *Zip7$^{f/f}$* or *Zip7$^{f/f}$ Ert2-cre*)

relative to internal control MD4 WT B cells in the spleens of unimmunized recipients on Day 3 (A) and Day 9 (B). Each column represents an individual mouse. The dashed line indicates the expected 50:50 input ratio.

5.4 Discussion

This chapter demonstrates that ZIP7 is essential for effective B cell responses to both TI and TD antigens. ZIP7-deficient B cells exhibit impaired antibody production, reduced GC formation, and diminished affinity maturation. These defects result from two key mechanisms: possibly inefficient recruitment into GCs at early stages and intrinsic survival disadvantages during immune responses.

The initial IgM response of *Zip7*$^{P198A/f}$ *Cr2-cre* mice to NP-CGG was lower than that of WT mice, suggesting a reduced extrafollicular short-lived plasma cell response in the absence of ZIP7. In contrast, the IgM response to NP-Ficoll was more profoundly impaired, to some extent due to the depletion of MZ B cells in this model. Despite eventual increases in IgG titres following NP-CGG immunization, ZIP7-deficient mice exhibited persistently lower antibody levels and reduced affinity maturation, reflecting a diminished pool of responding B cells.

Adoptive transfer models further confirmed that ZIP7-deficient B cells are less efficiently recruited into GCs and undergo progressive loss over time, even in non-immunized hosts. These effects cannot be explained by spatial mislocalisation or proliferation failure within GCs, as GC B cells displayed normal DZ/LZ distribution and intact BrdU incorporation. Instead, the progressive decline in both GC and non-GC compartments points to a fundamental survival defect, which is exacerbated in the highly competitive GC environment.

Together, these findings highlight a cell-intrinsic requirement for ZIP7 in supporting B cell recruitment, persistence, and antibody refinement during humoral immune responses.

Chapter

6 ZIP7-dependent transcriptional stress programs revealed by scRNA-seq

6.1 Introduction

Flow cytometry revealed a marked reduction of MZ B cells and GC B cells in ZIP7-deficient mice, whereas T cell populations appeared relatively preserved. However, flow cytometry is inherently limited to predefined subsets defined by established surface markers and may miss transcriptionally distinct or intermediate states. To explore how ZIP7 deficiency differentially impacts B and T cells at the transcriptomic level, I employed scRNA-seq as an unbiased, high-resolution approach to comprehensively profile lymphocyte heterogeneity and stress responses.

This approach aimed to identify transcriptional programs and pathways differentially engaged across ZIP7 genotypes, with a particular focus on stress-related signatures and adaptive mechanisms. By integrating gene expression data with surface protein markers and genotype information, I sought to uncover potential regulators that may explain the contrasting phenotypes observed between B- and T cell compartments.

6.2 Quality control and initial clustering reveal distinct B and T lymphocyte compartments

Pooled CD45.2^{+} splenic lymphocytes from *Zip7$^{+/f}$ Ert2-cre*, *Zip7$^{P198A/f}$ Ert2-cre*, and *Zip7$^{f/f}$ Ert2-cre* (n = 3 per genotype) were collected on Day 7 after tamoxifen treatment and profiled using the 10X Genomics scRNA-seq platform. Cells from individual samples were uniquely hashtagged[27] to retain genotype identity and labelled with CITE-seq[26] antibodies to simultaneously capture transcriptome and surface protein information (Figure 2-4). To improve detection of rare populations such as MZ B cells, the pooled sample was split into two technical replicates (Samples A and B) for sequencing.

Each replicate yielded ~14,000 high-quality cells with >2,000 median genes per cell and sequencing saturation levels above 70%, indicating optimal library complexity and sequencing depth. Sample-specific quality control was performed to filter doublets and low-quality cells (Figure 2-5, Figure 2-6), and no major batch effects were observed between replicates or genotype groups (Supplementary Figure 18A, B). Therefore, cells from both samples were merged without batch correction for downstream analysis.

Initial clustering at low resolution (Res = 0.1) identified 10 distinct clusters, broadly corresponding to two dominant immune lineages, namely, B and T cells, as confirmed by ADT labelling and canonical gene markers (Figure 6-1). A small transcriptionally distinct population (Cluster 8) expressed myeloid-associated genes[339,340] (e.g. *Csf1r*[341], *Lyz2*[342], *Siglech*[343]) but lacked B or T cell markers, suggesting a minor contaminant population of dendritic or myeloid origin (Figure 6-1C, D).

Cells corresponding to the B and T lymphocyte lineages were subsequently extracted and re-clustered at higher resolution to investigate lineage-specific transcriptional heterogeneity and genotype-associated phenotypes in the following sections.

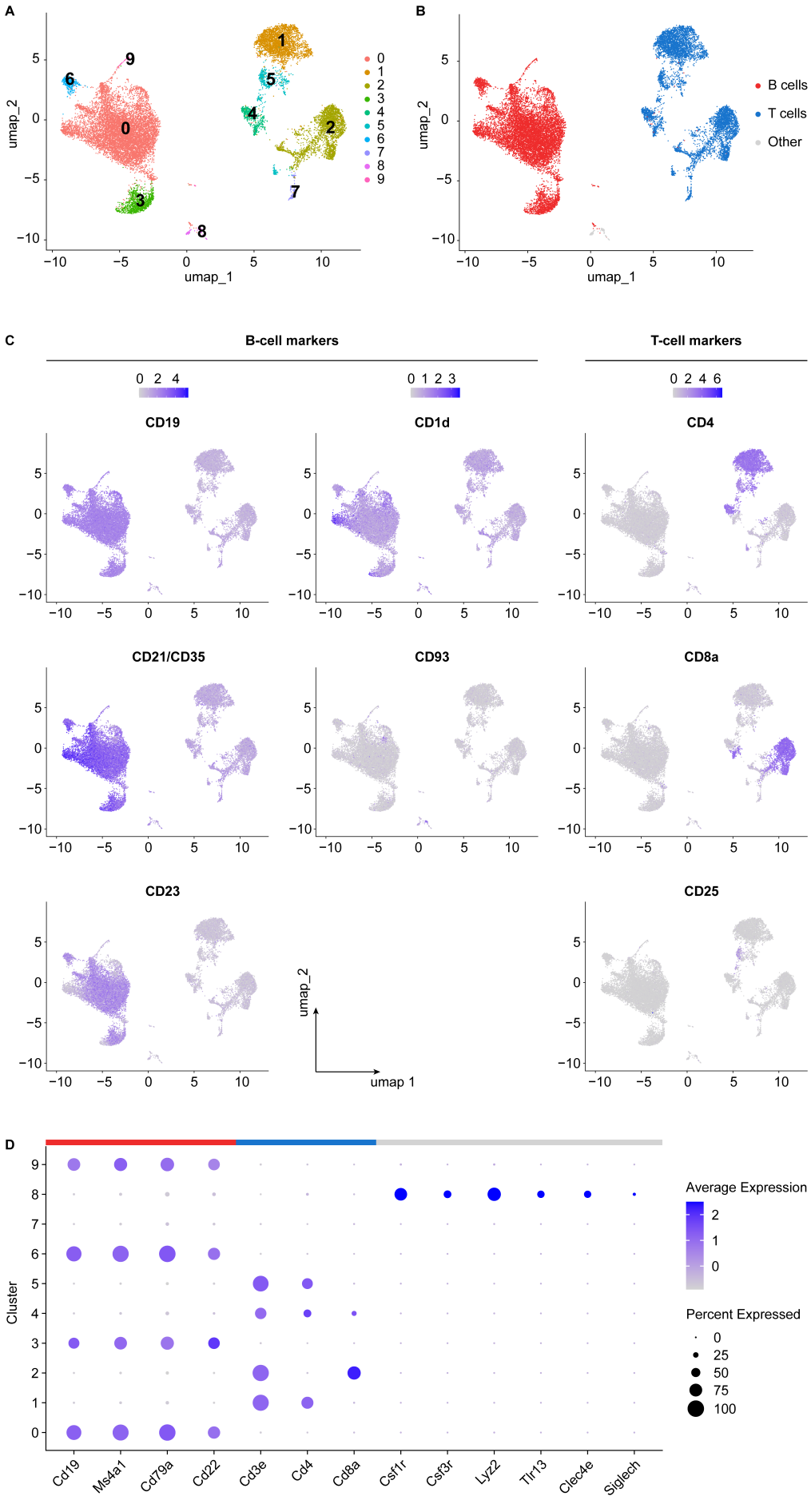
A
B
umap_1
umap_2
B cells
T cells
Other
C
B-cell markers
T-cell markers
CD19
CD1d
CD4
CD21/CD35
CD93
CD8a
CD23
CD25
umap 1
D
Cluster
Average Expression
Percent Expressed
Cd19
Ms4a1
Cd79a
Cd22
Cd3e
Cd4
Cd8a
Csf1r
Csf3r
Lyz2
Tlr13
Clec4e
Siglech

Figure 6-1: Integrated analysis of surface marker expression and transcriptional clustering of splenic lymphocytes.
(A) Unsupervised clustering of 17,651 CD45.2$^+$ splenic lymphocytes using scRNA-seq at resolution = 0.1. Each colour represents a distinct transcriptional cluster (0–9). (B) Lineage classification based on canonical surface and transcriptomic markers. Clusters were broadly assigned to B cells (clusters 0, 3, 6, 9), T cells (clusters 1, 2, 4, 5, 7), and myeloid cells (cluster 8). (C) UMAP plots showing the expression of selected B cell (CD19, CD21/CD35, CD23, CD1d, CD93) and T cell (CD4, CD8a, CD25) surface markers detected by CITE-seq antibody-derived tags (ADT). Colour intensity reflects normalised expression levels. (D) Dot plot summarising the expression of canonical B cell, T cell, and myeloid lineage markers across clusters. Dot size indicates the percentage of cells expressing each gene, and colour intensity represents average expression. Cluster 8 was excluded from lymphocyte-focused analyses.

6.3 Transcriptomic cluster annotation and ZIP7-dependent stress enrichment in T cells

Initial transcriptomic clustering of total T cells (resolution = 0.1) revealed 7 distinct populations (Supplementary Figure 19C). Among them, Clusters 0 and 3 corresponded predominantly to CD4$^+$ T cell subsets, while Cluster 1 corresponded to a CD8$^+$ T cell subset. In addition, Clusters 5 and 6 correspond to NK and NKT lineages, respectively. Although Cluster 2 and 4 co-expressed both CD4 and CD8 surface proteins, Cluster 4 also expressed CD19, suggesting significant B cell contamination, while Cluster 2 exhibited a memory-like transcriptomic signature (Supplementary Figure 19B, D).

To enable focused analysis of lineage-specific phenotypes, total T cells were stratified into CD4$^+$ and CD8$^+$ subsets based on ADT expression thresholds. These cutoffs were derived from the bimodal distributions observed in Cluster 2 and were consistently applicable across the broader T cell population (Supplementary Figure 19A, D and E). Cells with high CD4 but low CD8 expression were assigned to the CD4$^+$ subset, and vice versa for the CD8$^+$ subset.

6.3.1 Identification of a stressed CD4$^+$ T cell cluster under ZIP7 deficiency

To investigate whether ZIP7 deficiency alters the phenotypic composition of CD4$^+$ T cells, I examined transcriptomic clustering within this lineage. Unsupervised clustering at low resolution (Res = 0.1) identified six transcriptionally distinct clusters (Figure 6-2A). In addition to the major CD4$^+$ naïve T cell population (Cluster 0), two well-defined subsets were annotated as Treg (Cluster 1) and memory CD4$^+$ T cells (Cluster 2). The Treg cluster was characterized by high surface expression of CD25 and canonical RNA markers such as *Foxp3*[344], *Ctla4*[345], and *Nrp1*[346,347]. The memory CD4$^+$ T cell cluster expressed canonical central memory-associated markers including *Sell* (CD62L), *Ccr7*[214], and the transcriptional regulator *Lef1*[348,349], consistent with a central memory phenotype (Figure 6-2B).

Cluster 3 consisted exclusively of ZIP7-deficient cells, with *Zip7$^{f/f}$ Ert2-cre* contributing more cells than the *Zip7$^{P198A/f}$ Ert2-cre* genotype (Figure 6-2C, D). This population showed elevated expression of ER stress-related genes including *Atf4*, *Ddit3*, and *Trib3*, suggesting a stressed transcriptional state (Figure 6-2B). Cluster 4 and 5 were annotated as NKT cells and B cells, respectively, based on ADT and canonical transcriptomic markers (Figure 6-2A, B).

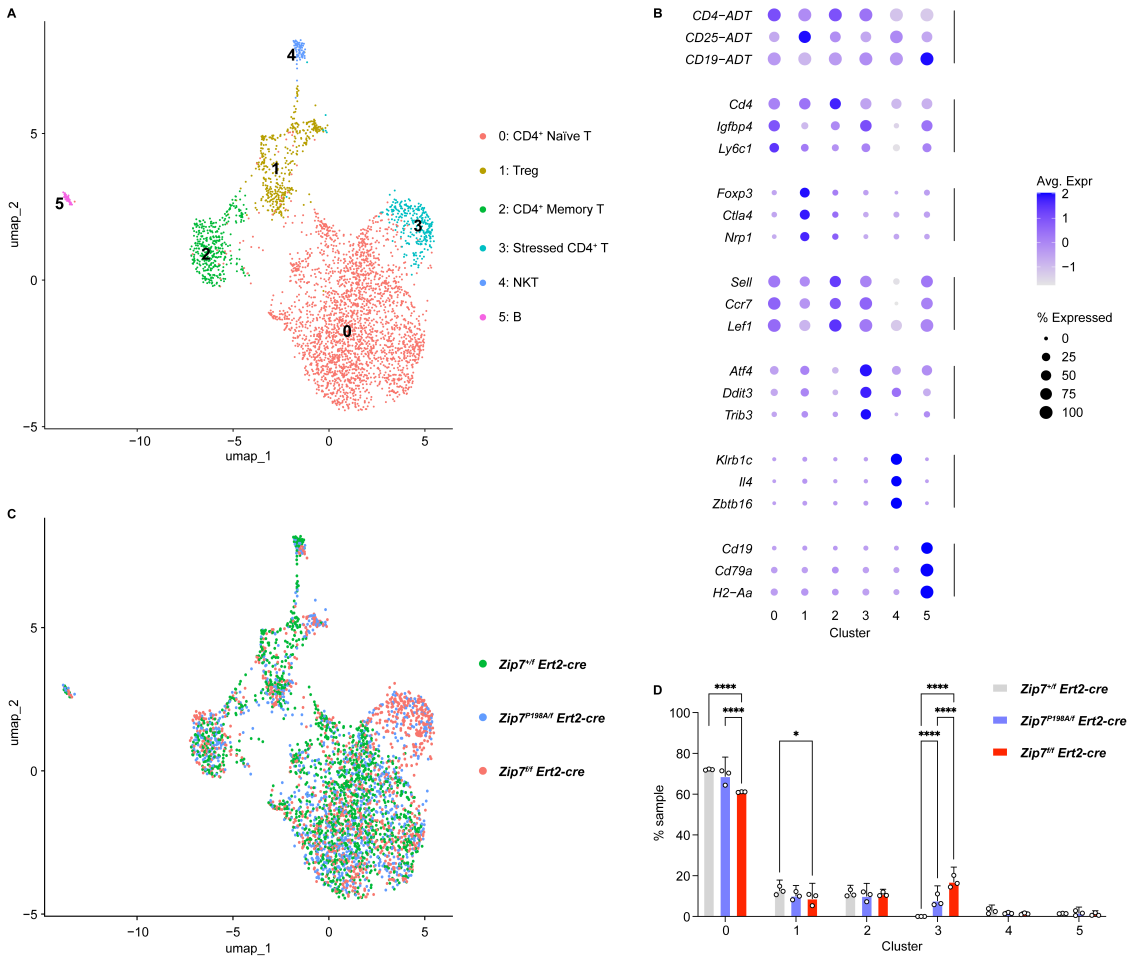

Figure 6-2: Phenotypic heterogeneity and genotype distribution of CD4⁺ T cell subsets. (A) UMAP of CD4⁺ T cell subset clustered at resolution 0.1, revealing six populations: CD4⁺ naïve T (0), Treg (1), memory T (2), stressed CD4⁺ T (3), NKT (4), and B cells (5). (B) Dot plot showing selected transcriptomic and ADT markers used for cluster annotation. (C) Genotype overlay on UMAP illustrating the distribution of cells from *Zip7*$^{+/f}$ *Ert2-cre* (green), *Zip7*$^{P198A/f}$ *Ert2-cre* (blue), and *Zip7*$^{f/f}$ *Ert2-cre* (red) mice. (D) Quantification of HTO-derived sample composition within each cluster. Data are presented as mean ± 95% CI (n = 3 per genotype). Statistical analysis was performed using two-way ANOVA followed by Šidák's multiple comparisons test (*$p < 0.05$, ****$p < 0.0001$).

6.3.2 CD8⁺ T cell subset: A ZIP7-linked stressed cell population

To test whether ZIP7-deficient cells also preferentially accumulated in a distinct cluster with a stress-associated signature, the distribution of CD8⁺ T cells from the three genotypic groups was projected onto a UMAP (Figure 6-3A). ZIP7-deficient samples (*Zip7*$^{P198A/f}$ *Ert2-cre* and *Zip7*$^{f/f}$ *Ert2-cre*) displayed preferential enrichment in a defined

region of the CD8$^+$ T cell landscape. To better resolve this region, clustering was performed at resolution 0.3 (Figure 6-3B), yielding 7 distinct transcriptional clusters. Of these, Cluster 1, was annotated as a CD8$^+$ stressed T cell population based on elevated expression of stress-response genes (e.g. *Atf4*, *Ddit3*, *Trib3*) and showed pronounced overrepresentation in ZIP7-deficient samples (Figure 6-3C, D), mirroring similar changes previously observed in CD4$^+$ T cells.

In contrast to the expanded stressed population, Cluster 0—representing CD8$^+$ naïve T cells—was markedly reduced in ZIP7-deficient mice (Figure 6-3D). Notably, this reduction in the naïve compartment had not been captured by conventional flow cytometry-based immunophenotyping. The reciprocal trends observed between Clusters 0 and 1 suggest a redistribution of cellular states, potentially reflecting early transcriptional perturbations in response to ZIP7 deficiency.

Beyond the naïve and stressed populations, several other clusters displayed distinct transcriptional programs (Figure 6-3C). Cluster 2 consisted of early-activated CD8$^+$ T cells, co-expressing activation markers such as *Pim2*[350], *Icam1*[351], *Junb*[352], alongside negative regulators including *Socs3*[353] and genes involved in NF-κB pathway attenuation. This signature suggests a self-limiting activation profile, potentially representing a transitional state shaped by negative feedback. Cluster 3 was enriched for effector-associated transcripts including *Gzma*, *Ccl5*[354], *Cxcr3*[215,355], and *Tbx21* (T-bet)[356], yet also expressed *Ikzf2* (Helios)[357] and *Il2rb* (CD122), indicating a subset with effector-like properties coupled to regulatory features. Cluster 5 further exemplified this regulatory axis, expressing high levels of *Ikzf2*, *Ctla4*, *Tigit*, and *Lag3*, consistent with a poised regulatory phenotype within the CD8$^+$ compartment. Cluster 4 was annotated as a CD8$^+$ memory T cell population, marked by the expression of *Sell* (CD62L), *Lef1*, and *Zbtb20*. These cells appeared transcriptionally quiescent and may adopt a low-energy, metabolically conserved state. Importantly, Clusters 2–5 did not show strong genotype-specific

differences in abundance (Figure 6-3D), suggesting that ZIP7 deficiency may primarily affect naïve and stressed CD8⁺ T cell subsets.

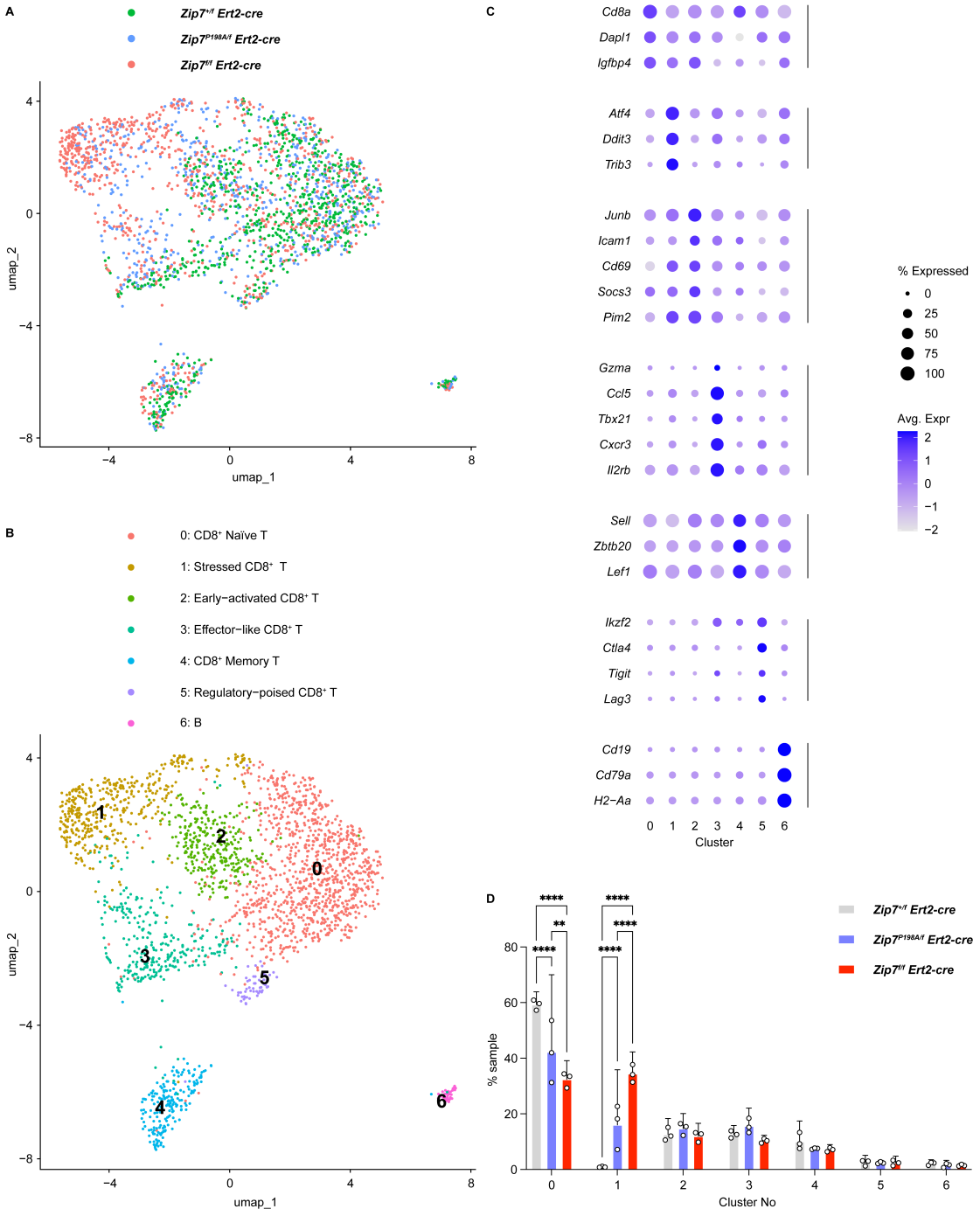

Figure 6-3: ZIP7 deficiency induces a stressed CD8⁺ T cell population and alters T cell subset distribution.
(A) UMAP of CD8⁺ T cells coloured by genotype group (*Zip7*$^{+/f}$ *Ert2-cre*, *Zip7*$^{P198A/f}$ *Ert2-cre*, and *Zip7*$^{f/f}$ *Ert2-cre*). (B) UMAP showing CD8⁺ T cell clustering at resolution 0.3, annotated based on marker gene expression. (C) Dot plot of selected marker genes used to define clusters. Dot size indicates the proportion of cells expressing each gene;

colour reflects average scaled expression. (D) Sample distribution across clusters, derived from HTO demultiplexing. Bars represent group means ± 95% CIs (n = 3 biological replicates per genotype). Significance was assessed using two-way ANOVA with Šidák correction for multiple comparisons. $^{**}p < 0.01$, $^{****}p < 0.0001$.

6.4 Transcriptional heterogeneity of splenic B cell populations

To investigate ZIP7-related changes within the B cell compartment, splenic B cells were subsetted for separate analysis. ADT signals confirmed uniform CD19 expression and revealed spatially distinct distributions of transitional ($CD93^+$) and marginal zone-like ($CD1d^+$ $CD23^-$) B cell populations (Figure 6-4A). Shifts in B cell distribution across ZIP7-deficient groups (Figure 6-4B) prompted refined clustering to better resolve transcriptional differences. A resolution of 0.6 was selected based on marker expression and cluster stability (Supplementary Figure 20), yielding 11 transcriptionally distinct B cell clusters.

Based on surface protein expression and the transcriptional profiles of canonical B cell subtype markers (Figure 6-5), several clusters were annotated with high confidence. Cluster 4 exhibited a $CD1d^{high}$ $CD21^{high}$ $CD23^{low}$ phenotype, alongside elevated expression of *Cd1d1*[358], *Cd9*[359], and *Fcrl5*[360], consistent with a MZ B cell identity. Cluster 9 showed a $CD93^{high}$ $CD21^{low}$ $CD23^{low}$ surface profile and upregulated expression of *Tnfrsf13c* (BAFF-R) and *Siglecg*, characteristic of transitional B cells. Cluster 8 demonstrated increased expression of *Egr1, Egr 2, Egr3* and *Nr4a1*, a transcriptional signature indicative of anergic B cells[361]. Cluster 10 displayed a bimodal pattern of CD19 surface protein expression, markedly reduced *Ighd* levels, and strong upregulation of GC-associated genes (*Aicda*, *Gcsam*, *Mki67*, *Fas*, *Rgs13*) as well as plasma cell-related genes (*Sdc1* [CD138], *Prdm1* [Blimp1], *Jchain*), suggesting this was a mixed GC/plasma cell population.

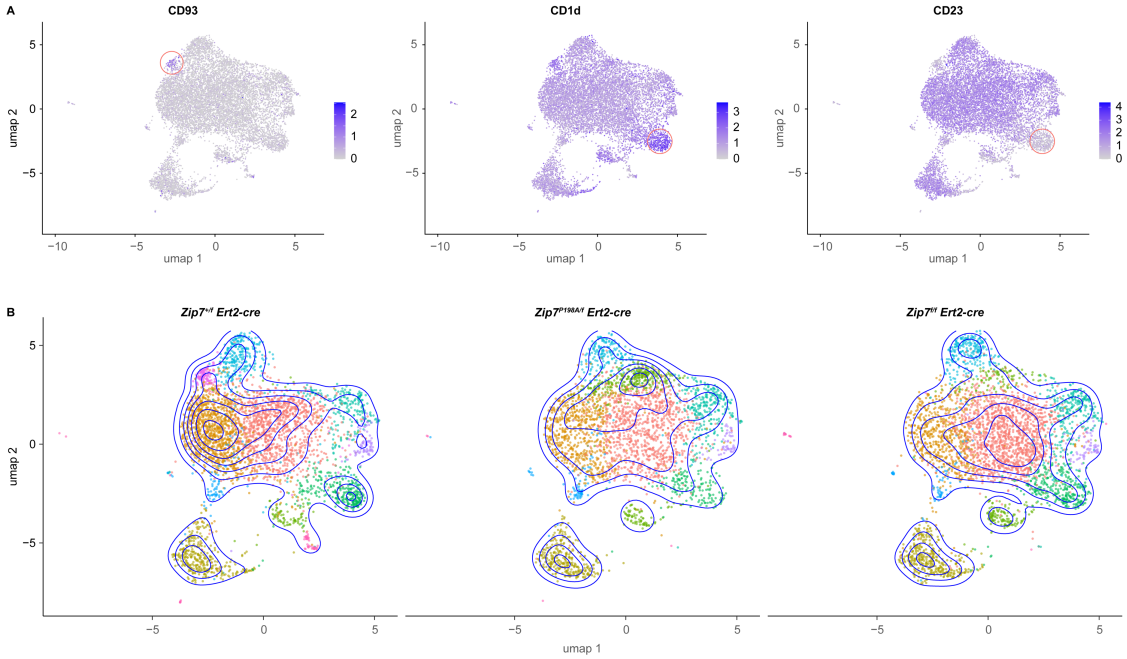

Figure 6-4: Surface marker–based B cell subset identification and genotype-driven shifts in transcriptionally defined clusters.
(A) UMAP plots showing protein expression levels of CD93, CD1d, and CD23, aiding initial identification of transitional ($CD93^+$) and marginal zone-like ($CD1d^+$ $CD23^-$) B cell populations. Highlighted circles indicate these subpopulations. (B) UMAP contour plots showing the spatial distribution of splenic B cells across three genotypes (*Zip7*$^{+/f}$ *Ert2-cre*, *Zip7*$^{P198A/f}$ *Ert2-cre*, *Zip7*$^{f/f}$ *Ert2-cre*), coloured by transcriptionally defined clusters (resolution = 0.6).

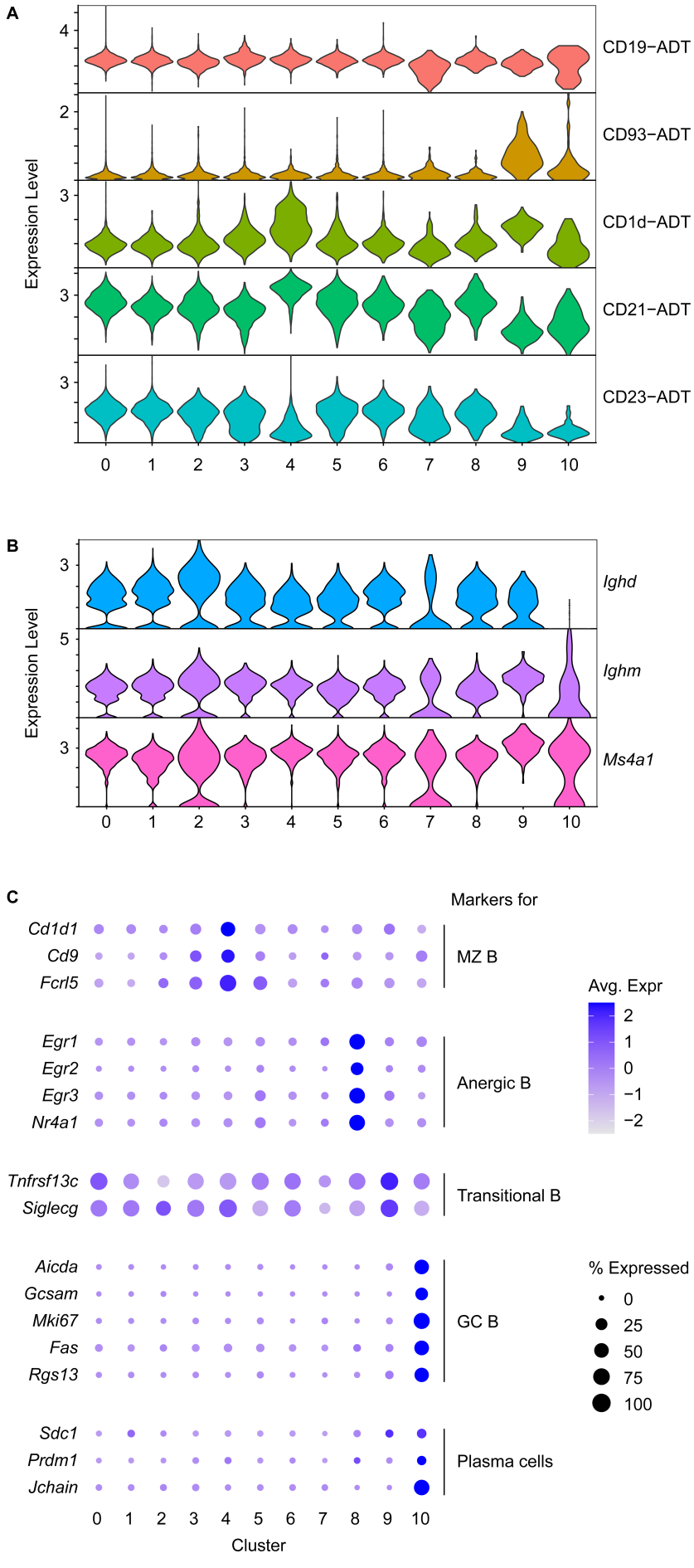
A
Expression Level
CD19−ADT
CD93−ADT
CD1d−ADT
CD21−ADT
CD23−ADT
0 1 2 3 4 5 6 7 8 9 10
B
Expression Level
Ighd
Ighm
Ms4a1
0 1 2 3 4 5 6 7 8 9 10
C
Markers for
Cd1d1
Cd9
Fcrl5
MZ B
Egr1
Egr2
Egr3
Nr4a1
Anergic B
Tnfrsf13c
Siglecg
Transitional B
Aicda
Gcsam
Mki67
Fas
Rgs13
GC B
Sdc1
Prdm1
Jchain
Plasma cells
0 1 2 3 4 5 6 7 8 9 10
Cluster
Avg. Expr
2
1
0
−1
−2
% Expressed
0
25
50
75
100

Figure 6-5: Phenotypic and transcriptional profiling of B cell clusters defined at resolution 0.6.
(A) Surface protein expression measured by ADTs across 11 transcriptionally defined B cell clusters. (B, C) RNA-level expression of general B cell identity genes (B), and canonical markers of MZ, anergic, transitional, GC, and plasma B cell subsets (C).

In addition to clusters that aligned with canonical B cell subtypes, given that splenic B cells were divided into 11 clusters with increased granularity, I therefore adopted a transcriptome-guided approach, incorporating cell cycle status and HTO distribution, to annotate the remaining clusters (Figure 6-6).

Clusters 0, 1, and 7 all displayed general characteristics of follicular B cells, but their differentially expressed genes (DEGs) were relatively limited and functionally broad, lacking highly distinctive markers compared to other clusters. To avoid overinterpretation, these clusters were provisionally designated as Follicular B_1 (Cluster 0), Follicular B_2 (Cluster 1), and Follicular B_3 (Cluster 7). Although transcriptional distinctions were subtle, each cluster exhibited minor features worth noting individually (Figure 6-6A). Cluster 1 expressed *Ccr7*[111], *S1pr4*, and *Klf2*[362]—genes associated with recirculating follicular B cells and migratory competence. Cluster 0 showed partial expression of genes associated with neighbouring subsets, but at lower levels than the defining clusters. For instance, *Vpreb3* was detectable but not as enriched as in transitional B cells (Cluster 9); *Cr2* was present but lower than in MZ B cells (Cluster 4); and *Xbp1* was expressed at levels below those observed in stressed B cells (Clusters 3 and 5) or GC/plasma-like B cells (Cluster 10). These features suggest that Cluster 0 may represent B cells in an intermediate or adaptive state, potentially undergoing early transcriptional changes in response to environmental cues such as stress cues or activation signals. Cluster 7 exhibited a heterogeneous expression pattern, with a subset of cells upregulating lysosomal and autophagy-related genes (*Lamp1*, *Rab7*, *Arl6ip5*). As these features were confined to a minor fraction of the cluster, interpretation remains cautious.

Cluster 2 exhibited minimal representation in the S phase (Figure 6-6B) and low expression of ribosomal and translation-related genes (*Rps26*, *Rpl34*, *Eef1b2*, *Atp5e*), indicating a quiescent cellular state. However, the upregulated expression of transcriptional regulators such as *Runx1* and *Tcf12*, along with chromatin-associated modifiers like *Hdac9*, *Smyd3*, and *Setbp1* (Figure 6-6A), suggests that these cells are epigenetically poised for rapid reactivation. This population lacked clear expression of germinal centre or plasma cell marker genes (Figure 6-5C), raising the possibility that they represent memory B cells. In unimmunized mice, however, identifying memory B cells is challenging without surface markers or BCR sequencing, and instead relies on transcriptional profiles. To support this annotation, I cross-referenced established transcriptomic markers of memory B cells described in immunized murine spleen, such as *Cd38*, *Tle3*, *Ski*[363], *Zbtb20*, *Bach2*, *Ptprc*, and *Cd22*[314], and annotated Cluster 2 as a memory B cell population.

Cluster 6 was characterised by robust upregulation of classical interferon-stimulated genes (ISGs)[364], including *Ifit3*, *Isg15*[365], *Bst2*, *Oasl1*, *Rtp4*[366], and *Eif2ak2* (PKR), suggesting an interferon-primed phenotype (Figure 6-6A). These cells also expressed the cytosolic pattern-recognition receptor (PRR) *Zbp1* (Dai), along with key transcriptional regulators (*Irf7*, *Irf9*, *Stat1*) and the negative feedback modulator *Usp18*, consistent with tonic type I interferon signalling. Notably, this population was not expanded in ZIP7-deficient samples (Figure 6-6D), suggesting that it represents a ZIP7-independent, interferon-primed B cell subset.

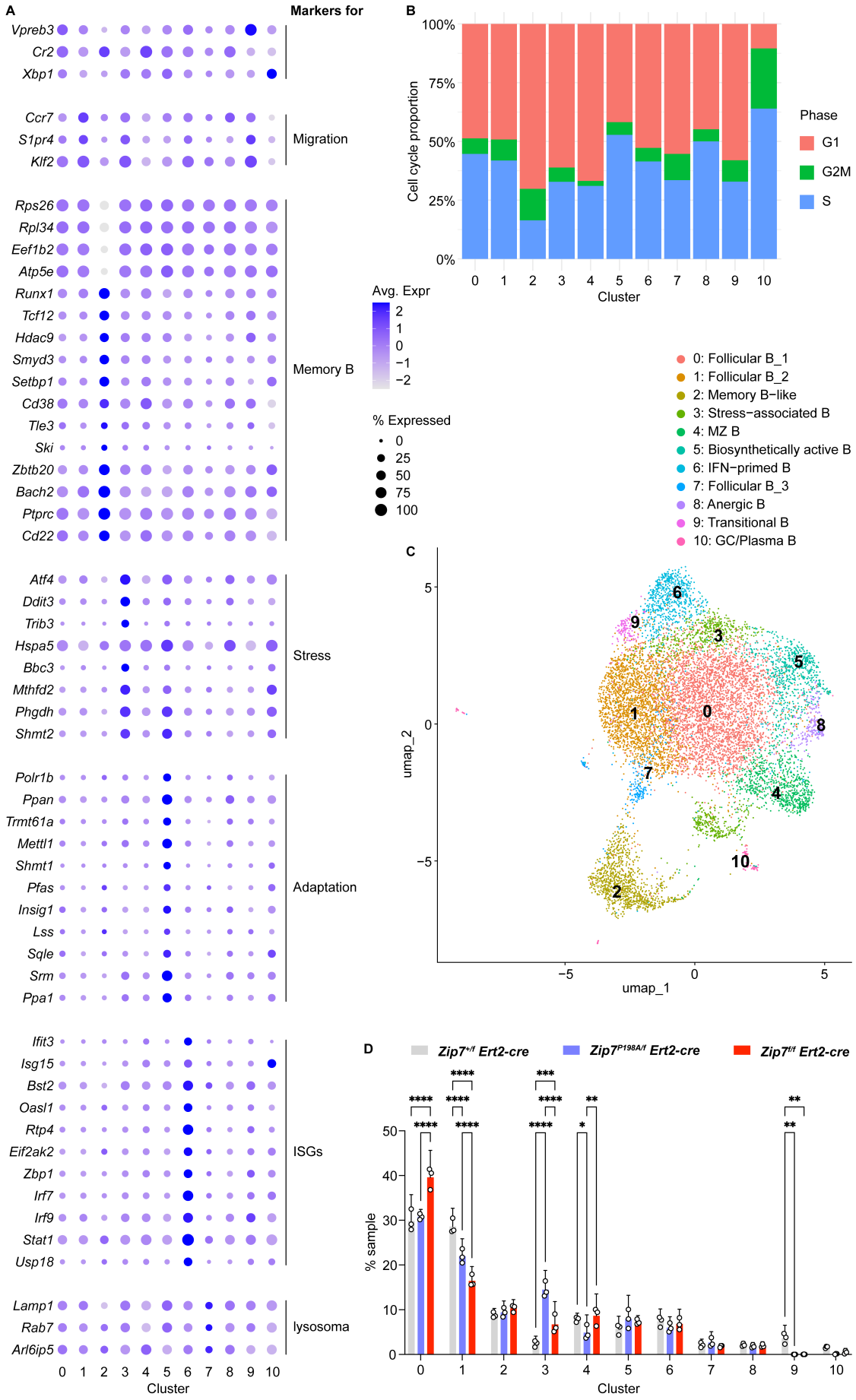
A
Markers for
Vpreb3
Cr2
Xbp1
Ccr7
S1pr4
Klf2
Migration
Rps26
Rpl34
Eef1b2
Atp5e
Runx1
Tcf12
Hdac9
Smyd3
Setbp1
Cd38
Tle3
Ski
Zbtb20
Bach2
Ptprc
Cd22
Memory B
Atf4
Ddit3
Trib3
Hspa5
Bbc3
Mthfd2
Phgdh
Shmt2
Stress
Polr1b
Ppan
Trmt61a
Mettl1
Shmt1
Pfas
Insig1
Lss
Sqle
Srm
Ppa1
Adaptation
Ifit3
Isg15
Bst2
Oasl1
Rtp4
Eif2ak2
Zbp1
Irf7
Irf9
Stat1
Usp18
ISGs
Lamp1
Rab7
Arl6ip5
lysosoma
0 1 2 3 4 5 6 7 8 9 10
Cluster
B
100%
75%
50%
25%
0%
Cell cycle proportion
0 1 2 3 4 5 6 7 8 9 10
Cluster
Phase
G1
G2M
S
Avg. Expr
2
1
0
−1
−2
% Expressed
0
25
50
75
100
0: Follicular B_1
1: Follicular B_2
2: Memory B−like
3: Stress−associated B
4: MZ B
5: Biosynthetically active B
6: IFN−primed B
7: Follicular B_3
8: Anergic B
9: Transitional B
10: GC/Plasma B
C
umap_2
umap_1
5
0
−5
−5
0
5
6
9
3
5
1
0
8
7
4
10
2
D
Zip7+/f Ert2-cre
Zip7P198A/f Ert2-cre
Zip7f/f Ert2-cre
% sample
50
40
30
20
10
0
0 1 2 3 4 5 6 7 8 9 10
Cluster
****
***
**
*

Figure 6-6: Transcriptional annotation and distribution of B cell clusters defined at resolution 0.6.
(A) DotPlot showing the expression of selected marker genes used to annotate clusters not clearly defined by canonical markers in Figure 6-5. These include transcriptional features associated with follicular B cell subsets (Clusters 0, 1, and 7), memory-like cells (Cluster 2), stress-associated cells (Cluster 3), biosynthetically active cells (Cluster 5), and interferon-primed cells (Cluster 6). (B) Cell cycle phase distribution across clusters based on transcriptomic signatures of G1, S, and G2/M phases[316]. (C) UMAP visualization of B cells coloured by cluster identity (resolution = 0.6). (D) Cluster composition across genotypes (*Zip7*$^{+/f}$ *Ert2-cre*, *Zip7*$^{P198A/f}$ *Ert2-cre*, and *Zip7*$^{f/f}$ *Ert2-cre*). Bars represent group means with 95% CIs from three biological replicates per genotype. Statistical comparisons were performed using two-way ANOVA with Šidák multiple comparisons test. *$p < 0.05$, **$p < 0.01$, ***$p < 0.001$, ****$p < 0.0001$.

Additionally, Cluster 3 and Cluster 5 exhibited distinct transcriptional and functional profiles (Figure 6-6A). Cluster 3 was enriched for genes associated with ER stress and apoptosis (*Atf4*, *Trib3*, *Ddit3*, *Bbc3*), as well as stress-responsive metabolic enzymes (*Mthfd2, Phgdh, Shmt2*), consistent with a stress-induced metabolic shift without evidence of proliferation. Notably, this stressed cluster was significantly expanded in ZIP7-deficient B cells (*Zip7*$^{P198A/f}$ *Ert2-cre* and *Zip7*$^{f/f}$ *Ert2-cre*) (Figure 6-6D), and shared a distinct transcriptional signature with expanded clusters observed in both the $CD4^+$ and $CD8^+$ T cell subsets (Figure 6-2, Figure 6-3).

In contrast, although Cluster 5 also displayed modest upregulation of *Atf4* and *Hspa5*, it lacked full activation of the ER stress program, distinguishing it from the stress-dominant phenotype of Cluster 3. It showed a distinct transcriptional program indicative of metabolic adaptation and proliferative activation. This cluster exhibited elevated expression of genes involved in RNA processing, ribosome biogenesis, and nucleotide synthesis (*Polr1b, Ppan, Trmt61a, Mettl1, Shmt1, Pfas*), as well as cholesterol and one-carbon metabolism (*Insig1*, *Lss*, *Sqle, Srm*, *Ppa1*). Consistent with this, Cluster 5 contained a higher proportion of cells in the S phase (Figure 6-6B), reflecting active cell cycle progression. Together, these features suggest that Cluster 5 represents a biosynthetically primed, metabolically active B cell subset. Importantly, the lack of significant

reduction of this cluster in ZIP7-deficient samples implies that ZIP7 is not essential for maintaining proliferative B cells under these conditions (Figure 6-6D), in contrast to the stress-prone phenotype of Cluster 3.

6.5 ZIP7 deficiency triggers a conserved but lineage-divergent stress-adaptive program

6.5.1 Shared stress-responsive features across lymphocyte subsets

To systematically identify transcriptional features shared by ZIP7-deficient expanded clusters in B cells (Cluster 3), $CD4^+$ T cells (Cluster 3), and $CD8^+$ T cells (Cluster 1), I defined a 'Shared Stress Signature' consisting of 11 genes: *Atf4, Ddit3, Trib3, Atf5, Cebpb, Bbc3, Eif4ebp1, Slc7a5, Shmt2, Aars, Cars*. These genes were selected from the top 30 upregulated markers of each stressed cluster and were enriched in at least two of the three cell types. The resulting signature includes well-established stress response regulators such as *Atf4*, *Ddit3* (CHOP), and *Trib3*.

To examine how these transcriptional features extend beyond the stressed clusters, I computed Shared Stress Signature module scores using Seurat's AddModuleScore and visualised their distribution via UMAP for each lineage (Figure 6-7). As expected, the stressed clusters in B cells, $CD4^+$ T cells, and $CD8^+$ T cells exhibited the highest signature scores. Interestingly, some cells within Biosynthetically active B cells (Cluster 5), Effector-like $CD8^+$ T cells (Cluster 3), and Treg cells (Cluster 1) also displayed high scores, despite comprising a mix of ZIP7 genotypes.

To better assess the contribution of genotype, I compared signature scores across ZIP7 genotypes within each cluster (Supplementary Figure 21). Consistent with overall UMAP-based observations, both $Zip7^{P198A/f}$ *Ert2-cre* and $Zip7^{f/f}$ *Ert2-cre* groups showed higher scores than the control in not only the stressed clusters, but also in other subsets.

These included Biosynthetically active B cells (Cluster 5), Effector-like $CD8^+$ T cells (Cluster 3), Treg cells (Cluster 1), as well as—albeit to varying degrees—GC/Plasma B cells (Cluster 10), IFN-primed B cells (Cluster 6), Follicular B cells (Cluster 1), $CD4^+$ Naïve T cells (Cluster 0), $CD8^+$ Naïve T cells (Cluster 0), and Early-activated $CD8^+$ T cells (Cluster 2).

Together, these findings reveal a conserved and genotype-dependent transcriptional stress response that is shared across all three lymphocyte lineages.

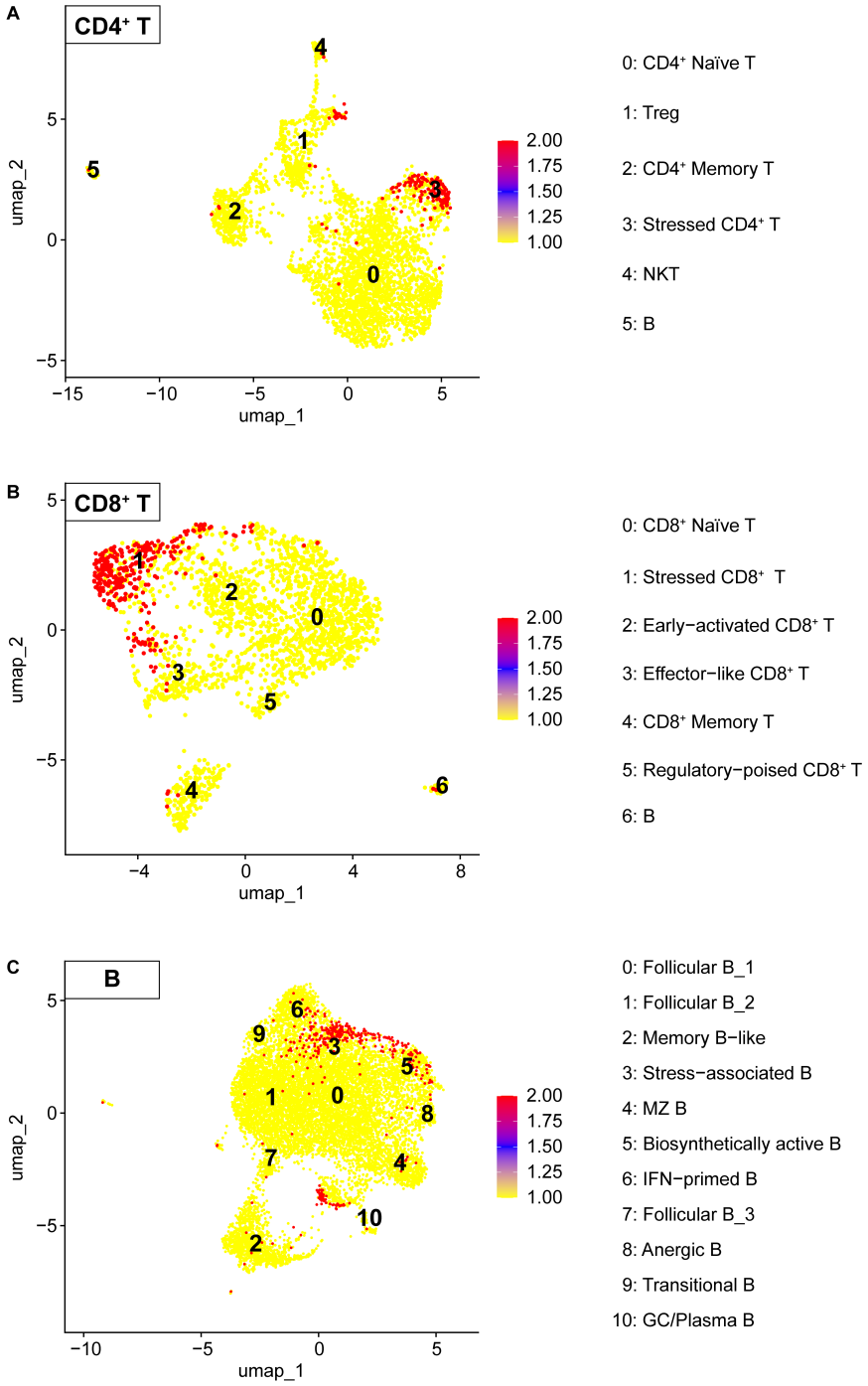

Figure 6-7: Lineage-specific expression of the Shared Stress Signature on UMAP. (A–C) UMAP plots displaying the distribution of Shared Stress Signature module scores in CD4$^+$ T cells (A), CD8$^+$ T cells (B), and B cells (C). The Shared Stress Signature was derived from the intersection of top marker genes from stressed clusters independently identified in each lineage. For each lineage, AddModuleScore was computed separately using the corresponding Seurat object without z-score normalization, in order to retain the original score distribution.

To further investigate how ZIP7 deficiency shapes stress responses across lymphocyte lineages, I examined the broader transcriptional programs activated in the most

stress-enriched clusters. Given the consistent elevation of the Shared Stress Signature—derived from top marker genes—in ZIP7-deficient B and T cell subsets, I hypothesised that the full set of significantly upregulated genes within these clusters may reveal lineage-specific strategies for coping with stress.

I performed GO enrichment analysis using upregulated DEGs from Cluster 3 in B cells, Cluster 3 in $CD4^+$ T cells, and Cluster 1 in $CD8^+$ T cells. Genes were selected based on an adjusted p-value < 0.05 and an average $\log_2$ fold-change > 0.3 (corresponding to at least a 1.23-fold increase in expression). To enable meaningful cross-lineage comparisons, enrichment was quantified using Fold Enrichment—the ratio between the observed gene frequency in the input gene set and its expected background frequency—which better reflects relative over-representation than raw gene counts or GeneRatio.

Despite lineage-specific context, all three subsets exhibited a shared core response centred on protein synthesis and homeostasis (Figure 6-8), rather than a global shutdown of translation typically observed under acute stress. Enriched GO terms included tRNA aminoacylation, oxidative phosphorylation, apoptosis, and ER stress response, suggesting a conserved adaptive transcriptional program aimed at restoring proteostasis.

Lineage-specific differences were nonetheless apparent. T cells activated a broader and more coordinated network of stress-alleviation pathways. These included ER-associated degradation (ERAD), N-linked protein glycosylation, and macroautophagy—indicating a more proactive strategy to reduce proteotoxic burden. $CD8^+$ T cells, in particular, showed unique enrichment of GO terms such as protein trafficking to mitochondrial membranes, PERK-mediated UPR, and RNA splicing. This combination may allow selective translation of stress-adaptive proteins while limiting ER overload.

By contrast, B cells lacked enrichment for these canonical protein clearance pathways. Instead, they showed unique upregulation of processes related to ionic

homeostasis, including calcium and iron ion transmembrane transport, particularly at the mitochondrial level. The functional relevance of these features under ZIP7 deficiency remains unclear, but may reflect a more constrained or less efficient stress adaptation strategy.

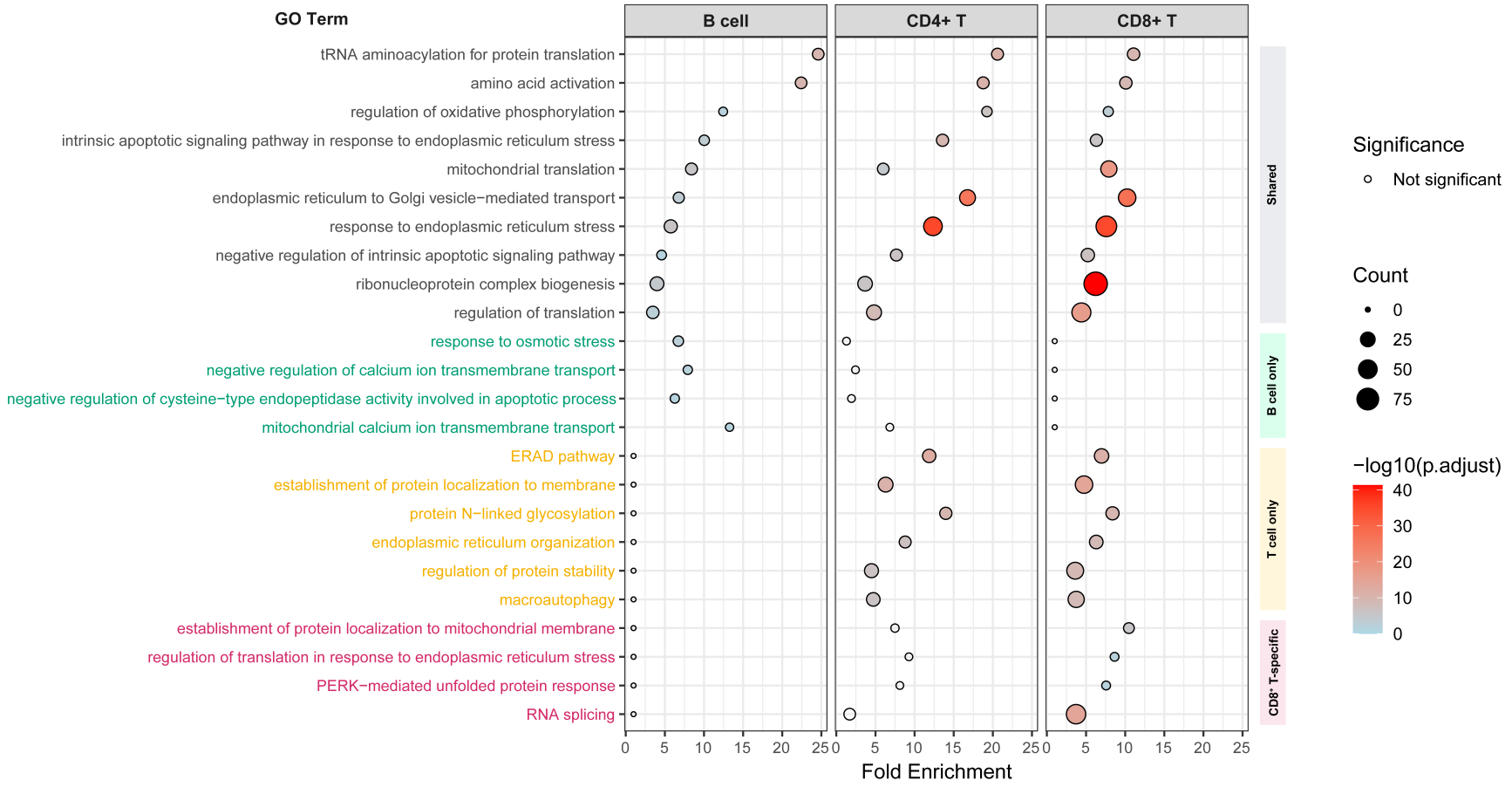

Figure 6-8: Comparative GO enrichment analysis of stressed clusters in B cells, $CD4^+$ T cells, and $CD8^+$ T cells.
Representative GO biological process terms enriched in stressed clusters from B cells, $CD4^+$ T cells, and $CD8^+$ T cells. Terms are grouped by enrichment pattern: shared across all three lineages or specific to one. Fold Enrichment was used to enable comparison across cell types regardless of input gene set size. Dot size indicates the number of associated genes (Count), and colour reflects enrichment significance. Filled dots represent significant terms (adjusted $p < 0.05$); hollow dots indicate non-significant enrichment.

6.5.2 ZIP7 deficiency activates a stress-adaptive program aligned with the split ISR

To avoid self-fulfilling bias associated with using a gene signature derived from my own dataset, I sought to independently verify the stress phenotype using an external reference. The split integrated stress response (s-ISR) is a transcriptional program triggered by mild stress or recessive mutations in *eIF2B* (such as in vanishing white matter disease), where impaired eIF2B function leads to ATF4 upregulation without increased eIF2α phosphorylation[317,367]. This non-canonical ISR response differs from the canonical ISR (c-ISR) and is marked by selective activation of metabolic and proteostasis-related genes, reflecting the plasticity of the ISR network.

To assess whether ZIP7-deficient lymphocytes exhibit features of c-ISR or s-ISR, I first examined the expression of several key ISR markers (Figure 6-9A). ATF4, a hallmark effector in both c-ISR and s-ISR, was robustly upregulated in stressed clusters from B cells, $CD4^+$ T cells, and $CD8^+$ T cells, and moderately elevated in metabolically active B cells. Gadd34, a classical c-ISR marker upregulated during both acute and chronic ISR phases[368,369] but independent of s-ISR activation[317], was selectively elevated in stressed $CD8^+$ T cells but not in the other stressed clusters. However, its interpretation is limited by the absence of phospho-eIF2α measurements and by the observation that Gadd34 can also be expressed under physiological conditions, as seen in GC/plasma and anergic B cells. In contrast, *Eif2b* expression was consistently downregulated in stressed clusters, consistent with s-ISR, but upregulated in biosynthetically active B cells, suggesting a distinct stress context in the latter. *Pck2*, a critical downstream effector of the s-ISR that operates via the eIF4E–ATF4–PCK2 axis in the absence of eIF2α phosphorylation[317], was strongly upregulated in all stressed clusters but not in biosynthetically active B cells. Together, the transcriptional profile of ZIP7-deficient stressed clusters—characterised

by high *Atf4* and *Pck2*, low *Eif2b*, and limited *Gadd34*—more closely resembles s-ISR than c-ISR.

To further investigate this possibility, I applied a s-ISR gene signature[317] comprising 27 genes to the B cell, $CD4^+$ T cell, and $CD8^+$ T cell datasets using AddModuleScore, and visualised their expression on UMAPs (Figure 6-9B). The full signature includes: *Aldh18a1*, *Arl14ep*, *Atf5*, *Calcrl*, *Cbs*, *Chac1*, *Cth*, *Cyb5r1*, *Ddit3*, *Ddr2*, *Igfbp4*, *Pck2*, *Phgdh*, *Phyhd1*, *Prnp*, *Rhbdd1*, *Sardh*, *Sesn2*, *Slc1a4*, *Slc7a1*, *Slc7a11*, *Slc7a5*, *Stc2*, *Tor3a*, *Trib3*, *Xpot*, *Atf4*[317]. The UMAP distribution of s-ISR scores closely mirrored that of the Shared Stress Signature, with highest expression localised to the stressed clusters of each lineage and biosynthetically active B cells, and variable activation in other clusters.

To quantify this relationship, I performed Spearman correlation analysis between the two scores at the single-cell level (Supplementary Figure 22). Across all ZIP7-deficient genotypes and lineages, strong correlations were observed. Cluster-level analysis further confirmed this trend: stressed clusters from $CD4^+$ T cells (Cluster 3), $CD8^+$ T cells (Cluster 1), and B cells (Cluster 3) showed R^2 values between 0.43 and 0.58. Additionally, biosynthetically active B cells (Cluster 5) and effector-like $CD8^+$ T cells (Cluster 3) also exhibited strong correlations ($R^2 > 0.45$).

These findings suggest that ZIP7 deficiency induces a transcriptional program resembling the s-ISR, particularly in metabolically active or stress-enriched immune subsets. Importantly, the consistency between the internally derived Shared Stress Signature and the independently defined s-ISR signature further supports the robustness and biological relevance of the stress phenotype observed.

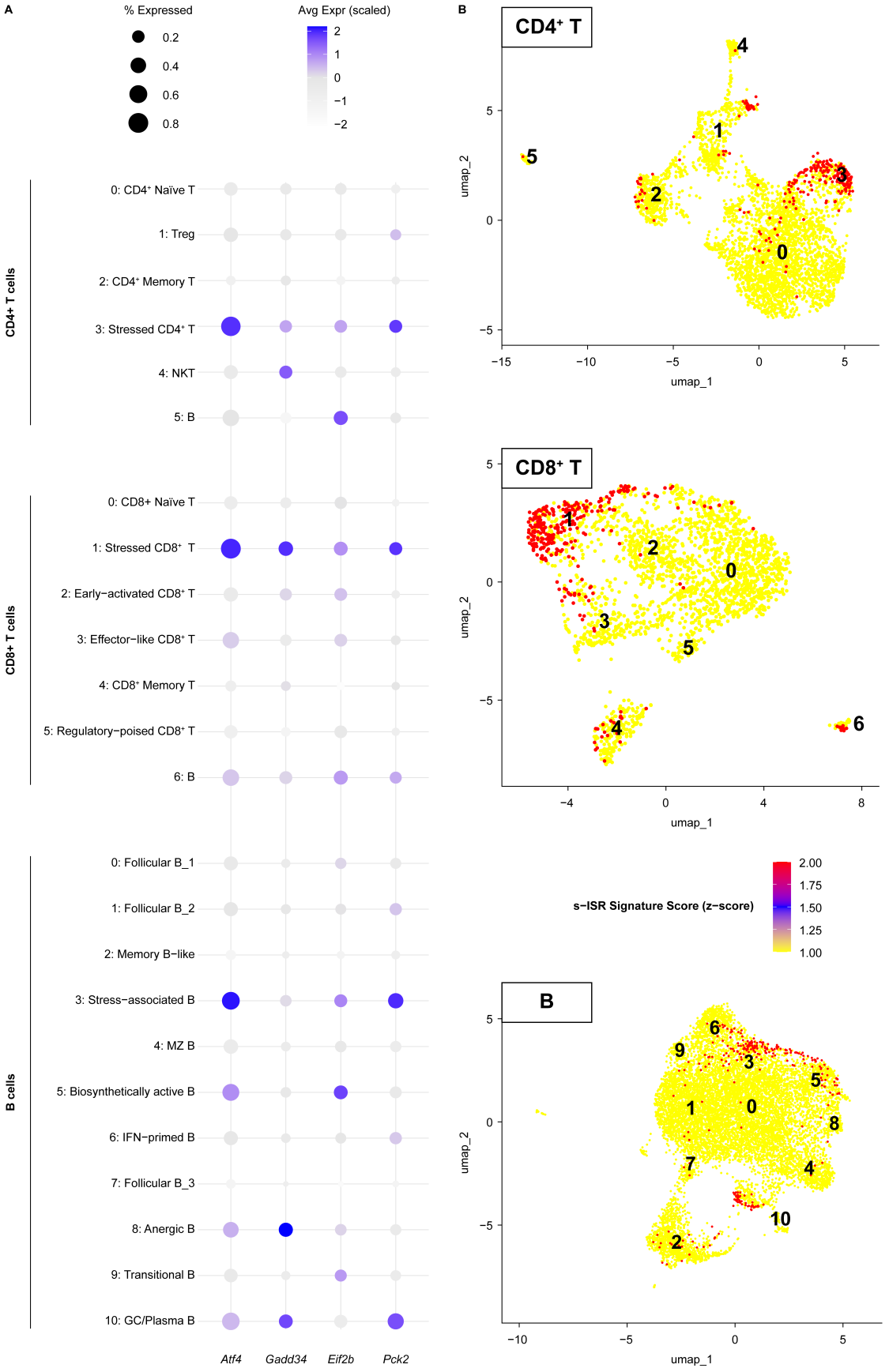

Figure 6-9: Transcriptional expression of s-ISR markers and module scores across lymphocyte subsets.

(A) Expression of key ISR-related genes—*Atf4*, *Gadd34* (*Ppp1r15a*), *Eif2b* (*Eif2b4*), and *Pck2*—across annotated clusters in $CD4^+$ T cells, $CD8^+$ T cells, and B cells. Circle size indicates the proportion of cells expressing each gene; colour intensity reflects average scaled expression. (B) UMAP plots showing s-ISR module scores computed using Seurat's AddModuleScore function in each lineage-specific dataset. Scores were calculated independently per lineage without z-score normalisation, to retain lineage-intrinsic expression patterns.

To investigate whether stressed B cells were undergoing terminal ER stress or instead mounting a more limited adaptive response, I first evaluated the activity of a published 16-gene Terminal UPR Signature[318], which includes *Aars*, *Cpox*, *Ddit3*, *Eif2a*, *Esrp1*, *Etf1*, *Gars*, *Qrich1*, *Srp72*, *Srpr*, *Stk40*, *Stt3b*, *Tars*, *Tgif1*, *Uso1*, *Vcp* and reflects the transcriptional program associated with irreversible ER damage. Module scores were calculated using Seurat's AddModuleScore across the entire scRNA-seq dataset and z-score were normalised across all clusters from the three major lineages to enable comparison between clusters and lineages (Figure 6-10). Although z-scores from different stress gene sets (e.g., s-ISR, Terminal UPR, etc.) were not directly comparable to each other, this strategy allowed direct comparison of a given gene signature (e.g., s-ISR) across B cells, $CD4^+$ T cells and $CD8^+$ T cells.

Terminal UPR scores in B cells revealed a nuanced pattern: most follicular subsets showed reduced expression, stressed-associated and biosynthetically active B cells exhibited near-average levels, even lower than in GC/plasma B cells. In contrast, stressed $CD4^+$ and $CD8^+$ T cells showed higher scores, suggesting that B cells had not yet committed to an irreversible stress response. While a true "positive control" for terminal UPR activation is lacking in this dataset, the relatively low scores in B cell clusters indicate that ZIP7-deficient B cells are more likely engaging a restricted or sub-threshold adaptive response rather than entering apoptosis-related terminal UPR.

Given this and considering both Shared Stress Signature and s-ISR Signature indicate a more adaptive metabolic rewiring in response to moderate cellular stress, I next

examined which adaptation pathways were obviously activated in these clusters (Figure 6-10). Analysis of curated Hallmark gene sets revealed obvious upregulation of MTORC1 signaling in the stressed clusters, especially in $CD4^+$ and $CD8^+$ T cells compared to other clusters within each lineage. In B cells, MTORC1 scores were moderately elevated in the stressed cluster compared to follicular B cells, but even higher in the biosynthetically active cluster. This raises the possibility that biosynthetically active B cells, while not transcriptionally stressed per se, are better equipped to meet protein production demands through enhanced mTORC1 signaling—a compensatory feature lacking in the stressed B cell subset and potentially contributing to their vulnerability.

Together, these findings support the idea that ZIP7-deficient lymphocytes engage a non-canonical, metabolically adaptive stress response aligned with the s-ISR, with B cells exhibiting a less coordinated compensatory program than T cells. This may underlie their heightened stress sensitivity and impaired survival.

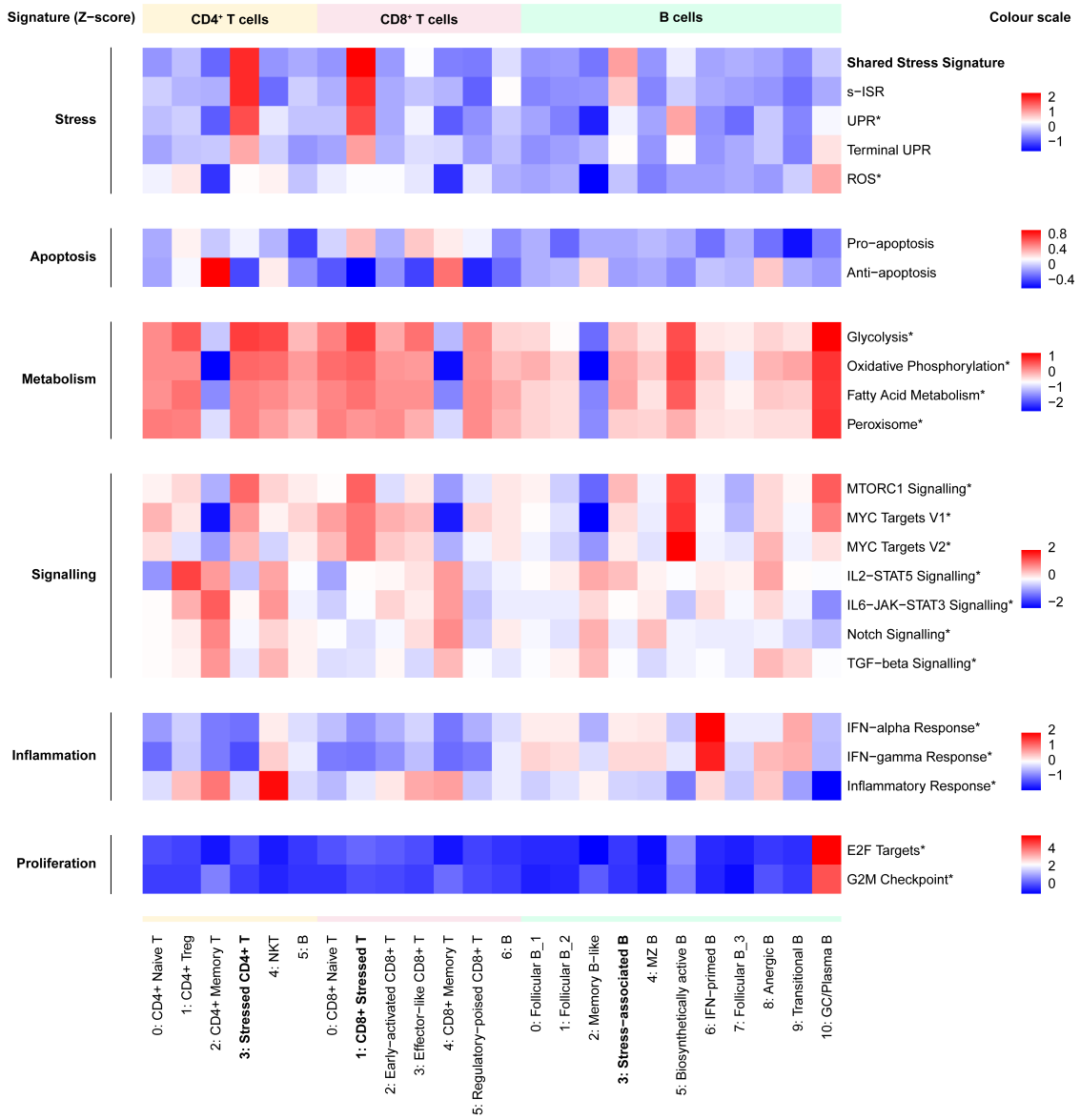

Figure 6-10: Pathway-level transcriptional landscape across lymphocyte subsets highlighting stress and functional module activity.
Heatmap showing z-scored module scores for curated transcriptional signatures across annotated clusters of CD4$^+$ T cells, CD8$^+$ T cells, and B cells. Gene sets were compiled from the Mouse MSigDB Hallmark Collection[319,320], literature-defined signatures[317,318,321], and internally derived stress-related modules. Signatures are grouped by functional category: Stress, Apoptosis, Metabolism, Signalling, Inflammation, and Proliferation. Module scores were calculated using Seurat's AddModuleScore and z-score normalised within each functional category to enable cross-cluster comparison. Asterisks (*) indicates gene sets from the Mouse MSigDB Hallmark collection.

6.6 Discussion

This single-cell transcriptomic analysis reveals a conserved yet heterogeneous stress response program across ZIP7-deficient lymphocyte subsets. By integrating gene

expression, surface marker data, and curated gene signatures, I identified lineage-specific stressed clusters in B cells, $CD4^+$ T cells, and $CD8^+$ T cells, all of which shared a core transcriptional stress signature centred on *Atf4*, *Ddit3*, and *Trib3*. This conserved program likely reflects a common cellular consequence of cytoplasmic zinc depletion caused by ZIP7 loss.

Interestingly, while the Shared Stress Signature was elevated across all three lineages, B cells appeared to exhibit a more restricted adaptive response. Unlike T cells, stressed B cells lacked enrichment of canonical protein clearance mechanisms such as ERAD and autophagy. In contrast, T cells—particularly $CD8^+$ T cells—activated a broader stress-alleviation network, including PERK-mediated UPR and transcriptional programs linked to metabolic rewiring.

Application of an independently defined s-ISR signature further validated the transcriptional stress phenotype and highlighted ZIP7 deficiency as a potential upstream trigger of the non-canonical integrated stress response. The consistent upregulation of *Pck2* and MTORC1 signaling in stressed clusters further supports a shift toward a metabolic strategy to sustain proteostasis under moderate, chronic stress conditions.

Together, these findings suggest that ZIP7 contributes to the lineage-specific tuning of stress responses in lymphocytes. They also raise the possibility that B cells, due to an inherently higher biosynthetic load, may be more vulnerable to disruptions in zinc-dependent proteostasis regulation. Further investigation is needed to determine whether the stress adaptations observed here are protective, maladaptive, or context-dependent.

Chapter

7 General Discussion

This thesis demonstrates that ZIP7 is essential for maintaining lymphocyte homeostasis and enabling effective humoral immunity, with peripheral B cells showing a marked reliance on adequate levels of intact ZIP7. Naturally occurring hypomorphic ZIP7 mutations causing B cell immunodeficiency and associated mouse studies highlight a requirement for ZIP7 at the pre-B to immature B cell selection point, but notably do not affect T cell development[20]. Higher levels of deficiency cause embryonic lethality, therefore the role of ZIP7 in other immune cells, biological processes and later development is unclear. Through inducible and lineage-specific models, I show here that greater ZIP7 deficiency leads to progressive loss of MZ B cells and select T cell subsets—reflecting a gene and allele dosage-sensitivity and a cell-intrinsic requirement for ZIP7 across both lineages.

While T cells retain partial resilience, B cells continue to appear to be more vulnerable to ZIP7 loss, particularly under competitive or immunogenic conditions. This differential sensitivity is not easily explained by impaired activation or proliferation, but instead correlates with the emergence of stress-prone transcriptional states. Single-cell profiling reveals a conserved stress signature in ZIP7-deficient B and T cells, aligning with features of the split integrated stress response. However, B cells mount a more

constrained adaptation, lacking the compensatory programs engaged by T cells. Whether these unique ZIP7-dependent transcriptional states are a consequence of or a response to metabolic reprogramming or selection pressures remains to be assessed.

Together, these findings support the initial hypothesis that ZIP7 is required for the maintenance of peripheral B cell populations, and establish ZIP7 as a critical regulator of lymphocyte lineage-specific stress adaptation and cellular persistence in the immune system.

7.1 ZIP7 supports peripheral B cell maintenance and differentiation

Although ZIP7 is essential for early B cell development, a non-redundant role for intact ZIP7 in peripheral B cell maintenance and B cell humoral responses had not been previously demonstrated.

In this thesis, distinct phenotypic outcomes were observed in the peripheral B cell compartment across ZIP7-deficient models. While the germline *Zip7*$^{P198A/P198A}$ and *Zip7*$^{H199QV/H199QV}$ mice lack B cells in the periphery, both *Zip7*$^{P198A/f}$ and *Zip7*$^{f/f}$ *Ert2*-cre chimeras had fewer transitional and MZ spleen B cells without significantly affecting the follicular B cell subset. The cell-intrinsic requirement for ZIP7 and the selective depletion of MZ B cells was also evident in long-term germline and lineage-specific knockout models. Both *Zip7* $^{H199QV/f}$ and *Zip7*$^{P198A/f}$ *Cr2-cre* mice exhibited reduced MZ precursor and MZ B cell populations in mixed chimeras. In addition, using the mixed chimeras and adoptive transfer models, we identified that ZIP7-deficient mice exhibit impaired GC formation and antibody secretion, as well as sub-optimal antibody secretion in response to TD and TI antigenic stimuli.

MZ B cells are NOTCH2 dependent, rely on STAT1 activity and are uniquely poised to sample the blood-borne antigenic space[133,370]. They maintain very low amounts of BACH2, a transcriptional repressor of PC differentiation, and high amounts of IRF4

and ZBTB20 that promote PC differentiation, in agreement with them being uniquely poised to differentiate into PCs. Furthermore, MZ B cells express higher amounts of UPR-related transcripts and maintain a proteome that can be quickly remodelled towards anabolic activities in response to environmental cues[98,371]. Taken together, these findings establish MZ B cells as a functionally and mechanistically distinct population with heightened dependence on ZIP7. Whether this reflects increased UPR and metabolic demands, a greater reliance on zinc-buffering capacity, or elevated sensitivity to cellular stress remains to be determined. Nonetheless, their reproducible loss across models highlights MZ B cells as a sensitive readout of intracellular zinc homeostasis and an early indicator of functional ZIP7 deficiency.

7.2 Comparative biology of B cell development and genetic defects in humans and mice

The core processes of B lymphocyte development are broadly conserved between humans and mice, with both progressing through sequential stages—from HSCs to pro-B, pre-B, immature, and mature B cells—defined by immunoglobulin gene rearrangement and developmental checkpoints. However, studies of primary immunodeficiencies and corresponding mouse models have highlighted significant species-specific differences, particularly in how certain genetic lesions affect pre-BCR forming stage.

In humans, BTK is vital for B cell development in the BM, around 90% early onset XLA patients carry *BTK* mutations[12,13,372]. Over 1000 unique variants in *Btk* have been identified. All kinds of mutation, such as missense mutations (40%), nonsense mutations (17%), deletions (20%), insertions (7%), and splice-stie mutations (16%) are scattered throughout its multidomains[373]. The majority of causative *BTK* variants result in decreased BTK levels and/or its activity. These patients exhibit a developmental arrest at the pre-B cell stage[11], resulting in an almost complete absence of peripheral B cells

and severe antibody deficiency. By contrast, Btk-deficient mice—whether carrying the *Xid* point mutation (*Btk*^{xid})[374-376] or a full knockout[103,377]—retain detectable pro-B, pre-B and immature B cell subsets (albeit with modest shifts in relative frequencies and a specific impairment of small pre-B cell expansion), as well as peripheral B cell numbers, underscoring a much milder requirement for BTK in early murine compared to human B lymphopoiesis.

Similarly, BLNK deficiency manifests differently, causing a stringent pro-B-cell developmental block and profound antibody deficiency in humans[378], while resulting in a less restrictive phenotype in mice[379,380], with partial B cell development beyond the pro–B stage and residual responses to T-dependent antigens. Furthermore, IL-7 signalling exemplifies another divergence, as it is indispensable for murine B-cell development[381,382] but dispensable in human B-cell lymphopoiesis[383-385], where IL-7 receptor mutations primarily impair T-cell rather than B-cell development.

ZIP7 deficiency relates with a developmental block at the BM. BM examination of two patients carrying *Zip7*$^{E363K/P190A}$ showed an increased proportion of pro-B cells relative to pre-B cells, and a further reduction in immature B cells compared to pre-B cells, suggesting a developmental arrest at the pro-B to pre-B cell transition[20]. *Zip7*$^{P198A/P198A}$ mice exhibit a cell-intrinsic block at a slightly later stage—from pre-B to immature B cells—marked by a striking reduction in late pre-B cells, immature B cells, and mature B cells[20]. The comparatively earlier block seen in *Zip7*$^{E363K/P190A}$ patients may result from the *Zip7*^{E363K} mutation introducing a positively charged residue near the putative active site, potentially causing a more severe functional impairment of ZIP7. Supporting this interpretation, severer ZIP7 deficiency models, such as *Zip7*$^{P198A/f}$ and *Zip7*$^{f/f}$ *Ert2*-cre inducible models, display an even earlier developmental arrest, as early as the pro-B stage (Hardy fraction B), mirroring the phenotype observed in human patients with the *Zip7*$^{E363K/P190A}$ genotype.

Beyond central B cell development, species-specific features also shape peripheral B cell maintenance and function. Humans harbour circulating class-switched memory B cells and somatically mutated MZ-like B cells from early life onwards[386,387], whereas mouse MZ B cells are largely spleen-resident and unmutated. Moreover, although peripheral B cell survival in both species depends on tonic BCR signalling and the BAFF–APRIL axis, their reliance on specific receptors differs: BAFF-R is essential for transitional and mature B cell survival in mice[91,143,388], while TACI plays a more prominent role in human MZ and class-switched memory B cells[389,390], particularly in T cell–independent responses. These differences in subset composition and survival requirements complicate direct cross-species comparisons when evaluating the impact of ZIP7 deficiency on peripheral B cells.

Given that ZIP7-deficient patients lack virtually all peripheral B cells[20], it remains unclear whether ZIP7 is differentially required for specific B-cell subsets in humans. In this context, our inducible Zip7-deficient mouse models, which bypass central developmental blocks, allow us to dissect the relative susceptibility of peripheral subsets—revealing that MZ B cells and GC responses are particularly dependent on intact ZIP7 function. These findings highlight how tractable mouse models can help infer lineage-specific requirements where human data are intrinsically limited.

7.3 Gene and allele dose effects in B and T cells

The phenotypic spectrum observed across models of ZIP7-deficiency supports a distinct gene and allelic dose effect in both B and T lymphocytes. Using *Zip7*$^{P198A/f}$ and *Zip7*$^{f/f}$ mouse models combined with the inducible *Ert2*-cre, I identified that ZIP7-deficient mice exhibited progressive defects in BM B cell development, with the complete *Zip7*$^{-/-}$ deletion model showing a more pronounced reduction at an earlier pro-B cell developmental stage than that seen with the *Zip7*$^{P198A/-}$ model. These findings extend previous

observations from mice bearing two germline copies of hypomorphic *Zip7* alleles, the *Zip7*$^{P198A/P198A}$ and the *Zip7*$^{H199QV/H199QV}$ mice, which exhibited impaired development from the late pre-B to immature stage onwards[20]. These differences likely reflect varying levels of residual ZIP7 function, with the P198A mutant protein retaining partial activity sufficient to support pro-B and pre-B stages. In contrast, severe or near-complete ZIP7 deficiency in our models disrupted development from pro-B onwards, suggesting that early B cell fitness is particularly sensitive to ZIP7 dosage.

Although the loss of MZ B cells was cell-intrinsic in both models, it appeared more penetrant in *Zip7*$^{P198A/f}$ *Ert2*-cre mice. Given that *Zip7*$^{f/f}$ cells require two Cre-mediated recombination events to generate a complete knockout, it is plausible that B cells with one copy of a functionally intact floxed allele (*Zip7*$^{-/f}$) outcompete ZIP7-deficient (*Zip7*$^{-/-}$) cells in competitive environments, thereby partially masking the phenotype. By contrast, *Zip7*$^{P198A/f}$ cells require a single-step inactivation of the floxed allele, allowing cellular vulnerabilities to be more readily exposed—particularly under stress or selection pressure. Similar allelic penetrance differences were also reflected in transcriptional stress signatures: *Zip7*$^{P198A/f}$ *Ert2*-cre B cells exhibited higher stress module scores than *Zip7*$^{f/f}$ *Ert2*-cre B cells in the scRNA-seq dataset. In inducible knockout models, ZIP7 protein turnover—reported to have a half-life of ~12 days in B cells[391]—may delay complete protein depletion, thereby blunting the observable phenotype.

While the germline *Zip7*$^{P198A/P198A}$ mice exhibit a profound B cell loss early during development in the BM, they retain normal T cell numbers in both the thymus and the periphery[20], indicating that partial ZIP7 activity via two copies of a hypomorphic allele is sufficient for T cell maintenance under homeostatic conditions (Figure 7-1). However, inducible ZIP7 deletion using the *Zip7*$^{f/f}$ *Ert2*-cre mice demonstrated a distinct thymic phenotype with a progressive loss of thymocytes from the DN2 to DP stages. This was in contrast with the observations from the *Zip7*$^{P198A/P198A}$ cells but consistent

with a requirement for ZIP7 in metabolically active, proliferative thymocytes undergoing selection. Although *Zip7*$^{P198A/f}$ *Ert2*-cre mice showed a marginally milder defect, reductions at the DP1 and DP2 stages indicate that loss of even one of the hypomorphic *Zip7* alleles compromises early thymic T cell development.

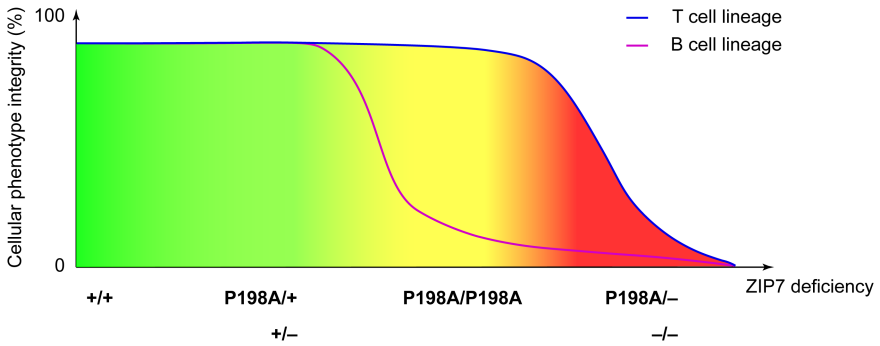

Figure 7-1: Differential impact of ZIP7 deficiency on B and T cell phenotype integrity across progressive genotypes.
The x-axis represents increasing degrees of ZIP7 loss, from WT to complete deficiency. The y-axis indicates the integrity of lineage-specific cellular phenotype, incorporating metrics such as BM B cell development, thymocyte maintenance, and functional competence. T cells largely maintain their phenotype under moderate ZIP7 deficiency (*Zip7*$^{P198A/P198A}$), while B cells exhibit early vulnerability due to a BM developmental block. More severe genotypes (*Zip7*$^{P198A/–}$ or *Zip7*$^{–/–}$) lead to progressive defects in both lineages, especially in proliferative subsets.

In contrast to B cells, T cells showed greater tolerance to ZIP7 insufficiency in the periphery, despite clear developmental defects in the thymus. ZIP7 deletion in peripheral T cells yielded divergent outcomes depending on the model used. In *Ert2*-cre mice, naïve T cells were largely preserved despite thymic defects, whereas *Zip7*$^{P198A/f}$ *Cd4-cre* mice exhibited a near-complete loss of peripheral T cells. These differences likely reflect the short observation window following tamoxifen induction. Given that thymic development was already impaired from the DP stages in the *Ert2*-cre model, it is plausible that continued depletion of thymic output would eventually exhaust the naïve T cell pool, as no new thymocytes can replenish the periphery. By contrast, the *Zip7*$^{P198A/f}$ *Cd4-cre* model—where *Zip7* is deleted almost throughout T cell development from the

earliest DP stage when CD4 is expressed—revealed a much more severe and sustained defect, underscoring the importance of both timing and duration of ZIP7 deficiency in shaping T cell outcomes. These findings suggest that while peripheral T cells appear to tolerate ZIP7 loss, sustained thymic input is ultimately required to preserve the T cell compartment.

These observations resonate with findings from other gene dosage studies in lymphocyte biology. For example, lineage-specific rescue of *Taok3* in B cells partially restored marginal zone B cell numbers in *Taok3*$^{-/-}$ mice, and even *Taok3*$^{+/-}$ mice showed intermediate phenotypes, underscoring a dosage-sensitive requirement in this compartment[139]. Similarly, monoallelic versus biallelic mutations in genes like *TCF3* or *IRF4* yield different forms and severities of immunodeficiency in patients[322,323]. In the case of ZIP7, the differential impacts observed across B- and T cell compartments, and across models with varying allele combinations, suggest that each lineage may operate under a distinct threshold of ZIP7 sufficiency. These findings also illustrate how combining gene editing with lineage-specific or inducible deletion strategies can reveal subtle yet biologically meaningful patterns of gene dependence.

7.4 ZIP7-dependent stress responses and survival vulnerability

Across multiple models, ZIP7 deficiency imposed a survival disadvantage that selectively affected metabolically active immune cells—particularly those undergoing activation, proliferation, or differentiation. This vulnerability was consistently observed in pro-B to immature B cells, MZ B cells, GC B cells, and proliferating thymocytes. Even in the absence of antigenic stimulation, ZIP7-deficient B cells progressively declined following adoptive transfer, highlighting an intrinsic survival defect that is likely exacerbated during immune activation.

To understand the nature of this vulnerability, I applied curated gene signatures to single-cell datasets. In addition to a distinct stress-signature with shared features across an UPR and ER stress response, ZIP7-deficient lymphocytes exhibited increased *Atf4* and *Pck2* expression with minimal induction of *Gadd34*—features characteristic of a "s-ISR"[317]. This stress mode is induced by reduced eIF2B activity and metabolic disturbance, characterised by ATF4 upregulation without the eIF2α phosphorylation characteristic of "c-ISR".

IRE1, an ER stress sensor with nuclease activity that promotes *Xbp1* splicing, is detectable in developing B cells in the BM as early as at the pro-B cell stage through to the pre-B cell stage, and is required for antigen receptor V(D)J rearrangement[392,393]. However, an essential role for downstream UPR mediators PERK and XBP1 in early B cell development has not been identified. In the thymus, IRE1 activity is detectable at the $CD4^+$ $CD8^+$ DP stage through to the SP stage when thymocytes are poised to exit the thymus[393]. Loss of SEL1L, a critical component of ERAD, triggers unresolved ER stress, PERK signaling and apoptosis, leading to impaired DN3 to DN4 thymocyte transition; furthermore, the dual loss of SEL1L and XBP1 exacerbates thymocyte loss, suggesting that the XBP1 mediated UPR pathway might function as a compensatory adaptation to survive ER stress[394]. This might explain, in part, how loss of ZIP7 function and the up-regulation of a stress signature (ER stress and ISR) could have a significant effect on the survival of developing lymphocytes of the B and T cell lineage.

As previously mentioned, MZ B cells have lower BACH2 levels, which inhibit BLIMP1 expression and PC differentiation, and higher amounts of baseline UPR-related transcripts[98]. The PKR (eIF2AK2) kinase that controls NF-κB activation and inhibits eIF2B activity is also abundant in MZ B cells[98]. Further, the spatiotemporal regulation of NOTCH2 signaling is critical for MZ B cells and ZIP7 has been implicated in NOTCH trafficking with disrupted ERAD[309,395]. In activated pre-GC B cells, mTORC1

coordinates the induction of an 'anticipatory' UPR; and BLIMP1 induces a 'classical' IRE1α-XBP1–dependent UPR as B cells commit to the PC fate and undergo terminal differentiation to an antibody-secreting cell state[371]. Disrupted mTORC1 signaling, impaired autophagy and ER proteostasis, and a compromised ability to adapt to metabolic and ER stress might together contribute to impaired survival of MZ B cells, GC B cells and PCs[396,397].

Despite a shared transcriptional response consisting of stress-associated signals, lineage-specific adaptation strategies diverge within the lymphocyte lineages. In T cells, particularly $CD8^+$ subsets, stressed clusters activated classical proteostasis pathways, including ER-associated degradation, N-linked glycosylation, and macroautophagy. These responses suggest a more coordinated attempt to maintain protein homeostasis. In tissue-resident $CD4^+$ memory T cells, steady state ISR allows the maintenance of a poised state with stored cytokine transcripts such that an activation signal can immediately promote cytokine production and release[398]. In contrast, stressed B cell clusters lacked these canonical clearance mechanisms and instead upregulated pathways associated with mitochondrial ion transport, potentially reflecting a compensatory attempt to restore redox and metabolic balance. mTORC1 signalling, known to support nutrient availability, was more robustly induced in stressed T cells and biosynthetically active B cells, but remained relatively limited in stressed B cells.

These differences may explain the heightened susceptibility of ZIP7-deficient B cells to stress-induced attrition. In the absence of sufficient proteostatic and metabolic compensation, even modest disruptions in zinc handling may compromise B cell fitness. By contrast, T cells appear to possess more effective stress-adaptation strategies, consistent with a lower dependency on ZIP7 under homeostatic conditions. Further analysis of various eIF2 transcription factors, mTORC1-dependent pathways, and other modules

that regulate UPR and ISR across lymphocyte subsets could offer insights into how and why these cell types have distinct responses to ZIP7 deficiency.

External evidence supports the interpretation that ZIP7 is required to maintain the effectiveness of the underlying stress response. ZIP7 expression is upregulated early during UPR and ER stress responses[296,305], and CRISPR screening data showed that *ZIP7* deletion significantly reduced a XBP1s–GFP signal[318]. Whether ZIP7 contributes to the maintenance of basal UPR activity or mediates acute ER crisis responses remains to be investigated.

Mechanistically, ZIP7 regulates cytoplasmic zinc availability via ER-to-cytosol transport. Its loss disrupts zinc-buffering capacity and perturbs intracellular signaling and proteostasis. These effects are particularly detrimental in cell states characterised by high protein synthesis and metabolic demand[20,305,309,399]. Previous studies have implicated ZIP7 in ER homeostasis[20,305], mitophagy[310], ferroptosis susceptibility[399], and ERAD regulation[309]. For example, intestinal stem cells with complete *Zip7* deletion exhibit impaired regeneration and exaggerated UPR activation, while a 50% reduction in ZIP7 is tolerated without phenotype[305], underscoring a dose-dependent requirement.

Taken together, these findings establish ZIP7 as a key determinant of intracellular stress resilience. Its function is particularly important for lymphocyte populations operating under high biosynthetic pressure, such as GC B cells. Loss of ZIP7 triggers a destabilising stress mode that undermines cell survival in competitive or metabolically demanding environments. This mechanistic insight integrates and explains the observed phenotypes across models, positioning ZIP7 as a non-redundant regulator of immune cell fitness. The pre-B to immature B cell transition may represent a similar stress-related checkpoint.

7.5 Revisiting the *Zip7*$^{P198A/P198A}$ mouse model through the lens of dose and adaptation

The *Zip7*$^{P198A/P198A}$ mouse model previously reported by Anzilotti *et al.* exhibited a severe B cell–intrinsic developmental block from the late pre-B to immature stage, with relative sparing of thymic and peripheral T cells[20]. These findings established ZIP7 as essential for early B cell development. In this study, by employing *Zip7*$^{P198A/f}$ or *Zip7*$^{f/f}$ models in combination with inducible or lineage-specific Cre drivers, I demonstrate that more severe ZIP7 deficiency also impairs T-cell development and maintenance—suggesting a gene dose–dependent requirement for ZIP7 across lymphocyte lineages.

Because the germline *Zip7*$^{P198A/P198A}$ model leads to a developmental arrest that precludes investigation of peripheral phenotypes, I used conditional models to delete ZIP7 in mature B or T cells. This enabled the dissection of ZIP7-dependent processes beyond early checkpoints, including peripheral subset composition, maintenance, and antigen responses. For instance, *Cr2-cre*–mediated deletion revealed that MZ B cells and GC responses are particularly dependent on ZIP7, while *Cd4-cre*–mediated deletion uncovered an essential role for ZIP7 in long-term T-cell survival. These results extend the previous model by uncovering peripheral vulnerabilities masked by early developmental arrest.

Anzilotti *et al.* attributed the BM B cell immunodeficiency phenotype primarily to impaired BCR signal transduction[20], showing that ZIP7-deficient pro– and pre–B cells exhibited reduced phosphorylation of key signalling molecules such as Syk and PLCγ2. I tested BCR signalling related events, such as calcium flux and phosphorylation, remains largely intact despite greater ZIP7 loss in more mature peripheral B cells (data not shown). Instead, I observed the emergence of stress-prone transcriptional states associated with the ISR and ER stress, highlighting an alternative mechanism by which ZIP7 deficiency compromises peripheral B cell function and survival. This raises the

possibility that certain BM B cell subsets may also be intrinsically stress-sensitive under physiological conditions, and that ZIP7 deficiency could exacerbate this vulnerability. Future single-cell analyses of normal BM B cells may help identify whether developmental stages such as Fraction C–E naturally exhibit elevated stress signals, offering a complementary explanation for the developmental block seen in ZIP7-deficient mice.

Fourth, while the *Zip7*$^{P198A/P198A}$ germline mouse model and 4/6 ZIP7-deficient patients described by Anzilotti *et al.* exhibited predominantly B cell-specific defects, two early-onset agammaglobulinemia patients carrying compound *Zip7*$^{E363K/P190A}$ mutations showed broader immunodeficiency involving both B and T cells[20]. At the time, the mechanistic basis for this difference remained unclear. In this study, using models with more severe ZIP7 deficiency (e.g., *Zip7*$^{P198A/f}$ or *Zip7*$^{f/f}$ with inducible or lineage-specific Cre), I demonstrate that T-cell subsets are indeed compromised under heightened ZIP7 insufficiency. These findings suggest that T cells are not intrinsically spared but instead require a higher threshold of ZIP7 loss to be affected, supporting a dose-sensitive requirement for ZIP7 across lymphoid lineages. Viewed in this light, the broader immunodeficiency seen in *Zip7*$^{E363K/P190A}$ patients may reflect a more profound functional impairment, as discussed in Section 7.2. Importantly, single-cell analysis reveals that although ZIP7-deficient B and T cells share stress-related transcriptional signatures, peripheral T cells exhibit more adaptive responses. These results refine our understanding of ZIP7 deficiency as not strictly B cell–specific, but as involving lineage-specific thresholds of resilience and stress adaptation.

Thus, while building upon the *Zip7*$^{P198A/P198A}$ model, this study provides a phenotypic and mechanistic extension that clarifies how ZIP7 regulates lymphocyte persistence beyond early developmental checkpoints.

7.6 Limitations

Several limitations of this study should be acknowledged. First, while this study comprehensively charts ZIP7 deficiency phenotypes using inducible and lineage-specific models, the downstream molecular mechanisms, such as direct targets or pathway-level mediators, remain to be elucidated. Second, although appropriate controls and competitive chimeras were used to reduce confounding effects, I could not directly verify whether B cells recruited into GCs were fully ZIP7-deficient or had escaped recombination. Cells retaining one intact Zip7 allele may have a competitive advantage in the GC, potentially masking the full phenotype of complete knockout cells. Third, while single-cell transcriptomic analyses revealed consistent stress responses, particularly features of s-ISR, their functional impact—such as whether they are protective or deleterious—remains unclear and requires experimental validation, especially in relation to cell fate under stress.

7.7 Future work and outlook

A key short-term priority is to confirm ZIP7 protein deletion at the cellular level. Although antibody specificity was validated in overexpression systems, ZIP7 protein levels have not yet been assessed in knockout lymphocytes. Flow cytometry or immunoblotting in sorted B and T cells would provide direct evidence of protein-level deletion. In parallel, the 5′ scRNA-seq platform used in this study allows transcript-level inspection of *Zip7* exon usage. By mapping reads to the *loxP*-flanked region, it may be possible to estimate deletion efficiency at single-cell resolution and assess whether recombination varies across lineages or developmental stages. These analyses would help clarify whether ZIP7-deficient cells are genuinely absent from certain compartments or are outcompeted by partially recombined cells.

A second area requiring follow-up concerns thymic T cell development. Previous observations suggested that *Zip7*$^{P198A/P198A}$ mice displayed relatively preserved thymic T cells, in contrast to the developmental block seen in BM B cells[20]. However, recent findings from more severe deficiency models revealed progressive loss from the DN2 to DP stages, raising the possibility that thymocytes also experience ZIP7-related stress. Single-cell RNA-seq of thymic T cells from *Zip7*$^{P198A/P198A}$, *Zip7*$^{P198A/f}$ *Ert2*-cre, and *Zip7*$^{f/f}$ *Ert2*-cre mice will help capture early transcriptional responses and refine our understanding of ZIP7 dependency during T cell development.

Third, the stress-related transcriptional features observed in ZIP7-deficient lymphocytes—such as upregulation of *Atf4* and *Pck2* without *Gadd34* induction—are consistent with activation of the s-ISR[317]. Assessing markers of ISR, such as eIF2α phosphorylation status, ATF4 levels, etc., may provide a more sensitive indicator of stress responses than conventional *Xbp1* splicing. In parallel, the upregulation of mTORC1 signaling observed in stressed clusters prompts questions about its role in buffering stress versus contributing to maladaptive responses. Dissecting how mTORC1 integrates with s-ISR and cell fate regulation may yield insights into the vulnerability of metabolically active immune cells. To complement *in vivo* models, nutrient-limited *ex vivo* systems may offer a sensitised environment for revealing ZIP7-dependent stress phenotypes.

Returning to the broader question posed at the beginning of this thesis—what insights can primary immunodeficiencies offer into immune regulation—this work highlights the translational potential of studying monogenic immune disorders. A notable example is RIPK1 deficiency: although *Ripk1* mutations had been extensively characterised in mouse models[400,401], their pathogenic relevance in humans remained uncertain until 2020, when two patients carrying heterozygous *RIPK1* variants (*D324V* or *D324H*) presented with recurrent fevers and lymphadenopathy. Single-cell RNA-seq of patient PBMCs revealed activation of NF-κB and type-I interferon pathways, and treatment with

tocilizumab (anti–IL-6R) achieved clinical improvement—despite not directly targeting the mutant protein[402].

The relevance of these findings to potential therapeutic strategies for ZIP7-related immune dysfunction deserves consideration. In the case of ZIP7, zinc supplementation failed to rescue the developmental block in BM B cells[20], suggesting that intracellular zinc imbalance alone does not account for the phenotype. The stress-related transcriptomic signatures observed in ZIP7-deficient cells, particularly s-ISR features, highlight downstream vulnerabilities that may be amenable to therapeutic modulation. In other models of proteostasis or metabolic dysregulation, small-molecule regulators of stress pathways have shown potential in restoring cell function[317,398,403]. While clinical translation remains a distant goal, further dissecting the stress adaptation and proteostasis mechanisms associated with ZIP7 deficiency—particularly those involving the ISR—may ultimately help identify pharmacologically tractable nodes and bridge the gap between gene discovery and therapeutic innovation.

References

1 Ameratunga, R. *et al.* Are all primary immunodeficiency disorders inborn errors of immunity? *Front Immunol* **12**, 706796 (2021). https://doi.org/10.3389/fimmu.2021.706796

2 Kobrynski, L., Powell, R. W. & Bowen, S. Prevalence and morbidity of primary immunodeficiency diseases, United States 2001-2007. *J Clin Immunol* **34**, 954-961 (2014). https://doi.org/10.1007/s10875-014-0102-8

3 Gathmann, B. *et al.* The European internet-based patient and research database for primary immunodeficiencies: results 2006-2008. *Clin Exp Immunol* **157 Suppl 1**, 3-11 (2009). https://doi.org/10.1111/j.1365-2249.2009.03954.x

4 Kirkpatrick, P. & Riminton, S. Primary immunodeficiency diseases in Australia and New Zealand. *J Clin Immunol* **27**, 517-524 (2007). https://doi.org/10.1007/s10875-007-9105-z

5 Wang, L. L. *et al.* Distribution and clinical features of primary immunodeficiency diseases in Chinese children (2004-2009). *J Clin Immunol* **31**, 297-308 (2011). https://doi.org/10.1007/s10875-010-9493-3

6 Abolhassani, H. *et al.* Global systematic review of primary immunodeficiency registries. *Expert Rev Clin Immunol* **16**, 717-732 (2020). https://doi.org/10.1080/1744666x.2020.1801422

7 Zhang, Q., Frange, P., Blanche, S. & Casanova, J. L. Pathogenesis of infections in HIV-infected individuals: Insights from primary immunodeficiencies. *Curr Opin Immunol* **48**, 122-133 (2017). https://doi.org/10.1016/j.coi.2017.09.002

8 Amaya-Uribe, L., Rojas, M., Azizi, G., Anaya, J. M. & Gershwin, M. E. Primary immunodeficiency and autoimmunity: A comprehensive review. *J Autoimmun* **99**, 52-72 (2019). https://doi.org/10.1016/j.jaut.2019.01.011

9 Bruton, O. C. Agammaglobulinemia. *Pediatrics* **9**, 722-728 (1952). https://doi.org/10.1542/peds.9.6.722

10 Raff, M. C., Megson, M., Owen, J. J. T. & Cooper, M. D. Early production of intracellular IgM by B-lymphocyte precursors in mouse. *Nature* **259**, 224-226 (1976). https://doi.org/10.1038/259224a0

11 Pearl, E. R. *et al.* B lymphocyte precursors in human bone marrow: an analysis of normal individuals and patients with antibody-deficiency states. *J Immunol* **120**, 1169-1175 (1978). https://doi.org/10.4049/jimmunol.120.4.1169

12 Vetrie, D. *et al.* The gene involved in X-linked agammaglobulinaemia is a member of the *src* family of protein-tyrosine kinases. *Nature* **361**, 226-233 (1993). https://doi.org/10.1038/361226a0

13 Tsukada, S. *et al.* Deficient expression of a B cell cytoplasmic tyrosine kinase in human X-linked agammaglobulinemia. *Cell* **72**, 279-290 (1993). https://doi.org/10.1016/0092-8674(93)90667-f

14 Pal Singh, S., Dammeijer, F. & Hendriks, R. W. Role of Bruton's tyrosine kinase in B cells and malignancies. *Molecular Cancer* **17**, 57 (2018). https://doi.org/10.1186/s12943-018-0779-z

15 International Human Genome Sequencing, C. Finishing the euchromatic sequence of the human genome. *Nature* **431**, 931-945 (2004). https://doi.org/10.1038/nature03001

16 Ng, S. B. *et al.* Targeted capture and massively parallel sequencing of 12 human exomes. *Nature* **461**, 272-276 (2009). https://doi.org/10.1038/nature08250

17 Thaventhiran, J. E. D. *et al.* Whole-genome sequencing of a sporadic primary immunodeficiency cohort. *Nature* **583**, 90-95 (2020). https://doi.org/10.1038/s41586-020-2265-1

18 Fang, M., Abolhassani, H., Lim, C. K., Zhang, J. & Hammarström, L. Next generation sequencing data analysis in primary immunodeficiency disorders – future directions. *Journal of Clinical Immunology* **36**, 68-75 (2016). https://doi.org/10.1007/s10875-016-0260-y

19 Kuehn, H. S. *et al.* Loss of B cells in patients with heterozygous mutations in IKAROS. *N Engl J Med* **374**, 1032-1043 (2016). https://doi.org/10.1056/NEJMoa1512234

20 Anzilotti, C. *et al.* An essential role for the Zn^{2+} transporter ZIP7 in B cell development. *Nat Immunol* **20**, 350-361 (2019). https://doi.org/10.1038/s41590-018-0295-8

21 Cong, L. *et al.* Multiplex genome engineering using CRISPR/Cas systems. *Science* **339**, 819-823 (2013). https://doi.org/10.1126/science.1231143

22 Ventura, A. *et al.* Restoration of p53 function leads to tumour regression *in vivo*. *Nature* **445**, 661-665 (2007). https://doi.org/10.1038/nature05541

23 Kraus, M., Alimzhanov, M. B., Rajewsky, N. & Rajewsky, K. Survival of resting mature B lymphocytes depends on BCR signaling via the Igalpha/beta heterodimer. *Cell* **117**, 787-800 (2004). https://doi.org/10.1016/j.cell.2004.05.014

24 Lee, P. P. *et al.* A critical role for Dnmt1 and DNA methylation in T cell development, function, and survival. *Immunity* **15**, 763-774 (2001). https://doi.org/https://doi.org/10.1016/S1074-7613(01)00227-8

25 Svensson, V., Vento-Tormo, R. & Teichmann, S. A. Exponential scaling of single-cell RNA-seq in the past decade. *Nature Protocols* **13**, 599-604 (2018). https://doi.org/10.1038/nprot.2017.149

26 Stoeckius, M. *et al.* Simultaneous epitope and transcriptome measurement in single cells. *Nat Methods* **14**, 865-868 (2017). https://doi.org/10.1038/nmeth.4380

27 Stoeckius, M. *et al.* Cell Hashing with barcoded antibodies enables multiplexing and doublet detection for single cell genomics. *Genome Biology* **19**, 224 (2018). https://doi.org/10.1186/s13059-018-1603-1

28 Cooper, M. D., Peterson, R. D. A. & Good, R. A. Delineation of the thymic and bursal lymphoid systems in the chicken. *Nature* **205**, 143-146 (1965). https://doi.org/10.1038/205143a0

29 Yagi, M. *et al.* Sustained *ex vivo* expansion of hematopoietic stem cells mediated by thrombopoietin. *Proc Natl Acad Sci U S A* **96**, 8126-8131 (1999). https://doi.org/10.1073/pnas.96.14.8126

30 Reya, T., Morrison, S. J., Clarke, M. F. & Weissman, I. L. Stem cells, cancer, and cancer stem cells. *Nature* **414**, 105-111 (2001). https://doi.org/10.1038/35102167

31 Laurenti, E. & Göttgens, B. From haematopoietic stem cells to complex differentiation landscapes. *Nature* **553**, 418-426 (2018). https://doi.org/10.1038/nature25022

32 Adolfsson, J. *et al.* Identification of Flt3+ lympho-myeloid stem cells lacking erythro-megakaryocytic potential a revised road map for adult blood lineage commitment. *Cell* **121**, 295-306 (2005). https://doi.org/10.1016/j.cell.2005.02.013

33 Doulatov, S. *et al.* Revised map of the human progenitor hierarchy shows the origin of macrophages and dendritic cells in early lymphoid development. *Nat Immunol* **11**, 585-593 (2010). https://doi.org/10.1038/ni.1889

34 Laurenti, E. *et al.* The transcriptional architecture of early human hematopoiesis identifies multilevel control of lymphoid commitment. *Nat Immunol* **14**, 756-763 (2013). https://doi.org/10.1038/ni.2615

35 Tokoyoda, K., Egawa, T., Sugiyama, T., Choi, B. I. & Nagasawa, T. Cellular niches controlling B lymphocyte behavior within bone marrow during development. *Immunity* **20**, 707-718 (2004). https://doi.org/10.1016/j.immuni.2004.05.001

36 Brioschi, S. *et al.* Heterogeneity of meningeal B cells reveals a lymphopoietic niche at the CNS borders. *Science* **373** (2021). https://doi.org/10.1126/science.abf9277

37 Wang, Y. *et al.* Early developing B cells undergo negative selection by central nervous system-specific antigens in the meninges. *Immunity* **54**, 2784-2794.e2786 (2021). https://doi.org/10.1016/j.immuni.2021.09.016

38 Uchida, N., Aguila, H. L., Fleming, W. H., Jerabek, L. & Weissman, I. L. Rapid and sustained hematopoietic recovery in lethally irradiated mice transplanted with purified Thy-1.1lo Lin-Sca-1+ hematopoietic stem cells. *Blood* **83**, 3758-3779 (1994). https://doi.org/https://doi.org/10.1182/blood.V83.12.3758.3758

39 Okada, S. *et al.* Sequential analysis of hematopoietic reconstitution achieved by transplantation of hematopoietic stem cells. *Blood* **81**, 1720-1725 (1993).

40 Mercier, F. E., Sykes, D. B. & Scadden, D. T. Single targeted exon mutation creates a true congenic mouse for competitive hematopoietic stem cell transplantation: The C57BL/6-CD45.1(STEM) mouse. *Stem Cell Reports* **6**, 985-992 (2016). https://doi.org/10.1016/j.stemcr.2016.04.010

41 Hardy, R. R., Carmack, C. E., Shinton, S. A., Kemp, J. D. & Hayakawa, K. Resolution and characterization of pro-B and pre-pro-B cell stages in normal mouse bone marrow. *J Exp Med* **173**, 1213-1225 (1991). https://doi.org/10.1084/jem.173.5.1213

42 Hardy, R. R. & Hayakawa, K. B cell development pathways. *Annu Rev Immunol* **19**, 595-621 (2001). https://doi.org/10.1146/annurev.immunol.19.1.595

43 Li, Y. S., Wasserman, R., Hayakawa, K. & Hardy, R. R. Identification of the earliest B lineage stage in mouse bone marrow. *Immunity* **5**, 527-535 (1996). https://doi.org/10.1016/s1074-7613(00)80268-x

44 Allman, D., Li, J. & Hardy, R. R. Commitment to the B lymphoid lineage occurs before DH-JH recombination. *J Exp Med* **189**, 735-740 (1999). https://doi.org/10.1084/jem.189.4.735

45 Medina, K. L. *et al.* Assembling a gene regulatory network for specification of the B cell fate. *Dev Cell* **7**, 607-617 (2004). https://doi.org/10.1016/j.devcel.2004.08.006

46 Fedl, A. S. *et al.* Transcriptional function of E2A, Ebf1, Pax5, Ikaros and Aiolos analyzed by in vivo acute protein degradation in early B cell development.

Nature Immunology **25**, 1663-1677 (2024). https://doi.org/10.1038/s41590-024-01933-7

47 Nutt, S. L., Heavey, B., Rolink, A. G. & Busslinger, M. Commitment to the B-lymphoid lineage depends on the transcription factor Pax5. *Nature* **401**, 556-562 (1999). https://doi.org/10.1038/44076

48 Rolink, A. G., Nutt, S. L., Melchers, F. & Busslinger, M. Long-term in vivo reconstitution of T-cell development by Pax5-deficient B-cell progenitors. *Nature* **401**, 603-606 (1999). https://doi.org/10.1038/44164

49 Alt, F. W. *et al.* Ordered rearrangement of immunoglobulin heavy chain variable region segments. *Embo j* **3**, 1209-1219 (1984). https://doi.org/10.1002/j.1460-2075.1984.tb01955.x

50 Zhang, Y., Zhang, X., Dai, H.-Q., Hu, H. & Alt, F. W. The role of chromatin loop extrusion in antibody diversification. *Nature Reviews Immunology* **22**, 550-566 (2022). https://doi.org/10.1038/s41577-022-00679-3

51 Zhang, Y. *et al.* The fundamental role of chromatin loop extrusion in physiological V(D)J recombination. *Nature* **573**, 600-604 (2019). https://doi.org/10.1038/s41586-019-1547-y

52 Jain, S., Ba, Z., Zhang, Y., Dai, H. Q. & Alt, F. W. CTCF-binding elements mediate accessibility of RAG substrates during chromatin scanning. *Cell* **174**, 102-116.e114 (2018). https://doi.org/10.1016/j.cell.2018.04.035

53 Dai, H. Q. *et al.* Loop extrusion mediates physiological Igh locus contraction for RAG scanning. *Nature* **590**, 338-343 (2021). https://doi.org/10.1038/s41586-020-03121-7

54 Kim, M. S., Lapkouski, M., Yang, W. & Gellert, M. Crystal structure of the V(D)J recombinase RAG1-RAG2. *Nature* **518**, 507-511 (2015). https://doi.org/10.1038/nature14174

55 Ru, H. *et al.* Molecular mechanism of V(D)J recombination from synaptic RAG1-RAG2 complex structures. *Cell* **163**, 1138-1152 (2015). https://doi.org/10.1016/j.cell.2015.10.055

56 Gwyn, L. M., Peak, M. M., De, P., Rahman, N. S. & Rodgers, K. K. A zinc site in the C-terminal domain of RAG1 is essential for DNA cleavage activity. *J Mol Biol* **390**, 863-878 (2009). https://doi.org/10.1016/j.jmb.2009.05.076

57 Rodgers, K. K. *et al.* A zinc-binding domain involved in the dimerization of RAG1. *J Mol Biol* **260**, 70-84 (1996). https://doi.org/10.1006/jmbi.1996.0382

58 Tonegawa, S. Somatic generation of antibody diversity. *Nature* **302**, 575-581 (1983). https://doi.org/10.1038/302575a0

59 Pillai, S. & Baltimore, D. Formation of disulphide-linked mu 2 omega 2 tetramers in pre-B cells by the 18K omega-immunoglobulin light chain. *Nature* **329**, 172-174 (1987). https://doi.org/10.1038/329172a0

60 Sakaguchi, N. & Melchers, F. Lambda 5, a new light-chain-related locus selectively expressed in pre-B lymphocytes. *Nature* **324**, 579-582 (1986). https://doi.org/10.1038/324579a0

61 ten Boekel, E., Melchers, F. & Rolink, A. G. Changes in the V(H) gene repertoire of developing precursor B lymphocytes in mouse bone marrow mediated by the pre-B cell receptor. *Immunity* **7**, 357-368 (1997). https://doi.org/10.1016/s1074-7613(00)80357-x

62 Melchers, F. The pre-B-cell receptor: selector of fitting immunoglobulin heavy chains for the B-cell repertoire. *Nature Reviews Immunology* **5**, 578-584 (2005). https://doi.org/10.1038/nri1649

63 Muljo, S. A. & Schlissel, M. S. A small molecule Abl kinase inhibitor induces differentiation of Abelson virus-transformed pre-B cell lines. *Nat Immunol* **4**, 31-37 (2003). https://doi.org/10.1038/ni870

64 Grawunder, U. *et al.* Down-regulation of RAG1 and RAG2 gene expression in preB cells after functional immunoglobulin heavy chain rearrangement. *Immunity* **3**, 601-608 (1995). https://doi.org/10.1016/1074-7613(95)90131-0

65 ten Boekel, E., Melchers, F. & Rolink, A. G. Precursor B cells showing H chain allelic inclusion display allelic exclusion at the level of pre-B cell receptor surface expression. *Immunity* **8**, 199-207 (1998). https://doi.org/10.1016/s1074-7613(00)80472-0

66 Neuberger, M. S., Caskey, H. M., Pettersson, S., Williams, G. T. & Surani, M. A. Isotype exclusion and transgene down-regulation in immunoglobulin-lambda transgenic mice. *Nature* **338**, 350-352 (1989). https://doi.org/10.1038/338350a0

67 Wardemann, H. *et al.* Predominant autoantibody production by early human B cell precursors. *Science* **301**, 1374-1377 (2003). https://doi.org/10.1126/science.1086907

68 Wienands, J., Larbolette, O. & Reth, M. Evidence for a preformed transducer complex organized by the B cell antigen receptor. *Proc Natl Acad Sci U S A* **93**, 7865-7870 (1996). https://doi.org/10.1073/pnas.93.15.7865

69 Lam, K. P., Kühn, R. & Rajewsky, K. In vivo ablation of surface immunoglobulin on mature B cells by inducible gene targeting results in rapid cell death. *Cell* **90**, 1073-1083 (1997). https://doi.org/10.1016/s0092-8674(00)80373-6

70 Srinivasan, L. *et al.* PI3 kinase signals BCR-dependent mature B cell survival. *Cell* **139**, 573-586 (2009). https://doi.org/10.1016/j.cell.2009.08.041

71 Kraus, M., Alimzhanov, M. B., Rajewsky, N. & Rajewsky, K. Survival of resting mature B lymphocytes depends on BCR signaling via the Igα/β heterodimer. *Cell* **117**, 787-800 (2004). https://doi.org/https://doi.org/10.1016/j.cell.2004.05.014

72 Hartley, S. B. *et al.* Elimination from peripheral lymphoid tissues of self-reactive B lymphocytes recognizing membrane-bound antigens. *Nature* **353**, 765-769 (1991). https://doi.org/10.1038/353765a0

73 Hippen, K. L. *et al.* In vivo assessment of the relative contributions of deletion, anergy, and editing to B cell self-tolerance. *J Immunol* **175**, 909-916 (2005). https://doi.org/10.4049/jimmunol.175.2.909

74 Goodnow, C. C. *et al.* Altered immunoglobulin expression and functional silencing of self-reactive B lymphocytes in transgenic mice. *Nature* **334**, 676-682 (1988). https://doi.org/10.1038/334676a0

75 Halverson, R., Torres, R. M. & Pelanda, R. Receptor editing is the main mechanism of B cell tolerance toward membrane antigens. *Nat Immunol* **5**, 645-650 (2004). https://doi.org/10.1038/ni1076

76 Chen, C. *et al.* The site and stage of anti-DNA B-cell deletion. *Nature* **373**, 252-255 (1995). https://doi.org/10.1038/373252a0

77 Ait-Azzouzene, D. *et al.* An immunoglobulin C kappa-reactive single chain antibody fusion protein induces tolerance through receptor editing in a normal polyclonal immune system. *J Exp Med* **201**, 817-828 (2005). https://doi.org/10.1084/jem.20041854

78 Duong, B. H. *et al.* Negative selection by IgM superantigen defines a B cell central tolerance compartment and reveals mutations allowing escape. *J Immunol* **187**, 5596-5605 (2011). https://doi.org/10.4049/jimmunol.1102479

79 Tiegs, S. L., Russell, D. M. & Nemazee, D. Receptor editing in self-reactive bone marrow B cells. *J Exp Med* **177**, 1009-1020 (1993). https://doi.org/10.1084/jem.177.4.1009

80 Gay, D., Saunders, T., Camper, S. & Weigert, M. Receptor editing: an approach by autoreactive B cells to escape tolerance. *J Exp Med* **177**, 999-1008 (1993). https://doi.org/10.1084/jem.177.4.999

81 Nemazee, D. A. & Bürki, K. Clonal deletion of B lymphocytes in a transgenic mouse bearing anti-MHC class I antibody genes. *Nature* **337**, 562-566 (1989). https://doi.org/10.1038/337562a0

82 Amin, R. H. & Schlissel, M. S. Foxo1 directly regulates the transcription of recombination-activating genes during B cell development. *Nat Immunol* **9**, 613-622 (2008). https://doi.org/10.1038/ni.1612

83 Verkoczy, L. *et al.* Basal B cell receptor-directed phosphatidylinositol 3-kinase signaling turns off RAGs and promotes B cell-positive selection. *J Immunol* **178**, 6332-6341 (2007). https://doi.org/10.4049/jimmunol.178.10.6332

84 Allman, D. M., Ferguson, S. E., Lentz, V. M. & Cancro, M. P. Peripheral B cell maturation. II. Heat-stable antigen(hi) splenic B cells are an immature developmental intermediate in the production of long-lived marrow-derived B cells. *The Journal of Immunology* **151**, 4431-4444 (1993). https://doi.org/10.4049/jimmunol.151.9.4431

85 Rolink, A. G., Andersson, J. & Melchers, F. Characterization of immature B cells by a novel monoclonal antibody, by turnover and by mitogen reactivity. *European Journal of Immunology* **28**, 3738-3748 (1998). https://doi.org/https://doi.org/10.1002/(SICI)1521-4141(199811)28:11<3738::AID-IMMU3738>3.0.CO;2-Q

86 Loder, F. *et al.* B cell development in the spleen takes place in discrete steps and is determined by the quality of B cell receptor-derived signals. *J Exp Med* **190**, 75-89 (1999). https://doi.org/10.1084/jem.190.1.75

87 Allman, D. *et al.* Resolution of three nonproliferative immature splenic B cell subsets reveals multiple selection points during peripheral B cell maturation. *J Immunol* **167**, 6834-6840 (2001). https://doi.org/10.4049/jimmunol.167.12.6834

88 Simpson, M. J. *et al.* Peripheral apoptosis and limited clonal deletion during physiologic murine B lymphocyte development. *Nature Communications* **15**, 4691 (2024). https://doi.org/10.1038/s41467-024-49062-x

89 Hüttl, S. *et al.* Processing of CD74 by the intramembrane protease SPPL2a is critical for B cell receptor signaling in transitional B cells. *J Immunol* **195**, 1548-1563 (2015). https://doi.org/10.4049/jimmunol.1403171

90 Rowland, S. L., Leahy, K. F., Halverson, R., Torres, R. M. & Pelanda, R. BAFF receptor signaling aids the differentiation of immature B cells into transitional B cells following tonic BCR signaling. *J Immunol* **185**, 4570-4581 (2010). https://doi.org/10.4049/jimmunol.1001708

91 Sasaki, Y., Casola, S., Kutok, J. L., Rajewsky, K. & Schmidt-Supprian, M. TNF family member B cell-activating factor (BAFF) receptor-dependent and -independent roles for BAFF in B cell physiology. *J Immunol* **173**, 2245-2252 (2004). https://doi.org/10.4049/jimmunol.173.4.2245

92 Gross, J. A. *et al.* TACI-Ig neutralizes molecules critical for B cell development and autoimmune disease. impaired B cell maturation in mice lacking BLyS. *Immunity* **15**, 289-302 (2001). https://doi.org/10.1016/s1074-7613(01)00183-2

93 Cyster, J. G. *et al.* Regulation of B-lymphocyte negative and positive selection by tyrosine phosphatase CD45. *Nature* **381**, 325-328 (1996). https://doi.org/10.1038/381325a0

94 Chung, J. B., Sater, R. A., Fields, M. L., Erikson, J. & Monroe, J. G. CD23 defines two distinct subsets of immature B cells which differ in their responses to T cell help signals. *International Immunology* **14**, 157-166 (2002). https://doi.org/10.1093/intimm/14.2.157

95 Förster, R. *et al.* A putative chemokine receptor, BLR1, directs B cell migration to defined lymphoid organs and specific anatomic compartments of the spleen. *Cell* **87**, 1037-1047 (1996). https://doi.org/10.1016/s0092-8674(00)81798-5

96 Benschop, R. J. *et al.* Activation and anergy in bone marrow B cells of a novel immunoglobulin transgenic mouse that is both hapten specific and autoreactive. *Immunity* **14**, 33-43 (2001). https://doi.org/10.1016/s1074-7613(01)00087-5

97 Merrell, K. T. *et al.* Identification of anergic B cells within a wild-type repertoire. *Immunity* **25**, 953-962 (2006). https://doi.org/10.1016/j.immuni.2006.10.017

98 Salerno, F. *et al.* An integrated proteome and transcriptome of B cell maturation defines poised activation states of transitional and mature B cells. *Nature Communications* **14**, 5116 (2023). https://doi.org/10.1038/s41467-023-40621-2

99 Glynne, R., Ghandour, G., Rayner, J., Mack, D. H. & Goodnow, C. C. B-lymphocyte quiescence, tolerance and activation as viewed by global gene expression profiling on microarrays. *Immunol Rev* **176**, 216-246 (2000). https://doi.org/10.1034/j.1600-065x.2000.00614.x

100 Zheng, Y., Zha, Y., Driessens, G., Locke, F. & Gajewski, T. F. Transcriptional regulator early growth response gene 2 (Egr2) is required for T cell anergy in vitro and in vivo. *J Exp Med* **209**, 2157-2163 (2012). https://doi.org/10.1084/jem.20120342

101 Masle-Farquhar, E. *et al.* Uncontrolled CD21low age-associated and B1 B cell accumulation caused by failure of an EGR2/3 tolerance checkpoint. *Cell Reports* **38**, 110259 (2022). https://doi.org/https://doi.org/10.1016/j.celrep.2021.110259

102 Wen, R. *et al.* Phospholipase Cgamma2 provides survival signals via Bcl2 and A1 in different subpopulations of B cells. *J Biol Chem* **278**, 43654-43662 (2003). https://doi.org/10.1074/jbc.M307318200

103 Khan, W. N. *et al.* Defective B cell development and function in Btk-deficient mice. *Immunity* **3**, 283-299 (1995). https://doi.org/10.1016/1074-7613(95)90114-0

104 Ansel, K. M. *et al.* A chemokine-driven positive feedback loop organizes lymphoid follicles. *Nature* **406**, 309-314 (2000). https://doi.org/10.1038/35018581

105 Schiemann, B. *et al.* An essential role for BAFF in the normal development of B cells through a BCMA-independent pathway. *Science* **293**, 2111-2114 (2001). https://doi.org/10.1126/science.1061964

106 Zhang, Y. *et al.* Microbiota-mediated shaping of mouse spleen structure and immune function characterized by scRNA-seq and Stereo-seq. *Journal of Genetics and Genomics* **50**, 688-701 (2023). https://doi.org/https://doi.org/10.1016/j.jgg.2023.04.012

107 Cariappa, A. *et al.* The recirculating B cell pool contains two functionally distinct, long-lived, posttransitional, follicular B cell populations. *J Immunol* **179**, 2270-2281 (2007). https://doi.org/10.4049/jimmunol.179.4.2270

108 Kleiman, E. *et al.* Distinct transcriptomic features are associated with transitional and mature B-cell populations in the mouse spleen. *Front Immunol* **6**, 30 (2015). https://doi.org/10.3389/fimmu.2015.00030

109 Farmer, J. R. *et al.* Induction of metabolic quiescence defines the transitional to follicular B cell switch. *Sci Signal* **12** (2019). https://doi.org/10.1126/scisignal.aaw5573

110 Sáez de Guinoa, J., Barrio, L., Mellado, M. & Carrasco, Y. R. CXCL13/CXCR5 signaling enhances BCR-triggered B-cell activation by shaping cell dynamics. *Blood* **118**, 1560-1569 (2011). https://doi.org/10.1182/blood-2011-01-332106

111 Reif, K. *et al.* Balanced responsiveness to chemoattractants from adjacent zones determines B-cell position. *Nature* **416**, 94-99 (2002). https://doi.org/10.1038/416094a

112 Gatto, D., Paus, D., Basten, A., Mackay, C. R. & Brink, R. Guidance of B cells by the orphan G protein-coupled receptor EBI2 shapes humoral immune responses. *Immunity* **31**, 259-269 (2009). https://doi.org/10.1016/j.immuni.2009.06.016

113 Pereira, J. P., Kelly, L. M., Xu, Y. & Cyster, J. G. EBI2 mediates B cell segregation between the outer and centre follicle. *Nature* **460**, 1122-1126 (2009). https://doi.org/10.1038/nature08226

114 Martin, F. & Kearney, J. F. Positive selection from newly formed to marginal zone B cells depends on the rate of clonal production, CD19, and btk. *Immunity* **12**, 39-49 (2000). https://doi.org/10.1016/s1074-7613(00)80157-0

115 Oliver, A. M., Martin, F. & Kearney, J. F. $IgM^{high}CD21^{high}$ lymphocytes enriched in the splenic marginal zone generate effector cells more rapidly than the bulk of follicular B cells. *J Immunol* **162**, 7198-7207 (1999). https://doi.org/https://doi.org/10.4049/jimmunol.162.12.7198

116 Martin, F., Oliver, A. M. & Kearney, J. F. Marginal zone and B1 B cells unite in the early response against T-independent blood-borne particulate antigens. *Immunity* **14**, 617-629 (2001). https://doi.org/10.1016/s1074-7613(01)00129-7

117 Balázs, M., Martin, F., Zhou, T. & Kearney, J. Blood dendritic cells interact with splenic marginal zone B cells to initiate T-independent immune responses. *Immunity* **17**, 341-352 (2002). https://doi.org/10.1016/s1074-7613(02)00389-8

118 Cinamon, G., Zachariah, M. A., Lam, O. M., Foss, F. W. & Cyster, J. G. Follicular shuttling of marginal zone B cells facilitates antigen transport. *Nature Immunology* **9**, 54-62 (2008). https://doi.org/10.1038/ni1542

119 Schriek, P. *et al.* Marginal zone B cells acquire dendritic cell functions by trogocytosis. *Science* **375**, eabf7470 (2022). https://doi.org/10.1126/science.abf7470

120 Cinamon, G. *et al.* Sphingosine 1-phosphate receptor 1 promotes B cell localization in the splenic marginal zone. *Nat Immunol* **5**, 713-720 (2004). https://doi.org/10.1038/ni1083

121 Barral, P. *et al.* B cell receptor-mediated uptake of CD1d-restricted antigen augments antibody responses by recruiting invariant NKT cell help in vivo. *Proc Natl Acad Sci U S A* **105**, 8345-8350 (2008). https://doi.org/10.1073/pnas.0802968105

122 Leadbetter, E. A. *et al.* NK T cells provide lipid antigen-specific cognate help for B cells. *Proc Natl Acad Sci U S A* **105**, 8339-8344 (2008). https://doi.org/10.1073/pnas.0801375105

123 Chappell, C. P., Draves, K. E., Giltiay, N. V. & Clark, E. A. Extrafollicular B cell activation by marginal zone dendritic cells drives T cell-dependent antibody responses. *J Exp Med* **209**, 1825-1840 (2012). https://doi.org/10.1084/jem.20120774

124 Kraus, M. *et al.* Interference with immunoglobulin (Ig)alpha immunoreceptor tyrosine-based activation motif (ITAM) phosphorylation modulates or blocks B cell development, depending on the availability of an Igbeta cytoplasmic tail. *J Exp Med* **194**, 455-469 (2001). https://doi.org/10.1084/jem.194.4.455

125 Makowska, A., Faizunnessa, N. N., Anderson, P., Midtvedt, T. & Cardell, S. CD1high B cells: a population of mixed origin. *Eur J Immunol* **29**, 3285-3294 (1999). https://doi.org/10.1002/(sici)1521-4141(199910)29:10<3285::Aid-immu3285>3.0.Co;2-p

126 You, Y., Zhao, H., Wang, Y. & Carter, R. H. Cutting edge: Primary and secondary effects of CD19 deficiency on cells of the marginal zone. *J Immunol* **182**, 7343-7347 (2009). https://doi.org/10.4049/jimmunol.0804295

127 Rickert, R. C., Rajewsky, K. & Roes, J. Impairment of T-cell-dependent B-cell responses and B-1 cell development in CD19-deficient mice. *Nature* **376**, 352-355 (1995). https://doi.org/10.1038/376352a0

128 Sato, S. *et al.* CD22 is both a positive and negative regulator of B lymphocyte antigen receptor signal transduction: altered signaling in CD22-deficient mice. *Immunity* **5**, 551-562 (1996). https://doi.org/10.1016/s1074-7613(00)80270-8

129 Cariappa, A. *et al.* The follicular versus marginal zone B lymphocyte cell fate decision is regulated by Aiolos, Btk, and CD21. *Immunity* **14**, 603-615 (2001). https://doi.org/10.1016/s1074-7613(01)00135-2

130 Wang, J. H. *et al.* Aiolos regulates B cell activation and maturation to effector state. *Immunity* **9**, 543-553 (1998). https://doi.org/10.1016/s1074-7613(00)80637-8

131 Tan, J. B. *et al.* Lunatic and manic fringe cooperatively enhance marginal zone B cell precursor competition for delta-like 1 in splenic endothelial niches. *Immunity* **30**, 254-263 (2009). https://doi.org/10.1016/j.immuni.2008.12.016

132 Hozumi, K. *et al.* Delta-like 1 is necessary for the generation of marginal zone B cells but not T cells in vivo. *Nat Immunol* **5**, 638-644 (2004). https://doi.org/10.1038/ni1075

133 Saito, T. *et al.* Notch2 is preferentially expressed in mature B cells and indispensable for marginal zone B lineage development. *Immunity* **18**, 675-685 (2003). https://doi.org/10.1016/s1074-7613(03)00111-0

134 Tanigaki, K. *et al.* Notch-RBP-J signaling is involved in cell fate determination of marginal zone B cells. *Nat Immunol* **3**, 443-450 (2002). https://doi.org/10.1038/ni793

135 Cariappa, A., Liou, H. C., Horwitz, B. H. & Pillai, S. Nuclear factor kappa B is required for the development of marginal zone B lymphocytes. *J Exp Med* **192**, 1175-1182 (2000). https://doi.org/10.1084/jem.192.8.1175

136 Gibb, D. R. *et al.* ADAM10 is essential for Notch2-dependent marginal zone B cell development and CD23 cleavage in vivo. *J Exp Med* **207**, 623-635 (2010). https://doi.org/10.1084/jem.20091990

137 Srivastava, B., Quinn, W. J., 3rd, Hazard, K., Erikson, J. & Allman, D. Characterization of marginal zone B cell precursors. *J Exp Med* **202**, 1225-1234 (2005). https://doi.org/10.1084/jem.20051038

138 Carey, J. B., Moffatt-Blue, C. S., Watson, L. C., Gavin, A. L. & Feeney, A. J. Repertoire-based selection into the marginal zone compartment during B cell development. *J Exp Med* **205**, 2043-2052 (2008). https://doi.org/10.1084/jem.20080559

139 Hammad, H. *et al.* Transitional B cells commit to marginal zone B cell fate by Taok3-mediated surface expression of ADAM10. *Nature Immunology* **18**, 313-320 (2017). https://doi.org/10.1038/ni.3657

140 Jones, D. D., Wilmore, J. R. & Allman, D. Cellular dynamics of memory B cell populations: IgM+ and IgG+ memory B cells persist indefinitely as quiescent cells. *J Immunol* **195**, 4753-4759 (2015). https://doi.org/10.4049/jimmunol.1501365

141 Hao, Z. & Rajewsky, K. Homeostasis of peripheral B cells in the absence of B cell influx from the bone marrow. *Journal of Experimental Medicine* **194**, 1151-1164 (2001). https://doi.org/10.1084/jem.194.8.1151

142 Do, R. K. *et al.* Attenuation of apoptosis underlies B lymphocyte stimulator enhancement of humoral immune response. *J Exp Med* **192**, 953-964 (2000). https://doi.org/10.1084/jem.192.7.953

143 Batten, M. *et al.* BAFF mediates survival of peripheral immature B lymphocytes. *J Exp Med* **192**, 1453-1466 (2000). https://doi.org/10.1084/jem.192.10.1453

144 Tardivel, A. *et al.* The anti-apoptotic factor Bcl-2 can functionally substitute for the B cell survival but not for the marginal zone B cell differentiation activity of BAFF. *Eur J Immunol* **34**, 509-518 (2004). https://doi.org/10.1002/eji.200324692

145 Rahman, Z. S. & Manser, T. B cells expressing Bcl-2 and a signaling-impaired BAFF-specific receptor fail to mature and are deficient in the formation of lymphoid follicles and germinal centers. *J Immunol* **173**, 6179-6188 (2004). https://doi.org/10.4049/jimmunol.173.10.6179

146 Liu, J. *et al.* Fcμ receptor promotes the survival and activation of marginal zone B cells and protects mice against bacterial sepsis. *Front Immunol* **9**, 160 (2018). https://doi.org/10.3389/fimmu.2018.00160

147 Newman, R. *et al.* Maintenance of the marginal-zone B cell compartment specifically requires the RNA-binding protein ZFP36L1. *Nature Immunology* **18**, 683-693 (2017). https://doi.org/10.1038/ni.3724

148 Figgett, W. A. *et al.* The TACI receptor regulates T-cell-independent marginal zone B cell responses through innate activation-induced cell death. *Immunity* **39**, 573-583 (2013). https://doi.org/10.1016/j.immuni.2013.05.019

149 Arnon, T. I. *et al.* GRK2-dependent S1PR1 desensitization is required for lymphocytes to overcome their attraction to blood. *Science* **333**, 1898-1903 (2011). https://doi.org/10.1126/science.1208248

150 Muppidi, J. R. *et al.* Cannabinoid receptor 2 positions and retains marginal zone B cells within the splenic marginal zone. *Journal of Experimental Medicine* **208**, 1941-1948 (2011). https://doi.org/10.1084/jem.20111083

151 Lu, T. T. & Cyster, J. G. Integrin-mediated long-term B cell retention in the splenic marginal zone. *Science* **297**, 409-412 (2002). https://doi.org/10.1126/science.1071632

152 Guinamard, R., Okigaki, M., Schlessinger, J. & Ravetch, J. V. Absence of marginal zone B cells in Pyk-2–deficient mice defines their role in the humoral response. *Nature Immunology* **1**, 31-36 (2000). https://doi.org/10.1038/76882

153 Girkontaite, I. *et al.* Lsc is required for marginal zone B cells, regulation of lymphocyte motility and immune responses. *Nat Immunol* **2**, 855-862 (2001). https://doi.org/10.1038/ni0901-855

154 Westerberg, L. S. *et al.* WASP confers selective advantage for specific hematopoietic cell populations and serves a unique role in marginal zone B-cell homeostasis and function. *Blood* **112**, 4139-4147 (2008). https://doi.org/10.1182/blood-2008-02-140715

155 Walmsley, M. J. *et al.* Critical roles for Rac1 and Rac2 GTPases in B cell development and signaling. *Science* **302**, 459-462 (2003). https://doi.org/10.1126/science.1089709

156 Croker, B. A. *et al.* The Rac2 guanosine triphosphatase regulates B lymphocyte antigen receptor responses and chemotaxis and is required for establishment of B-1a and marginal zone B lymphocytes. *J Immunol* **168**, 3376-3386 (2002). https://doi.org/10.4049/jimmunol.168.7.3376

157 Liu, D. *et al.* Dynamic encounters with red blood cells trigger splenic marginal zone B cell retention and function. *Nature Immunology* **25**, 142-154 (2024). https://doi.org/10.1038/s41590-023-01690-z

158 Karlsson , M. C. I. *et al.* Macrophages control the retention and trafficking of B lymphocytes in the splenic marginal zone. *Journal of Experimental Medicine* **198**, 333-340 (2003). https://doi.org/10.1084/jem.20030684

159 Okada, T. *et al.* Antigen-engaged B cells undergo chemotaxis toward the T zone and form motile conjugates with helper T cells. *PLoS Biol* **3**, e150 (2005). https://doi.org/10.1371/journal.pbio.0030150

160 Kerfoot, S. M. *et al.* Germinal center B cell and T follicular helper cell development initiates in the interfollicular zone. *Immunity* **34**, 947-960 (2011). https://doi.org/10.1016/j.immuni.2011.03.024

161 Qi, H., Cannons, J. L., Klauschen, F., Schwartzberg, P. L. & Germain, R. N. SAP-controlled T–B cell interactions underlie germinal centre formation. *Nature* **455**, 764-769 (2008). https://doi.org/10.1038/nature07345

162 Kitano, M. *et al.* Bcl6 protein expression shapes pre-germinal center B cell dynamics and follicular helper T cell heterogeneity. *Immunity* **34**, 961-972 (2011). https://doi.org/10.1016/j.immuni.2011.03.025

163 Qi, H., Egen, J. G., Huang, A. Y. & Germain, R. N. Extrafollicular activation of lymph node B cells by antigen-bearing dendritic cells. *Science* **312**, 1672-1676 (2006). https://doi.org/10.1126/science.1125703

164 Jacob, J., Kelsoe, G., Rajewsky, K. & Weiss, U. Intraclonal generation of antibody mutants in germinal centres. *Nature* **354**, 389-392 (1991). https://doi.org/10.1038/354389a0

165 Allen, C. D. *et al.* Germinal center dark and light zone organization is mediated by CXCR4 and CXCR5. *Nat Immunol* **5**, 943-952 (2004). https://doi.org/10.1038/ni1100

166 Victora, G. D. *et al.* Germinal center dynamics revealed by multiphoton microscopy with a photoactivatable fluorescent reporter. *Cell* **143**, 592-605 (2010). https://doi.org/10.1016/j.cell.2010.10.032

167 Wang, X. *et al.* Follicular dendritic cells help establish follicle identity and promote B cell retention in germinal centers. *J Exp Med* **208**, 2497-2510 (2011). https://doi.org/10.1084/jem.20111449

168 Gitlin, A. D., Shulman, Z. & Nussenzweig, M. C. Clonal selection in the germinal centre by regulated proliferation and hypermutation. *Nature* **509**, 637-640 (2014). https://doi.org/10.1038/nature13300

169 Mayer, C. T. *et al.* The microanatomic segregation of selection by apoptosis in the germinal center. *Science* **358** (2017). https://doi.org/10.1126/science.aao2602

170 Takahashi, Y. *et al.* Relaxed negative selection in germinal centers and impaired affinity maturation in bcl-xL transgenic mice. *J Exp Med* **190**, 399-410 (1999). https://doi.org/10.1084/jem.190.3.399

171 Liu, D. *et al.* T–B-cell entanglement and ICOSL-driven feed-forward regulation of germinal centre reaction. *Nature* **517**, 214-218 (2015). https://doi.org/10.1038/nature13803

172 Liu, B. *et al.* Affinity-coupled CCL22 promotes positive selection in germinal centres. *Nature* **592**, 133-137 (2021). https://doi.org/10.1038/s41586-021-03239-2

173 Tarlinton, D. & Good-Jacobson, K. Diversity among memory B cells: origin, consequences, and utility. *Science* **341**, 1205-1211 (2013). https://doi.org/10.1126/science.1241146

174 Kallies, A. *et al.* Initiation of plasma-cell differentiation is independent of the transcription factor Blimp-1. *Immunity* **26**, 555-566 (2007). https://doi.org/10.1016/j.immuni.2007.04.007

175 Sciammas, R. *et al.* Graded expression of interferon regulatory factor-4 coordinates isotype switching with plasma cell differentiation. *Immunity* **25**, 225-236 (2006). https://doi.org/10.1016/j.immuni.2006.07.009

176 Klein, U. *et al.* Transcription factor IRF4 controls plasma cell differentiation and class-switch recombination. *Nat Immunol* **7**, 773-782 (2006). https://doi.org/10.1038/ni1357

177 Diehl, S. A. *et al.* STAT3-mediated up-regulation of BLIMP1 Is coordinated with BCL6 down-regulation to control human plasma cell differentiation. *J Immunol* **180**, 4805-4815 (2008). https://doi.org/10.4049/jimmunol.180.7.4805

178 Kwon, H. *et al.* Analysis of interleukin-21-induced Prdm1 gene regulation reveals functional cooperation of STAT3 and IRF4 transcription factors. *Immunity* **31**, 941-952 (2009). https://doi.org/10.1016/j.immuni.2009.10.008

179 Ozaki, K. *et al.* Regulation of B cell differentiation and plasma cell generation by IL-21, a novel inducer of Blimp-1 and Bcl-6. *J Immunol* **173**, 5361-5371 (2004). https://doi.org/10.4049/jimmunol.173.9.5361

180 Tellier, J. *et al.* Blimp-1 controls plasma cell function through the regulation of immunoglobulin secretion and the unfolded protein response. *Nat Immunol* **17**, 323-330 (2016). https://doi.org/10.1038/ni.3348

181 Shaffer, A. L. *et al.* Blimp-1 orchestrates plasma cell differentiation by extinguishing the mature B cell gene expression program. *Immunity* **17**, 51-62 (2002). https://doi.org/https://doi.org/10.1016/S1074-7613(02)00335-7

182 Allman, D. *et al.* Thymopoiesis independent of common lymphoid progenitors. *Nature Immunology* **4**, 168-174 (2003). https://doi.org/10.1038/ni878

183 Donskoy, E. & Goldschneider, I. Thymocytopoiesis is maintained by blood-borne precursors throughout postnatal life. A study in parabiotic mice. *J Immunol* **148**, 1604-1612 (1992).

184 Godfrey, D. I., Kennedy, J., Suda, T. & Zlotnik, A. A developmental pathway involving four phenotypically and functionally distinct subsets of CD3-CD4-CD8- triple-negative adult mouse thymocytes defined by CD44 and CD25 expression. *J Immunol* **150**, 4244-4252 (1993).

185 Petrie, H. T., Hugo, P., Scollay, R. & Shortman, K. Lineage relationships and developmental kinetics of immature thymocytes: CD3, CD4, and CD8 acquisition in vivo and in vitro. *J Exp Med* **172**, 1583-1588 (1990). https://doi.org/10.1084/jem.172.6.1583

186 Porritt, H. E. *et al.* Heterogeneity among DN1 prothymocytes reveals multiple progenitors with different capacities to generate T cell and non-T cell lineages. *Immunity* **20**, 735-745 (2004). https://doi.org/10.1016/j.immuni.2004.05.004

187 Koch, U. *et al.* Delta-like 4 is the essential, nonredundant ligand for Notch1 during thymic T cell lineage commitment. *J Exp Med* **205**, 2515-2523 (2008). https://doi.org/10.1084/jem.20080829

188 Sambandam, A. *et al.* Notch signaling controls the generation and differentiation of early T lineage progenitors. *Nature Immunology* **6**, 663-670 (2005). https://doi.org/10.1038/ni1216

189 Germar, K. *et al.* T-cell factor 1 is a gatekeeper for T-cell specification in response to Notch signaling. *Proc Natl Acad Sci U S A* **108**, 20060-20065 (2011). https://doi.org/10.1073/pnas.1110230108

190 Weber, B. N. *et al.* A critical role for TCF-1 in T-lineage specification and differentiation. *Nature* **476**, 63-68 (2011). https://doi.org/10.1038/nature10279

191 Garcia-Perez, L. *et al.* Functional definition of a transcription factor hierarchy regulating T cell lineage commitment. *Sci Adv* **6**, eaaw7313 (2020). https://doi.org/10.1126/sciadv.aaw7313

192 Hosoya, T. *et al.* GATA-3 is required for early T lineage progenitor development. *Journal of Experimental Medicine* **206**, 2987-3000 (2009). https://doi.org/10.1084/jem.20090934

193 Li, L., Leid, M. & Rothenberg, E. V. An early T cell lineage commitment checkpoint dependent on the transcription factor Bcl11b. *Science* **329**, 89-93 (2010). https://doi.org/10.1126/science.1188989

194 Ikawa, T. *et al.* An essential developmental checkpoint for production of the T cell lineage. *Science* **329**, 93-96 (2010). https://doi.org/10.1126/science.1188995

195 Fehling, H. J., Krotkova, A., Saint-Ruf, C. & von Boehmer, H. Crucial role of the pre-T-cell receptor alpha gene in development of alpha beta but not gamma delta T cells. *Nature* **375**, 795-798 (1995). https://doi.org/10.1038/375795a0

196 Zarin, P., Wong, G. W., Mohtashami, M., Wiest, D. L. & Zúñiga-Pflücker, J. C. Enforcement of γδ-lineage commitment by the pre-T-cell receptor in precursors with weak γδ-TCR signals. *Proc Natl Acad Sci U S A* **111**, 5658-5663 (2014). https://doi.org/10.1073/pnas.1312872111

197 Ciofani, M., Knowles, G. C., Wiest, D. L., von Boehmer, H. & Zúñiga-Pflücker, J. C. Stage-specific and differential notch dependency at the alphabeta and gammadelta T lineage bifurcation. *Immunity* **25**, 105-116 (2006). https://doi.org/10.1016/j.immuni.2006.05.010

198 Taghon, T., Yui, M. A., Pant, R., Diamond, R. A. & Rothenberg, E. V. Developmental and molecular characterization of emerging beta- and gammadelta-selected pre-T cells in the adult mouse thymus. *Immunity* **24**, 53-64 (2006). https://doi.org/10.1016/j.immuni.2005.11.012

199 Garbe, A. I., Krueger, A., Gounari, F., Zúñiga-Pflücker, J. C. & von Boehmer, H. Differential synergy of Notch and T cell receptor signaling determines alphabeta versus gammadelta lineage fate. *J Exp Med* **203**, 1579-1590 (2006). https://doi.org/10.1084/jem.20060474

200 Daniels, M. A. *et al.* Thymic selection threshold defined by compartmentalization of Ras/MAPK signalling. *Nature* **444**, 724-729 (2006). https://doi.org/10.1038/nature05269

201 Murata, S. *et al.* Regulation of CD8+ T cell development by thymus-specific proteasomes. *Science* **316**, 1349-1353 (2007). https://doi.org/10.1126/science.1141915

202 Nakagawa, T. *et al.* Cathepsin L: critical role in Ii degradation and CD4 T cell selection in the thymus. *Science* **280**, 450-453 (1998). https://doi.org/10.1126/science.280.5362.450

203 Anderson, M. S. *et al.* Projection of an immunological self shadow within the thymus by the aire protein. *Science* **298**, 1395-1401 (2002). https://doi.org/10.1126/science.1075958

204 Li, J., Park, J., Foss, D. & Goldschneider, I. Thymus-homing peripheral dendritic cells constitute two of the three major subsets of dendritic cells in the steady-state thymus. *J Exp Med* **206**, 607-622 (2009). https://doi.org/10.1084/jem.20082232

205 Aichinger, M., Wu, C., Nedjic, J. & Klein, L. Macroautophagy substrates are loaded onto MHC class II of medullary thymic epithelial cells for central tolerance. *J Exp Med* **210**, 287-300 (2013). https://doi.org/10.1084/jem.20122149

206 Hadeiba, H. *et al.* Plasmacytoid dendritic cells transport peripheral antigens to the thymus to promote central tolerance. *Immunity* **36**, 438-450 (2012). https://doi.org/10.1016/j.immuni.2012.01.017

207 Itoh, M. *et al.* Thymus and autoimmunity: production of CD25+CD4+ naturally anergic and suppressive T cells as a key function of the thymus in maintaining immunologic self-tolerance. *J Immunol* **162**, 5317-5326 (1999).

208 Egerton, M., Scollay, R. & Shortman, K. Kinetics of mature T-cell development in the thymus. *Proc Natl Acad Sci U S A* **87**, 2579-2582 (1990). https://doi.org/10.1073/pnas.87.7.2579

209 Veiga-Fernandes, H., Walter, U., Bourgeois, C., McLean, A. & Rocha, B. Response of naïve and memory CD8+ T cells to antigen stimulation in vivo. *Nat Immunol* **1**, 47-53 (2000). https://doi.org/10.1038/76907

210 Cho, B. K., Wang, C., Sugawa, S., Eisen, H. N. & Chen, J. Functional differences between memory and naive CD8 T cells. *Proc Natl Acad Sci U S A* **96**, 2976-2981 (1999). https://doi.org/10.1073/pnas.96.6.2976

211 Wherry, E. J. *et al.* Lineage relationship and protective immunity of memory CD8 T cell subsets. *Nature Immunology* **4**, 225-234 (2003). https://doi.org/10.1038/ni889

212 Warnock, R. A., Askari, S., Butcher, E. C. & von Andrian, U. H. Molecular mechanisms of lymphocyte homing to peripheral lymph nodes. *J Exp Med* **187**, 205-216 (1998). https://doi.org/10.1084/jem.187.2.205

213 Stein, J. V. *et al.* The CC chemokine thymus-derived chemotactic agent 4 (TCA-4, secondary lymphoid tissue chemokine, 6Ckine, exodus-2) triggers lymphocyte function-associated antigen 1-mediated arrest of rolling T lymphocytes in peripheral lymph node high endothelial venules. *J Exp Med* **191**, 61-76 (2000). https://doi.org/10.1084/jem.191.1.61

214 Sallusto, F., Lenig, D., Förster, R., Lipp, M. & Lanzavecchia, A. Two subsets of memory T lymphocytes with distinct homing potentials and effector functions. *Nature* **401**, 708-712 (1999). https://doi.org/10.1038/44385

215 Kurachi, M. *et al.* Chemokine receptor CXCR3 facilitates CD8(+) T cell differentiation into short-lived effector cells leading to memory degeneration. *J Exp Med* **208**, 1605-1620 (2011). https://doi.org/10.1084/jem.20102101

216 Kamogawa, Y., Minasi, L. A., Carding, S. R., Bottomly, K. & Flavell, R. A. The relationship of IL-4- and IFN gamma-producing T cells studied by lineage ablation of IL-4-producing cells. *Cell* **75**, 985-995 (1993). https://doi.org/10.1016/0092-8674(93)90542-x

217 Mackay, C. R., Marston, W. L. & Dudler, L. Naive and memory T cells show distinct pathways of lymphocyte recirculation. *J Exp Med* **171**, 801-817 (1990). https://doi.org/10.1084/jem.171.3.801

218 van der Windt, G. J. *et al.* Mitochondrial respiratory capacity is a critical regulator of CD8+ T cell memory development. *Immunity* **36**, 68-78 (2012). https://doi.org/10.1016/j.immuni.2011.12.007

219 Pearce, E. L. *et al.* Enhancing CD8 T-cell memory by modulating fatty acid metabolism. *Nature* **460**, 103-107 (2009). https://doi.org/10.1038/nature08097

220 van der Windt, G. J. *et al.* CD8 memory T cells have a bioenergetic advantage that underlies their rapid recall ability. *Proc Natl Acad Sci U S A* **110**, 14336-14341 (2013). https://doi.org/10.1073/pnas.1221740110

221 O'Sullivan, D. *et al.* Memory CD8(+) T cells use cell-intrinsic lipolysis to support the metabolic programming necessary for development. *Immunity* **41**, 75-88 (2014). https://doi.org/10.1016/j.immuni.2014.06.005

222 Tan, J. T. *et al.* IL-7 is critical for homeostatic proliferation and survival of naive T cells. *Proc Natl Acad Sci U S A* **98**, 8732-8737 (2001). https://doi.org/10.1073/pnas.161126098

223 Tanchot, C., Lemonnier, F. A., Pérarnau, B., Freitas, A. A. & Rocha, B. Differential requirements for survival and proliferation of CD8 naïve or memory T cells. *Science* **276**, 2057-2062 (1997). https://doi.org/10.1126/science.276.5321.2057

224 Kirberg, J., Berns, A. & von Boehmer, H. Peripheral T cell survival requires continual ligation of the T cell receptor to major histocompatibility complex-encoded molecules. *J Exp Med* **186**, 1269-1275 (1997). https://doi.org/10.1084/jem.186.8.1269

225 Kurtulus, S. *et al.* Bcl-2 allows effector and memory CD8+ T cells to tolerate higher expression of Bim. *J Immunol* **186**, 5729-5737 (2011). https://doi.org/10.4049/jimmunol.1100102

226 Murali-Krishna, K. *et al.* Persistence of memory CD8 T cells in MHC class I-deficient mice. *Science* **286**, 1377-1381 (1999). https://doi.org/10.1126/science.286.5443.1377

227 Garboczi, D. N. *et al.* Structure of the complex between human T-cell receptor, viral peptide and HLA-A2. *Nature* **384**, 134-141 (1996). https://doi.org/10.1038/384134a0

228 Reinherz, E. L. *et al.* The crystal structure of a T cell receptor in complex with peptide and MHC class II. *Science* **286**, 1913-1921 (1999). https://doi.org/10.1126/science.286.5446.1913

229 Shahinian, A. *et al.* Differential T cell costimulatory requirements in CD28-deficient mice. *Science* **261**, 609-612 (1993). https://doi.org/10.1126/science.7688139

230 Harding, F. A., McArthur, J. G., Gross, J. A., Raulet, D. H. & Allison, J. P. CD28-mediated signalling co-stimulates murine T cells and prevents induction of anergy in T-cell clones. *Nature* **356**, 607-609 (1992). https://doi.org/10.1038/356607a0

231 Hsieh, C. S. *et al.* Development of TH1 CD4+ T cells through IL-12 produced by Listeria-induced macrophages. *Science* **260**, 547-549 (1993). https://doi.org/10.1126/science.8097338

232 Long, L. *et al.* CRISPR screens unveil signal hubs for nutrient licensing of T cell immunity. *Nature* **600**, 308-313 (2021). https://doi.org/10.1038/s41586-021-04109-7

233 Shi, H. *et al.* Amino acids license kinase mTORC1 activity and Treg cell function via small G proteins Rag and Rheb. *Immunity* **51**, 1012-1027.e1017 (2019). https://doi.org/10.1016/j.immuni.2019.10.001

234 Blagih, J. *et al.* The energy sensor AMPK regulates T cell metabolic adaptation and effector responses in vivo. *Immunity* **42**, 41-54 (2015). https://doi.org/10.1016/j.immuni.2014.12.030

235 Kidani, Y. *et al.* Sterol regulatory element–binding proteins are essential for the metabolic programming of effector T cells and adaptive immunity. *Nature Immunology* **14**, 489-499 (2013). https://doi.org/10.1038/ni.2570

236 Harding, H. P. *et al.* An integrated stress response regulates amino acid metabolism and resistance to oxidative stress. *Mol Cell* **11**, 619-633 (2003). https://doi.org/10.1016/s1097-2765(03)00105-9

237 Munn, D. H. *et al.* GCN2 kinase in T cells mediates proliferative arrest and anergy induction in response to indoleamine 2,3-dioxygenase. *Immunity* **22**, 633-642 (2005). https://doi.org/10.1016/j.immuni.2005.03.013

238 Cao, T. *et al.* Cancer SLC6A6-mediated taurine uptake transactivates immune checkpoint genes and induces exhaustion in CD8(+) T cells. *Cell* **187**, 2288-2304.e2227 (2024). https://doi.org/10.1016/j.cell.2024.03.011

239 Jin, J. *et al.* Deletion of Trpm7 disrupts embryonic development and thymopoiesis without altering Mg2+ homeostasis. *Science* **322**, 756-760 (2008). https://doi.org/10.1126/science.1163493

240 Krishnamoorthy, M. *et al.* The ion channel TRPM7 is required for B cell lymphopoiesis. *Sci Signal* **11** (2018). https://doi.org/10.1126/scisignal.aan2693

241 Romagnani, A. *et al.* TRPM7 kinase activity is essential for T cell colonization and alloreactivity in the gut. *Nature Communications* **8**, 1917 (2017). https://doi.org/10.1038/s41467-017-01960-z

242 Schmitz, C. *et al.* Regulation of vertebrate cellular Mg2+ homeostasis by TRPM7. *Cell* **114**, 191-200 (2003). https://doi.org/10.1016/s0092-8674(03)00556-7

243 Santos, R. *et al.* A comprehensive map of molecular drug targets. *Nat Rev Drug Discov* **16**, 19-34 (2017). https://doi.org/10.1038/nrd.2016.230

244 Tapiero, H. & Tew, K. D. Trace elements in human physiology and pathology: zinc and metallothioneins. *Biomedicine & Pharmacotherapy* **57**, 399-411 (2003). https://doi.org/https://doi.org/10.1016/S0753-3322(03)00081-7

245 Prasad, A. S., Halsted, J. A. & Nadimi, M. Syndrome of iron deficiency anemia, hepatosplenomegaly, hypogonadism, dwarfism and geophagia. *The American Journal of Medicine* **31**, 532-546 (1961). https://doi.org/10.1016/0002-9343(61)90137-1

246 Black, R. E. *et al.* Maternal and child undernutrition: global and regional exposures and health consequences. *The Lancet* **371**, 243-260 (2008). https://doi.org/https://doi.org/10.1016/S0140-6736(07)61690-0

247 Victora, C. G. *et al.* Revisiting maternal and child undernutrition in low-income and middle-income countries: variable progress towards an unfinished agenda. *Lancet* **397**, 1388-1399 (2021). https://doi.org/10.1016/s0140-6736(21)00394-9

248 Jothimani, D. *et al.* COVID-19: Poor outcomes in patients with zinc deficiency. *International Journal of Infectious Diseases* **100**, 343-349 (2020). https://doi.org/https://doi.org/10.1016/j.ijid.2020.09.014

249 Nault, D. *et al.* Zinc for prevention and treatment of the common cold. *Cochrane Database of Systematic Reviews* (2024). https://doi.org/10.1002/14651858.CD014914.pub2

250 Ben Abdallah, S. *et al.* Twice-daily oral zinc in the treatment of patients with Coronavirus disease 2019: A randomized double-blind controlled trial. *Clin Infect Dis* **76**, 185-191 (2023). https://doi.org/10.1093/cid/ciac807

251 Andreini, C., Bertini, I. & Rosato, A. Metalloproteomes: a bioinformatic approach. *Acc Chem Res* **42**, 1471-1479 (2009). https://doi.org/10.1021/ar900015x

252 Yamasaki, S. *et al.* Zinc is a novel intracellular second messenger. *J Cell Biol* **177**, 637-645 (2007). https://doi.org/10.1083/jcb.200702081

253 Yu, M. *et al.* Regulation of T cell receptor signaling by activation-induced zinc influx. *J Exp Med* **208**, 775-785 (2011). https://doi.org/10.1084/jem.20100031

254 Fang, H. *et al.* Simultaneous Zn2+ tracking in multiple organelles using super-resolution morphology-correlated organelle identification in living cells. *Nature Communications* **12**, 109 (2021). https://doi.org/10.1038/s41467-020-20309-7

255 Aydemir, T. B., Liuzzi, J. P., McClellan, S. & Cousins, R. J. Zinc transporter ZIP8 (SLC39A8) and zinc influence IFN-gamma expression in activated human T cells. *J Leukoc Biol* **86**, 337-348 (2009). https://doi.org/10.1189/jlb.1208759

256 Colomar-Carando, N. *et al.* Zip6 transporter is an essential component of the lymphocyte activation machinery. *J Immunol* **202**, 441-450 (2019). https://doi.org/10.4049/jimmunol.1800689

257 Outten, C. E. & O'Halloran, T. V. Femtomolar sensitivity of metalloregulatory proteins controlling zinc homeostasis. *Science* **292**, 2488-2492 (2001). https://doi.org/10.1126/science.1060331

258 Maret, W. Redox biochemistry of mammalian metallothioneins. *JBIC Journal of Biological Inorganic Chemistry* **16**, 1079-1086 (2011). https://doi.org/10.1007/s00775-011-0800-0

259 Hojyo, S. *et al.* Zinc transporter SLC39A10/ZIP10 controls humoral immunity by modulating B-cell receptor signal strength. *Proc Natl Acad Sci U S A* **111**, 11786-11791 (2014). https://doi.org/10.1073/pnas.1323557111

260 Du, M. & Chen, Z. J. DNA-induced liquid phase condensation of cGAS activates innate immune signaling. *Science* **361**, 704-709 (2018). https://doi.org/doi:10.1126/science.aat1022

261 Kim, P. W., Sun, Z. Y., Blacklow, S. C., Wagner, G. & Eck, M. J. A zinc clasp structure tethers Lck to T cell coreceptors CD4 and CD8. *Science* **301**, 1725-1728 (2003). https://doi.org/10.1126/science.1085643

262 West, A. P. *et al.* TLR signalling augments macrophage bactericidal activity through mitochondrial ROS. *Nature* **472**, 476-480 (2011). https://doi.org/10.1038/nature09973

263 Heijmans, J. *et al.* ER stress causes rapid loss of intestinal epithelial stemness through activation of the unfolded protein response. *Cell Rep* **3**, 1128-1139 (2013). https://doi.org/10.1016/j.celrep.2013.02.031

264 Oteiza, P. I., Clegg, M. S., Zago, M. P. & Keen, C. L. Zinc deficiency induces oxidative stress and AP-1 activation in 3T3 cells. *Free Radic Biol Med* **28**, 1091-1099 (2000). https://doi.org/10.1016/s0891-5849(00)00200-8

265 Homma, K. *et al.* SOD1 as a molecular switch for initiating the homeostatic ER stress response under zinc deficiency. *Mol Cell* **52**, 75-86 (2013). https://doi.org/10.1016/j.molcel.2013.08.038

266 Sun, Q. *et al.* Zinc deficiency mediates alcohol-induced apoptotic cell death in the liver of rats through activating ER and mitochondrial cell death pathways. *Am J Physiol Gastrointest Liver Physiol* **308**, G757-766 (2015). https://doi.org/10.1152/ajpgi.00442.2014

267 Cui, J., Xu, T., Lv, H. & Guo, M. Y. Zinc deficiency causes oxidative stress, endoplasmic reticulum stress, apoptosis and inflammation in hepatocytes in grass carp. *Fish Shellfish Immunol* **139**, 108905 (2023). https://doi.org/10.1016/j.fsi.2023.108905

268 Ellis, C. D. *et al.* Zinc and the Msc2 zinc transporter protein are required for endoplasmic reticulum function. *J Cell Biol* **166**, 325-335 (2004). https://doi.org/10.1083/jcb.200401157

269 Aimo, L., Cherr, G. N. & Oteiza, P. I. Low extracellular zinc increases neuronal oxidant production through nadph oxidase and nitric oxide synthase activation. *Free Radic Biol Med* **48**, 1577-1587 (2010). https://doi.org/10.1016/j.freeradbiomed.2010.02.040

270 Ho, E. & Ames, B. N. Low intracellular zinc induces oxidative DNA damage, disrupts p53, NFkappa B, and AP1 DNA binding, and affects DNA repair in a rat glioma cell line. *Proc Natl Acad Sci U S A* **99**, 16770-16775 (2002). https://doi.org/10.1073/pnas.222679399

271 Miyai, T. *et al.* Zinc transporter SLC39A10/ZIP10 facilitates antiapoptotic signaling during early B-cell development. *Proc Natl Acad Sci U S A* **111**, 11780-11785 (2014). https://doi.org/10.1073/pnas.1323549111
272 Gaither, L. A. & Eide, D. J. Eukaryotic zinc transporters and their regulation. *Biometals* **14**, 251-270 (2001). https://doi.org/10.1023/a:1012988914300
273 Zhang, T. *et al.* Crystal structures of a ZIP zinc transporter reveal a binuclear metal center in the transport pathway. *Sci Adv* **3**, e1700344 (2017). https://doi.org/10.1126/sciadv.1700344
274 Jeong, J. & Eide, D. J. The SLC39 family of zinc transporters. *Molecular Aspects of Medicine* **34**, 612-619 (2013). https://doi.org/https://doi.org/10.1016/j.mam.2012.05.011
275 Taniguchi, M. *et al.* Essential role of the zinc transporter ZIP9/SLC39A9 in regulating the activations of Akt and Erk in B-cell receptor signaling pathway in DT40 cells. *PLoS One* **8**, e58022 (2013). https://doi.org/10.1371/journal.pone.0058022
276 Heng, T. S. & Painter, M. W. The Immunological Genome Project: networks of gene expression in immune cells. *Nat Immunol* **9**, 1091-1094 (2008). https://doi.org/10.1038/ni1008-1091
277 Zhao, L. *et al.* SLC39A6/ZIP6 is essential for zinc homeostasis and T-cell development in zebrafish. *Biochem Biophys Res Commun* **511**, 896-902 (2019). https://doi.org/10.1016/j.bbrc.2019.02.148
278 Dufner-Beattie, J., Huang, Z. L., Geiser, J., Xu, W. & Andrews, G. K. Generation and characterization of mice lacking the zinc uptake transporter ZIP3. *Mol Cell Biol* **25**, 5607-5615 (2005). https://doi.org/10.1128/mcb.25.13.5607-5615.2005
279 Endre, L., Katona, Z. & Gyurkovits, K. Zinc deficiency and cellular immune deficiency in acrodermatitis enteropathica. *Lancet* **1**, 1196 (1975). https://doi.org/10.1016/s0140-6736(75)93186-4
280 Oleske, J. M. *et al.* Zinc therapy of depressed cellular immunity in acrodermatitis enteropathica. Its correction. *Am J Dis Child* **133**, 915-918 (1979). https://doi.org/10.1001/archpedi.1979.02130090043007
281 Küry, S. *et al.* Identification of SLC39A4, a gene involved in acrodermatitis enteropathica. *Nature Genetics* **31**, 239-240 (2002). https://doi.org/10.1038/ng913
282 Wang, K., Zhou, B., Kuo, Y. M., Zemansky, J. & Gitschier, J. A novel member of a zinc transporter family is defective in acrodermatitis enteropathica. *Am J Hum Genet* **71**, 66-73 (2002). https://doi.org/10.1086/341125
283 Geiser, J., Venken, K. J., De Lisle, R. C. & Andrews, G. K. A mouse model of acrodermatitis enteropathica: loss of intestine zinc transporter ZIP4 (Slc39a4) disrupts the stem cell niche and intestine integrity. *PLoS Genet* **8**, e1002766 (2012). https://doi.org/10.1371/journal.pgen.1002766
284 Kim, B., Kim, H. Y. & Lee, W. W. Zap70 regulates TCR-mediated Zip6 activation at the immunological synapse. *Front Immunol* **12**, 687367 (2021). https://doi.org/10.3389/fimmu.2021.687367
285 Rosenkranz, E. *et al.* Zinc supplementation induces regulatory T cells by inhibition of Sirt-1 deacetylase in mixed lymphocyte cultures. *Mol Nutr Food Res* **60**, 661-671 (2016). https://doi.org/10.1002/mnfr.201500524
286 Maywald, M., Meurer, S. K., Weiskirchen, R. & Rink, L. Zinc supplementation augments TGF-β1-dependent regulatory T cell induction. *Mol Nutr Food Res* **61** (2017). https://doi.org/10.1002/mnfr.201600493
287 Beck, F. W., Prasad, A. S., Kaplan, J., Fitzgerald, J. T. & Brewer, G. J. Changes in cytokine production and T cell subpopulations in experimentally induced zinc-

deficient humans. *Am J Physiol* **272**, E1002-1007 (1997). https://doi.org/10.1152/ajpendo.1997.272.6.E1002

288 Uciechowski, P. *et al.* TH1 and TH2 cell polarization increases with aging and is modulated by zinc supplementation. *Exp Gerontol* **43**, 493-498 (2008). https://doi.org/10.1016/j.exger.2007.11.006

289 Nishida, K. *et al.* Zinc transporter Znt5/Slc30a5 is required for the mast cell-mediated delayed-type allergic reaction but not the immediate-type reaction. *J Exp Med* **206**, 1351-1364 (2009). https://doi.org/10.1084/jem.20082533

290 Lazarczyk, M. *et al.* Regulation of cellular zinc balance as a potential mechanism of EVER-mediated protection against pathogenesis by cutaneous oncogenic human papillomaviruses. *J Exp Med* **205**, 35-42 (2008). https://doi.org/10.1084/jem.20071311

291 Palmiter, R. D. & Findley, S. D. Cloning and functional characterization of a mammalian zinc transporter that confers resistance to zinc. *Embo j* **14**, 639-649 (1995). https://doi.org/10.1002/j.1460-2075.1995.tb07042.x

292 Yang, D. *et al.* ZNT1 and Zn 2+ control TLR4 and PD-L1 endocytosis in macrophages to improve chemotherapy efficacy against liver tumor. *Hepatology* **80**, 312-329 (2024). https://doi.org/10.1097/hep.0000000000000629

293 Sun, C. *et al.* Structural insights into the calcium-coupled zinc export of human ZnT1. *Sci Adv* **10**, eadk5128 (2024). https://doi.org/10.1126/sciadv.adk5128

294 Li, Y. *et al.* Zinc transporter 1 functions in copper uptake and cuproptosis. *Cell Metab* **36**, 2118-2129.e2116 (2024). https://doi.org/10.1016/j.cmet.2024.07.009

295 Lasswell, J., Rogg, L. E., Nelson, D. C., Rongey, C. & Bartel, B. Cloning and characterization of IAR1, a gene required for auxin conjugate sensitivity in Arabidopsis. *Plant Cell* **12**, 2395-2408 (2000). https://doi.org/10.1105/tpc.12.12.2395

296 Groth, C., Sasamura, T., Khanna, M. R., Whitley, M. & Fortini, M. E. Protein trafficking abnormalities in Drosophila tissues with impaired activity of the ZIP7 zinc transporter Catsup. *Development* **140**, 3018-3027 (2013). https://doi.org/10.1242/dev.088336

297 TAYLOR, K. M., MORGAN, H. E., JOHNSON, A. & NICHOLSON, R. I. Structure-function analysis of HKE4, a member of the new LIV-1 subfamily of zinc transporters. *Biochemical Journal* **377**, 131-139 (2004). https://doi.org/10.1042/bj20031183

298 Huang, L., Kirschke, C. P., Zhang, Y. & Yu, Y. Y. The ZIP7 gene (Slc39a7) encodes a zinc transporter involved in zinc homeostasis of the Golgi apparatus. *J Biol Chem* **280**, 15456-15463 (2005). https://doi.org/10.1074/jbc.M412188200

299 Song, Y. *et al.* The NLRX1-SLC39A7 complex orchestrates mitochondrial dynamics and mitophagy to rejuvenate intervertebral disc by modulating mitochondrial Zn(2+) trafficking. *Autophagy* **20**, 809-829 (2024). https://doi.org/10.1080/15548627.2023.2274205

300 Friedman, J. R. *et al.* ER tubules mark sites of mitochondrial division. *Science* **334**, 358-362 (2011). https://doi.org/10.1126/science.1207385

301 Viana, M. P. *et al.* Integrated intracellular organization and its variations in human iPS cells. *Nature* **613**, 345-354 (2023). https://doi.org/10.1038/s41586-022-05563-7

302 Liang, P. *et al.* ACSL4-mediated ZIP7-VDAC3 interaction regulates endoplasmic reticulum-mitochondria iron transfer in hepatocytes under PFOS exposure. *Sci Total Environ* **957**, 177679 (2024). https://doi.org/10.1016/j.scitotenv.2024.177679

303 Erdős, M. *et al.* A novel mutation in SLC39A7 identified in a patient with autosomal recessive agammaglobulinemia: The impact of the J Project. *Pediatr Allergy Immunol* **33**, e13805 (2022). https://doi.org/10.1111/pai.13805

304 Barbati, F. *et al.* Monogenic common variable immunodeficiency (Mo-CVID) score for optimizing the genetic diagnosis in pediatric CVID cohort. *Eur J Immunol* **55**, e202451433 (2025). https://doi.org/10.1002/eji.202451433

305 Ohashi, W. *et al.* Zinc transporter SLC39A7/ZIP7 promotes intestinal epithelial self-renewal by resolving ER stress. *PLoS Genet* **12**, e1006349 (2016). https://doi.org/10.1371/journal.pgen.1006349

306 Senior, A. W. *et al.* Improved protein structure prediction using potentials from deep learning. *Nature* **577**, 706-710 (2020). https://doi.org/10.1038/s41586-019-1923-7

307 Jumper, J. *et al.* Highly accurate protein structure prediction with AlphaFold. *Nature* **596**, 583-589 (2021). https://doi.org/10.1038/s41586-021-03819-2

308 Kim, M. H., Aydemir, T. B., Kim, J. & Cousins, R. J. Hepatic ZIP14-mediated zinc transport is required for adaptation to endoplasmic reticulum stress. *Proc Natl Acad Sci U S A* **114**, E5805-e5814 (2017). https://doi.org/10.1073/pnas.1704012114

309 Guo, X. *et al.* The Zn^{2+} transporter ZIP7 enhances endoplasmic-reticulum-associated protein degradation and prevents neurodegeneration in *Drosophila*. *Dev Cell* (2024). https://doi.org/10.1016/j.devcel.2024.04.003

310 Yang, N., Zhang, R., Zhang, H., Yu, Y. & Xu, Z. ZIP7 contributes to the pathogenesis of diabetic cardiomyopathy by suppressing mitophagy in mouse hearts. *Cardiovasc Diabetol* **23**, 399 (2024). https://doi.org/10.1186/s12933-024-02499-2

311 Sheng, N. *et al.* Knockdown of SLC39A7 inhibits cell growth and induces apoptosis in human colorectal cancer cells. *Acta Biochim Biophys Sin (Shanghai)* **49**, 926-934 (2017). https://doi.org/10.1093/abbs/gmx094

312 Wei, Y., Dong, J., Li, F., Wei, Z. & Tian, Y. Knockdown of SLC39A7 suppresses cell proliferation, migration and invasion in cervical cancer. *Excli j* **16**, 1165-1176 (2017). https://doi.org/10.17179/excli2017-690

313 Quadros, R. M. *et al. Easi*-CRISPR: a robust method for one-step generation of mice carrying conditional and insertion alleles using long ssDNA donors and CRISPR ribonucleoproteins. *Genome Biology* **18**, 92 (2017). https://doi.org/10.1186/s13059-017-1220-4

314 Deobagkar-Lele, M. *et al.* B cells require DOCK8 to elicit and integrate T cell help when antigen is limiting. *Sci Immunol* **9**, eadd4874 (2024). https://doi.org/10.1126/sciimmunol.add4874

315 Hsu, J. *et al.* Comparing 10x Genomics single-cell 3' and 5' assay in short-and long-read sequencing. *bioRxiv*, 2022.2010.2027.514084 (2022). https://doi.org/10.1101/2022.10.27.514084

316 Tirosh, I. *et al.* Dissecting the multicellular ecosystem of metastatic melanoma by single-cell RNA-seq. *Science* **352**, 189-196 (2016). https://doi.org/10.1126/science.aad0501

317 Chen, C.-W. *et al.* Plasticity of the mammalian integrated stress response. *Nature* (2025). https://doi.org/10.1038/s41586-025-08794-6

318 You, K. *et al.* QRICH1 dictates the outcome of ER stress through transcriptional control of proteostasis. *Science* **371** (2021). https://doi.org/10.1126/science.abb6896

319 Subramanian, A. *et al.* Gene set enrichment analysis: a knowledge-based approach for interpreting genome-wide expression profiles. *Proc Natl Acad Sci U S A* **102**, 15545-15550 (2005). https://doi.org/10.1073/pnas.0506580102

320 Mootha, V. K. *et al.* PGC-1α-responsive genes involved in oxidative phosphorylation are coordinately downregulated in human diabetes. *Nature Genetics* **34**, 267-273 (2003). https://doi.org/10.1038/ng1180

321 Chu, Y. *et al.* Pan-cancer T cell atlas links a cellular stress response state to immunotherapy resistance. *Nature Medicine* **29**, 1550-1562 (2023). https://doi.org/10.1038/s41591-023-02371-y

322 Boast, B. *et al.* TCF3 haploinsufficiency defined by immune, clinical, gene-dosage, and murine studies. *Journal of Allergy and Clinical Immunology* **152**, 736-747 (2023). https://doi.org/10.1016/j.jaci.2023.05.017

323 Fornes, O. *et al.* A multimorphic mutation in IRF4 causes human autosomal dominant combined immunodeficiency. *Sci Immunol* **8**, eade7953 (2023). https://doi.org/10.1126/sciimmunol.ade7953

324 Finkin, S., Hartweger, H., Oliveira, T. Y., Kara, E. E. & Nussenzweig, M. C. Protein amounts of the MYC transcription factor determine germinal center B cell division capacity. *Immunity* **51**, 324-336.e325 (2019). https://doi.org/https://doi.org/10.1016/j.immuni.2019.06.013

325 Kim, H., Kim, M., Im, S. K. & Fang, S. Mouse Cre-LoxP system: general principles to determine tissue-specific roles of target genes. *Lab Anim Res* **34**, 147-159 (2018). https://doi.org/10.5625/lar.2018.34.4.147

326 Indra, A. K. *et al.* Temporally-controlled site-specific mutagenesis in the basal layer of the epidermis: comparison of the recombinase activity of the tamoxifen-inducible Cre-ER(T) and Cre-ER(T2) recombinases. *Nucleic Acids Res* **27**, 4324-4327 (1999). https://doi.org/10.1093/nar/27.22.4324

327 Madisen, L. *et al.* A robust and high-throughput Cre reporting and characterization system for the whole mouse brain. *Nature Neuroscience* **13**, 133-140 (2010). https://doi.org/10.1038/nn.2467

328 Sohal, D. S. *et al.* Temporally regulated and tissue-specific gene manipulations in the adult and embryonic heart using a Tamoxifen-inducible Cre protein. *Circulation Research* **89**, 20-25 (2001). https://doi.org/doi:10.1161/hh1301.092687

329 Spangrude, G. J., Heimfeld, S. & Weissman, I. L. Purification and characterization of mouse hematopoietic stem cells. *Science* **241**, 58-62 (1988). https://doi.org/doi:10.1126/science.2898810

330 Zhang, Y. *et al.* Regulation of pDC fate determination by histone deacetylase 3. *eLife* **12**, e80477 (2023). https://doi.org/10.7554/eLife.80477

331 Wilson, A. & MacDonald, H. R. Expression of genes encoding the pre-TCR and CD3 complex during thymus development. *Int Immunol* **7**, 1659-1664 (1995). https://doi.org/10.1093/intimm/7.10.1659

332 Levelt, C. N., Carsetti, R. & Eichmann, K. Regulation of thymocyte development through CD3. II. Expression of T cell receptor beta CD3 epsilon and maturation to the CD4+8+ stage are highly correlated in individual thymocytes. *J Exp Med* **178**, 1867-1875 (1993). https://doi.org/10.1084/jem.178.6.1867

333 Carroll, M. C. The role of complement and complement receptors in induction and regulation of immunity. *Annu Rev Immunol* **16**, 545-568 (1998). https://doi.org/10.1146/annurev.immunol.16.1.545

334 Hobeika, E. *et al.* Testing gene function early in the B cell lineage in mb1-cre mice. *Proc Natl Acad Sci U S A* **103**, 13789-13794 (2006). https://doi.org/10.1073/pnas.0605944103

335 García de Vinuesa, C., O'Leary, P., Sze, D. M., Toellner, K. M. & MacLennan, I. C. T-independent type 2 antigens induce B cell proliferation in multiple splenic sites, but exponential growth is confined to extrafollicular foci. *Eur J Immunol* **29**, 1314-1323 (1999). https://doi.org/10.1002/(SICI)1521-4141(199904)29:04<1314::AID-IMMU1314>3.0.CO;2-4

336 Hsu, M. C., Toellner, K. M., Vinuesa, C. G. & Maclennan, I. C. B cell clones that sustain long-term plasmablast growth in T-independent extrafollicular antibody responses. *Proc Natl Acad Sci U S A* **103**, 5905-5910 (2006). https://doi.org/10.1073/pnas.0601502103

337 Pirgova, G., Chauveau, A., MacLean, A. J., Cyster, J. G. & Arnon, T. I. Marginal zone SIGN-R1(+) macrophages are essential for the maturation of germinal center B cells in the spleen. *Proc Natl Acad Sci U S A* **117**, 12295-12305 (2020). https://doi.org/10.1073/pnas.1921673117

338 Arnon, T. I., Horton, R. M., Grigorova, I. L. & Cyster, J. G. Visualization of splenic marginal zone B-cell shuttling and follicular B-cell egress. *Nature* **493**, 684-688 (2013). https://doi.org/10.1038/nature11738

339 Yamasaki, S. *et al.* C-type lectin Mincle is an activating receptor for pathogenic fungus, Malassezia. *Proc Natl Acad Sci U S A* **106**, 1897-1902 (2009). https://doi.org/10.1073/pnas.0805177106

340 Oldenburg, M. *et al.* TLR13 recognizes bacterial 23S rRNA devoid of erythromycin resistance-forming modification. *Science* **337**, 1111-1115 (2012). https://doi.org/10.1126/science.1220363

341 Hawley, C. A. *et al.* Csf1r-mApple transgene expression and ligand binding in vivo reveal dynamics of CSF1R expression within the mononuclear phagocyte system. *J Immunol* **200**, 2209-2223 (2018). https://doi.org/10.4049/jimmunol.1701488

342 Ganz, T. *et al.* Increased inflammation in lysozyme M-deficient mice in response to Micrococcus luteus and its peptidoglycan. *Blood* **101**, 2388-2392 (2003). https://doi.org/10.1182/blood-2002-07-2319

343 Blasius, A. L., Cella, M., Maldonado, J., Takai, T. & Colonna, M. Siglec-H is an IPC-specific receptor that modulates type I IFN secretion through DAP12. *Blood* **107**, 2474-2476 (2006). https://doi.org/10.1182/blood-2005-09-3746

344 Hori, S., Nomura, T. & Sakaguchi, S. Control of regulatory T cell development by the transcription factor Foxp3. *Science* **299**, 1057-1061 (2003). https://doi.org/10.1126/science.1079490

345 Takahashi, T. *et al.* Immunologic self-tolerance maintained by Cd25+Cd4+regulatory T cells constitutively expressing cytotoxic T lymphocyte–associated antigen 4. *Journal of Experimental Medicine* **192**, 303-310 (2000). https://doi.org/10.1084/jem.192.2.303

346 Bruder, D. *et al.* Frontline: Neuropilin-1: a surface marker of regulatory T cells. *European Journal of Immunology* **34**, 623-630 (2004). https://doi.org/https://doi.org/10.1002/eji.200324799

347 Yadav, M. *et al.* Neuropilin-1 distinguishes natural and inducible regulatory T cells among regulatory T cell subsets in vivo. *J Exp Med* **209**, 1713-1722, s1711-1719 (2012). https://doi.org/10.1084/jem.20120822

348 Zhou, X. & Xue, H. H. Cutting edge: generation of memory precursors and functional memory CD8+ T cells depends on T cell factor-1 and lymphoid enhancer-binding factor-1. *J Immunol* **189**, 2722-2726 (2012). https://doi.org/10.4049/jimmunol.1201150

349 Durek, P. *et al.* Epigenomic profiling of human CD4(+) T cells supports a linear differentiation model and highlights molecular regulators of memory

development. *Immunity* **45**, 1148-1161 (2016). https://doi.org/10.1016/j.immuni.2016.10.022

350 Tahvanainen, J. *et al.* Proviral integration site for Moloney murine leukemia virus (PIM) kinases promote human T helper 1 cell differentiation. *J Biol Chem* **288**, 3048-3058 (2013). https://doi.org/10.1074/jbc.M112.361709

351 Zumwalde, N. A., Domae, E., Mescher, M. F. & Shimizu, Y. ICAM-1-dependent homotypic aggregates regulate CD8 T cell effector function and differentiation during T cell activation. *J Immunol* **191**, 3681-3693 (2013). https://doi.org/10.4049/jimmunol.1201954

352 Wu, J. *et al.* Regulatory T cells sense effector T-cell activation through synchronized JunB expression. *FEBS Lett* **593**, 1020-1029 (2019). https://doi.org/10.1002/1873-3468.13393

353 Brender, C. *et al.* Suppressor of cytokine signaling 3 regulates CD8 T-cell proliferation by inhibition of interleukins 6 and 27. *Blood* **110**, 2528-2536 (2007). https://doi.org/10.1182/blood-2006-08-041541

354 Swanson, B. J., Murakami, M., Mitchell, T. C., Kappler, J. & Marrack, P. RANTES production by memory phenotype T cells is controlled by a posttranscriptional, TCR-dependent process. *Immunity* **17**, 605-615 (2002). https://doi.org/10.1016/s1074-7613(02)00456-9

355 Hu, J. K., Kagari, T., Clingan, J. M. & Matloubian, M. Expression of chemokine receptor CXCR3 on T cells affects the balance between effector and memory CD8 T-cell generation. *Proc Natl Acad Sci U S A* **108**, E118-127 (2011). https://doi.org/10.1073/pnas.1101881108

356 McLane, L. M. *et al.* Differential localization of T-bet and Eomes in CD8 T cell memory populations. *J Immunol* **190**, 3207-3215 (2013). https://doi.org/10.4049/jimmunol.1201556

357 Kim, H. J. *et al.* Stable inhibitory activity of regulatory T cells requires the transcription factor Helios. *Science* **350**, 334-339 (2015). https://doi.org/10.1126/science.aad0616

358 Roark, J. H. *et al.* CD1.1 expression by mouse antigen-presenting cells and marginal zone B cells. *J Immunol* **160**, 3121-3127 (1998).

359 Won, W. J. & Kearney, J. F. CD9 is a unique marker for marginal zone B cells, B1 cells, and plasma cells in mice. *J Immunol* **168**, 5605-5611 (2002). https://doi.org/10.4049/jimmunol.168.11.5605

360 Won, W. J. *et al.* Fc receptor homolog 3 is a novel immunoregulatory marker of marginal zone and B1 B cells. *J Immunol* **177**, 6815-6823 (2006). https://doi.org/10.4049/jimmunol.177.10.6815

361 Sabouri, Z. *et al.* IgD attenuates the IgM-induced anergy response in transitional and mature B cells. *Nature Communications* **7**, 13381 (2016). https://doi.org/10.1038/ncomms13381

362 Hoek, K. L. *et al.* Follicular B cell trafficking within the spleen actively restricts humoral immune responses. *Immunity* **33**, 254-265 (2010). https://doi.org/10.1016/j.immuni.2010.07.016

363 Laidlaw, B. J., Duan, L., Xu, Y., Vazquez, S. E. & Cyster, J. G. The transcription factor Hhex cooperates with the corepressor Tle3 to promote memory B cell development. *Nature Immunology* **21**, 1082-1093 (2020). https://doi.org/10.1038/s41590-020-0713-6

364 Schneider, W. M., Chevillotte, M. D. & Rice, C. M. Interferon-stimulated genes: a complex web of host defenses. *Annu Rev Immunol* **32**, 513-545 (2014). https://doi.org/10.1146/annurev-immunol-032713-120231

365 Bogunovic, D. *et al.* Mycobacterial disease and impaired IFN-γ immunity in humans with inherited ISG15 deficiency. *Science* **337**, 1684-1688 (2012). https://doi.org/10.1126/science.1224026

366 Schoggins, J. W. *et al.* A diverse range of gene products are effectors of the type I interferon antiviral response. *Nature* **472**, 481-485 (2011). https://doi.org/10.1038/nature09907

367 Abbink, T. E. M. *et al.* Vanishing white matter: deregulated integrated stress response as therapy target. *Ann Clin Transl Neurol* **6**, 1407-1422 (2019). https://doi.org/10.1002/acn3.50826

368 Novoa, I. *et al.* Stress-induced gene expression requires programmed recovery from translational repression. *Embo j* **22**, 1180-1187 (2003). https://doi.org/10.1093/emboj/cdg112

369 Guan, B. J. *et al.* A unique ISR program determines cellular responses to chronic stress. *Mol Cell* **68**, 885-900.e886 (2017). https://doi.org/10.1016/j.molcel.2017.11.007

370 Chen, T. T. *et al.* STAT1 regulates marginal zone B cell differentiation in response to inflammation and infection with blood-borne bacteria. *J Exp Med* **213**, 3025-3039 (2016). https://doi.org/10.1084/jem.20151620

371 Gaudette, B. T., Jones, D. D., Bortnick, A., Argon, Y. & Allman, D. mTORC1 coordinates an immediate unfolded protein response-related transcriptome in activated B cells preceding antibody secretion. *Nat Commun* **11**, 723 (2020). https://doi.org/10.1038/s41467-019-14032-1

372 Conley, M. E., Mathias, D., Treadaway, J., Minegishi, Y. & Rohrer, J. Mutations in *Btk* in patients with presumed X-Linked Agammaglobulinemia. *The American Journal of Human Genetics* **62**, 1034-1043 (1998). https://doi.org/10.1086/301828

373 Väliaho, J., Smith, C. I. & Vihinen, M. BTKbase: the mutation database for X-linked agammaglobulinemia. *Hum Mutat* **27**, 1209-1217 (2006). https://doi.org/10.1002/humu.20410

374 Rawlings, D. J. *et al.* Mutation of unique region of Bruton's tyrosine kinase in immunodeficient XID mice. *Science* **261**, 358-361 (1993). https://doi.org/10.1126/science.8332901

375 Thomas, J. D. *et al.* Colocalization of X-linked agammaglobulinemia and X-linked immunodeficiency genes. *Science* **261**, 355-358 (1993). https://doi.org/10.1126/science.8332900

376 Reid, G. K. & Osmond, D. G. B lymphocyte production in the bone marrow of mice with X-linked immunodeficiency (xid). *J Immunol* **135**, 2299-2302 (1985).

377 Kerner, J. D. *et al.* Impaired expansion of mouse B cell progenitors lacking Btk. *Immunity* **3**, 301-312 (1995). https://doi.org/10.1016/1074-7613(95)90115-9

378 Minegishi, Y. *et al.* An essential role for BLNK in human B cell development. *Science* **286**, 1954-1957 (1999). https://doi.org/10.1126/science.286.5446.1954

379 Pappu, R. *et al.* Requirement for B cell linker protein (BLNK) in B cell development. *Science* **286**, 1949-1954 (1999). https://doi.org/10.1126/science.286.5446.1949

380 Xu, S. *et al.* B cell development and activation defects resulting in xid-like immunodeficiency in BLNK/SLP-65-deficient mice. *Int Immunol* **12**, 397-404 (2000). https://doi.org/10.1093/intimm/12.3.397

381 Dias, S., Silva, H., Jr., Cumano, A. & Vieira, P. Interleukin-7 is necessary to maintain the B cell potential in common lymphoid progenitors. *J Exp Med* **201**, 971-979 (2005). https://doi.org/10.1084/jem.20042393

382 Wei, C., Zeff, R. & Goldschneider, I. Murine pro-B cells require IL-7 and its receptor complex to up-regulate IL-7R alpha, terminal deoxynucleotidyltransferase, and c mu expression. *J Immunol* **164**, 1961-1970 (2000). https://doi.org/10.4049/jimmunol.164.4.1961

383 Macchi, P. *et al.* Mutations of Jak-3 gene in patients with autosomal severe combined immune deficiency (SCID). *Nature* **377**, 65-68 (1995). https://doi.org/10.1038/377065a0

384 Puel, A., Ziegler, S. F., Buckley, R. H. & Leonard, W. J. Defective IL7R expression in T(-)B(+)NK(+) severe combined immunodeficiency. *Nat Genet* **20**, 394-397 (1998). https://doi.org/10.1038/3877

385 Noguchi, M. *et al.* Interleukin-2 receptor gamma chain: a functional component of the interleukin-7 receptor. *Science* **262**, 1877-1880 (1993). https://doi.org/10.1126/science.8266077

386 Weill, J. C., Weller, S. & Reynaud, C. A. Human marginal zone B cells. *Annu Rev Immunol* **27**, 267-285 (2009). https://doi.org/10.1146/annurev.immunol.021908.132607

387 Weller, S. *et al.* Human blood IgM "memory" B cells are circulating splenic marginal zone B cells harboring a prediversified immunoglobulin repertoire. *Blood* **104**, 3647-3654 (2004). https://doi.org/10.1182/blood-2004-01-0346

388 Schneider, P. *et al.* BAFF, a novel ligand of the tumor necrosis factor family, stimulates B cell growth. *J Exp Med* **189**, 1747-1756 (1999). https://doi.org/10.1084/jem.189.11.1747

389 Salzer, U. *et al.* Mutations in TNFRSF13B encoding TACI are associated with common variable immunodeficiency in humans. *Nat Genet* **37**, 820-828 (2005). https://doi.org/10.1038/ng1600

390 Castigli, E. *et al.* TACI is mutant in common variable immunodeficiency and IgA deficiency. *Nat Genet* **37**, 829-834 (2005). https://doi.org/10.1038/ng1601

391 Mathieson, T. *et al.* Systematic analysis of protein turnover in primary cells. *Nature Communications* **9**, 689 (2018). https://doi.org/10.1038/s41467-018-03106-1

392 Zhang, K. *et al.* The unfolded protein response sensor IRE1alpha is required at 2 distinct steps in B cell lymphopoiesis. *J Clin Invest* **115**, 268-281 (2005). https://doi.org/10.1172/jci21848

393 Brunsing, R. *et al.* B- and T-cell development both involve activity of the unfolded protein response pathway. *J Biol Chem* **283**, 17954-17961 (2008). https://doi.org/10.1074/jbc.M801395200

394 Liu, X. *et al.* Notch-induced endoplasmic reticulum-associated degradation governs mouse thymocyte β-selection. *Elife* **10** (2021). https://doi.org/10.7554/eLife.69975

395 Nolin, E. *et al.* Discovery of a ZIP7 inhibitor from a Notch pathway screen. *Nat Chem Biol* **15**, 179-188 (2019). https://doi.org/10.1038/s41589-018-0200-7

396 Al Qureshah, F. *et al.* Activated PI3Kδ signals compromise plasma cell survival via limiting autophagy and increasing ER stress. *J Exp Med* **218** (2021). https://doi.org/10.1084/jem.20211035

397 Jones, D. D. *et al.* mTOR has distinct functions in generating versus sustaining humoral immunity. *J Clin Invest* **126**, 4250-4261 (2016). https://doi.org/10.1172/jci86504

398 Asada, N. *et al.* The integrated stress response pathway controls cytokine production in tissue-resident memory CD4(+) T cells. *Nat Immunol* **26**, 557-566 (2025). https://doi.org/10.1038/s41590-025-02105-x

399 Chen, P.-H. *et al.* Zinc transporter ZIP7 is a novel determinant of ferroptosis. *Cell Death & Disease* **12**, 198 (2021). https://doi.org/10.1038/s41419-021-03482-5

400 Lalaoui, N. *et al.* Mutations that prevent caspase cleavage of RIPK1 cause autoinflammatory disease. *Nature* **577**, 103-108 (2020). https://doi.org/10.1038/s41586-019-1828-5

401 Newton, K. *et al.* Cleavage of RIPK1 by caspase-8 is crucial for limiting apoptosis and necroptosis. *Nature* **574**, 428-431 (2019). https://doi.org/10.1038/s41586-019-1548-x

402 Tao, P. *et al.* A dominant autoinflammatory disease caused by non-cleavable variants of RIPK1. *Nature* **577**, 109-114 (2020). https://doi.org/10.1038/s41586-019-1830-y

403 Calamini, B. *et al.* Small-molecule proteostasis regulators for protein conformational diseases. *Nat Chem Biol* **8**, 185-196 (2011). https://doi.org/10.1038/nchembio.763

Appendices

Table S2-1. Biochemical reagents

Brand	Name	Catalogue number	CAS
Thermo Scientific	Glycine, 99%	A13816.36	56-40-6
Insight Biotechnology	Tris hydrochloride solution, pH 7.4	sc-301950	1185-53-1
Scientific Laboratory Supplies	Sodium Chloride, >99.5%	CHE3320	7647-14-5
Sigma-Aldrich	Tamoxifen free base	T5648	10540-29-1
	Corn oil	C8267	8001-30-7
	Bovine Serum Albumin	A7906	9048-46-8
	TWEEN 20	P7949	9005-64-5
	Sodium chloride solution, 5 M	S6546-4L	7647-14-5
	2-Propanol	24137-M	67-63-0
	Ethanol	32221-M	64-17-5

Table S2-2. Antibodies and reagents used for *ex vivo* stimulation

Brand	Name	Catalogue number	Clone
Jackson ImmunoResearch	AffiniPure F(ab')$_2$ Fragment Donkey Anti-Mouse IgM, μ chain specific	715-006-020	Polyclonal
Sigma-Aldrich	Lipopolysaccharides from Salmonella enterica serotype enteritidis	L7770-1M	NA
BioLegend	Recombinant Mouse IL-4 (carrier-free)	574304	NA
	Purified anti-mouse CD40 Antibody	102902	HM40-3

Table S2-3. Buffers, reagents, and kits

Brand	Name	Catalogue number
Thermo Scientific	Oxoid™ Sheep blood in alsevers solution liquid	12977755
Invitrogen	PureLink™ DNase Set	12185010
BioLegend	Recombinant Mouse IL-4 (carrier-free)	574304
	MojoSort™ Mouse Pan B Cell Isolation Kit II	480088
	MojoSort™ Mouse CD3 T Cell Isolation Kit	480024
Meridian Bioscience	BIOTAQ™ PCR Kit	BIO-21071
QIAGEN	DNeasy Blood & Tissue Kit	69504
BD	Cytoperm™ Permeabilization Buffer Plus	561651
	Cytofix/Cytoperm™ Fixation and Permeabilization Solution	554722
	BD FACSFlow™ Sheath Fluid	342003
	BD FACSClean Solution	340345
	Shutdown Solution	334224
BioGene	Agarose Hi-Pure Low EEO	300-300
Bayer	Baytril 10% Oral Solution (enrofloxacin)	2150886
Day-Impex	Rely+On™ Virkon (potassium peroxymonosulfate) tablets	115-0021

Table S2-4. Antibodies used for flow cytometry and phospho-flow

Target antigen	Brand	Clone
B220	BioLegend	RA3-6B2
BP-1	BioLegend	6C3
BrdU	BD Pharmingen	3D4
CD138	BioLegend	281-2
CD19	BioLegend	6D5
CD1d	BioLegend	1B1
CD21/CD35	BD Pharmingen	7G6
CD23	BioLegend	B3B4
CD24	BioLegend	M1/69
CD25	BioLegend	PC61
CD3e	BioLegend	17A2
CD4	BioLegend	GK1.5
CD43	BD Pharmingen	S7
CD44	BioLegend	IM7
CD45.1	BioLegend	A20
CD45.2	eBioscience	104
CD5	BioLegend	53-7.3
CD62L	BioLegend	MEL-14
CD69	BioLegend	H1.2F3
CD86	BioLegend	GL-1
CD8a	BioLegend	53-6.7

Table S2-4. Antibodies used for flow cytometry and phospho-flow (continued)

Target antigen	Brand	Clone
CD93	BioLegend	AA4.1
CD95	BD Pharmingen	Jo2
CXCR5	BioLegend	L138D7
GL7	BioLegend	GL7
HEL	S.J. Gill-Smith	HyHEL9
IgD	BioLegend	11-26c.2a
IgDa	BioLegend	AMS-9.1
IgG1	BD Horizon	RMG1-1
IgM	BioLegend	RMM-1
IgMa	BioLegend	MA-69
NK1.1	eBioscience	PK136
Phospho-ERK1/2 (Thr202, Tyr204)	eBioscience	MILAN8R
Phospho-PLCγ2 (Tyr759)	BD Phosflow	K86-689.37
Phospho-Syk (Tyr348)	eBioscience	moch1ct
PNA	Vector Laboratories FL-1071	NA
TCR β	eBioscience	H57-597
TCR γ/δ	Biolegend	GL3
Zombie Aqua Live/Dead	Biolegend 423102	NA
Zombie NIR Live/Dead	Biolegend 423106	NA

Table S2-5. BioLegend antibodies used for CITE-seq and cell-hashing

Name	Catalogue number	Clone	Barcode sequence	Dilution
TotalSeq™-C0001 anti-mouse CD4 Antibody	100571	RM4-5	AACAAGACCCTTGAG	1:300
TotalSeq™-C0002 anti-mouse CD8a Antibody	100785	53-6.7	TACCCGTAATAGCGT	1:300
TotalSeq™-C0093 anti-mouse CD19 Antibody	115571	6D5	ATCAGCCATGTCAGT	1:300
TotalSeq™-C0097 anti-mouse CD25 Antibody	102065	PC61	ACCATGAGACACAGT	1:400
TotalSeq™-C0107 anti-mouse CD21/CD35 Antibody	123441	7E9	GGATAATTTCGATCC	1:400
TotalSeq™-C0108 anti-mouse CD23 Antibody	101639	B3B4	TCTCTTGGAAGATGA	1:300
TotalSeq™-C0113 anti-mouse CD93 Antibody	136515	AA4.1	GGTATTTCCTGTGGT	1:200
TotalSeq™-C0851 anti-mouse CD1d Antibody	123533	1B1	CAACTTGGCCGAATC	1:500
TotalSeq™-C0301 anti-mouse Hashtag 1 Antibody	155861	M1/42; 30-F11	ACCCACCAGTAAGAC	0.5 μg Hashtag per million cells in 200 μL
TotalSeq™-C0302 anti-mouse Hashtag 2 Antibody	155863	M1/42; 30-F11	GGTCGAGAGCATTCA	
TotalSeq™-C0303 anti-mouse Hashtag 3 Antibody	155865	M1/42; 30-F11	CTTGCCGCATGTCAT	
TotalSeq™-C0304 anti-mouse Hashtag 4 Antibody	155867	M1/42; 30-F11	AAAGCATTCTTCACG	
TotalSeq™-C0305 anti-mouse Hashtag 5 Antibody	155869	M1/42; 30-F11	CTTTGTCTTTGTGAG	
TotalSeq™-C0306 anti-mouse Hashtag 6 Antibody	155871	M1/42; 30-F11	TATGCTGCCACGGTA	
TotalSeq™-C0307 anti-mouse Hashtag 7 Antibody	155873	M1/42; 30-F11	GAGTCTGCCAGTATC	
TotalSeq™-C0308 anti-mouse Hashtag 8 Antibody	155875	M1/42; 30-F11	TATAGAACGCCAGGC	
TotalSeq™-C0309 anti-mouse Hashtag 9 Antibody	155877	M1/42; 30-F11	TGCCTATGAAACAAG	

Table S2-6. Laboratory consumables and equipment

Brand	Name	Catalogue number
Medicina	5 mL Luer Slip IV Syringe (Concentric Tip)	IVS05
Invitrogen	Qubit™ Assay Tubes	Q32856
Greiner Bio-One	EASYstrainer™ Cell sieve for 50 mL tubes, 70 µm mesh, sterile	542070
	CELLSTAR® 96-well, Cell Culture-Treated, U-Shaped-Bottom Microplate	650180
Miltenyi Biotec	LS Columns	130-042-401
BD	FACSCanto™ Flow Cytometer 10-Color Configuration	657338
Bio-Rad	ChemiDoc™ MP Imaging System	Universal Hood III
Thermo Fisher Scientific	NanoDrop 1000 spectrophotometer	ND-1000
MJ Research	Gradient Thermal Cycler	PTC225 Tetrad

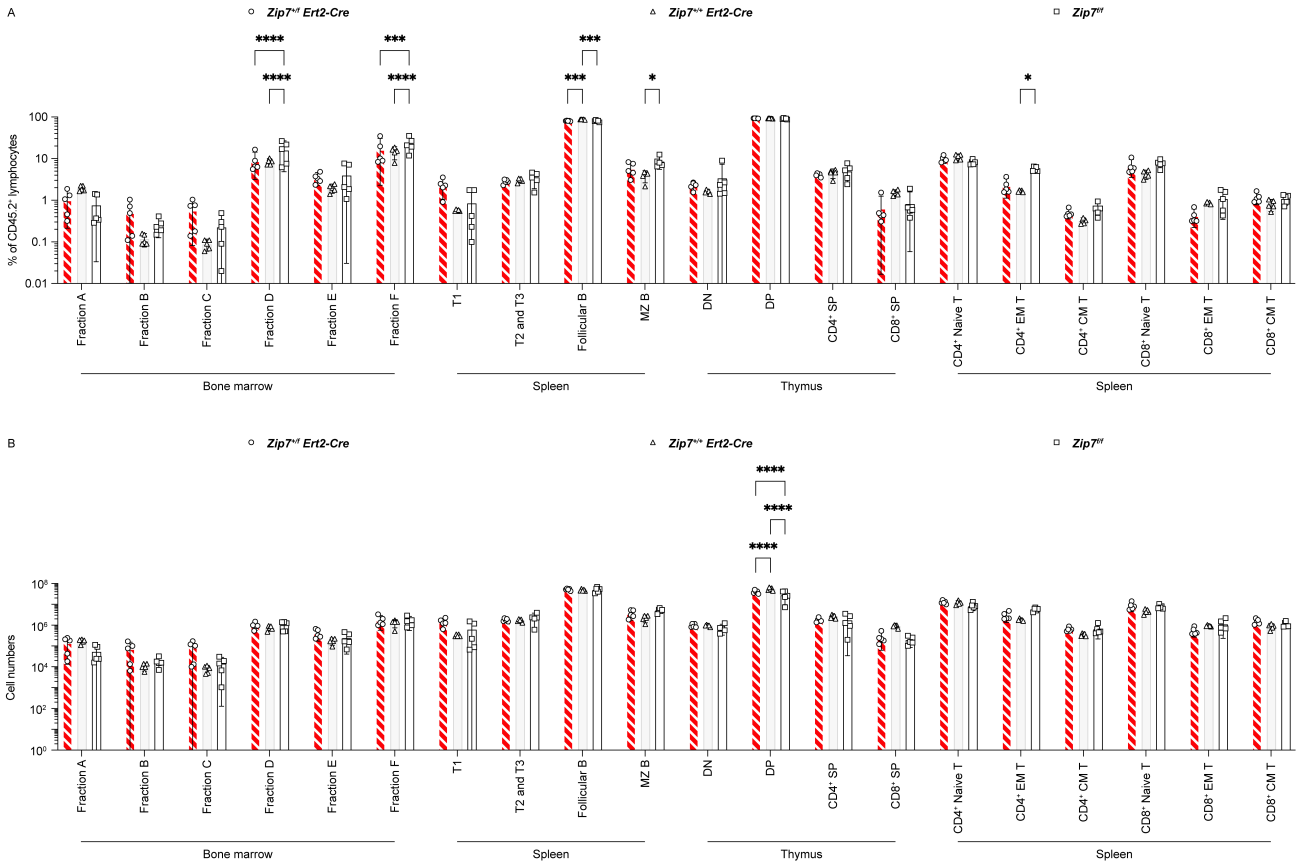

Supplementary Figure 1: Control groups of *Ert2-cre*-induced mouse models treated with tamoxifen.
The percentage of CD45.2$^+$ donor-derived cells (A) and the corresponding absolute cell numbers (B) for various B- and T cell subtypes in the BM, thymus, and spleen of CD45.1$^+$ recipient mice. These mice were transplanted with CD45.2$^+$ BM form *Zip7*$^{+/+}$ *Ert2-cre*, *Zip7*$^{+/f}$ *Ert2-cre* or *Zip7*$^{f/f}$ (without Cre) donor mice. Recipients were treated with 4-5 doses of tamoxifen after at least eight-week BM reconstitution, and samples were collected 1-2 weeks post-treatment. Data were pooled from different experiment batches. The statistical analysis was conducted using two-way ANOVA, followed by Tukey's multiple comparisons test.

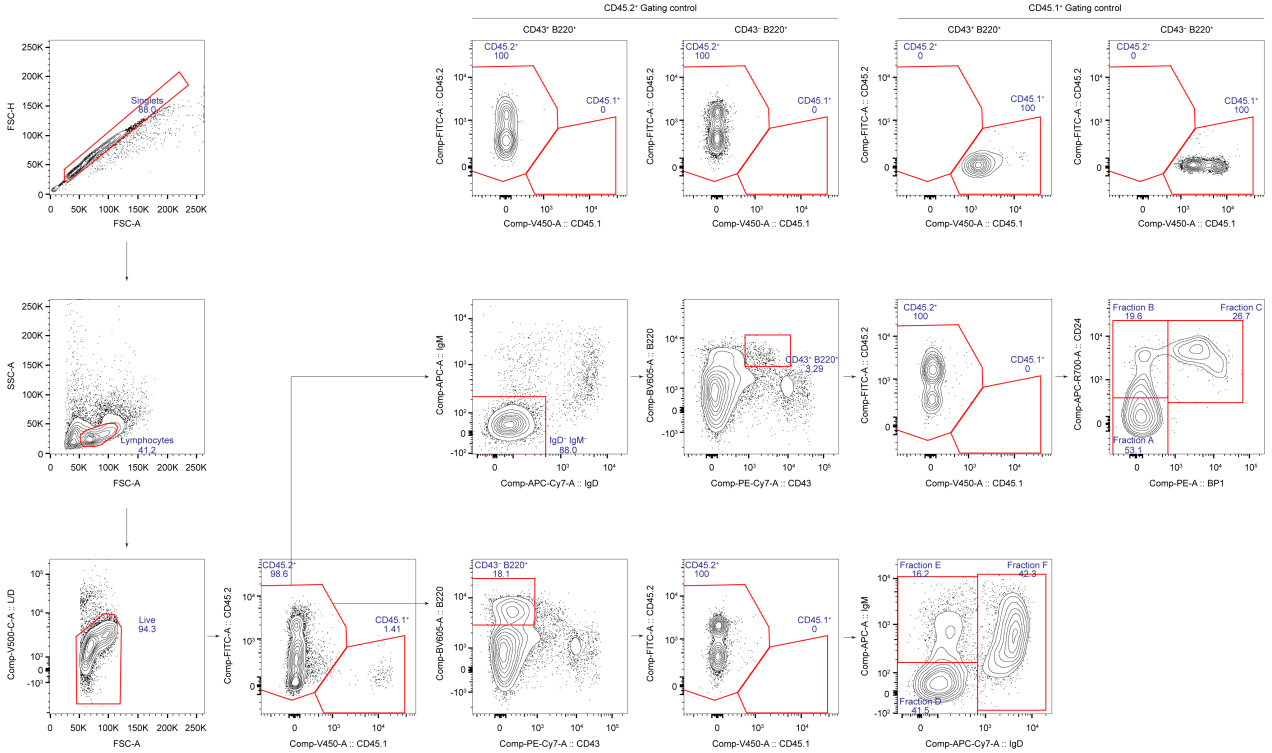

Supplementary Figure 2: Gating strategy for identifying B cell subtypes in the BM of single BM-transplanted chimeric mice.
The gating process begins with the selection of single, live CD45.2$^+$ lymphocytes. BM B cells are subsequently classified into Hardy Fractions A-F to distinguish developmental stages. (Middle row) Early B cell precursors (Fractions A-C) are gated first on IgD$^-$ IgM$^-$, followed by selecting B220$^+$ CD43$^+$ populations. These populations are further classified into: Fraction A: Early pro-B cells (B220$^+$ CD43$^+$ CD45.2$^+$ CD24$^-$ BP1$^-$), Fraction B: Pro-B cells (B220$^+$ CD43$^+$ CD45.2$^+$ CD24$^+$ BP1$^-$), and Fraction C/C': Early pre-B cells (B220$^+$ CD43$^+$ CD45.2$^+$ CD24$^+$ BP1$^+$). (Bottom row) Later stages of BM B cell development are gated from the live donor-derived lymphocytes. Fraction D: Late pre-B cells (B220$^+$ CD43$^-$ CD45.2$^+$ IgM$^-$ IgD$^-$), Fraction E: Immature B cells (B220$^+$ CD43$^-$ CD45.2$^+$ IgM$^+$ IgD$^-$), and Fraction F: Recirculating mature B cells (B220$^+$ CD43$^-$ CD45.2$^+$ IgM$^+$ IgD$^+$). (Top row) CD45.1 and CD45.2 homozygous samples were used as gating controls to ensure accurate discrimination between donor and recipient cell populations.

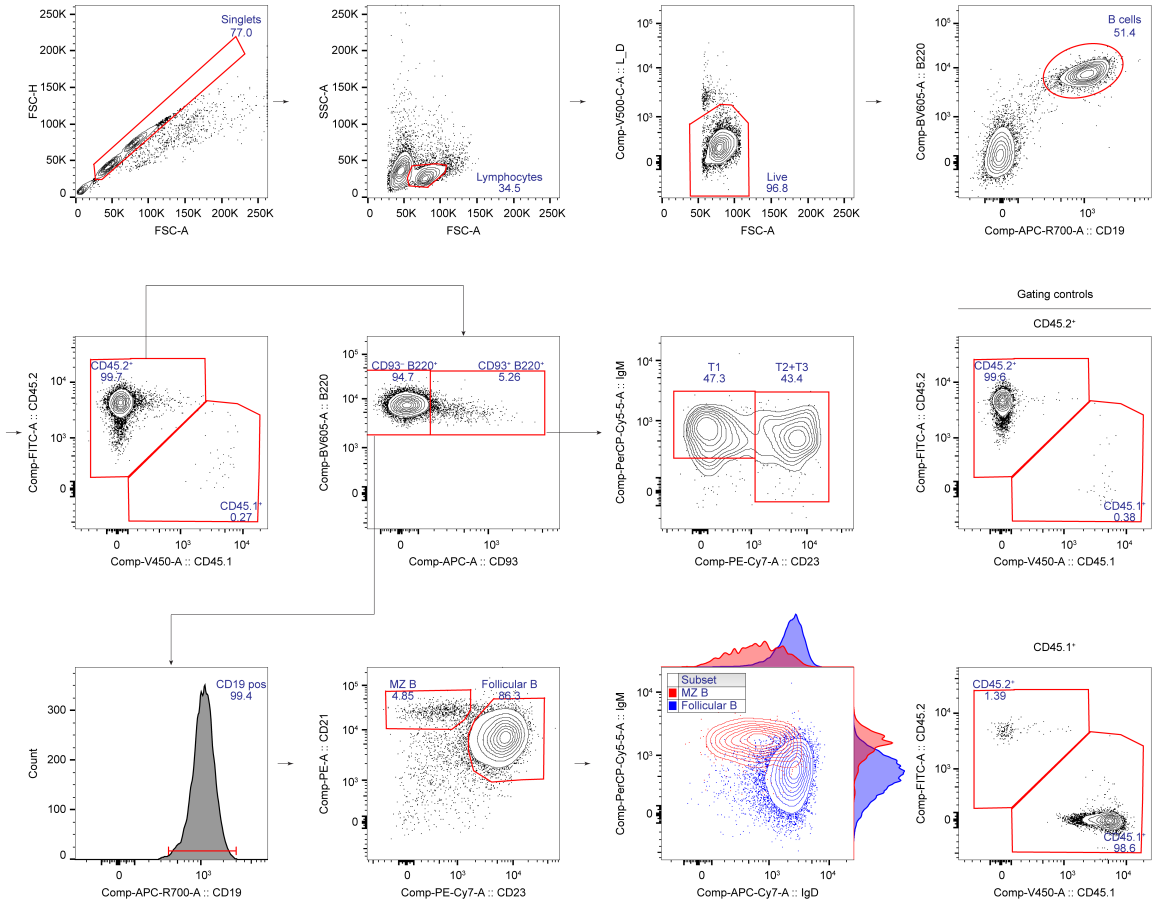

Supplementary Figure 3: Gating strategy for identifying B cell subtypes in the spleen of single BM-transplanted chimeric mice.
The gating strategy begins by selecting single live CD45.2$^+$ B cells, followed by gating based on CD93 expression. CD93$^+$ transitional B cells are further classified into T1 (IgM$^+$ CD23$^-$) and T2/T3 (IgM$^{-\text{ to }+}$ CD23$^+$) subsets. CD93$^-$ cells are gated into marginal zone B cells (CD21$^+$ CD23$^{\text{low-to-moderate}}$) and Follicular B cells (CD21$^{\text{Mod to }+}$ CD23$^+$), then confirmed by their expression patterns of IgM and IgD: MZ B cells (IgM$^{\text{high}}$ IgD$^-$) and Follicular B cells (IgM$^{\text{low-to-mod}}$ IgD$^{\text{high}}$). Spleen samples from CD45.2 or CD45.1 homozygous mice are used as gating controls.

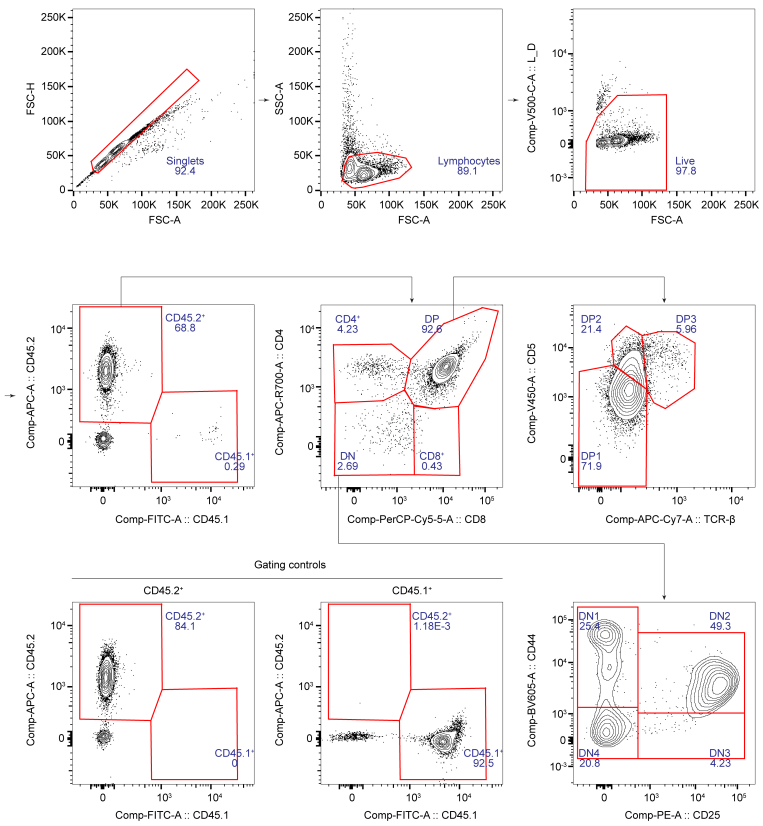

Supplementary Figure 4: Gating strategy for identifying thymocyte subpopulations in single BM-transplanted chimeric mice.
The gating strategy begins by selecting single, live CD45.2^{+} lymphocytes from the thymus. Thymocyte subsets are classified into double-negative (DN), double-positive (DP), CD4^{+} single-positive, or CD8^{+} single-positive populations. DN cells are broadly subdivided into DN1-DN4 stages based on the expression of CD44 and CD25: DN1 (CD44^{+} CD25^{-}), DN2 (CD44^{+} CD25^{+}), DN3 (CD44^{-} CD25^{+}), and DN4 (CD44^{-} CD25^{-}). DP cells are roughly subdivided into DP1-DP3 stages according to CD5 and TCR-β expression levels: DP1 (CD5^{low} TCR-β^{low}), DP2 (CD5^{high} TCR-β^{mod}), and DP3 (CD5^{mod} TCR-β^{high}). CD45.1 and CD45.2 homozygous control thymocytes are included to ensure clear distinction between donor and recipient cell populations.

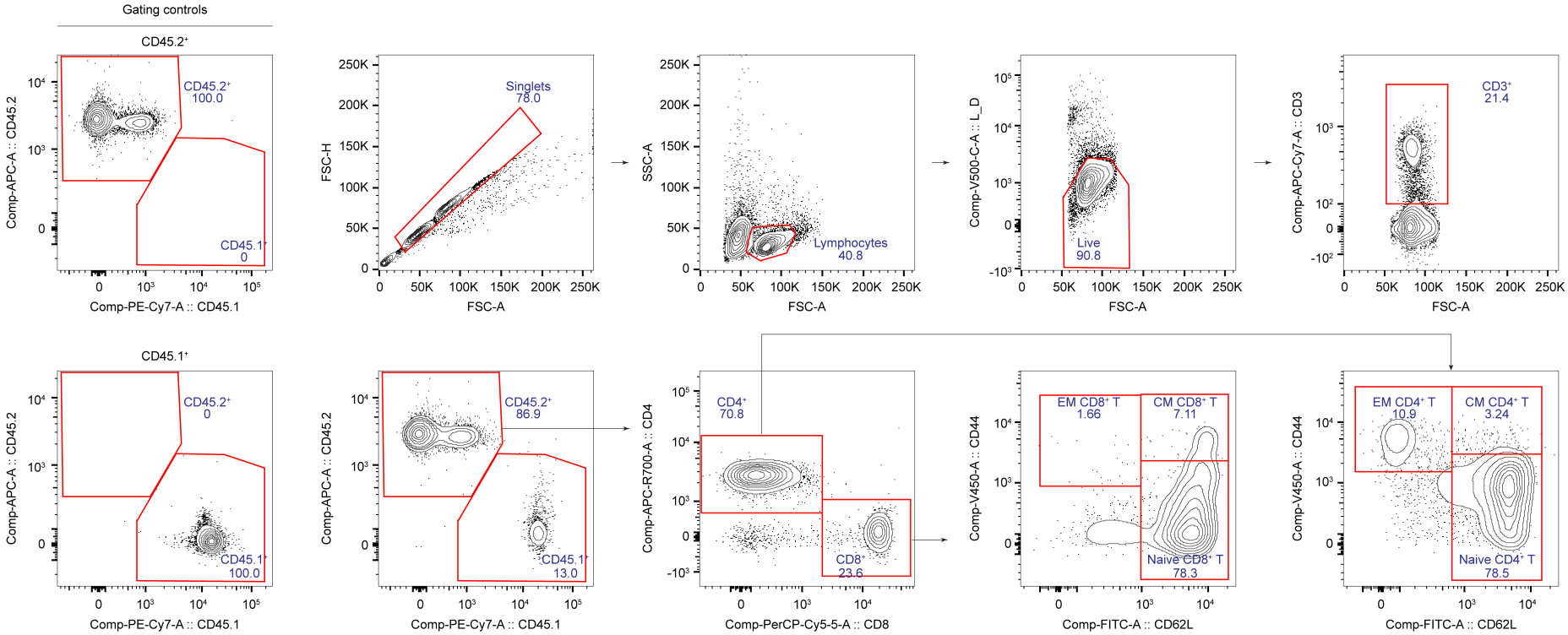

Supplementary Figure 5: Gating strategy for identifying splenic T cell subsets in single BM-transplanted chimeric mice.
The gating strategy starts by selecting single, live CD3$^+$ CD45.2$^+$ cells. These are further separated into CD4$^+$ and CD8$^+$ T cells. Within each of these populations, EM T cells (CD44$^+$ CD62L$^-$), CM T cells (CD44$^+$ CD62L$^+$), and Naïve T cells (CD44$^-$ CD62L$^+$) are identified. Homozygous CD45.1 and CD45.2 spleen samples are used as controls to ensure accurate gating between donor and recipient cells.

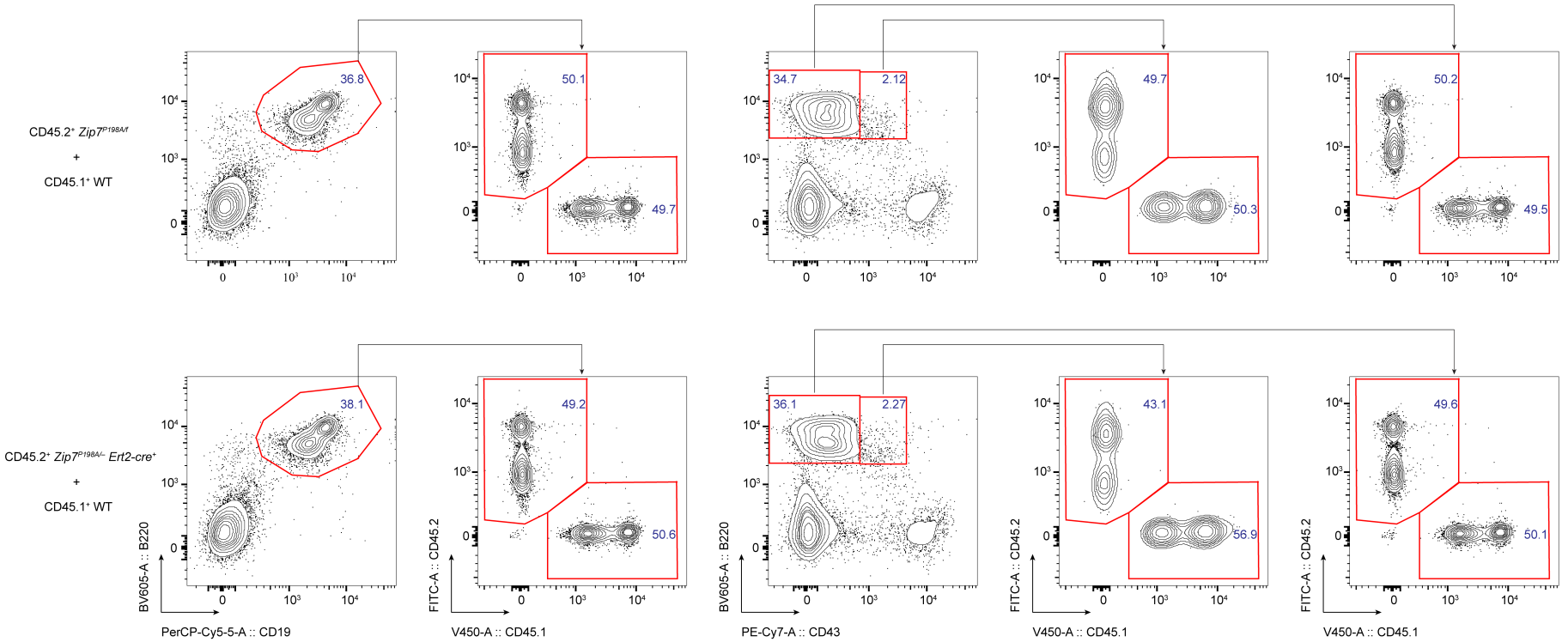

Supplementary Figure 6: Gating strategy to verify the mixed ratio of CD45.1$^+$ and CD45.2$^+$ BM cells.
BM cells from CD45.2$^+$ ZIP7-deficient or its control were mixed with CD45.1$^+$ internal control cells in a 1:1 ratio before transplantation into lethally irradiated CD45.1$^+$ WT recipient mice. The mixed ratio was confirmed based on the gating of Hardy Fraction B-F cells (CD19$^+$ B220$^+$), Hardy Fraction D-F B cells (CD43$^-$ B220$^+$), or Hardy Fraction A-C cells (CD43$^+$ B220$^+$). The origin of each population, whether from CD45.1$^+$ or CD45.2$^+$ cells, was identified by the expression of the respective CD45 alleles.

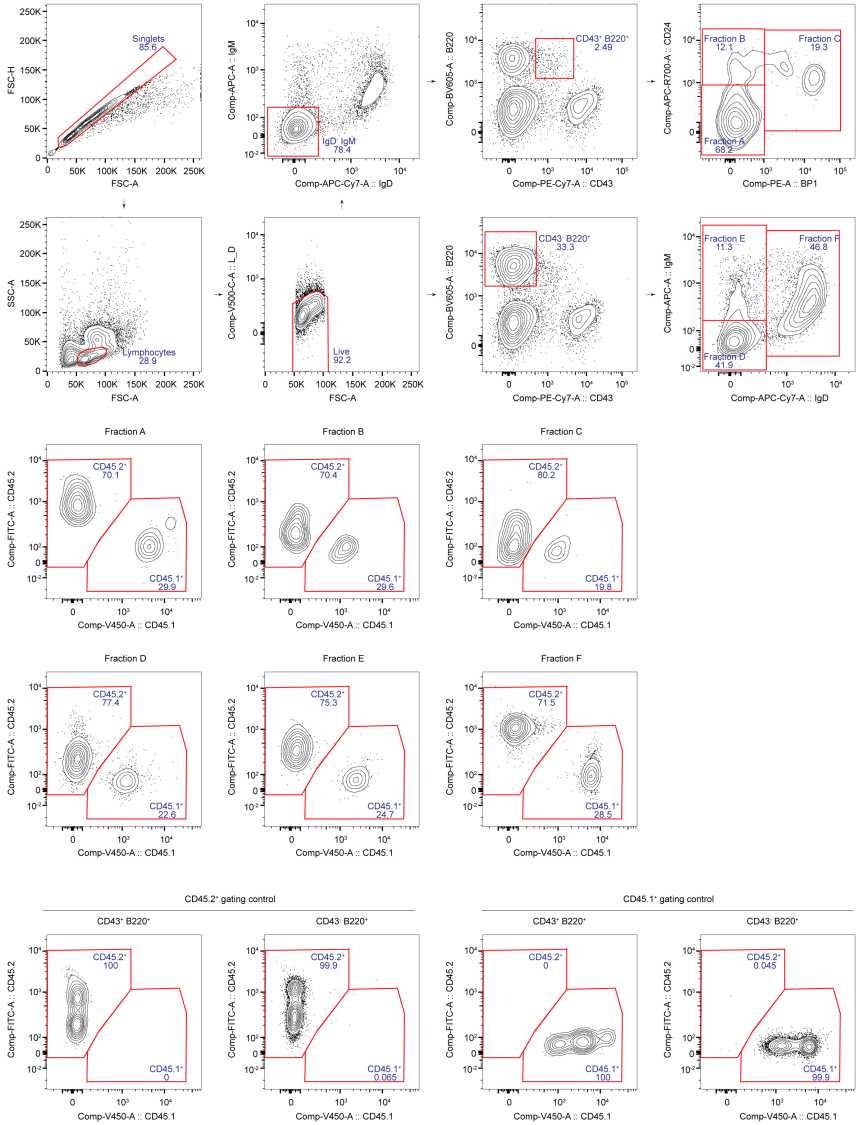
Singlets
85.6
FSC-H
FSC-A
Comp-APC-A :: IgM
Comp-APC-Cy7-A :: IgD
IgD+ IgM+
76.4
Comp-BV605-A :: B220
Comp-PE-Cy7-A :: CD43
CD43+ B220+
2.49
Comp-APC-R700-A :: CD24
Comp-PE-A :: BP1
Fraction B
12.1
Fraction C
19.3
Fraction A
68.2
SSC-A
Lymphocytes
28.9
Comp-V500-C-A :: L_D
Live
92.2
CD43- B220+
33.3
Fraction E
11.3
Fraction F
46.8
Fraction D
41.9
Fraction A
Fraction B
Fraction C
Comp-FITC-A :: CD45.2
Comp-V450-A :: CD45.1
CD45.2+
70.1
CD45.1+
29.9
CD45.2+
70.4
CD45.1+
29.6
CD45.2+
80.2
CD45.1+
19.8
Fraction D
Fraction E
Fraction F
CD45.2+
77.4
CD45.1+
22.6
CD45.2+
75.3
CD45.1+
24.7
CD45.2+
71.5
CD45.1+
28.5
CD45.2+ gating control
CD45.1+ gating control
CD43+ B220+
CD43- B220+
CD45.2+
100
CD45.1+
0
CD45.2+
99.9
CD45.1+
0.065
CD45.2+
0
CD45.1+
100
CD45.2+
0.045
CD45.1+
99.9

Supplementary Figure 7: Gating strategy for identifying B cell developmental stages in the BM of mixed chimeras.
The gating strategy begins by identifying Hardy Fractions A-F in the BM, representing different stages of B cell development (top two rows). Within each fraction, $CD45.2^+$ donor-derived cells and $CD45.1^+$ internal controls are separated (middle two rows). This distinction is validated using homozygous CD45.1 and CD45.2 control samples (bottom row).

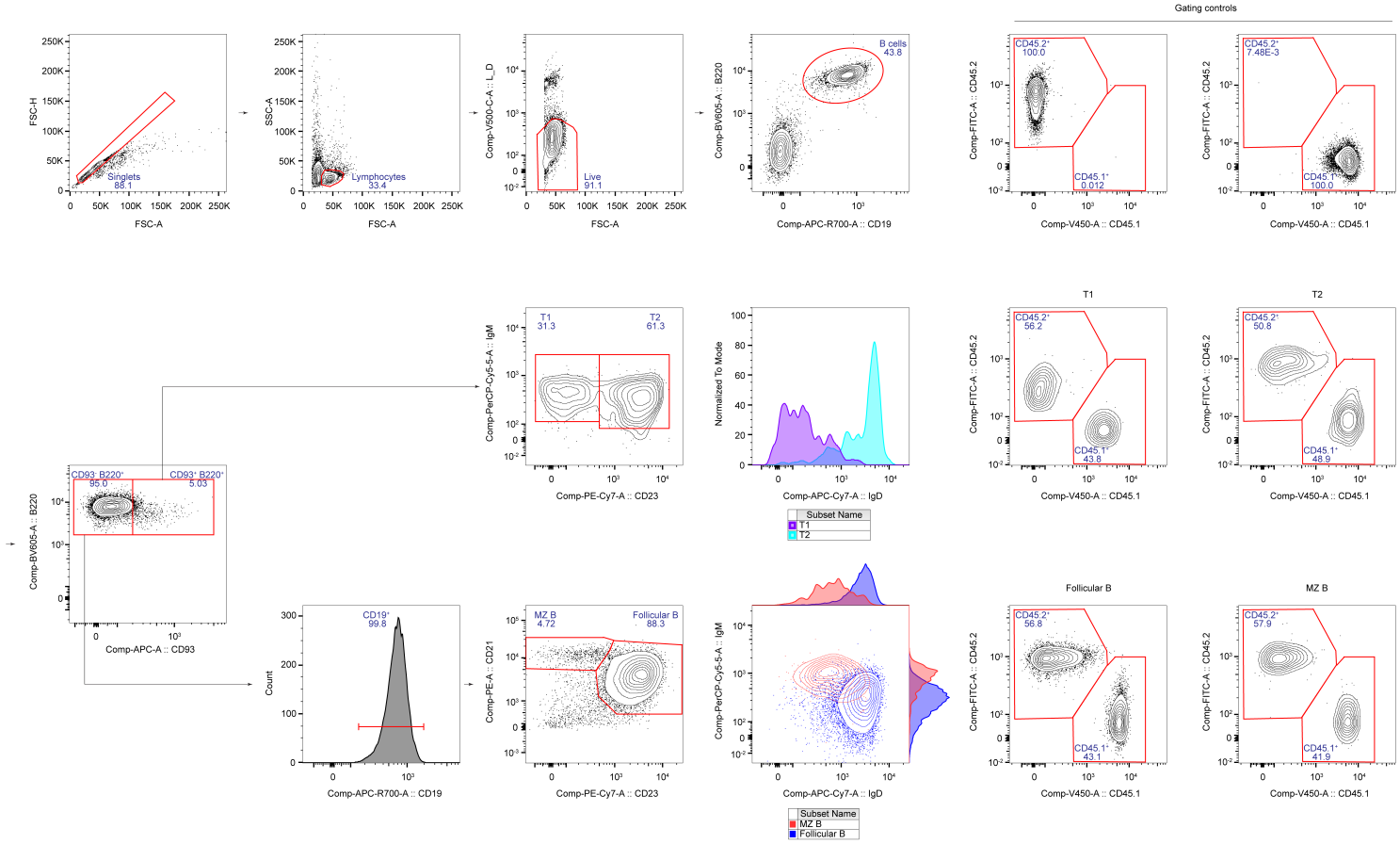

Supplementary Figure 8: Gating strategy for identifying splenic B cell subpopulations in mixed chimeras.
This strategy distinguishes the origins of T1, T2, Follicular, and MZ B cells by identifying CD45.1 and CD45.2 donor populations. The gating process starts with selecting single, live B cells, followed by separation into respective subpopulations. T1 and T2 cells are gated based on their IgM and CD23 expression, while Follicular and MZ B cells are identified by their CD21 and CD23 expression patterns, with additional confirmation by assessing their IgM and IgD levels. The same identification approach is applied to Follicular B cells in both the spleen and the MLN.

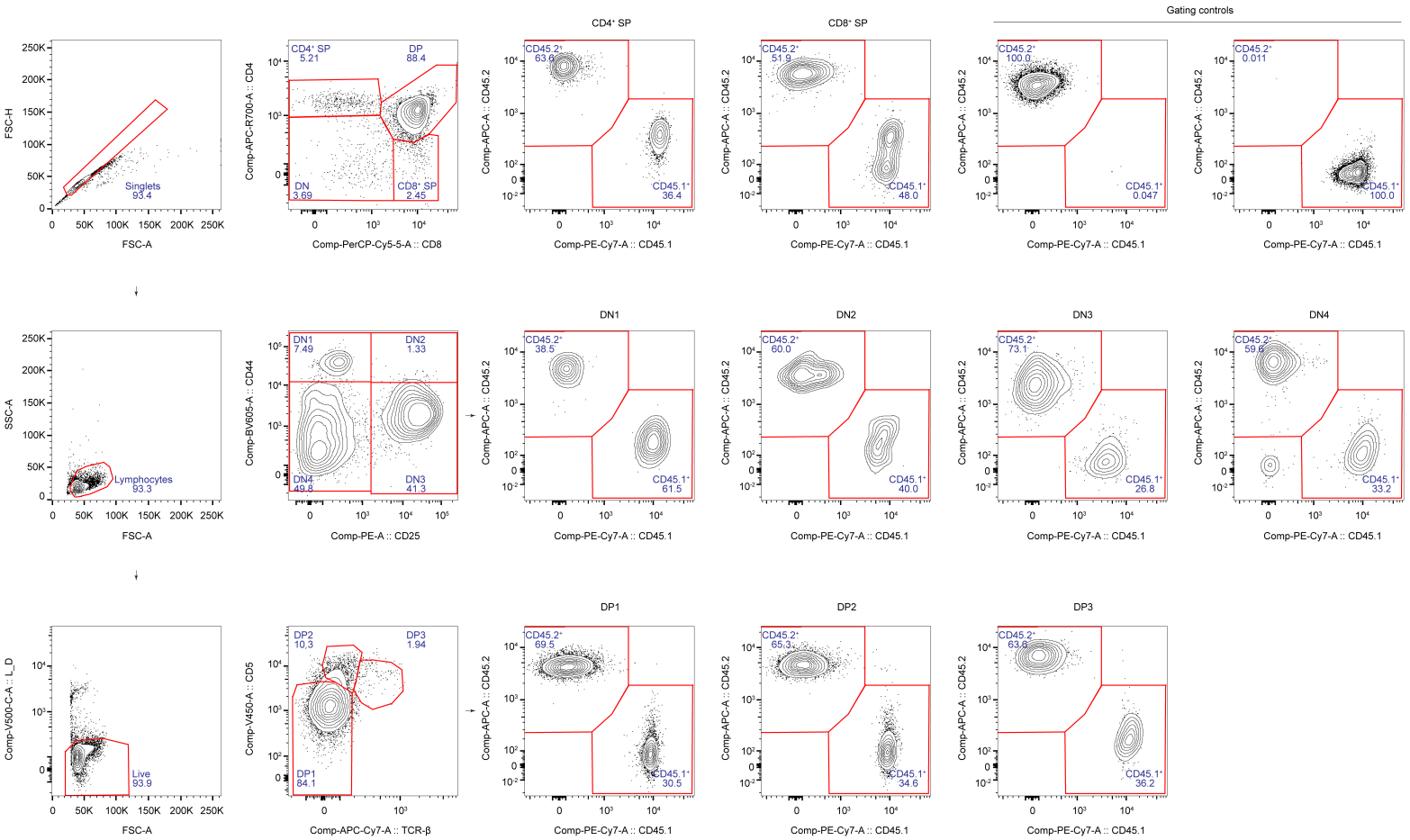

Supplementary Figure 9: Gating strategy for identifying thymocyte subtypes in mixed chimeric mice.
Thymocyte subsets were identified using a gating strategy consistent with that described for single BM-transplanted chimeras. The focus here is on distinguishing cells derived from CD45.2$^+$ and CD45.1$^+$ donors within each subtype. Homozygous CD45.1 and CD45.2 gating controls are displayed in the top right corner for reference.

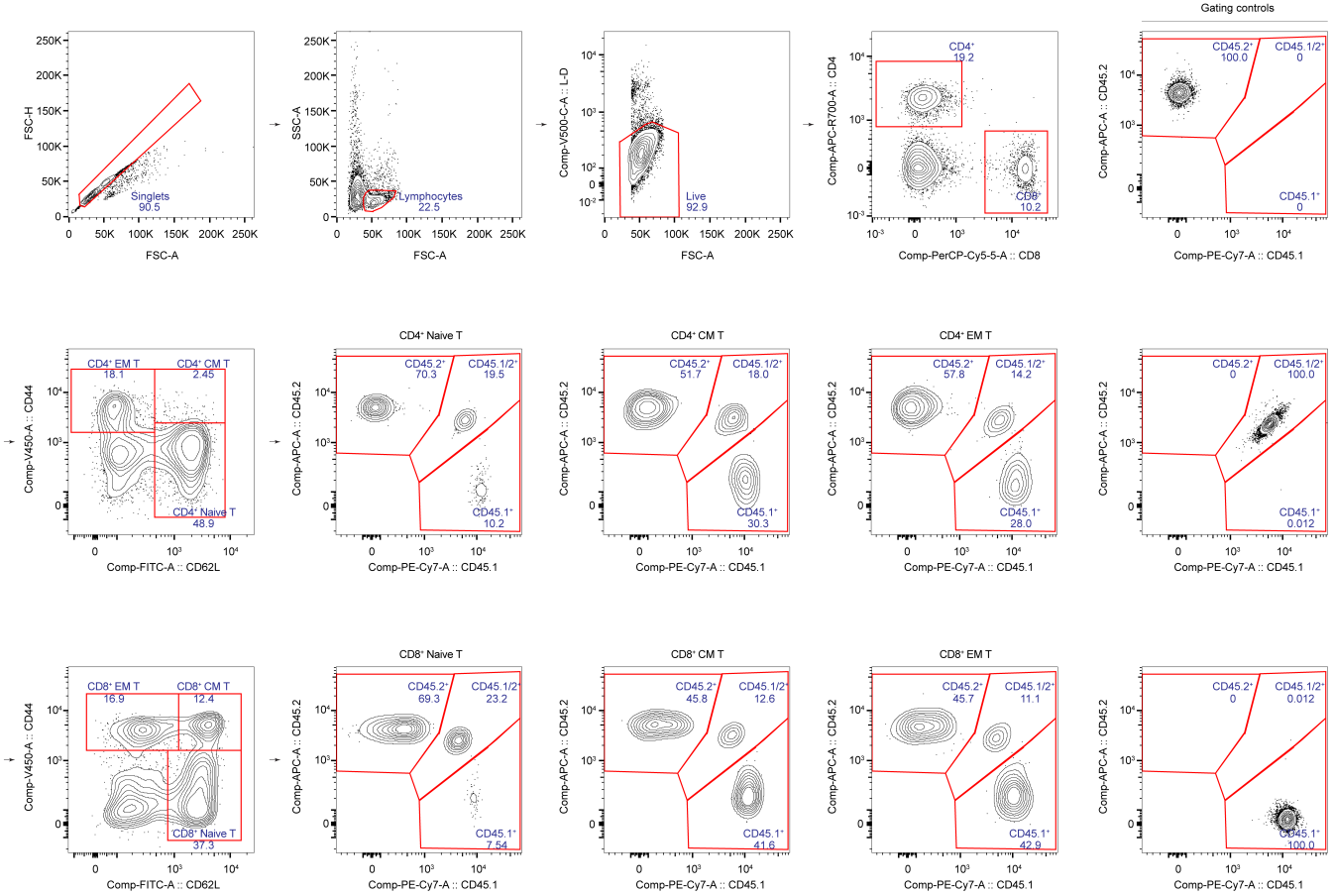

Supplementary Figure 10: Gating strategy for identifying splenic T cell sub-populations in the mixed BM chimera.
This figure illustrates the gating of splenic T cell subsets (naïve, CM and EM) within $CD4^+$ and $CD8^+$ T populations. The gating strategy to distinguish their subtypes follows the same method used in single-BM transplanted chimeras. However, this figure specifically highlights the differentiation among cells from the internal control WT donor (CD45.1/2), ZIP7 WT or deficient donor (CD45.2) and WT recipients (CD45.1).
Gating controls for CD45.1 and CD45.2 expression ensure accurate identification of each donor or recipient source.

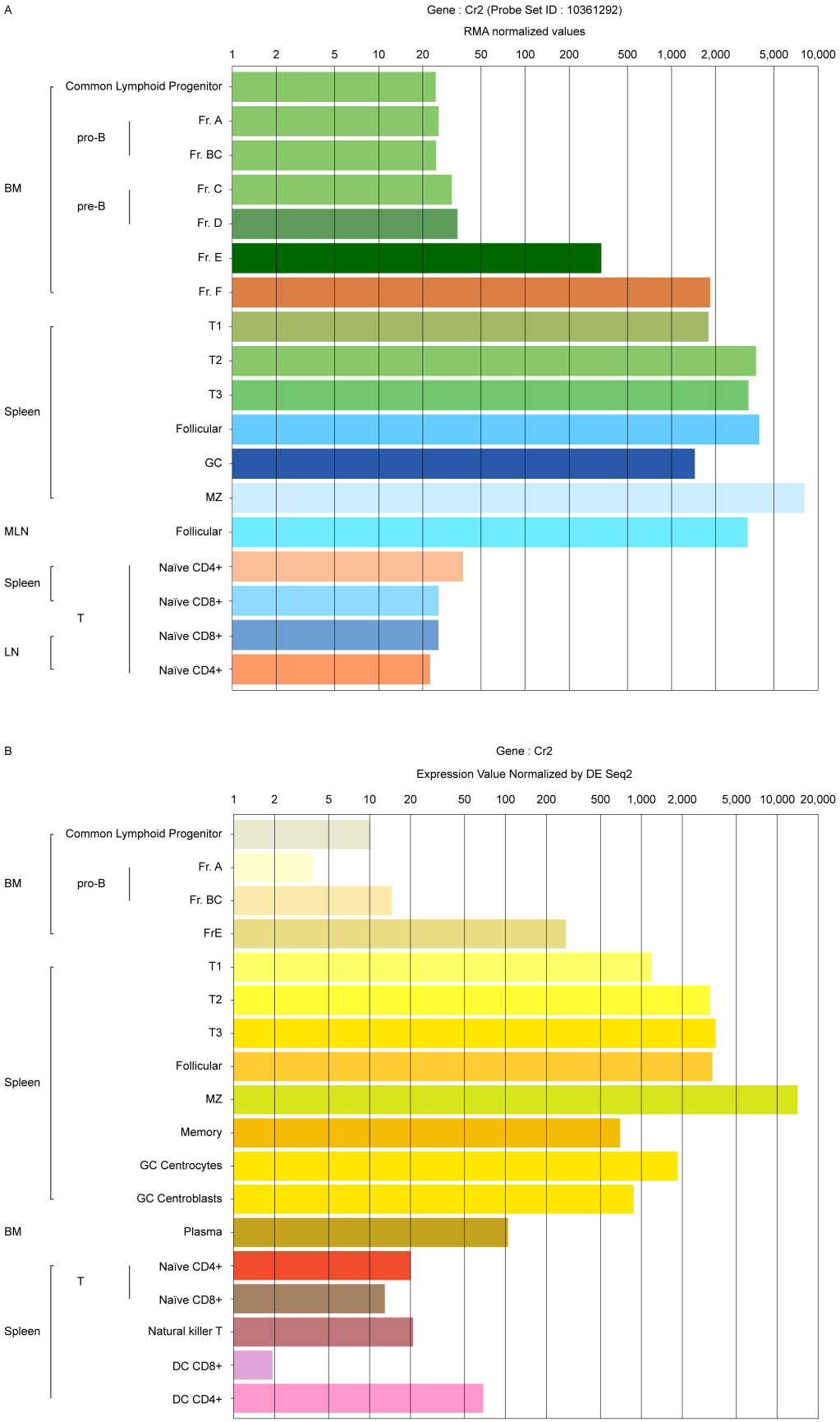

Supplementary Figure 11: Expression profiles of *Cr2* across various immune cell subsets. Expression levels are displayed on a Log10 scale, based on data from (A) microarray and (B) RNA-seq analyses in the ImmGen dataset[276].

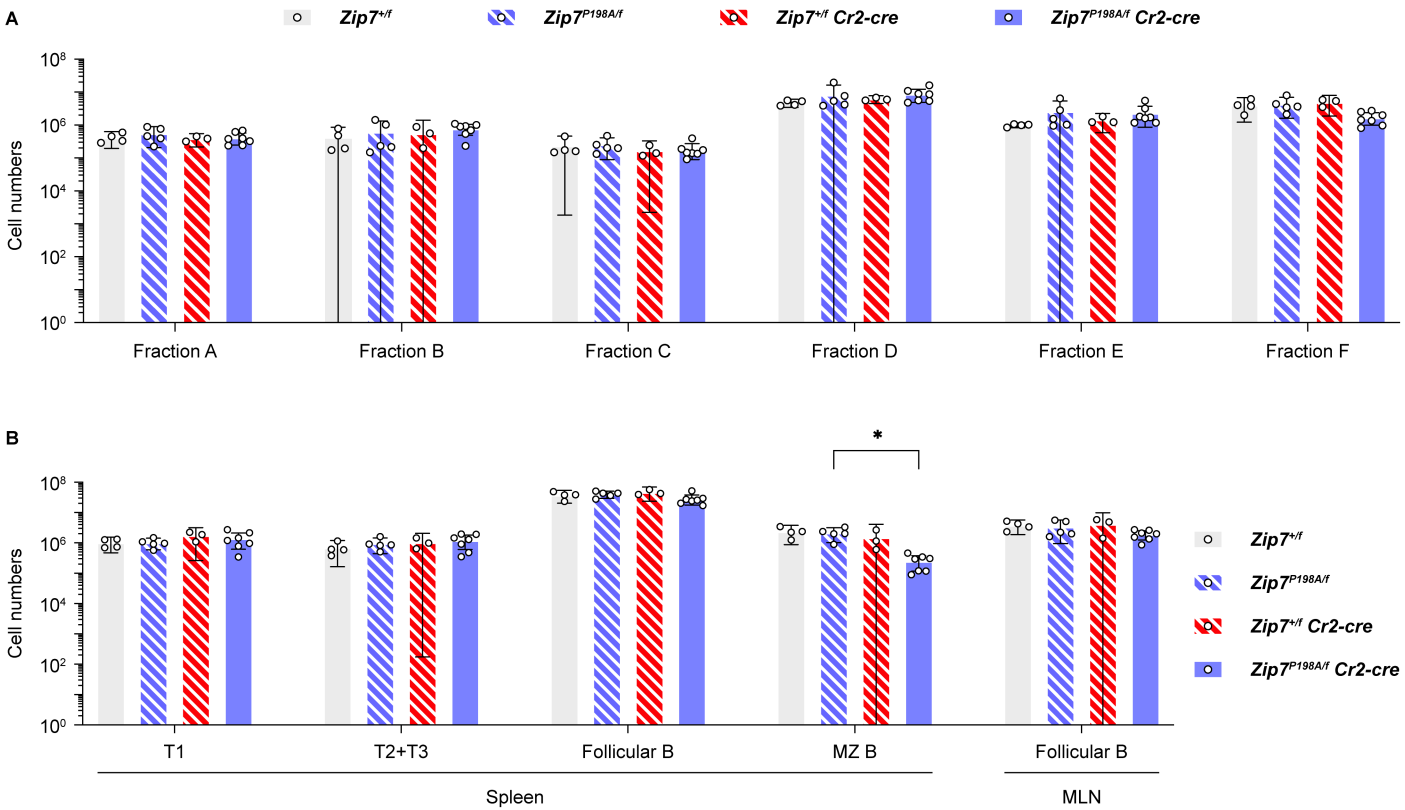

Supplementary Figure 12: ZIP7 deficiency in mature B cells leads to a reduction in MZ B cells without affecting B cell development in the BM. These mice were generated from a separate *Zip7*^{f} founder line. (A) Absolute cell numbers of B cell subsets in the BM. (B) Absolute cell numbers of peripheral B cell subtypes. Each dot represents an individual mouse. Statistical analysis was conducted using mixed-effects analysis followed by Tukey's multiple comparisons test. *, $p = 0.0278$.

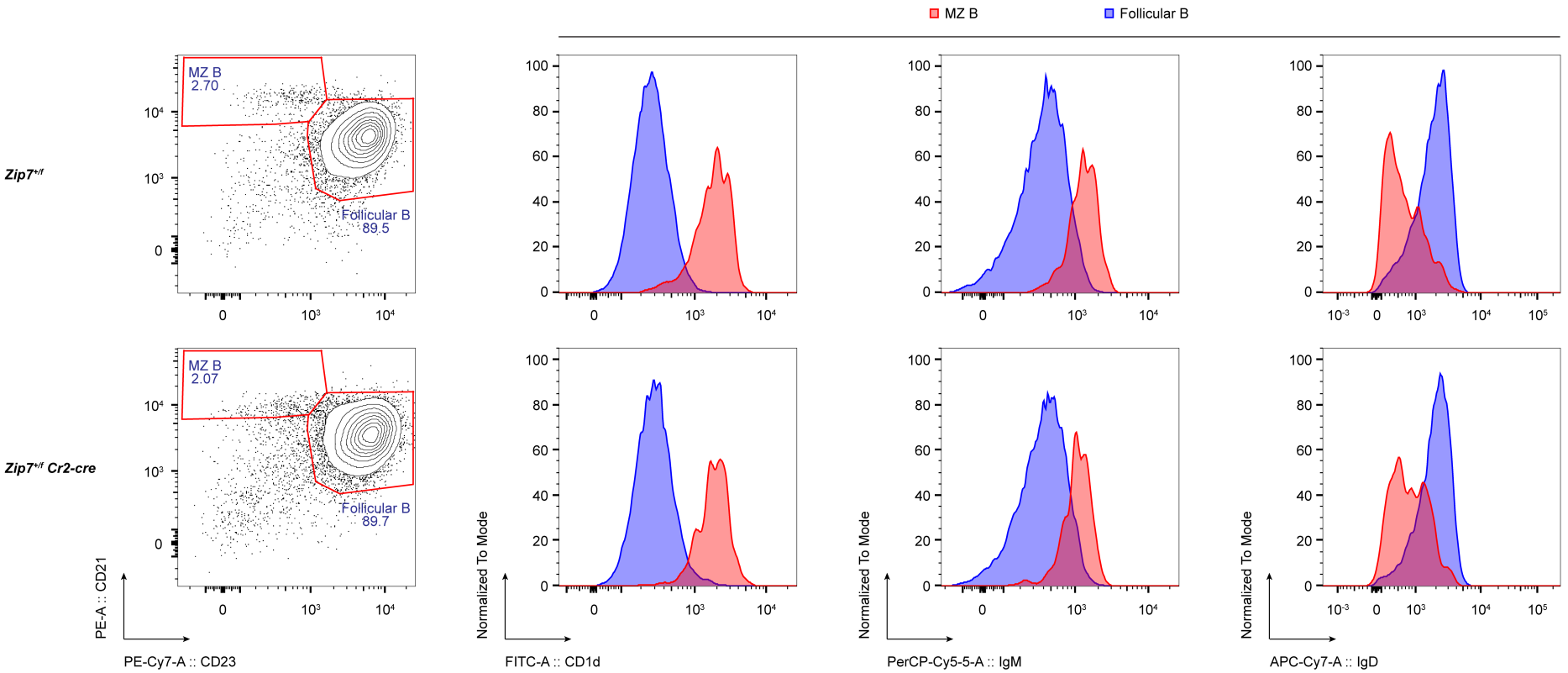

Supplementary Figure 13: Confirmation that CD21^{+} CD23$^{low/–}$ gated MZ B cells in *Zip7*$^{+/f}$ *Cr2-cre* mice exhibit characteristic MZ B cell markers. Flow cytometry plots show MZ B cells (CD21^{+} CD23$^{low/–}$) and follicular B cells in *Zip7*$^{+/f}$ (top) and *Zip7*$^{+/f}$ *Cr2-cre* (bottom) mice. Histograms on the right confirm that MZ B cells in both genotypes exhibit characteristic markers: CD1d^{high}, IgM^{high}, and IgD^{low}, indicating that CD21^{+} CD23$^{low/–}$ gated cells in *Zip7*$^{+/f}$ *Cr2-cre* mice display the expected MZ B cell phenotype.

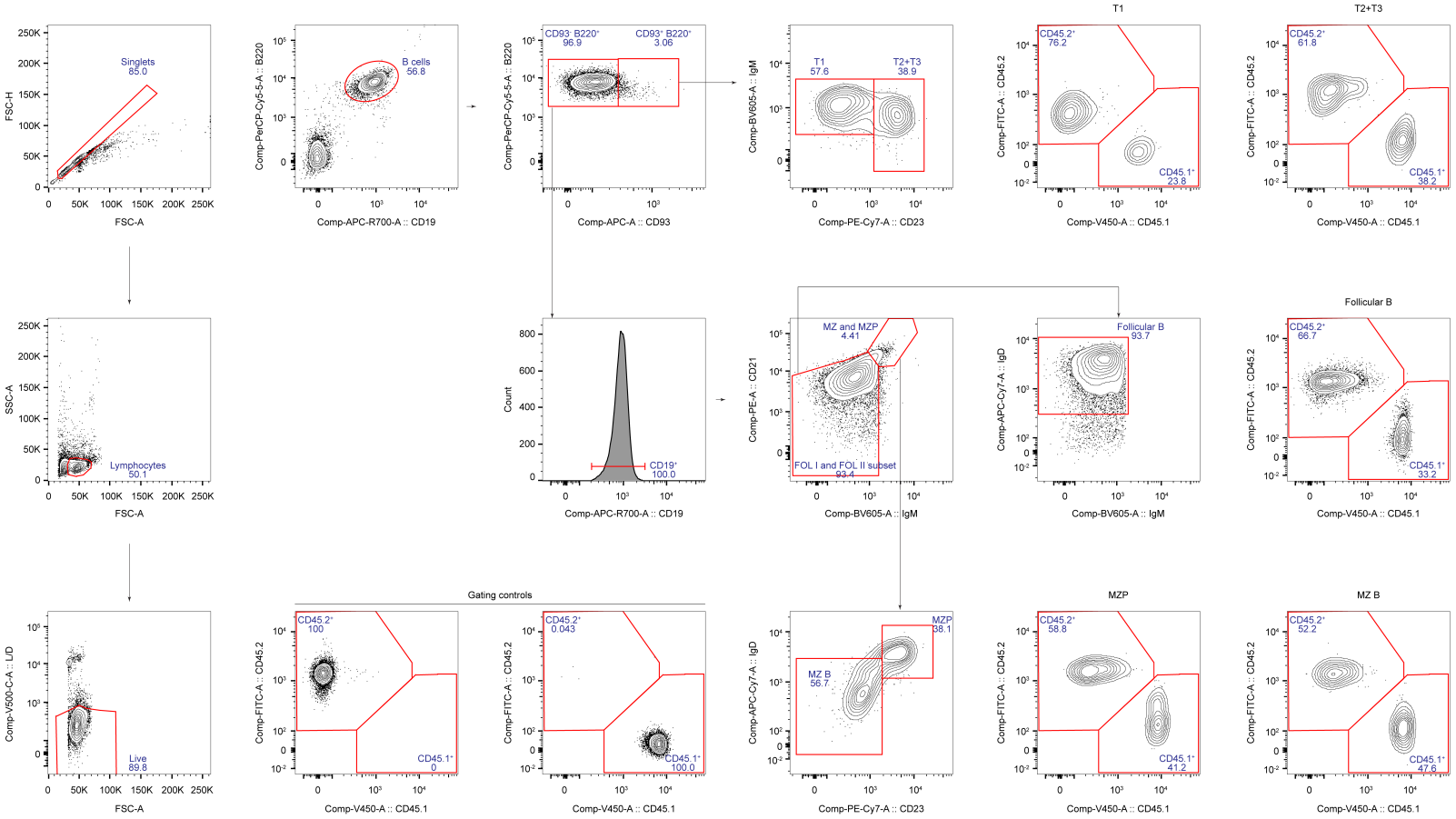

Supplementary Figure 14: Gating strategy for identifying MZ B precursor cells in mixed chimeras.
This gating strategy highlights the identification of MZP within splenic B cell subpopulations in mixed chimeras. MZP and MZ B cells are characterized by high CD21 and high IgM expression, with further confirmation using CD23 and IgD profiles. Follicular B cells are gated as $CD21^{-\text{ to Mod}}$, $IgM^{-\text{ to Low}}$ and IgD^{+}. This approach is consistent with the gating strategy previously shown in Supplementary Figure 8 for other splenic B cell subsets.

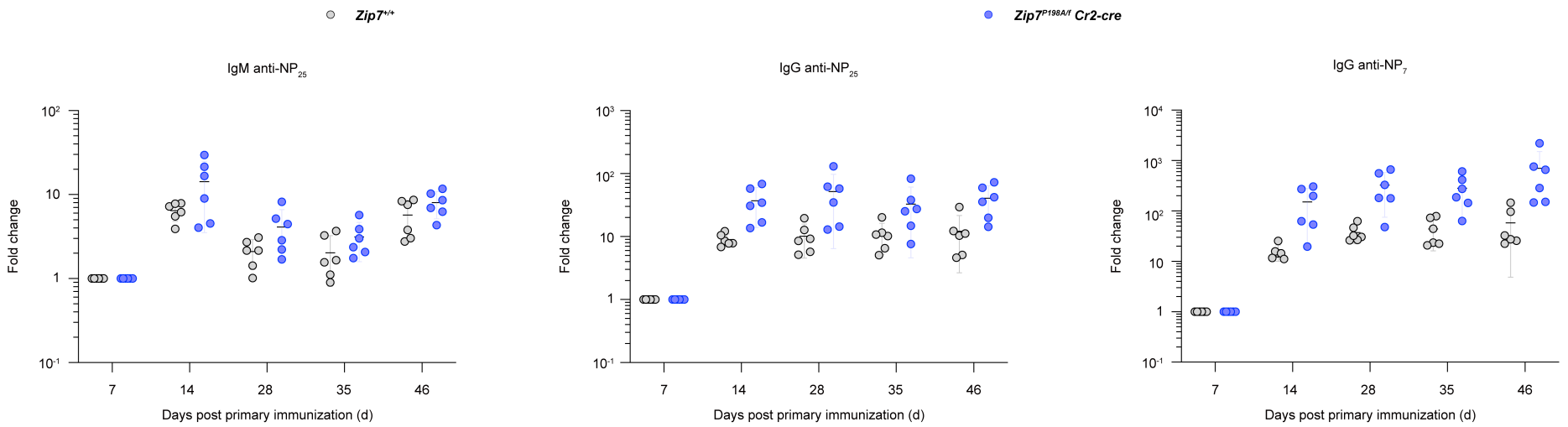

Supplementary Figure 15: Fold change of NP-specific antibodies following NP-CGG immunization.
The fold change of NP-specific IgM (anti-NP_{25}, left panel), low-affinity IgG (anti-NP_{25}, middle panel) and high-affinity IgG (anti-NP_7, right panel) were measured in *Zip7*$^{+/+}$ and *Zip7*$^{P198A/f}$ *Cr2-cre* mice at multiple time points post-primary immunization with NP-CGG. Fold change was calculated as the antibody level at each time point divided by the corresponding antibody level on Day 7. Dots represent individual mice, with means ± 95% CIs shown for each group. Statistical significance was assessed using unpaired *t*-test with Welch correction, followed by Holm-Šídák's multiple comparisons test.

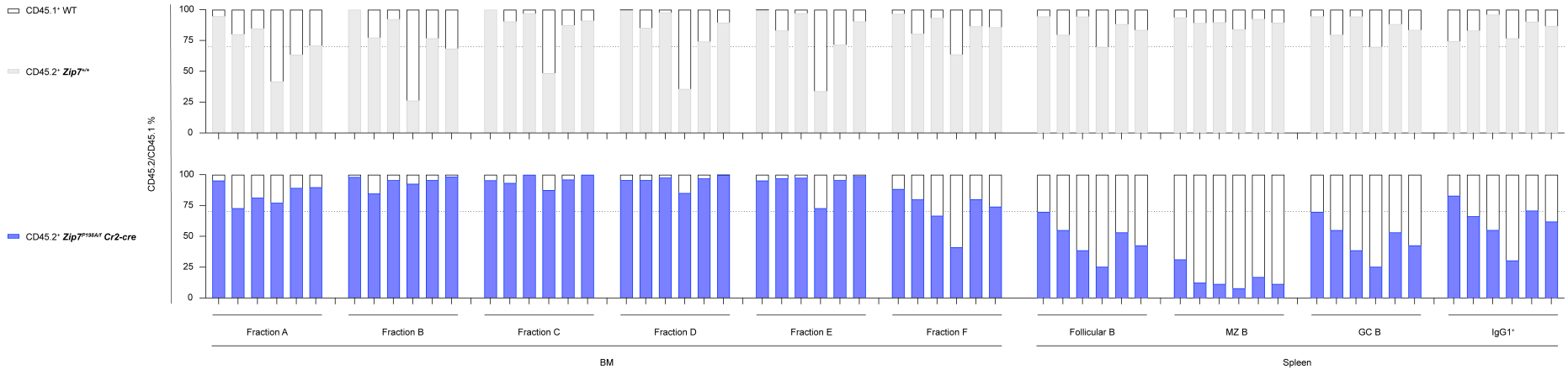

Supplementary Figure 16: Consistent GC response defects in an independent batch of *Zip7*$^{P198A/f}$ *Cr2-cre* mixed chimeric mice after SRBC immunization.
This experiment utilized an independent founder line of *Zip7*$^{P198A/f}$ *Cr2-cre* mice to confirm the observed phenotypes. Mixed chimeras were generated using 70/30 BM mixtures of CD45.2^{+} *Zip7*$^{+/+}$ or *Zip7*$^{P198A/f}$ *Cr2-cre* and CD45.1^{+} WT cells. After eight weeks of reconstitution, the chimeric mice were immunized with SRBC, and samples were collected on Day 8 post-immunization. The white and coloured columns indicate the percentages of CD45.1^{+} and CD45.2^{+} cells in different B cell subsets from the BM and spleen, respectively. Data from six mice in each group are shown.

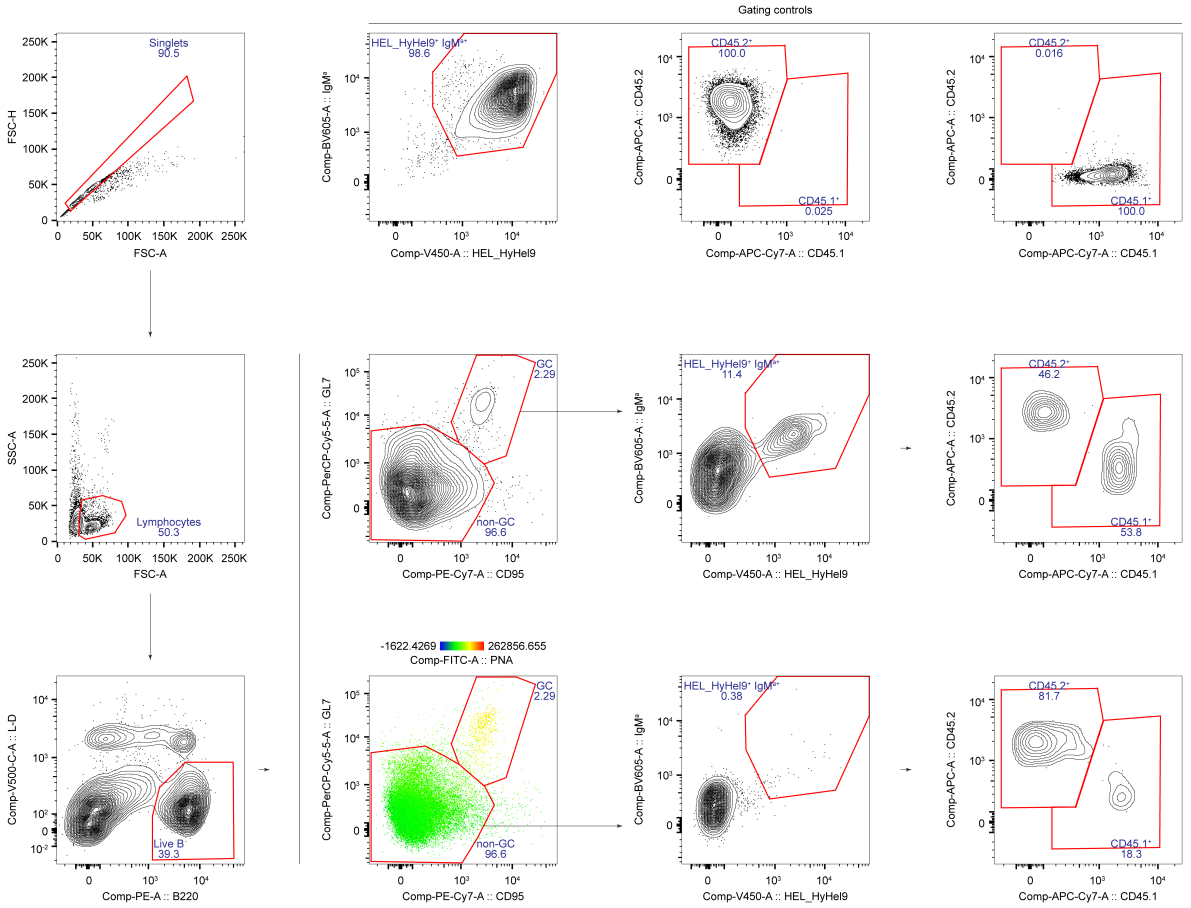

Supplementary Figure 17: Gating strategy for identifying donor-derived GC B cells in the adoptive transfer model followed by HEL-SRBC immunization.
Single live B220^{+} cells were first gated, followed by identification of GC B cells as GL7^{+} CD95^{+} PNA^{+}. MD4 donor-derived B cells were defined as HEL_HyHEL9^{+} IgM^{+} cells within both GC and non-GC populations. Subsequent gating distinguished ZIP7-deficient or WT-derived cells (CD45.2^{+}) from internal control-derived cells (CD45.1^{+}). Percentages of each gated population are displayed within the respective plots.

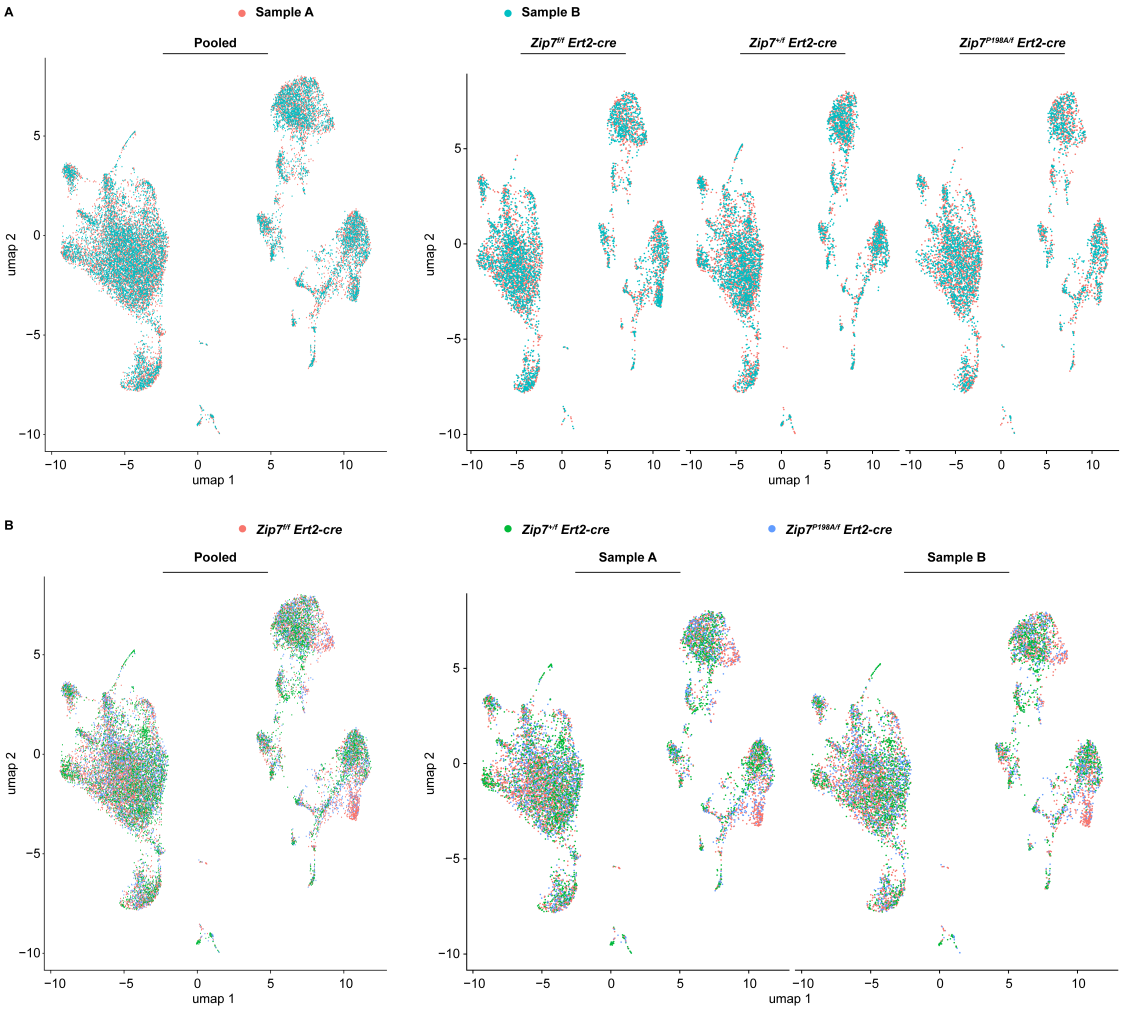

Supplementary Figure 18: Evaluation of technical reproducibility and sample distribution.
UMAP plots showing cell distribution across technical duplicates and ZIP7 genotypes.
(A) Cells from Sample A (red) and Sample B (blue) exhibit strong overlap, indicating minimal batch effects.
(B) Cells from different genotypes (*Zip7*$^{+/f}$ *Ert2-cre*: green, *Zip7*$^{P198A/f}$ *Ert2-cre*: blue, *Zip7*$^{f/f}$ *Ert2-cre*: red) display similar distribution patterns across pooled and individual samples, supporting data consistency.

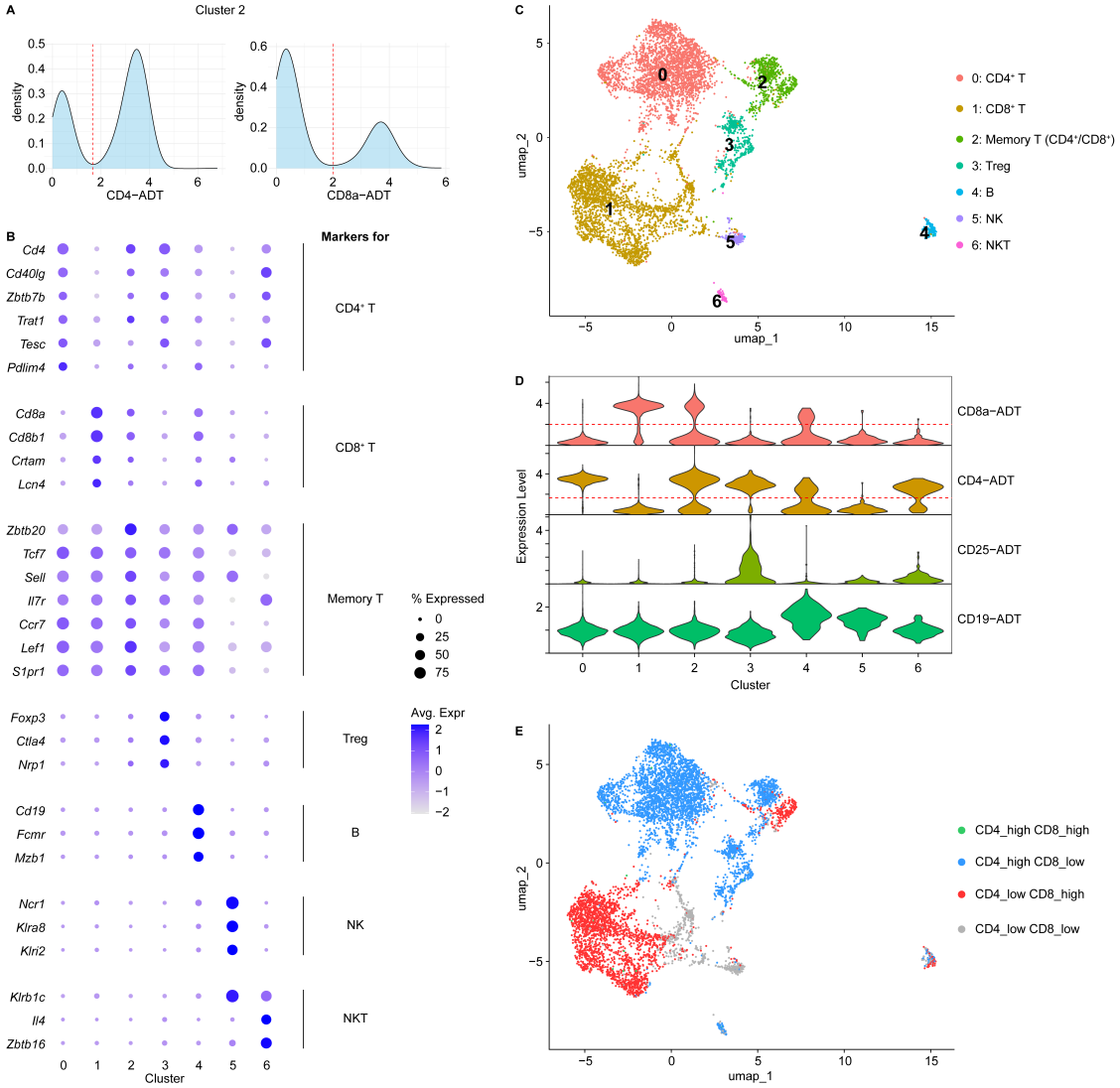

Supplementary Figure 19: Initial clustering and ADT-based stratification of the total T cell population.
(A) Density plots of CD4 and CD8a ADT expression within Cluster 2 ($CD4^+/CD8^+$ memory-like population). Dashed red lines indicate the thresholds used to define single-positive cells (CD8a > 2; CD4 > 1.67). (B) Dot plot showing the expression of selected transcriptomic markers across clusters, grouped by cell type lineage. (C) Transcriptomic clustering of total T cells at low resolution (resolution = 0.1), identifying 7 clusters (0–6). (D) Violin plots of CD8a, CD4, CD25, and CD19 ADT expression across clusters. Thresholds for $CD4^+$ and $CD8^+$ selection are indicated by red lines. (E) UMAP projection showing stratification of total T cells into four subpopulations based on CD4 and CD8a ADT expression levels.

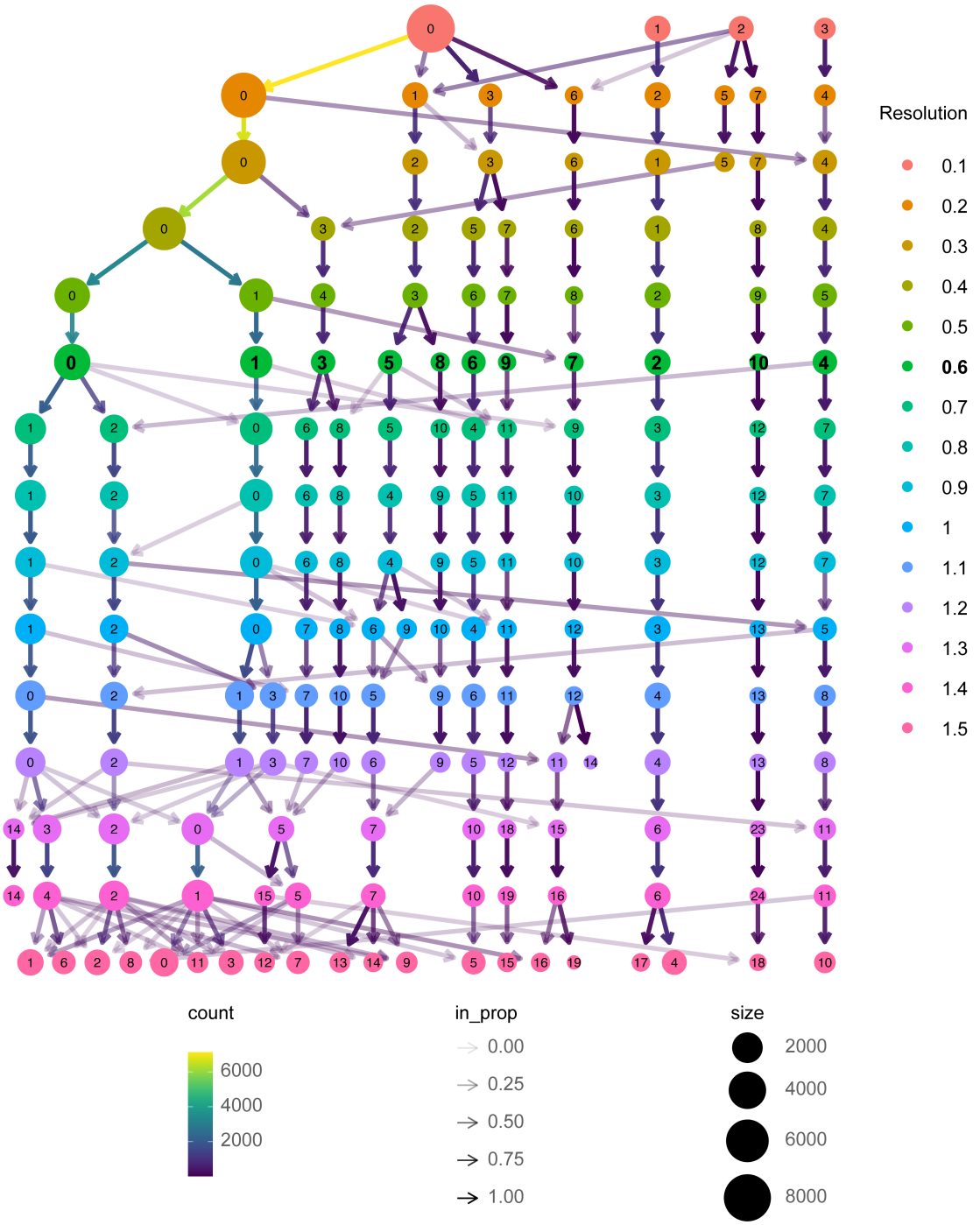

Supplementary Figure 20: Clustering stability analysis for B cells.
Clustree analysis was conducted on pooled splenic B cells to evaluate cluster stability across a range of resolution parameters. Node size reflects the number of cells per cluster; edge transparency indicates the proportion of cells retained between resolutions. A resolution of 0.6 was selected for downstream analysis based on stability and interpretability.

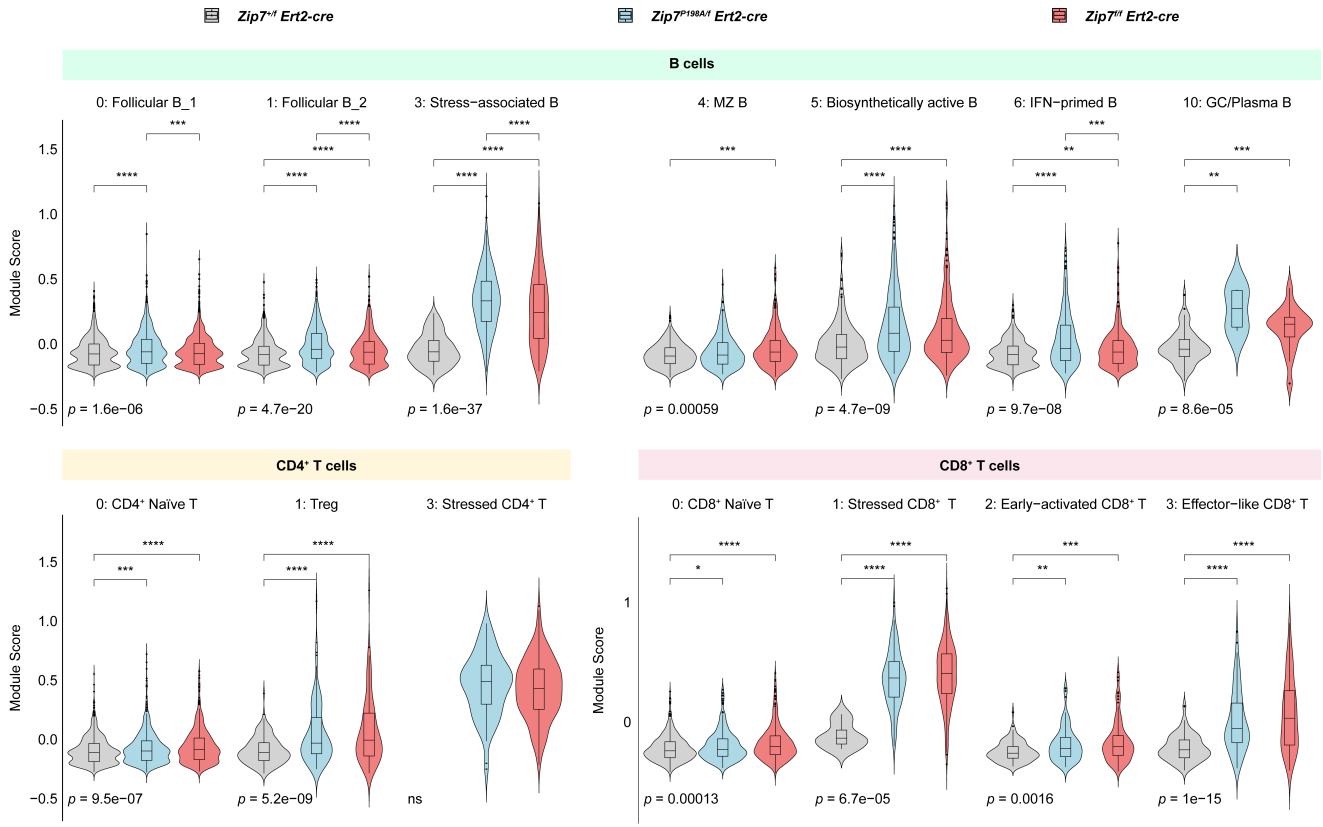

Supplementary Figure 21: Elevated Shared Stress Signature scores in ZIP7-deficient B and T cell subsets.
Violin plots show module scores for the Shared Stress Signature across representative clusters of B cells, $CD4^+$ T cells, and $CD8^+$ T cells. Scores were computed using Seurat's AddModuleScore function separately within each lineage-specific object, without z-score normalization, to retain biologically meaningful differences. Statistical comparisons were performed using the Kruskal–Wallis test to assess overall genotype effects (un-adjusted p-values shown below each plot), followed by pairwise Wilcoxon rank-sum tests with Bonferroni correction. Asterisks indicate significance of adjusted p-values from pairwise comparisons: $p < 0.05$ (*), < 0.01 (**), < 0.001 (***), < 0.0001 (****); ns = not significant.
Note: Shared Stress Signature scores in Figure 6-10 were computed jointly across all subsets using unified AddModuleScore and z-score normalisation to enable cross-lineage comparison.

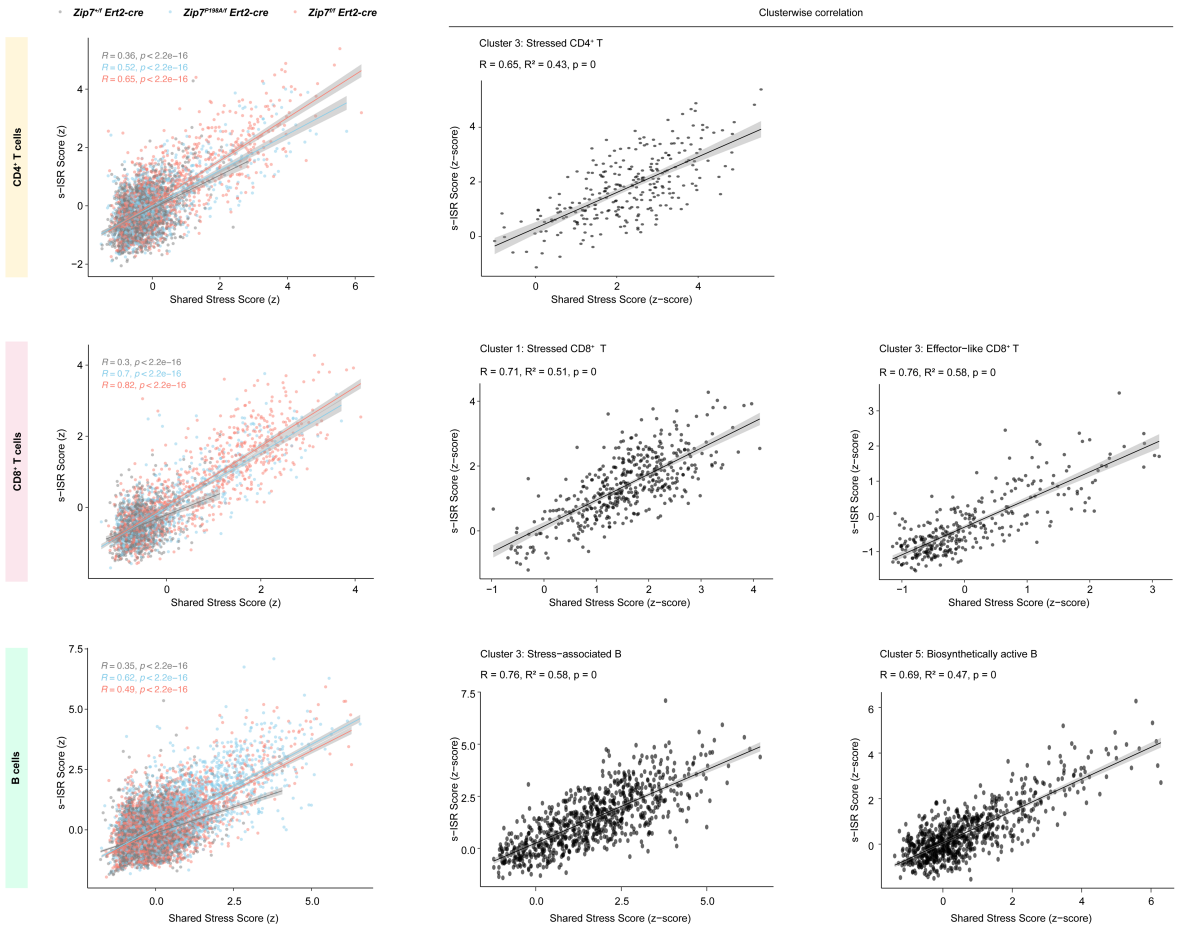

Supplementary Figure 22: Shared Stress and s-ISR Signatures are strongly correlated in ZIP7-deficient lymphocyte subsets.
Left panels show the correlation between z-scored Shared Stress Signature and split ISR (s-ISR) Signature module scores across indicated cell type, coloured by genotype group (*Zip7*$^{+/f}$ *Ert2-cre*, *Zip7*$^{P198A/f}$ *Ert2-cre*, *Zip7*$^{f/f}$ *Ert2-cre*). Right panels display selected clusters with strong correlation ($R^2 \geqslant 0.4$, $p < 0.05$), including stressed or metabolically active subsets from CD4$^+$ T cells, CD8$^+$ T cells, and B cells. Each plot reports Spearman correlation coefficient (R), R^2, and p-value.